The IAPWS Formulation 1995 for the Thermodynamic Properties of Ordinary Water Substance for General and Scientific Use

Cite as: Journal of Physical and Chemical Reference Data **31**, 387 (2002); https://doi.org/10.1063/1.1461829
Submitted: 20 September 2001 . Published Online: 07 June 2002

W. Wagner, and A. Pruß

The IAPWS Formulation 1995 for the Thermodynamic Properties of Ordinary Water Substance for General and Scientific Use

W. Wagner[a] and A. Pruß[b]

Lehrstuhl für Thermodynamik, Ruhr-Universität Bochum, D-44780 Bochum, Germany

(Received 20 September 2001; revised manuscript received 20 December 2001; published 7 June 2002)

In 1995, the International Association for the Properties of Water and Steam (IAPWS) adopted a new formulation called ''The IAPWS Formulation 1995 for the Thermodynamic Properties of Ordinary Water Substance for General and Scientific Use'', which we abbreviate to IAPWS-95 formulation or IAPWS-95 for short. This IAPWS-95 formulation replaces the previous formulation adopted in 1984. This work provides information on the selected experimental data of the thermodynamic properties of water used to develop the new formulation, but information is also given on newer data. The article presents all details of the IAPWS-95 formulation, which is in the form of a fundamental equation explicit in the Helmholtz free energy. The function for the residual part of the Helmholtz free energy was fitted to selected data for the following properties: (a) thermal properties of the single-phase region ($p\rho T$) and of the vapor–liquid phase boundary ($p_\sigma \rho' \rho'' T$), including the phase-equilibrium condition (Maxwell criterion), and (b) the caloric properties specific isochoric heat capacity, specific isobaric heat capacity, speed of sound, differences in the specific enthalpy and in the specific internal energy, Joule–Thomson coefficient, and isothermal throttling coefficient. By applying modern strategies for optimizing the functional form of the equation of state and for the simultaneous nonlinear fitting to the data of all mentioned properties, the resulting IAPWS-95 formulation covers a validity range for temperatures from the melting line (lowest temperature 251.2 K at 209.9 MPa) to 1273 K and pressures up to 1000 MPa. In this entire range of validity, IAPWS-95 represents even the most accurate data to within their experimental uncertainty. In the most important part of the liquid region, the estimated uncertainty of IAPWS-95 ranges from $\pm 0.001\%$ to $\pm 0.02\%$ in density, $\pm 0.03\%$ to $\pm 0.2\%$ in speed of sound, and $\pm 0.1\%$ in isobaric heat capacity. In the liquid region at ambient pressure, IAPWS-95 is extremely accurate in density (uncertainty $\leqslant \pm 0.0001\%$) and in speed of sound ($\pm 0.005\%$). In a large part of the gas region the estimated uncertainty in density ranges from $\pm 0.03\%$ to $\pm 0.05\%$, in speed of sound it amounts to $\pm 0.15\%$ and in isobaric heat capacity it is $\pm 0.2\%$. In the critical region, IAPWS-95 represents not only the thermal properties very well but also the caloric properties in a reasonable way. Special interest has been focused on the extrapolation behavior of the new formulation. At least for the basic properties such as pressure and enthalpy, IAPWS-95 can be extrapolated up to extremely high pressures and temperatures. In addition to the IAPWS-95 formulation, independent equations for vapor pressure, the densities, and the most important caloric properties along the vapor–liquid phase boundary, and for the pressure on the melting and sublimation curve, are given. Moreover, a so-called gas equation for densities up to 55 kg m^{-3} is also included. Tables of the thermodynamic properties calculated from the IAPWS-95 formulation are listed in the Appendix.

Key words: critical region, data evaluation, equation of state, extrapolation, fundamental equation, H_2O, IAPWS-95 formulation, melting curve, property tables, sublimation curve, thermal and caloric properties, vapor–liquid phase boundary, water substance.

Contents

1. Introduction. 395
   1.1. Background. 395
   1.2. Previous Equations of State. 395
   1.3. Need for the Development of a New Scientific Formulation and Adoption of the IAPWS-95 Formulation. 397
   1.4. Existence of the New Industrial Formulation IAPWS-IF97. 397
   1.5. Note on the Values of Temperature Used Throughout this Article. 397
2. Phase Equilibria of Water. 397

[a]Author to whom correspondence should be addressed; Electronic mail: Wagner@thermo.ruhr-uni-bochum.de
[b]Present address: Degussa AG, Paul-Baumann Str. 1, D-45764 Marl, Germany.

2.1. The Triple Point. 398
2.2. The Critical Point. 398
2.3. The Vapor–Liquid Phase Boundary. 398
2.3.1. Experimental Data and Equations for the Vapor Pressure and the Densities of the Saturated Liquid and Vapor. . . . 398
2.3.2. Experimental Data for the Caloric Difference Property $\Delta\alpha$ and Equations for the Enthalpy and Entropy of the Saturated Liquid and Saturated Vapor. 400
2.4. The Solid–Liquid and Solid–Vapor Phase Boundaries. 401
2.4.1. The Melting–Pressure Equations. 401
2.4.2. The Sublimation–Pressure Equation. . . 401
3. The Gas Equation. 401
3.1. Density Range and Input Data. 402
3.2. Details of the Gas Equation. 402
3.3. Comparison of the Gas Equation with Experimental Data. 403
4. The Selected Experimental Data and Other Data Used to Develop IAPWS-95 and Further Experimental Data for Comparison. 403
4.1. Vapor–Liquid Phase Boundary. 405
4.1.1. Thermal Properties in the Saturation State. 405
4.1.2. Caloric Properties in the Saturation State. 405
4.2. Single-Phase Region. 406
4.2.1. $p\rho T$ Data. 407
4.2.2. Second Virial Coefficients. 410
4.3. Speeds of Sound. 410
4.4. Isochoric Heat Capacities. 412
4.5. Isobaric Heat Capacities. 413
4.5.1. Data of the Specific Isobaric Heat Capacity in the Ideal-Gas State. 413
4.5.2. Experimental Data of the Specific Isobaric Heat Capacity. 414
4.6. Enthalpy Differences. 416
4.7. Joule–Thomson Coefficient. 416
4.8. Isothermal Throttling Coefficient. 416
4.9. Hugoniot-Curve Data and Derived $p\rho T$ Data. 417
4.10. Calculated Data for the Gas Region. 418
4.11. Data for Special Applications. 418
5. Details of the Development of the IAPWS-95 Formulation. 419
5.1. Basic Structure of an Equation of State Explicit in the Helmholtz Free Energy. 419
5.2. The Equation for the Helmholtz Free Energy of the Ideal Gas. 419
5.3. Basic Statements for Fitting and Optimizing the Structure of an Equation for the Residual Part of the Helmholtz Free Energy. 420
5.3.1. Fitting an Equation for ϕ^r to Data. . . . 420
5.3.2. Basic Statements for Optimizing the Mathematical Form of ϕ^r. 422
5.4. Functional Forms for ϕ^r and the Bank of Terms. 423
5.4.1. Polynomial Terms. 423
5.4.2. Polynomial Terms in Combination with Exponential Functions. 423
5.4.3. Modified Gaussian Bell-Shaped Terms. 424
5.4.4. Nonanalytical Terms. 424
5.4.5. Bank of Terms. 425
5.5. Determination of the Final Form of the IAPWS-95 Formulation. 426
5.5.1. Summarizing Information on the Sorts of Data Used. 426
5.5.2. Iterative Process of the Development of the IAPWS-95 Formulation. 426
6. The IAPWS-95 Formulation. 427
6.1. Reference Constants. 428
6.2. Numerical Description of the IAPWS-95 Formulation. 429
6.3. Basic Information on the Application of the IAPWS-95 Formulation. 432
6.3.1. Range of Validity. 432
6.3.2. Estimates of Uncertainty. 432
6.3.3. Computer-Program Verification. 435
6.4. Features of the Nonanalytical Terms Used for IAPWS-95. 435
6.4.1. Positive Features of the Nonanalytical Terms. 435
6.4.2. Weaknesses of the Nonanalytical Terms. 437
6.4.3. Nonanalytical Terms Proposed by Kiselev and Friend. 441
6.4.4. Summary of the Advantages and Weaknesses of the Nonanalytical Terms in IAPWS-95. 441
7. Comparison of the IAPWS-95 Formulation with Experimental Data and Values from Other Equations of State. 442
7.1. The Vapor–Liquid Phase Boundary. 443
7.1.1. Thermal Properties at Saturation. 443
7.1.2. Speeds of Sound at Saturation. 444
7.1.3. Isochoric Heat Capacities at Saturation. 445
7.1.4. Isobaric Heat Capacities at Saturation. 445
7.1.5. The Caloric Difference Property $\Delta\alpha$ and the Enthalpies at Saturation. 446
7.2. The Representation of Properties in the Single-Phase Region. 446
7.2.1. $p\rho T$ Data. 446
7.2.1.1. Temperature Range $T < 273.16$ K. 446
7.2.1.2. Temperature Range 273.16 K $\leqslant T <$ 643.15 K. 447
7.2.1.3. Critical Region 643.15 K $\leqslant T <$ 663.15 K. 449
7.2.1.4. Temperature Range 663.15 K $\leqslant T <$ 1273.15 K. 450

7.2.1.5. Comparison with the IAPS Skeleton Table Values at High Pressures and High Temperatures. 450
7.2.2. Second and Third Virial Coefficients. . 451
7.2.3. Speed of Sound. 452
7.2.4. Isochoric Heat Capacity. 455
7.2.5. Isobaric Heat Capacity. 459
7.2.6. Enthalpy Differences. 464
7.2.7. Joule–Thomson and Isothermal Throttling Coefficient. 465
7.2.8. Isentropic Temperature–Pressure Coefficient. 468
7.3. Selected Attributes of the IAPWS-95 Formulation. 468
7.3.1. Derivatives of the Thermal Properties in the Liquid Phase. 468
7.3.2. Representation of Thermodynamic Properties in Metastable Regions. 472
7.3.2.1. Subcooled Liquid. 472
7.3.2.2. Superheated Liquid. 473
7.3.2.3. Subcooled Vapor. 474
7.3.3. Extrapolation Behavior. 475
7.3.3.1. Hugoniot Curve and $p\rho T$ Behavior at Extreme Pressures and Temperatures. . . 475
7.3.3.2. Ideal Curves. 476
8. Uncertainty of the IAPWS-95 Formulation. 478
9. Recommendations for Improving the Basis of the Experimental Data. 479
10. Conclusions. 480
11. Acknowledgments. 480
12. References. 481
13. Appendix: Tables of Thermodynamic Properties of Water. 485

List of Tables

1.1. Information on selected equations of state for water. 396
2.1. Information on the selected measuring runs for the vapor pressure p_σ, the saturated liquid density ρ', and the saturated vapor density ρ''... 399
2.2. Information on the selected data for the caloric difference quantity $\Delta\alpha$. 400
3.1. Coefficients and exponents of the residual part ϕ^r of the dimensionless Helmholtz free energy, Eq. (3.3). 402
4.1. Information on the selected values of the thermal saturation properties used to develop the IAPWS-95 formulation. 405
4.2. Information on the selected values for the specific internal energy on the vapor–liquid phase boundary. 405
4.3. Information on the selected data for the caloric properties speed of sound w and specific isobaric heat capacity c_p of the saturated liquid and vapor. 406
4.4. Information on the selected $p\rho T$ data. 406
4.5. Information on the selected data for the speed of sound w. 411
4.6. Information on the selected data for the specific isochoric heat capacity. 413
4.7. Information on data sets for the isobaric heat capacity of water in the ideal-gas state. 413
4.8. Information on the selected data for the specific isobaric heat capacity c_p. 414
4.9. Information on the selected data of the caloric properties enthalpy difference Δh, Joule–Thomson coefficient μ, and isothermal throttling coefficient δ_T. 416
5.1. Contribution of the several linear, nonlinear, and linearized data to the weighted sum of squares for the fitting and optimization process. 421
5.2. Parameters of the modified Gaussian bell-shaped terms according to Eq. (5.37) which are contained in the bank of terms, Eq. (5.41). 425
5.3. Parameters of the nonanalytical terms according to Eq. (5.40) which are contained in the bank of terms, Eq. (5.41). 426
5.4. Summarizing information on the selected data used in the linear optimization procedure and in the nonlinear fitting process when developing the IAPWS-95 formulation. 427
6.1. Coefficients of Eq. (6.5). 429
6.2. Coefficients and exponents of Eq. (6.6). 430
6.3. Relations of thermodynamic properties to the ideal-gas part ϕ°, Eq. (6.5), and the residual part ϕ^r, Eq. (6.6), of the dimensionless Helmholtz free energy and their derivatives. . . . 431
6.4. The ideal-gas part ϕ°, Eq. (6.5), of the dimensionless Helmholtz free energy and its derivatives. 432
6.5. The residual part ϕ^r, Eq. (6.6), of the dimensionless Helmholtz free energy and its derivatives. 433
6.6. Values for the ideal-gas part ϕ°, Eq. (6.5), and for the residual part ϕ^r, Eq. (6.6), of the dimensionless Helmholtz free energy together with the corresponding derivatives for two combinations of temperature and density. 436
7.1. The zeroth and first order ideal curves for the compression factor Z and their definitions in terms of the compression factor $Z(\rho,T)$ and of the residual part of the reduced Helmholtz free energy $\phi^r(\rho,T)$ and the condition for the second virial coefficient B at the temperature T_{end} 477
13.1. Thermodynamic properties of water on the vapor–liquid phase boundary as a function on temperature. 486
13.2. Thermodynamic properties of water in the single-phase region. 495

List of Figures

2.1. The phase–boundary curves of water in a $p-T$ diagram.. 398
2.2. Percentage deviations of the experimental data of the vapor pressure p_σ, the saturated liquid density ρ', and the saturated vapor density ρ'' from the values calculated from the corresponding Eqs. (2.5), (2.6), or (2.7).. 399
2.3. Percentage deviations $100\Delta(\Delta\alpha)/\Delta\alpha = 100(\Delta\alpha_{\rm exp}-\Delta\alpha_{\rm calc})/\Delta\alpha_{\rm exp}$ between experimental data of the caloric difference quantity $\Delta\alpha$ and values calculated from Eq. (2.9).. 400
3.1. Percentage density deviations between experimental $p\rho T$ data and values calculated from the gas equation, Eq. (3.2).. 402
3.2. Percentage deviations between experimental data of the speed of sound w and values calculated from the gas equation, Eq. (3.2).. . . . 403
3.3. Percentage deviations between experimental data of the isobaric heat capacity c_p and values calculated from the gas equation, Eq. (3.2).. 404
3.4. Percentage deviations between experimental data of the Joule–Thomson coefficient μ and values calculated from the gas equation, Eq. (3.2).. 404
4.1. Distribution of the selected $p\rho T$ data used to develop the residual part of IAPWS-95, Eq. (6.6), in a $p-T$ diagram.. 407
4.2. Percentage density deviations $100\Delta\rho/\rho = 100(\rho_{\rm exp}-\rho_{\rm calc})/\rho_{\rm exp}$ of experimental $p\rho T$ data of Grindley and Lind (1971) and Kell and Whalley (1975) from values calculated from a preliminary equation of state.. 408
4.3. Percentage density deviations between experimental $p\rho T$ data of Kell *et al.* (1989) and values calculated from a preliminary equation of state.. 408
4.4. Percentage density deviations between experimental $p\rho T$ data and values calculated from a preliminary equation of state.. 408
4.5. Distribution of the selected data of the speed of sound used to develop the residual part of IAPWS-95, Eq. (6.6), in a $p-T$ diagram.. 411
4.6. Distribution of experimental data of the isochoric heat capacity in a $T-\rho$ diagram.. 412
4.7. Percentage deviations between the data of the isobaric heat capacity in the ideal-gas state c_p° from statistical mechanical models and from property tables, respectively, and values calculated from the ϕ° equation of IAPWS-95, Eq. (6.5).. 414
4.8. Distribution of the selected data of the isobaric heat capacity used to develop the residual part of IAPWS-95, Eq. (6.6), in a $p-T$ diagram.. . . . 415
4.9. Distribution of the selected data of the three properties enthalpy difference, Joule–Thomson coefficient, and isothermal throttling coefficient used to develop the residual part of IAPWS-95, Eq. (6.6), in a $p-T$ diagram.. 417
5.1. Scheme of one step of the entire iteration cycle to develop the residual part $\phi^{\rm r}$ of IAPWS-95, Eq. (6.6).. 428
6.1. Percentage uncertainties in density estimated for IAPWS-95, Eq. (6.4).. 434
6.2. Percentage uncertainties in speed of sound estimated for IAPWS-95, Eq. (6.4).. 434
6.3. Percentage uncertainties in specific isobaric heat capacity estimated for IAPWS-95, Eq. (6.4).. 435
6.4. Percentage uncertainties in vapor pressure $100\,\Delta p_\sigma/p_\sigma$, in saturated liquid density $100\,\Delta\rho'/\rho'$, and in saturated vapor density $100\,\Delta\rho''/\rho''$ estimated for IAPWS-95, Eq. (6.4).. 435
6.5. Isochoric heat capacity in the critical region as a function of temperature (on the critical isochore of the single-phase region) calculated from IAPWS-95, Eq. (6.4), an IAPWS-95-like equation but without nonanalytical terms, and the equation of Saul and Wagner (1989).. . 436
6.6. Isochoric heat capacity in the critical region as a function of density on two isotherms calculated from IAPWS-95, Eq. (6.4), IAPS-84, and the crossover equation of Kostrowicka Wyczalkowska *et al.* (2000).. 436
6.7. Speed of sound in the critical region as a function of density on two isotherms calculated from IAPWS-95, Eq. (6.4), IAPS-84, and the crossover equation of Kostrowicka Wyczalkowska *et al.* (2000).. 437
6.8. Isochoric heat capacity along the critical isochore of the single-phase region in a double logarithmic diagram calculated from IAPWS-95, Eq. (6.4), IAPS-84, and the crossover equation of Kostrowicka Wyczalkowska *et al.* (2000).. 437
6.9. Partial derivative of pressure with respect to density at constant temperature as a function of density calculated from IAPWS-95, Eq. (6.4), along the isotherm $T=T_{\rm c}+10$ mK.. 438
6.10. Partial derivative of density with respect to pressure at constant temperature as a function of density calculated from IAPWS-95, Eq. (6.4), along the isotherm $T=T_{\rm c}+10$ mK.. 438
6.11. Isobaric heat capacity as a function of density calculated from IAPWS-95, Eq. (6.4), along the isotherm $T=T_{\rm c}+10$ mK.. 439
6.12. Isobaric heat capacity as a function of density calculated from IAPWS-95, Eq. (6.4), along the two isotherms $T=T_{\rm c}+1$ K and $T=T_{\rm c}+2$ K.. 439

6.13. Isochoric heat capacity along several near-critical isochores $\rho<\rho_c$ (gas region) calculated from IAPWS-95, Eq. (6.4), in a small temperature range above the saturation temperature.. 440
6.14. Speed of sound along several near-critical isochores $\rho>\rho_c$ (liquid region) calculated from IAPWS-95, Eq. (6.4), in a small temperature range above the saturation temperature.. 440
6.15. Isochoric heat capacity along the vapor–liquid phase boundary as a function of density calculated from IAPWS-95, an IAPWS-95-like equation without nonanalytical terms, and the crossover equation of Kostrowicka Wyczalkowska *et al.* (2000).. 440
6.16. Speed of sound along the vapor–liquid phase boundary as a function of density calculated from IAPWS-95, an IAPWS-95-like equation without nonanalytical terms, and the crossover equation of Kostrowicka Wyczalkowska *et al.* (2000).. 441
7.1. Percentage deviations of the experimental data of the vapor pressure p_σ, the saturated liquid density ρ', and the saturated vapor density ρ'' from the corresponding values calculated from IAPWS-95, Eq. (6.4).. 442
7.2. Percentage deviations $100\,\Delta\rho'/\rho' = 100(\rho'_{\rm exp} - \rho'_{\rm calc})/\rho'_{\rm exp}$ between experimental data of the saturated liquid density ρ' and values calculated from IAPWS-95, Eq. (6.4).. 443
7.3. Percentage deviations of the experimental data of the vapor pressure p_σ, the saturated liquid density ρ', and the saturated vapor density ρ'' from the corresponding values calculated from IAPWS-95, Eq. (6.4), for the temperature range from 10 K below the critical temperature up to T_c.. 443
7.4. The vapor–liquid phase boundary in the critical region of the $p-\rho$ diagram calculated from IAPWS-95, Eq. (6.4), IAPS-84, the equation of Hill (1990), and the crossover equation of Kostrowicka Wyczalkowska *et al.* (2000).. 444
7.5. Percentage deviations of the experimental data of the speed of sound of the saturated liquid w' and the speed of sound of the saturated vapor w'' from the corresponding values calculated from IAPWS-95, Eq. (6.4).. 444
7.6. Percentage deviations $100\,\Delta c'_v/c'_v = 100(c'_{v,\rm exp} - c'_{v,\rm calc})/c'_{v,\rm exp}$ between experimental data of the isochoric heat capacity of the saturated liquid c'_v and values calculated from IAPWS-95, Eq. (6.4). 445
7.7. Percentage deviations of the experimental data of the isobaric heat capacity of the saturated liquid c'_p and the isobaric heat capacity of the saturated vapor c''_p from the corresponding values calculated from IAPWS-95, Eq. (6.4).. . . 445
7.8. The caloric difference quantity $\Delta\alpha$ related to ΔT (with $\Delta T = 1$ K) as a function of temperature calculated from IAPWS-95, Eq. (6.4), IAPS-84, and the equation of Hill (1990).. 446
7.9. Percentage deviations of the experimental data of the caloric difference quantity $\Delta\alpha$ and values of the Skeleton Tables IST-85 with their tolerances [IAPWS (1994)] of the enthalpy of the saturated liquid h' and the enthalpy of the saturated vapor h'' from the corresponding values calculated from IAPWS-95, Eq. (6.4).. . . 446
7.10. Percentage density deviations between experimental $p\rho T$ data and values calculated from IAPWS-95, Eq. (6.4).. 447
7.11. Percentage density deviations between experimental $p\rho T$ data and values calculated from IAPWS-95, Eq. (6.4).. 448
7.12. Percentage density deviations between very accurate experimental $p\rho T$ data and values calculated from IAPWS-95, Eq. (6.4).. 449
7.13. Percentage density deviations $100\,\Delta\rho/\rho = 100(\rho_{\rm exp} - \rho_{\rm calc})/\rho_{\rm exp}$ between highly accurate experimental $p\rho T$ data along the isobar $p = 0.101\,325$ MPa and values calculated from IAPWS-95, Eq. (6.4). 449
7.14. Parts-per-million density deviations $10^6\Delta\rho/\rho = 10^6(\rho_{\rm exp} - \rho_{\rm calc})/\rho_{\rm exp}$ between highly accurate experimental $p\rho T$ data along the isobar $p = 0.101\,325$ MPa and values calculated from IAPWS-95, Eq. (6.4).. 449
7.15. Percentage density deviations $100\Delta\rho/\rho = 100(\rho_{\rm exp} - \rho_{\rm calc})/\rho_{\rm exp}$ between the $p\rho T$ data of Wiryana *et al.* (1998) for temperatures from 353.15 to 473.15 K and values calculated with IAPWS-95, Eq. (6.4).. 450
7.16. Percentage pressure deviations between experimental $p\rho T$ data in the critical region and values calculated from IAPWS-95, Eq. (6.4); the density range of the diagrams clearly exceeds the critical region.. 450
7.17. Percentage density deviations between experimental $p\rho T$ data and values calculated from IAPWS-95, Eq. (6.4).. 451
7.18. Percentage density deviations of experimental $p\rho T$ data and values of the Skeleton Tables IST-85 [IAPWS (1994)] together with their tolerances from values calculated with IAPWS-95, Eq. (6.4).. 452
7.19. Second virial coefficient B as a function of temperature as calculated from IAPWS-95, Eq. (6.4); the experimental data are plotted for

comparison.. 453
7.20. Third virial coefficient C as a function of temperature as calculated from IAPWS-95, Eq. (6.4); the experimental data are plotted for comparison.. 453
7.21. Percentage deviations between experimental data of the speed of sound w and values calculated from IAPWS-95, Eq. (6.4).. 454
7.22. Percentage deviations between very accurate experimental data of the speed of sound w along the isobar $p=0.101\,325$ MPa and values calculated from IAPWS-95, Eq. (6.4).. 455
7.23. Speed of sound in the critical region as a function of pressure on three isotherms as calculated from IAPWS-95, the equation of Hill (1990), and the crossover equation of Kostrowicka Wyczalkowska *et al.* (2000); values from the crossover equation are only shown within its range of validity.. 456
7.24. Percentage deviations between experimental data of the speed of sound w and values calculated from IAPWS-95, Eq. (6.4).. 457
7.25. Percentage deviations $100\Delta w/w=100(w_{\rm exp}-w_{\rm calc})/w_{\rm exp}$ between the experimental data of the speed of sound w of Wiryana *et al.* (1998) for temperatures from 353.15 to 473.15 K and values calculated with IAPWS-95, Eq. (6.4).. 457
7.26. Comparison between experimental data of the isochoric heat capacity c_v and values calculated from IAPWS-95, Eq. (6.4), IAPS-84, and the equation of Hill (1990).. 458
7.27. Percentage deviations between experimental data of the isochoric heat capacity c_v in the extended critical region and values calculated from IAPWS-95, Eq. (6.4).. 458
7.28. Percentage deviations between experimental data of the isochoric heat capacity c_v in the extended critical region and values calculated from IAPWS-95, Eq. (6.4).. 459
7.29. Isochoric heat capacity in the near-critical region along a subcritical isochore as a function of temperature (near-critical temperature range, $T>T_\sigma$, single-phase region) as calculated from IAPWS-95, Eq. (6.4), and from the crossover equation of Kostrowicka Wyczalkowska *et al.* (2000).. 460
7.30. Isochoric heat capacity in the critical region along a supercritical isochore as a function of temperature as calculated from IAPWS-95, Eq. (6.4).. 461
7.31. Percentage deviations between experimental data of the isochoric heat capacity c_v and values calculated from IAPWS-95, Eq. (6.4).. . . 461
7.32. Percentage deviations between experimental data of the isobaric heat capacity c_p and values calculated from IAPWS-95, Eq. (6.4).. . . 462
7.33. Isobaric heat capacity as a function of temperature as calculated from IAPWS-95, Eq. (6.4), along a part of the saturated-vapor line and in the gas region.. 462
7.34. Isobaric heat capacity in the critical region as a function of density on four isobars as calculated from IAPWS-95, Eq. (6.4).. 463
7.35. Percentage deviations between experimental data of the isobaric heat capacity c_p and values calculated from IAPWS-95, Eq. (6.4).. . . 463
7.36. Percentage deviations between experimental data of the isobaric heat capacity c_p in the extended critical region and values calculated from IAPWS-95, Eq. (6.4).. 464
7.37. Percentage deviations $100\Delta c_p/c_p=100(c_{p,\rm exp}-c_{p,\rm calc})/c_{p,\rm exp}$ between experimental data of the isobaric heat capacity c_p measured by Czarnota (1984) and values calculated from IAPWS-95, Eq. (6.4).. 464
7.38. Percentage deviations $100\Delta c_p/c_p=100(c_{p,\rm exp}-c_{p,\rm calc})/c_{p,\rm exp}$ between the data of the isobaric heat capacity c_p of Wiryana *et al.* (1998) for temperatures from 353.15 to 473.15 K and values calculated with IAPWS-95, Eq. (6.4).. . . 464
7.39. Percentage deviations between experimental data of the enthalpy differences Δh and values calculated from IAPWS-95, Eq. (6.4).. 465
7.40. Percentage deviations between experimental data of the Joule–Thomson coefficient μ and values calculated from IAPWS-95, Eq. (6.4).. . . 466
7.41. Percentage deviations between experimental data of the isothermal throttling coefficient δ_T of Ertle (1979) and values calculated from IAPWS-95, Eq. (6.4).. 466
7.42. Percentage deviations between experimental data of the isothermal throttling coefficient δ_T of McGlashan and Wormald (2000) and values calculated from IAPWS-95, Eq. (6.4).. . . 467
7.43. Absolute deviations $\Delta\delta_{T,0}=(\delta_{T,0,\rm exp}-\delta_{T,0,\rm calc})$ between experimental data of the isothermal throttling coefficient at zero pressure $\delta_{T,0}$ of McGlashan and Wormald (2000) and values calculated from IAPWS-95, Eq. (6.4).. 467
7.44. Percentage deviations between experimental data of the isentropic temperature–pressure coefficient β_s and values calculated from IAPWS-95, Eq. (6.4).. 468
7.45. Percentage differences of values of the derivative $(\partial\rho/\partial T)_p$ for $p=100$ MPa calculated from IAPS-84, the equation of Saul and Wagner (1989), and the equation of Hill (1990) from values calculated from an equation of Ter Minassian and Pruzan (1981) for the expansivity of water and values of the derivative $(\partial^2\rho/\partial p^2)_T$ for $T=273.15$ K as a function of pressure as calculated from the same equations of state.. 469

7.46. Percentage density deviations $100\Delta\rho/\rho = 100(\rho_{exp}-\rho_{calc})/\rho_{exp}$ between accurate experimental $p\rho T$ data for the isotherm $T = 273.15$ K and values calculated from IAPWS-95, Eq. (6.4).. 469
7.47. Percentage differences of values of the derivatives $(\partial\rho/\partial p)_T$ and $(\partial\rho/\partial T)_p$ for the four pressures 0.1, 1, 10, and 100 MPa calculated with IAPS-84 and the equation of Hill (1990) from values calculated with IAPWS-95, Eq. (6.4).. 470
7.48. Values of the derivatives $(\partial^2\rho/\partial p^2)_T$, $(\partial^2\rho/\partial T^2)_p$, and $(\partial^2\rho/\partial p\partial T)$ as a function of pressure for the temperatures 273.15 and 298.15 K and $(\partial^2\rho/\partial T^2)_p$ as a function of temperature for $p = 0.101\,325$ MPa as calculated from IAPWS-95, IAPS-84, and the equation of Hill (1990).. 471
7.49. Percentage density deviations $100\Delta\rho/\rho = 100(\rho_{exp}-\rho_{calc})/\rho_{exp}$ between experimental $p\rho T$ data in the subcooled liquid along the isobar $p = 0.101\,325$ MPa and values calculated from IAPWS-95, Eq. (6.4).. 472
7.50. Percentage deviations $100\Delta w/w = 100(w_{exp} - w_{calc})/w_{exp}$ between experimental data of the speed of sound w in the subcooled liquid along the isobar $p = 0.101\,325$ MPa and values calculated from IAPWS-95, Eq. (6.4).. 472
7.51. Comparison between experimental data of the isobaric heat capacity c_p in the subcooled liquid for the isobar $p = 0.101\,325$ MPa and values calculated from IAPWS-95, Eq. (6.4), IAPS-84, and the equation of Hill (1990).. 472
7.52. Percentage density deviations between experimental $p\rho T$ data in the superheated liquid (left of the phase-boundary line) and values calculated from IAPWS-95, Eq. (6.4).. 473
7.53. Percentage deviations between experimental data of the speed of sound w in the superheated liquid (left of the phase-boundary line) and values calculated from IAPWS-95, Eq. (6.4).. . . 474
7.54. The liquid spinodal of the vapor–liquid two-phase region as calculated from IAPWS-95, Eq. (6.4), IAPS-84, and the equation of Hill (1990).. 474
7.55. Comparison of the Hugoniot curve as calculated from IAPWS-95, Eq. (6.4), IAPS-84, the equation of Saul and Wagner (1989), and the equation of Hill (1990) with the corresponding experimental data.. 475
7.56. Plot of three $p\rho T$ isotherms in the pressure–density diagram at extremely high pressures as calculated from IAPWS-95, Eq. (6.4), IAPS-84, and the equation of Hill (1990).. 475
7.57. The so-called ideal curves in a double logarithmic p/p_c vs T/T_c diagram as calculated from IAPWS-95, Eq. (6.4).. 477
7.58. The ideal curves in a double logarithmic p/p_c vs T/T_c diagram as calculated from IAPS-84 and the equation of Hill (1990); the curves calculated from IAPWS-95 are plotted for comparison.. 478
7.59. Second virial coefficient at very high temperatures as calculated from IAPWS-95, Eq. (6.4), IAPS-84, the equation of Hill (1990), and the virial equation of Hill and MacMillan (1988).. 478
7.60. The ideal curves in a ρ/ρ_c vs log (T/T_c) diagram as calculated from IAPWS-95, Eq. (6.4), IAPS-84, and the equation of Hill (1990).. 478

Nomenclature

Latin symbols

$a,b,c,d,$	
A,B,C,D	Adjustable parameters
B	Second virial coefficient
c	Density exponent
c_p	Specific isobaric heat capacity
c_v	Specific isochoric heat capacity
c_σ	Specific heat capacity along the saturated-liquid line
C	Third virial coefficient
d	Density exponent
d	Derivative
D	Fourth virial coefficient
E	Fifth virial coefficient
f	Specific Helmholtz free energy
g	Specific Gibbs free energy
h	Specific enthalpy
i,j,k,l,m	Serial numbers
I,J,K,L,M	Maximum values of the serial numbers i,j,k,l,m
M	Molar mass, number of data
n	Adjustable coefficient
p	Pressure
R	Specific gas constant
R_m	Molar gas constant
s	Specific entropy
t	Temperature exponent
T	Thermodynamic temperature, ITS-90
u	Specific internal energy
v	Specific volume
w	Speed of sound
x,y	Independent variables
z	Any thermodynamic property
Z	Compression factor $[Z = p/(\rho RT)]$

Greek symbols

$\alpha,\beta,\gamma,\Delta,\epsilon,\theta$	Adjustable parameters
$\alpha,\beta,\gamma,\delta$	Critical exponents
α	Special caloric property, Eq. (2.9)
β	Special caloric property, Eq. (2.3)

β_s	Isentropic temperature-pressure coefficient $[\beta_s=(\partial T/\partial p)_s]$
γ	Special caloric property, Eq. (2.4)
γ^{p}	Precorrelation factor $(\gamma=c_p/c_v)$
δ	Reduced density $(\delta=\rho/\rho_{\mathrm{c}})$
δ_T	Isothermal throttling coefficient $[\delta_T=(\partial h/\partial p)_T]$
$\delta_{T,0}$	Isothermal throttling coefficient at the limit of zero density
Δ	Difference in any quantity
Δ,θ,ψ	Functions in the nonanalytical terms
$\Delta\alpha$	Caloric difference quantity
$\Delta^{\mathrm{v}}h$	Heat of vaporization
∂	Partial differential
ϵ	Static dielectric constant
ϵ^{p}	Precorrelation factor $(\epsilon=c_p-c_v)$
θ	Reduced temperature $(\theta=T/T_{\mathrm{c}},\ \theta=T/T_{\mathrm{n}})$
ϑ	Transformed temperature $(\vartheta=1-T/T_{\mathrm{c}})$
κ_T	Isothermal compressibility $[\kappa_T=\rho^{-1}(\partial p/\partial p)_T]$
ϕ	Dimensionless Helmholtz free energy $[\phi=f/(RT)]$
μ	Joule–Thomson coefficient $[\mu=(\partial T/\partial p)_h]$
ρ	Mass density
σ	Standard deviation
σ^2	Variance
τ	Inverse reduced temperature $(\tau=T_{\mathrm{c}}/T)$
χ^2	Weighted sum of squares
ψ	Special caloric function

Superscripts

o	Ideal-gas state
p	Precorrelated quantity
r	Residual contribution
$'$	Saturated liquid state
$''$	Saturated vapor state
$\rightarrow$	Denotes a vector

Subscripts

b	At the normal boiling point
c	At the critical point
calc	Calculated
exp	Experimental
h	Isenthalpic
i,j,k,l,m	Indices
n	General reducing state
m	Denotes a state on the melting curve
max	Maximum value
p	Isobaric
s	Isentropic
subl	Denotes a state on the sublimation curve
σ	Denotes a state on the vapor–pressure curve
t	At the triple point
tot	Total
T	Isothermal
v	Isochoric
wt	Weighting
0H	In the initial state of the Hugoniot curve measurements

Physical constants and characteristic properties of water (H_2O)

Molar mass	$M = 18.015\,268\ \mathrm{g\,mol^{-1}}$	see Sec. 6.1
Specific gas constant	$R = 0.461\,518\,05\ \mathrm{kJ\,kg^{-1}\,K^{-1}}$	see Sec. 6.1
Critical point		
Temperature	$T_c = 647.096\ \mathrm{K}$	see Sec. 2.2
Pressure	$p_c = 22.064\ \mathrm{MPa}$	
Density	$\rho_c = 322\ \mathrm{kg\,m^{-3}}$	
Triple point		
Temperature	$T_t = 273.16\ \mathrm{K}$	see Sec. 2.1
Pressure	$p_t = 611.655\ \mathrm{Pa}$	Eq. (6.4)[c]
Density (liquid)	$\rho_t' = 999.793\ \mathrm{kg\,m^{-3}}$	
Density (vapor)	$\rho_t'' = 0.004\,854\,58\ \mathrm{kg\,m^{-3}}$	
Normal boiling point		
Temperature	$T_b = 373.124\ \mathrm{K}$	Eq. (6.4)[c]
Pressure	$p_b = 0.101\,325\ \mathrm{MPa}$	
Density (liquid)	$\rho_b' = 958.367\ \mathrm{kg\,m^{-3}}$	Eq. (6.4)[c]
Density (vapor)	$\rho_b'' = 0.597\,657\ \mathrm{kg\,m^{-3}}$	
Reference state (liquid state at the triple point)		
Specific internal energy	$u_t' = 0$	see Sec. 6.2
Specific entropy	$s_t' = 0$	
Specific enthalpy	$h_t' = 0.611\,872\ \mathrm{J\,kg^{-1}}$	Eq. (6.4)[c]

[c]Calculated from IAPWS-95, Eq. (6.4), by solving the phase-equilibrium condition, Eqs. (6.9a)–(6.9c).

1. Introduction

1.1. Background

Of all pure fluid substances, water and steam, or ''ordinary water substance'' as it is sometimes called, or simply H_2O, is without doubt the most important substance in existence. It is used as a working fluid in power cycles which supply electricity in huge amounts to power the industrialized world and for numerous other technical applications. In addition to its use in energy engineering, in chemical engineering and chemistry, water is the most common solvent. Not only is H_2O an extremely important substance in classical technical applications, but also in very modern technical fields such as supercritical water oxidation. Supercritical water has been examined as a very convenient medium for special chemical reactions to destroy hazardous waste. No less important than these technical applications is the fact that water plays an essential part in the variation of weather and climate, and its properties under extreme pressure and temperature are essential in the field of geology. Finally, water covers more than two thirds of the earth's surface, not to mention its seminal role in living organisms.

In view of this multitude of applications and the basic importance of water, a huge number of measurements in a great variety of its properties have been carried out from the beginning of the 20th century until today. Considering their quality, their different nature and the extremely large number of data (about 20 000 values), water cannot be compared with any other substance. However, a continuous description of the thermodynamic properties of water over the entire thermodynamic surface can only be achieved with a suitable equation of state that is able to represent all the data considered to be reliable to within their experimental uncertainty.

Since 1970, international research regarding the thermophysical properties of water and steam has been coordinated by the International Association for the Properties of Steam (IAPS), which later changed its name to the International Association for the Properties of Water and Steam (IAPWS). IAPWS members come from most of the important industrial countries. IAPWS is responsible for the international standards for several thermophysical properties. These standards and recommendations are given in the form of releases and guidelines. One of the most important standards in this sense is the equation of state for the thermodynamic properties of ordinary water substance for general and scientific use.

1.2. Previous Equations of State

Numerous correlations for the thermodynamic properties of water can be found in the literature, but most of them cover only small parts of the fluid region and do not meet

TABLE 1.1. Information on selected equations of state for water

Authors	Year	International standard as	Temperature range/K	Pressure range/MPa	Structure of the equation	Number of coefficients	Data used in the development
International Formulation Committee	1968	IFC-68	273–1073	0–100	Separate equations of the Gibbs and Helmholtz free energy for 7 subregions	240	$pvT, p_\sigma v' v'' T, h$
Keenan *et al.*	1969		273–1673	0–100	Helmholtz free energy	50	$pvT, p_\sigma v' v'' T, h', h''$
Pollak	1974[a]		273–1200	0–300	Helmholtz free energy	40	$p\rho T, p_\sigma \rho' \rho'' T$, Maxwell, h', h''
Haar *et al.*	1982[b]	IAPS-84[c]	273–1273	0–1000	Helmholtz free energy	48	$p\rho T, p_\sigma \rho' \rho'' T$, Maxwell
Saul & Wagner	1989		273–1273	0–25 000	Helmholtz free energy, optimized structure	58	$p\rho T, p_\sigma \rho' \rho'' T$, Maxwell, $c_v, w, w', c_p, \Delta h, \mu, \delta_T, u''-u'$
Hill	1990		273–1273	0–1000	Helmholtz free energy, optimized structure, combined with a scaled equation	80	pvT, p_σ, v', Maxwell, h', h''

[a]See also Pollak (1975).
[b]See also Haar *et al.* (1984).
[c]Published as IAPS-84 formulation by Kestin and Sengers (1986).

present demands on accuracy. Thus, Table 1.1 summarizes only the characteristic features of the best equations of state that have been published since 1968.

The first international standard for the thermodynamic properties of water and steam for scientific and general use was the equation package of the IFC-68 [IFC (1968)]. This formulation was a further development of the international standard for the thermodynamic properties of water and steam for industrial use, the IFC-67 formulation [IFC (1967)]; the improvement related essentially to a better representation of the critical region. IFC-68 used seven separate equations to cover its entire range of validity. However, due to these separate equations, there are clear consistency problems for some properties. The first wide-ranging single equation of state for water was developed by Keenan *et al.* (1969), which was one of the first fundamental equations in the form of the Helmholtz free energy. This equation, however, did not satisfy the phase-equilibrium condition (Maxwell criterion). A very good equation for water was the fundamental equation of Pollak (1974, 1975), which has a range of validity in pressure up to 300 MPa. This equation meets the phase-equilibrium condition so that the saturation properties along the vapor–liquid phase boundary can be calculated from this equation without using a separate vapor–pressure equation. In 1984, the Helmholtz-free-energy equation developed by Haar *et al.* (1982, 1984) was adopted by IAPS as a new international standard. We will refer to this formulation as IAPS-84; for the corresponding publication see Kestin and Sengers (1986). This equation was the first to cover a pressure range up to 1000 MPa, and over wide ranges of pressure and temperature IAPS-84 represents the thermodynamic properties of water very well. However, in the years following 1984 it became clear that IAPS-84 manifested some substantial weaknesses near the critical point (particularly regarding the phase boundary and in its ''derivative'' properties such as the isothermal compressibility) and when extrapolating this equation beyond its range of validity. The fundamental equation developed by Saul and Wagner (1989) was the first equation of state for water that was optimized regarding its functional structure and that was fitted simultaneously to the experimental data of many different properties (so-called multiproperty fitting, see Table 1.1). In 1990, Hill (1990) published a so-called unified fundamental equation for the thermodynamic properties of H_2O that includes the revised and extended scaled equation of Levelt Sengers *et al.* (1983). It was the first time that an analytical wide-range equation was combined with a scaled equation without problems in the transition range; this equation provides a smooth transition from the singular scaled equation to the nonsingular wide-range function. The price however, for realizing this behavior is the great number of 80 fitted coefficients, and more importantly, a rather complex functional structure of the entire equation plus, due to the incorporation of a scaled equation, the necessity of a recursive calculation of internal variables in the scaled part. Due to the use of the original scaled equation of 1983 [Levelt Sengers *et al.* (1983)] the critical point of Hill's equation is slightly different from the critical point of H_2O as agreed by IAPWS (1992).

It should be pointed out that none of these wide-range equations is based on the current International Temperature Scale of 1990 (ITS-90), see Preston-Thomas (1990), as they were all developed before 1990.

Besides the wide-range equations of state mentioned above, there are also special equations for the critical region of H_2O. One of these equations is the revised and extended scaled equation of Levelt-Sengers *et al.* (1983) which is a part of the unified fundamental equation of Hill (1990). The most recent equation of this kind is the crossover equation developed by Kostrowicka Wyczalkowska *et al.* (2000). This

equation has been included in the corresponding comparisons with experimental data of the critical region, see Sec. 7.

1.3. Need for the Development of a New Scientific Formulation and Adoption of the IAPWS-95 Formulation

It becomes apparent from the summary of previous scientific equations of state that they all have several smaller or greater deficiencies, and that a new equation of state for H_2O was needed.

At the IAPWS meeting in Buenos Aires in 1990, it was agreed that a new scientific standard equation should be developed in order to replace IAPS-84. The task group of IAPWS for dealing with this development consisted of Professor J. V. Sengers (USA) as chairman and Professors P. G. Hill (Canada) and W. Wagner (Germany). The new scientific formulation was required to meet the following three main requirements:

(i) based on ITS-90;
(ii) based on an updated data set; and
(iii) improved behavior in the critical region, in metastable regions, of the first and second derivatives in the liquid region at low temperatures and pressures, and when extrapolating to very high pressures and high temperatures.

Taking these requirements into account, new equations of state were developed in two groups, namely in Professor Hill's group at the University of British Columbia in Vancouver (Canada) and in Professor Wagner's group at the Ruhr-Universität Bochum in Bochum (Germany). After having finished these developments, the two candidate equations were comprehensively tested by the IAPWS Task Group ''New Scientific Formulation—Evaluation,'' which was chaired by J. Gallagher (USA). Both equations gave very good results with small advantages and disadvantages for each. In 1995, after careful consideration, IAPWS at its meeting in Paris adopted the equation of state developed by Pruß and Wagner (1995a,1995b) as the new scientific standard under the name ''The IAPWS Formulation 1995 for the Thermodynamic Properties of Ordinary Water Substance for General and Scientific Use,'' which we shall refer to in the following as the IAPWS-95 formulation or IAPWS-95 for short. The final form of the IAPWS release that describes IAPWS-95 in detail was adopted at the IAPWS meeting in Fredericia (Denmark) in 1996 [IAPWS (1996)]; the essential information from this release can be found in Sec. 6. The IAPWS-95 formulation replaces the previous scientific formulation IAPS-84.

1.4. Existence of the New Industrial Formulation IAPWS-IF97

The reader should be informed that in 1997 at the IAPWS meeting in Erlangen (Germany) a new formulation for industrial use called ''IAPWS Industrial Formulation 1997 for the Thermodynamic Properties of Water and Steam'' abbreviated to IAPWS-IF97 was adopted. IAPWS-IF97, which is designed for the special needs of the steam power industry, was developed based on input data calculated from the new scientific formulation IAPWS-95 described in this article. In this way, the industrial standard for the thermodynamic properties of water and steam is coupled to the corresponding scientific standard, the IAPWS-95 formulation. Full information on the industrial standard IAPWS-IF97 can be found in the article by Wagner *et al.* (2000).

1.5. Note on the Values of Temperature Used Throughout this Article

With regard to the numerical values used for the thermodynamic temperature throughout this article the following information is given:

(i) No distinction is made between the thermodynamic temperature T and the temperature T_{90} of the currently valid International Temperature Scale of 1990 (ITS-90), see Preston-Thomas (1990). This is because the ITS-90 is the best approximation of the thermodynamic temperature within the present experimental uncertainties.

(ii) All correlation equations for the thermodynamic properties along the several phase boundaries, the so-called gas equation, and the IAPWS-95 formulation refer to the ITS-90.

(iii) The temperature values of the available experimental data, based on older temperature scales and referred to in this article, were converted to ITS-90. The conversion from the IPTS-68 temperature scale to ITS-90 temperatures was carried out based on conversion equations given by Rusby (1991) for $T<903.15\,\mathrm{K}$ and by Rusby *et al.* (1994) for $903.15\,\mathrm{K}\leqslant T\leqslant 1337.15\,\mathrm{K}$. Data corresponding to the IPTS-48 temperature scale were converted to IPTS-68 according to the procedure given by Bedford and Kirby (1969).

(iv) Values calculated from literature equations that are used in the corresponding figures for comparison purposes, were, if necessary, converted from their original temperature scale to ITS-90 values.

2. Phase Equilibria of Water

Figure 2.1 shows several phase–boundary curves for water in a $p-T$ diagram. In this section information on the following data and equations is given:

(i) The internationally accepted values for the parameters of the triple point and critical point.
(ii) The selected experimental data for the vapor pressure, the saturated liquid density, the saturated vapor density, and the differences of the internal energy on the vapor–liquid phase boundary.
(iii) Correlation equations for the properties vapor pressure, saturation densities, specific enthalpy, specific internal energy, and specific entropy along the vapor–liquid phase boundary.

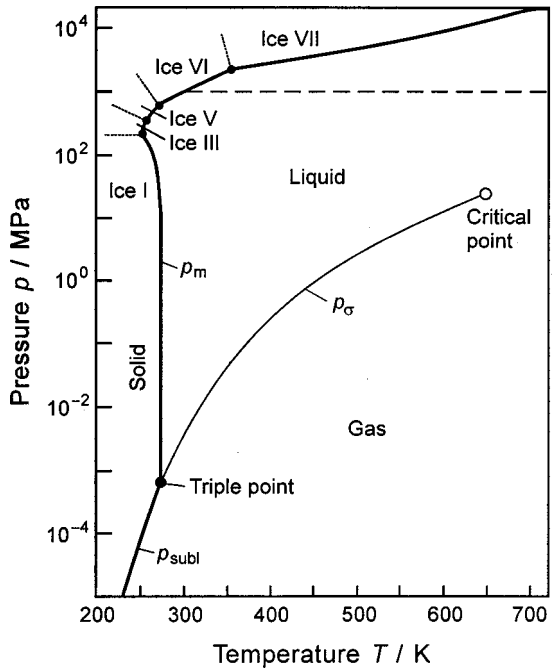

FIG. 2.1. The phase–boundary curves of water in a $p-T$ diagram. The sublimation curve p_{subl} and the several melting curves p_m plotted in bold correspond to the lower limit of the range of validity of IAPWS-95 with regard to temperature. The dashed line corresponds to the range of validity of IAPWS-95 with regard to pressure.

(iv) Correlation equations for the pressure along the melting–pressure curve and along the sublimation–pressure curve.

2.1. The Triple Point

The temperature of the gas–liquid–solid triple point of water corresponds by definition to one of the 17 defined fixed points of the temperature scale ITS-90 [Preston-Thomas (1990)]. Accordingly it is

$$T_t = 273.16 \text{ K}. \tag{2.1a}$$

Based on the internationally accepted measurements of Guildner *et al.* (1976), the triple-point pressure is

$$p_t = (611.657 \pm 0.010) \text{ Pa}. \tag{2.1b}$$

2.2. The Critical Point

Based on the comprehensive evaluation and assessment of the experimental data of the critical region of H_2O, Levelt Sengers *et al.* (1985) determined the most likely values of the critical parameters. Later on, these values were converted to ITS-90 temperatures and are given in the corresponding IAPWS release [IAPWS (1992)] as:

$$T_c = (647.096 \pm \epsilon) \text{ K} \quad \text{with} \quad \epsilon = 0.01, \tag{2.2a}$$

$$p_c = (22.064 \pm 0.27\epsilon \pm 0.005) \text{ MPa}, \tag{2.2b}$$

$$\rho_c = (322 \pm 3) \text{ kg m}^{-3}. \tag{2.2c}$$

2.3. The Vapor–Liquid Phase Boundary

In 1987, Saul and Wagner (1987) published correlation equations for properties of H_2O along the vapor–liquid phase boundary. The equations for the vapor pressure, the saturated liquid and vapor density, and the caloric difference property $\Delta\alpha$ were based on the temperature scale IPTS-68. At a later date, the experimental data on which these equations are based were converted into ITS-90 temperatures. With these converted data the equations were re-established, see Wagner and Pruss (1993); this article of 1993 also contains the IAPWS supplementary release of 1992 on this subject as the Appendix. For reasons of completeness and because these equations were used to develop the IAPWS-95 formulation, these auxiliary equations are given in the next two subsections. Remarks on the usefulness and the consistency of the equations in relation to IAPWS-95 can be found at the end of Sec. 2.3.1.

2.3.1. Experimental Data and Equations for the Vapor Pressure and the Densities of the Saturated Liquid and Vapor

Table 2.1 summarizes certain information on the selected experimental data of the vapor pressure and the densities of the saturated liquid and vapor used to develop the international equations for the saturation properties, Eqs. (2.5)–(2.7). The only vapor–pressure data of Table 2.1 that were not used for the development of the vapor–pressure equation [Wagner and Saul (1986), Saul and Wagner (1987)] are the data of Morita *et al.* (1989), which were published later; they are, however, included in the comparison of the selected data in Fig. 2.2.

The densities of the saturated liquid and the saturated vapor of Osborne *et al.* (1937), (1939) constitute a special case. These densities were not directly measured but were calculated by Wagner and Saul (1986) from the relations

$$\rho' = T \frac{dp_\sigma}{dT} \beta^{-1}, \tag{2.3}$$

$$\rho'' = T \frac{dp_\sigma}{dT} \gamma^{-1}, \tag{2.4}$$

by using Osborne *et al.*'s (1939) experimental values of the two caloric properties β and γ and the derivative dp_σ/dT determined from the vapor–pressure equation given by Wagner and Saul (1986) and Saul and Wagner (1987), see Eq. (2.5a). The international equations for the vapor pressure and the densities of the saturated liquid and vapor [Saul and Wagner (1987)], converted to ITS-90 temperatures by Wagner and Pruss (1993) are as follows:

Vapor–pressure equation and its derivative:

$$\ln\left(\frac{p_\sigma}{p_c}\right) = \frac{T_c}{T}(a_1\vartheta + a_2\vartheta^{1.5} + a_3\vartheta^3 + a_4\vartheta^{3.5} + a_5\vartheta^4 + a_6\vartheta^{7.5}), \tag{2.5}$$

TABLE 2.1. Information on the selected measuring runs for the vapor pressure p_σ, the saturated liquid density ρ', and the saturated vapor density ρ''

Authors	Property	Temperature range/K	Uncertainty ΔT/mK[a]	Uncertainty Δy[b]	Number of data Total	Number of data Selected
Osborne *et al.* (1933)	p_σ	373–647	···	±0.025%	390	382
Rivkin *et al.* (1964[a])	p_σ	646–647	···	±0.01%	18	13
Stimson (1969)	p_σ	298–373	±0.4	±0.002%	7	7
Guildner *et al.* (1976)	p_σ	273.16	···	±0.016%	1	1
Hanafusa *et al.* (1984)	p_σ	643–646	···	±0.01%	8	8
Kell *et al.* (1985)	p_σ	423–623	···	±0.04%	22	22
Morita *et al.* (1989)[c]	p_σ	620–647	±4	±0.02%	26	···[c]
Smith & Keyes (1934)	ρ'	303–593	···	±0.05%	13	9
Osborne *et al.* (1937)	ρ'	603–645	···	±0.5%	65	29
Kell (1975)	ρ'	273–423	···	$\Delta\rho'$[d]	32	32
Kell *et al.* (1985)	ρ'	423–623	···	±0.05%	22	22
Osborne *et al.* (1937)	ρ''	373–645	···	$\Delta\rho''$[e]	214	189
Osborne *et al.* (1939)	ρ''	273–373	···	±0.05%	152	146

[a]When no uncertainty value is given, then this uncertainty is taken into account in the uncertainty in y.
[b]y corresponds to p_σ, ρ', and ρ'', respectively.
[c]These data were only available after the vapor–pressure equation had been developed.
[d]$\Delta\rho' = \pm[2\times10^{-6} + 1\times10^{-7}(T/\mathrm{K}-273)]$ kg m^{-3}.
[e]$\Delta\rho'' = \pm 0.01[5 + 0.125(T/\mathrm{K}-423)]\%$.

$$\frac{\mathrm{d}p_\sigma}{\mathrm{d}T} = -\frac{p_\sigma}{T}\left[\ln\left(\frac{p_\sigma}{p_\mathrm{c}}\right) + a_1 + 1.5a_2\vartheta^{0.5} + 3a_3\vartheta^2 + 3.5a_4\vartheta^{2.5} + 4a_5\vartheta^3 + 7.5a_6\vartheta^{6.5}\right], \qquad (2.5a)$$

with $\vartheta = (1 - T/T_\mathrm{c})$, $T_\mathrm{c} = 647.096$ K, $p_\mathrm{c} = 22.064$ MPa, $a_1 = -7.859\,517\,83$, $a_2 = 1.844\,082\,59$, $a_3 = -11.786\,649\,7$, $a_4 = 22.680\,741\,1$, $a_5 = -15.961\,871\,9$, and $a_6 = 1.801\,225\,02$.

Saturated liquid density equation:

$$\frac{\rho'}{\rho_\mathrm{c}} = 1 + b_1\vartheta^{1/3} + b_2\vartheta^{2/3} + b_3\vartheta^{5/3} + b_4\vartheta^{16/3} + b_5\vartheta^{43/3} + b_6\vartheta^{110/3}, \qquad (2.6)$$

with $b_1 = 1.992\,740\,64$, $b_2 = 1.099\,653\,42$, $b_3 = -0.510\,839\,303$, $b_4 = -1.754\,934\,79$, $b_5 = -45.517\,035\,2$, and $b_6 = -6.746\,944\,50\times10^5$; for the definition of ϑ see Eq. (2.5).

Saturated vapor density equation:

$$\ln\left(\frac{\rho''}{\rho_\mathrm{c}}\right) = c_1\vartheta^{2/6} + c_2\vartheta^{4/6} + c_3\vartheta^{8/6} + c_4\vartheta^{18/6} + c_5\vartheta^{37/6} + c_6\vartheta^{71/6}, \qquad (2.7)$$

with $c_1 = -2.031\,502\,40$, $c_2 = -2.683\,029\,40$, $c_3 = -5.386\,264\,92$, $c_4 = -17.299\,160\,5$, $c_5 = -44.758\,658\,1$, and $c_6 = -63.920\,106\,3$; for the definition of ϑ see Eq. (2.5).

Figure 2.2 illustrates that Eqs. (2.5)–(2.7) represent the selected experimental data of p_σ, ρ', and ρ'' very well within their experimental uncertainty listed in Table 2.1. Values for

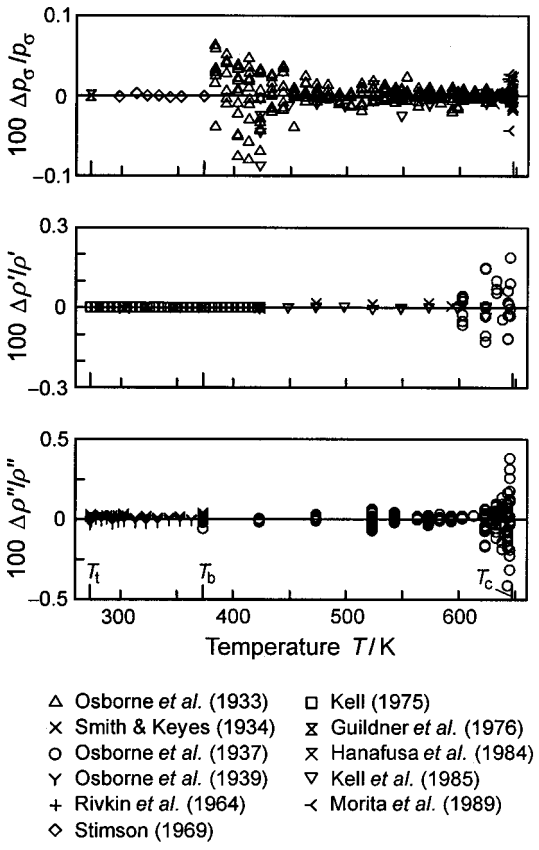

FIG. 2.2. Percentage deviations of the experimental data of the vapor pressure p_σ, the saturated liquid density ρ', and the saturated vapor density ρ'' from the values calculated from the corresponding Eqs. (2.5), (2.6), or (2.7): $100\Delta p_\sigma/p_\sigma = 100(p_{\sigma,\mathrm{exp}} - p_{\sigma,\mathrm{calc}})/p_{\sigma,\mathrm{exp}}$, $100\Delta\rho'/\rho' = 100(\rho'_{\mathrm{exp}} - \rho'_{\mathrm{calc}})/\rho'_{\mathrm{exp}}$, $100\Delta\rho''/\rho'' = 100(\rho''_{\mathrm{exp}} - \rho''_{\mathrm{calc}})/\rho''_{\mathrm{exp}}$.

TABLE 2.2. Information on the selected data for the caloric difference quantity $\Delta\alpha$

Authors	Temperature range/K	Uncertainty $\Delta(\Delta\alpha)$	Number of data	
			Total	Selected
Osborne *et al.* (1937)	373–647	±0.3%	142	142
Osborne *et al.* (1939)	273–373	±0.05%	256	256

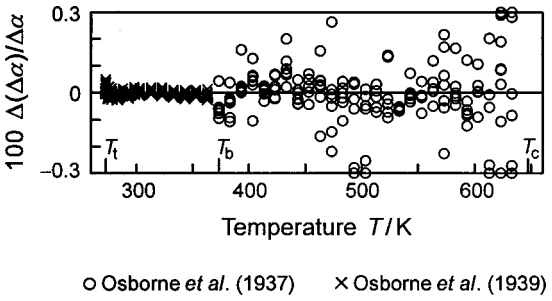

FIG. 2.3. Percentage deviations $100\Delta(\Delta\alpha)/\Delta\alpha = 100(\Delta\alpha_{exp} - \Delta\alpha_{calc})/\Delta\alpha_{exp}$ between experimental data of the caloric difference quantity $\Delta\alpha$ and values calculated from Eq. (2.9).

computer-program verification of Eqs. (2.5)–(2.7) can be found in the article of Wagner and Pruss (1993).

It should be pointed out that Eqs. (2.5)–(2.7) are only auxiliary equations for calculating properties along the vapor–liquid phase boundary. Although the differences between the results from these equations and the corresponding results from the IAPWS-95 formulation, Eq. (6.4), are extremely small, these equations are not thermodynamically consistent with IAPWS-95. Nevertheless, the application of these auxiliary equations might be useful for simple calculations of these saturation properties or for the determination of starting values when iteratively calculating the saturation properties from IAPWS-95 according to the phase-equilibrium condition.

2.3.2. Experimental Data for the Caloric Difference Property $\Delta\alpha$ and Equations for the Enthalpy and Entropy of the Saturated Liquid and Saturated Vapor

Up to now it has not been possible to measure directly values of the enthalpy and internal energy along the vapor–liquid phase boundary of H_2O. Thus, for a system consisting of a gas and liquid phase, [in addition to the quantities β and γ, see Eqs. (2.3) and (2.4)], Osborne measured the caloric difference quantity $\Delta\alpha$, which basically corresponds to the difference of the internal energy between two temperatures in the two-phase region. For this quantity the following relation exists:

$$\Delta\alpha = h' - \Delta^{v}h\,\frac{v'}{v''-v'}, \tag{2.8}$$

where $\Delta\alpha$ depends only on temperature. Table 2.2 summarizes the information on these selected measuring runs of the caloric difference quantity $\Delta\alpha$.

A correlation equation for $\alpha = \alpha(T)$ allows the calculation of the enthalpy, internal energy, and entropy along the phase boundary, for details see Saul and Wagner (1987). On the basis of this article, Wagner and Pruss (1993) made the coefficients of the equation for α and its integrated form ψ consistent with the ITS-90 temperature scale. The equations and the converted coefficients read:

$$\frac{\alpha}{\alpha_0} = d_\alpha + d_1\theta^{-19} + d_2\theta + d_3\theta^{4.5} + d_4\theta^5 + d_5\theta^{54.5}, \tag{2.9}$$

$$\frac{\psi}{\psi_0} = d_\psi + \frac{19}{20}d_1\theta^{-20} + d_2\ln\theta + \frac{9}{7}d_3\theta^{3.5} + \frac{5}{4}d_4\theta^4 + \frac{109}{107}d_5\theta^{53.5}, \tag{2.9a}$$

where $\alpha_0 = 1\ \mathrm{kJ\,kg^{-1}}$, $\psi_0 = \alpha_0/T_c$, $\theta = T/T_c$, $T_c = 647.096$ K, and the coefficients are $d_\alpha = -1135.905\,627\,715$, $d_\psi = 2319.5246$, $d_1 = -5.651\,349\,98\times10^{-8}$, $d_2 = 2690.666\,31$, $d_3 = 127.287\,297$, $d_4 = -135.003\,439$, and $d_5 = 0.981\,825\,814$. The values of the coefficients d_α and d_ψ were determined according to the international agreement so that the zero points of the specific internal energy and the specific entropy are met for the saturated liquid at the triple point [namely $u'_t = 0$, $s'_t = 0$, see also Eq. (6.7)]. Figure 2.3 shows the comparison between the experimental $\Delta\alpha$ values and the values calculated from Eq. (2.9). (In all such deviation plots, points shown at the top or bottom edge have deviations larger than the scale of the plot.)

The equations for calculating the specific values of the enthalpy h, the internal energy u, and the entropy s for the saturated liquid and the saturated vapor are summarized as follows:

Specific enthalpy

$$\frac{h'}{\mathrm{kJ\,kg^{-1}}} = \frac{\alpha}{\alpha_0} + 10^3\frac{T/\mathrm{K}}{\rho'/(\mathrm{kg\,m^{-3}})}\left(\frac{\mathrm{d}p_\sigma}{\mathrm{d}T}\right)\Bigg/\left(\frac{\mathrm{MPa}}{\mathrm{K}}\right), \tag{2.10}$$

$$\frac{h''}{\mathrm{kJ\,kg^{-1}}} = \frac{\alpha}{\alpha_0} + 10^3\frac{T/\mathrm{K}}{\rho''/(\mathrm{kg\,m^{-3}})}\left(\frac{\mathrm{d}p_\sigma}{\mathrm{d}T}\right)\Bigg/\left(\frac{\mathrm{MPa}}{\mathrm{K}}\right). \tag{2.11}$$

Specific internal energy

$$\frac{u'}{\mathrm{kJ\,kg^{-1}}} = \frac{\alpha}{\alpha_0} + 10^3\frac{\dfrac{T}{\mathrm{K}}\left(\dfrac{\mathrm{d}p_\sigma}{\mathrm{d}T}\right)\Big/\left(\dfrac{\mathrm{MPa}}{\mathrm{K}}\right) - \dfrac{p_\sigma}{\mathrm{MPa}}}{\rho'/(\mathrm{kg\,m^{-3}})}, \tag{2.12}$$

$$\frac{u''}{\mathrm{kJ\,kg^{-1}}} = \frac{\alpha}{\alpha_0} + 10^3\frac{\dfrac{T}{\mathrm{K}}\left(\dfrac{\mathrm{d}p_\sigma}{\mathrm{d}T}\right)\Big/\left(\dfrac{\mathrm{MPa}}{\mathrm{K}}\right) - \dfrac{p_\sigma}{\mathrm{MPa}}}{\rho''/(\mathrm{kg\,m^{-3}})}. \tag{2.13}$$

Specific entropy

$$\frac{s'}{\mathrm{kJ\,kg^{-1}\,K^{-1}}} = \frac{\psi}{\mathrm{kJ\,kg^{-1}\,K^{-1}}} + 10^3 \frac{\left(\frac{\mathrm{d}p_\sigma}{\mathrm{d}T}\right) \Big/ \left(\frac{\mathrm{MPa}}{\mathrm{K}}\right)}{\rho'/(\mathrm{kg\,m^{-3}})}, \tag{2.14}$$

$$\frac{s''}{\mathrm{kJ\,kg^{-1}\,K^{-1}}} = \frac{\psi}{\mathrm{kJ\,kg^{-1}\,K^{-1}}} + 10^3 \frac{\left(\frac{\mathrm{d}p_\sigma}{\mathrm{d}T}\right) \Big/ \left(\frac{\mathrm{MPa}}{\mathrm{K}}\right)}{\rho''/(\mathrm{kg\,m^{-3}})}. \tag{2.15}$$

In order to evaluate Eqs. (2.10)–(2.15) the quantities α/α_0, ψ, ρ', ρ'', p_σ, and $\mathrm{d}p_\sigma/\mathrm{d}T$ are calculated from Eqs. (2.9), (2.9a), (2.6), (2.7), (2.5), and (2.5a). Values for computer-program verification of these equations are given by Wagner and Pruss (1993).

For remarks regarding the usefulness of Eqs. (2.10)–(2.15) and their consistency related to IAPWS-95, see the end of Sec. 2.3.1.

2.4. The Solid–Liquid and Solid–Vapor Phase Boundaries

Depending on the pressure and temperature range, solid water forms different structures. Five of the known ice forms are bordered by the liquid phase of H_2O. Although the intersections of two melting–pressure curves are also called triple points (two solid phases are in equilibrium with the liquid phase), in this article the term ''triple point'' is only used for the solid–liquid–vapor triple point, see Sec. 2.1. Figure 2.1 illustrates the plot of the phase–boundary curves in a $p-T$ diagram.

Correlation equations for the melting–pressure curves (solid–liquid phase boundary) and the sublimation–pressure curve (solid–vapor phase boundary) are described by Wagner *et al.* (1994) and documented in the corresponding IAPWS release [IAPWS (1993)]; this release is appended to the above mentioned article. Although these equations were not directly used for the development of the IAPWS-95 formulation, the equations are presented here because they mark the boundaries between the fluid phase (for which IAPWS-95 is valid) and the solid phase.

2.4.1. The Melting–Pressure Equations

The melting–pressure equations adopted by IAPWS [see Wagner *et al.* (1994)] are as follows:

Melting–pressure equation for ice I (temperature range from 273.16 to 251.165 K):

$$\frac{p_{\mathrm{m,ice\ I}}}{p_\mathrm{n}} = 1 - 0.626\times10^6\cdot(1-\theta^{-3}) + 0.197\,135\times10^6(1-\theta^{21.2}), \tag{2.16}$$

with $\theta = T/T_\mathrm{n}$, $T_\mathrm{n} = 273.16\,\mathrm{K}$, and $p_\mathrm{n} = 0.000\,611\,657$ MPa.

Melting–pressure equation for ice III (temperature range from 251.165 to 256.164 K):

$$\frac{p_{\mathrm{m,ice\ III}}}{p_\mathrm{n}} = 1 - 0.295\,252(1-\theta^{60}), \tag{2.17}$$

with $\theta = T/T_\mathrm{n}$, $T_\mathrm{n} = 251.165\,\mathrm{K}$, and $p_\mathrm{n} = 209.9\,\mathrm{MPa}$.

Melting–pressure equation for ice V (temperature range from 256.164 to 273.31 K):

$$\frac{p_{\mathrm{m,ice\ V}}}{p_\mathrm{n}} = 1 - 1.187\,21(1-\theta^{8}), \tag{2.18}$$

with $\theta = T/T_\mathrm{n}$, $T_\mathrm{n} = 256.164\,\mathrm{K}$, and $p_\mathrm{n} = 350.1\,\mathrm{MPa}$.

Melting–pressure equation for ice VI (temperature range from 273.31 to 355 K):

$$\frac{p_{\mathrm{m,ice\ VI}}}{p_\mathrm{n}} = 1 - 1.074\,76(1-\theta^{4.6}), \tag{2.19}$$

with $\theta = T/T_\mathrm{n}$, $T_\mathrm{n} = 273.31\,\mathrm{K}$, and $p_\mathrm{n} = 632.4\,\mathrm{MPa}$.

Melting–pressure equation for ice VII (temperature range from 355 to 715 K):

$$\ln\left(\frac{p_{\mathrm{m,ice\ VII}}}{p_\mathrm{n}}\right) = 1.736\,83(1-\theta^{-1}) - 0.054\,4606(1-\theta^{5}) + 0.806\,106\times10^{-7}(1-\theta^{22}), \tag{2.20}$$

with $\theta = T/T_\mathrm{n}$, $T_\mathrm{n} = 355\,\mathrm{K}$, and $p_\mathrm{n} = 2216\,\mathrm{MPa}$.

Further details regarding Eqs. (2.16)–(2.20), including values for computer-program verification, are given by Wagner *et al.* (1994).

2.4.2. The Sublimation–Pressure Equation

According to Wagner *et al.* (1994), the sublimation pressure is given by:

$$\ln\left(\frac{p_\mathrm{subl}}{p_\mathrm{n}}\right) = -13.928\,169(1-\theta^{-1.5}) + 34.707\,823\,8(1-\theta^{-1.25}), \tag{2.21}$$

with $\theta = T/T_\mathrm{n}$, $T_\mathrm{n} = 273.16\,\mathrm{K}$, and $p_\mathrm{n} = 0.000\,611\,657\,\mathrm{MPa}$. For further details and values for computer-program verification see Wagner *et al.* (1994).

3. The Gas Equation

Reference equations of state for methane [Setzmann and Wagner (1991), Wagner and de Reuck (1996)] and carbon dioxide [Span and Wagner (1996)] that are valid for the entire fluid region have been successfully established by using not only the so-called nonlinear experimental data but also corresponding (precorrelated) linearized data at least for parts of the entire fluid region, for details see Sec. 5.3.2. In particular, the gas region has offered possibilities for such a procedure. Thus, a special gas equation for water was developed with the general aim of providing so-called synthetic data for the development of IAPWS-95. For the development of IAPWS-95 and for calculating values in the metastable

TABLE 3.1. Coefficients and exponents of the residual part ϕ^r of the dimensionless Helmholtz free energy, Eq. (3.3)

i	d_i	t_i	n_i
1	1	0.25	0.474 865 925 9
2	1	1.25	$-0.112\,437\,055\,3\times10^{1}$
3	1	3.5	−0.811 862 740 1
4	1	12	$-0.621\,301\,850\,1\times10^{-3}$
5	2	1.5	0.192 443 099 3
6	2	13.5	$-0.832\,286\,766\,2\times10^{-1}$
7	4	8.75	$0.139\,105\,223\,0\times10^{1}$

steam region, the establishment of this gas equation is of primary importance and is therefore described in this section.

3.1. Density Range and Input Data

For ''normal'' substances, a simple virial equation,

$$\frac{p}{\rho RT}=1+B(T)\cdot\rho+C(T)\cdot\rho^2+D(T)\cdot\rho^3+E(T)\cdot\rho^4+\ldots, \tag{3.1}$$

truncated after the term with the third virial coefficient $C(T)$ is able to cover the fluid region up to densities of $0.5\,\rho_c$ within the experimental uncertainty of the data. For the ''difficult'' substance water, such a truncated virial equation can only cover the gas region very accurately for densities up to about $0.1\,\rho_c$. It was, however, our aim that the gas equation should cover a region up to densities of $\rho=55\,\mathrm{kg\,m^{-3}}\approx0.17\,\rho_c$. In this region, the gas equation should represent all thermodynamic properties with the best possible accuracy.

In order to achieve this aim, the equation was developed by using selected experimental data of the thermal properties $(p\rho T)$ and the properties speed of sound w, specific isobaric heat capacity c_p, Joule–Thomson coefficient μ, and isothermal throttling coefficient δ_T. Due to the density range considered here, only data with $\rho\leqslant55\,\mathrm{kg\,m^{-3}}$ were used. Information on all data selected for the development of the IAPWS-95 formulation is summarized in Sec. 4; for the data considered in connection with the gas equation see Secs. 4.2, 4.3, 4.5, 4.7, and 4.8. Figures 4.1, 4.5, 4.8, and 4.9, which show the data distribution in corresponding $p-T$ diagrams, contain the isochoric line $\rho=55\,\mathrm{kg\,m^{-3}}$ to illustrate which part of the gas region and which data sets were involved. In total, 604 $p\rho T$ data, 112 w data, 90 c_p data, 234 μ data, and 180 δ_T data were used to develop the gas equation, Eq. (3.2). These data had to be represented by the gas equation to within their experimental uncertainty.

3.2. Details of the Gas Equation

Like the IAPWS-95 formulation, Eq. (6.4), the gas equation is a fundamental equation for the specific Helmholtz free energy f. This equation is expressed in dimensionless form, $\phi=f/(RT)$, and is separated into two parts, an ideal-gas part ϕ° and a residual part ϕ^r, so that:

$$\frac{f(\rho,T)}{RT}=\phi(\delta,\tau)=\phi^\circ(\delta,\tau)+\phi^r(\delta,\tau), \tag{3.2}$$

where $\delta=\rho/\rho_c$ and $\tau=T_c/T$ with $\rho_c=322\,\mathrm{kg\,m^{-3}}$, $T_c=647.096\,\mathrm{K}$, and $R=0.461\,518\,05\,\mathrm{kJ\,kg^{-1}\,K^{-1}}$. The ideal-gas part ϕ° of Eq. (3.2) is identical to the ideal-gas part of IAPWS-95, Eq. (6.5).

The form of the residual part ϕ^r of the dimensionless Helmholtz free energy is:

$$\phi^r=\sum_{i=1}^{7} n_i\delta^{d_i}\tau^{t_i}, \tag{3.3}$$

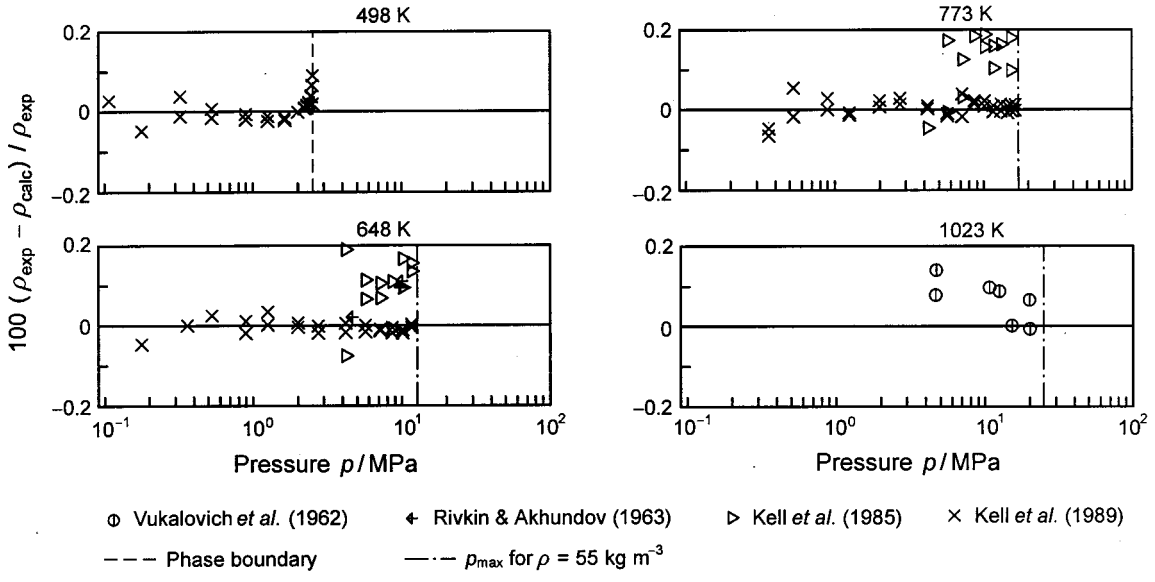

FIG. 3.1. Percentage density deviations between experimental $p\rho T$ data and values calculated from the gas equation, Eq. (3.2).

where $\delta=\rho/\rho_c$ and $\tau=T_c/T$ with $\rho_c=322\,\mathrm{kg\,m^{-3}}$ and $T_c=647.096\,\mathrm{K}$. The coefficients and exponents of Eq. (3.3) are listed in Table 3.1. The values of the exponents d_i in Eq. (3.3) are integers up to four; this corresponds to extending Eq. (3.1) to the fifth virial coefficient $E(T)$. This was necessary in order to represent the accurate $p\rho T$ data [Kell *et al.* (1985), (1989), see Fig. 4.1] and the speed-of-sound data [Novikov and Avdonin (1968), see Fig. 4.5].

All thermodynamic properties can be derived from Eq. (3.2) by using the appropriate combinations of the ideal-gas part ϕ°, Eq. (6.5), and the residual part ϕ^r, Eq. (3.3), of the dimensionless Helmholtz free energy and their derivatives. Relations between thermodynamic properties and ϕ° and ϕ^r and their derivatives are summarized in Table 6.3. All required derivatives of the ideal-gas part of the Helmholtz free energy, Eq. (6.5), are explicitly given in Table 6.4. The required derivatives of the residual part of the gas equation, Eq. (3.3), are identical with the first sum (first seven polynomial terms) given in Table 6.5.

Equation (3.2) is valid in the gas region of H_2O for temperatures from 273 to 1273 K and densities up to $55\,\mathrm{kg\,m^{-3}}$. In this region, Eq. (3.2) represents the experimental data to within their uncertainties, for further details see Sec. 3.3.

Proceeding from a general functional form for $\phi^r(\delta,\tau)$, called a bank of terms, and using the structure-optimization method of Setzmann and Wagner (1989), the development of an equation for the residual part ϕ^r, Eq. (3.3), of the gas equation, Eq. (3.2), occurred in a similar way to the residual part of the IAPWS-95 formulation, which is described in detail in Sec. 5. In this entire process, Eq. (3.2) was fitted to the $p\rho T$ data (so-called linear properties) and to the experimental data of the so-called nonlinear properties w, c_p, μ, and δ_T; for details see Pruß and Wagner (1995b).

3.3. Comparison of the Gas Equation with Experimental Data

For the density range $0\leqslant\rho\leqslant55\,\mathrm{kg\,m^{-3}}$ where the gas equation is valid, Figs. 3.1–3.4 show deviations between the experimental $p\rho T$, w, c_p, and μ data in this low density region and values calculated from Eq. (3.2).

Figure 3.1 shows a comparison between the experimental $p\rho T$ data and the densities calculated from Eq. (3.2) for four representative isotherms. It can be seen that Eq. (3.2) represents these data to within their scatter. Only the data of Vukalovich *et al.* (1961), (1962) show somewhat systematic deviations from the calculated densities. Based on our experience with the development of the IAPWS-95 formulation in this high-temperature range (see Sec. 7.2.1.4), we believe that these deviations are due to the data; nevertheless, the deviations remain well within the given experimental uncertainty of the data, see Table 4.4.

For three representative isotherms, Fig. 3.2 illustrates that the speed-of-sound data of Novikov and Avdonin (1968) are represented very well to within their experimental uncertainty given in Table 4.5.

For the specific isobaric heat capacity, the comparisons

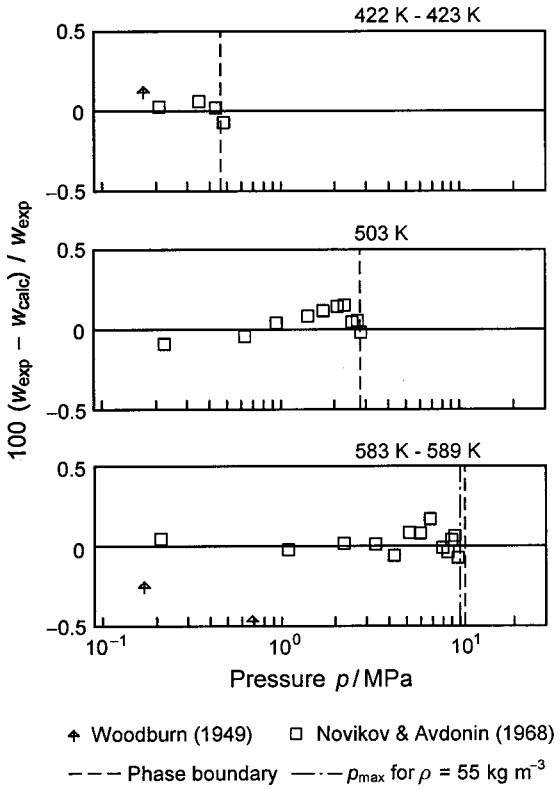

FIG. 3.2. Percentage deviations between experimental data of the speed of sound w and values calculated from the gas equation, Eq. (3.2).

between the experimental data and the corresponding values calculated from Eq. (3.2) are summarized in Fig. 3.3 for four isobars. Although Eq. (3.2) represents the c_p data to within their experimental uncertainty (see Table 4.8), there are clearly systematic deviations between the experimental and calculated values, for example, see the isobars $p=5.88\,\mathrm{MPa}$ and $p=9.8\,\mathrm{MPa}$. These systematic trends are based on the experimental data and not on a weakness of the gas equation, Eq. (3.2), regarding this property. For example, the $p\rho T$ data and the speeds of sound in this region are represented very well by Eq. (3.2). Moreover, the deviation of the c_p data from those values calculated with the IAPWS-95 formulation shows very similar trends, see Sec. 7.2.5.

Figure 3.4 shows that Eq. (3.2) represents the experimental data of the Joule–Thomson coefficient μ to within their experimental uncertainty given in Table 4.9. The deviation diagrams for the data of the isothermal throttling coefficient δ_T look very similar to the diagrams for μ in Fig. 3.4; thus the δ_T comparisons are not explicitly given here.

4. The Selected Experimental Data and Other Data Used to Develop IAPWS-95 and Further Experimental Data for Comparison

As seen by the quantity and quality of the experimental data of the several thermodynamic properties, water is one of

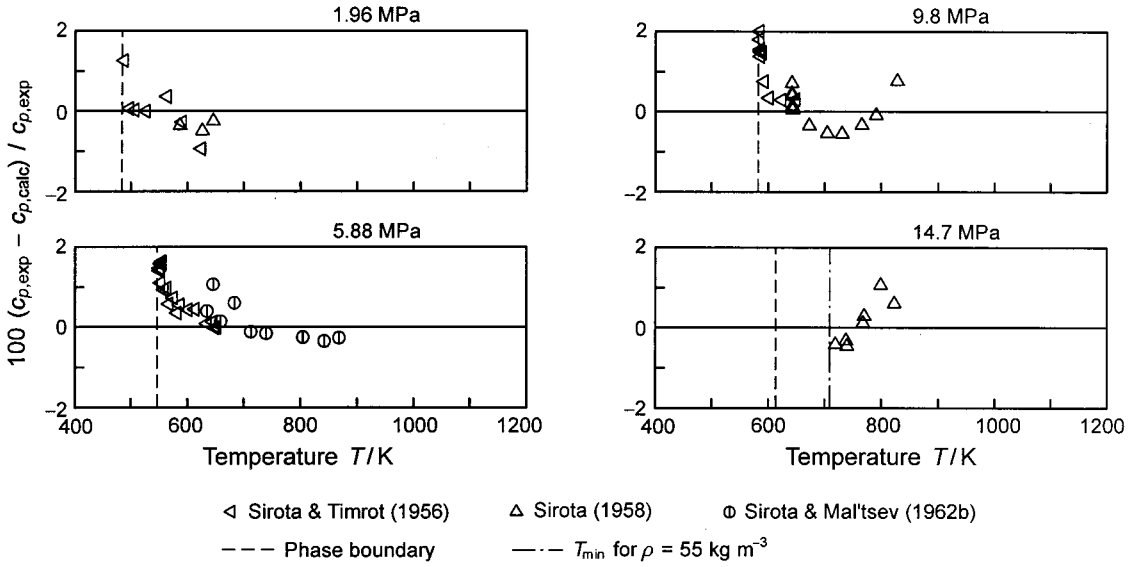

FIG. 3.3. Percentage deviations between experimental data of the isobaric heat capacity c_p and values calculated from the gas equation, Eq. (3.2).

the best experimentally investigated fluids. As a basis for the development of the new equation of state, a comprehensive and consistent data set had to be assembled from a total of about 20 000 experimental data.

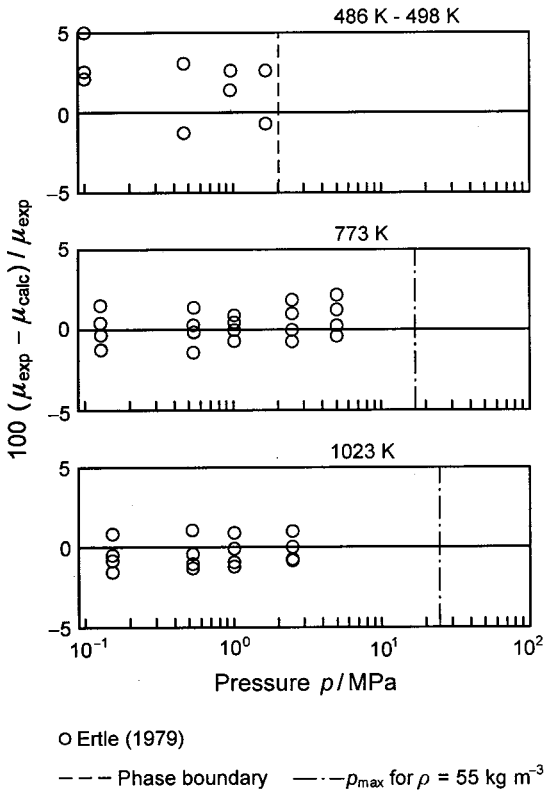

FIG. 3.4. Percentage deviations between experimental data of the Joule-Thomson coefficient μ and values calculated from the gas equation, Eq. (3.2).

In our comprehensive study to establish such a selected data set, we took into account all information given in several articles. The article of Sato *et al.* (1988), which describes the basis of the IAPWS Skeleton Tables of 1985 (IST-85), represents a comprehensive investigation regarding the $p\rho T$ data of the single-phase region; the IST-85 Skeleton Tables converted to ITS-90 temperatures are given in the corresponding revised IAPWS release [IAPWS (1994)]. Moreover, for our own assessment we considered the analyses of the data used to establish the equations of state of Saul and Wagner (1989) and of Hill (1990). In addition to this, there is also the data collection of Sato *et al.* (1991) that was initiated by IAPWS and forms the most comprehensive data collection presently available, consisting of more than 16 000 experimental data for several thermodynamic properties of H_2O. We examined this data set and the data judged to be of high quality were incorporated into our selected data set.

It should be clearly pointed out that we critically reexamined the data used by Saul and Wagner (1989) and by Hill (1990) for their equations of state. All data were again checked with regard to their internal consistency and their basic applicability for the development of an equation of state to form the new scientific standard. These selected data sets took into account experimental data which were available by the middle of 1994.

The experimental data published between May 1991 [the time up to which Sato *et al.* (1991) included data for their collection] and the middle of 1994 (the time at which we took into account data for the development of IAPWS-95) did not contain significant new experimental information; for a comprehensive view of the experimental data of H_2O, please refer to the study of Sato *et al.* (1991). Thus, in this article the information on experimental data is limited to those data used for the development of the IAPWS-95 for-

TABLE 4.1. Information on the selected values of the thermal saturation properties used to develop the IAPWS-95 formulation

Property	Number of data	Temperature range	Step size
		Data for linear fitting	
$p_\sigma\rho'\rho''T$ data from Eqs. (2.5) to (2.7)	218	273.16 K$<T\leqslant$641 K	ΔT=2 K
		641 K$<T\leqslant$646 K	ΔT=0.5 K
		646 K$<T\leqslant$646.946 K	ΔT=0.1 K
		646.946 K$<T\leqslant$647.096 K	ΔT=0.01 K
		Data for nonlinear fitting	
$p_\sigma(T)$ from Eq. (2.5)	109	273.16 K$<T\leqslant$647.096 K	every other point[a]
$\rho'(T)$ from Eq. (2.6)	109	273.16 K$<T\leqslant$647.096 K	every other point[a]
$\rho''(T)$ from Eq. (2.7)	35	273.16 K$<T\leqslant$640 K	every 10th point[a]
		640 K$<T\leqslant$647.096 K	every other point[a]

[a]From the total values used in the linear fitting.

mulation and to comparisons with data published between the middle of 1994 and the middle of 2001.

This section presents not only information on the experimental data (Secs. 4.2–4.9) used to develop IAPWS-95, but also presents information on calculated values (Secs. 4.1, 4.10, and 4.11) used as additional input data for the IAPWS-95 formulation.

4.1. Vapor–Liquid Phase Boundary

In the course of developing the IAPWS-95 formulation, the new equation of state was fitted to values defining the vapor–liquid phase boundary. These values are thermal and caloric properties calculated from the corresponding auxiliary equations summarized in Sec. 2. Since these auxiliary equations had resulted from a statistically founded fitting process to experimental data and since the step size of the calculated points is given, the corresponding input values for IAPWS-95 can be clearly identified.

4.1.1. Thermal Properties in the Saturation State

All thermal properties on the vapor–liquid phase boundary, i.e., $p_\sigma\rho'\rho''T$ data, which were used to develop the IAPWS-95 formulation, were calculated from the corresponding auxiliary equations given in Sec. 2.3.1 for preselected values of temperature. The exact data set is defined by Table 4.1. There, it can be seen that in actual fact two data sets distributed along the phase boundary were used. The $p_\sigma\rho'\rho''T$ data were used in the linear fitting of IAPWS-95 to $p\rho T$ data points at saturation and to the phase-equilibrium condition. The data set containing separate $p_\sigma(T)$, $\rho'(T)$, and $\rho''(T)$ data were used to fit IAPWS-95 nonlinearly to these single $p_\sigma-T$, $\rho'-T$, and $\rho''-T$ values, for further details see Sec. 5.5.2.

4.1.2. Caloric Properties in the Saturation State

The difference property $\Delta\alpha$ (see Sec. 2.3.2) is the only caloric property whose measurements cover the entire temperature range from the triple point to the critical point with high accuracy, see Table 2.2 and Fig. 2.3. The enthalpies h' and h'' of the saturated liquid and vapor, respectively, are directly based on the α values from Eq. (2.9), which represents the experimental $\Delta\alpha$ data. Since the previous scientific standard IAPS-84 could only represent the h' values of the IST-85 Skeleton Tables [IAPWS (1994)] with systematic deviations that are partly outside the IST-85 tolerances, it was desired that the IAPWS-95 formulation behaves clearly better in this respect. Thus, it was decided to incorporate values of one of the key quantities for a good representation of α, namely enthalpies or internal energies, into the selected data set. Since h is distinguishable from u by the product pv, which consists of purely thermal properties, the internal energy u is the decisive caloric quantity in the saturation state and its inclusion in the selected data set is a precondition for a good representation of the α values by IAPWS-95. Besides $(u_2'-u_1')$ values, specific internal energies of vaporization, $(u''-u')$, were included in the selected data set for developing IAPWS-95. Table 4.2 gives information on the design of these data sets, including the data distribution on the vapor–liquid phase boundary. For given values of temperature, the u' and u'' values were calculated from Eqs. (2.12)

TABLE 4.2. Information on the selected values for the specific internal energy on the vapor–liquid phase boundary

Property	Number of data	Temperature range	Step size
$(u_2'-u_1')$, ρ_2', ρ_1'', T_1, T_2	74	273.16 K$<T_1\leqslant$638 K (T_2-T_1)=5 K	ΔT_1=5 K
$(u''-u')$, ρ'', ρ', T	75	273.16 K$<T_1\leqslant$638 K	ΔT=5 K

TABLE 4.3. Information on the selected data for the caloric properties speed of sound w and specific isobaric heat capacity c_p of the saturated liquid and vapor

Authors	Property	Temperature range/K	Uncertainty Δy[a]	Number of data	
				Total	Selected
Novikov & Avdonin (1968)	w''	273–583	±1%	51	50
Chavez *et al.* (1985)	w'	273–372	±0.05%	108	108
Sirota (1963)	c_p'	273–628	±0.15%	44	36
Sirota (1963)	c_p''	273–628	±2%	44	36

[a]y corresponds to either w'', w', c_p', or c_p''.

and (2.13) and the corresponding ρ' and ρ'' values were determined from Eqs. (2.6) and (2.7), respectively.

Experimental data for other caloric properties on the vapor–liquid phase boundary of H_2O are rather limited regarding their number and quality. Information on the best data sets is given in Table 4.3; these data were used to develop IAPWS-95. There are also experimental data of the isochoric heat capacity at saturation (saturated liquid and saturated vapor from both the single-phase and two-phase region), which were measured by Kerimov (1964), Amirkhanov *et al.* (1969), and Abdulagatov *et al.* (1998). Unfortunately, however, these data sets from the Dagestan Scientific Center of the Russian Academy of Sciences are not very consistent with each other (see the discussion in Sec. 7.2.4 on the c_v data in the single-phase region). Therefore, these data were not used to develop IAPWS-95, but a comparison with c_v' data is carried out in Fig. 7.6.

4.2. Single-Phase Region

The International Skeleton Tables of 1985 [(IST-85), see Sato *et al.* (1988)] in its revision for the ITS-90 temperature scale [IAPWS (1994)] contain a comprehensive set of $p\rho T$ and enthalpy values. These values were chosen using measurements in combination with several equations of state of that time. Since these values are not direct measurements and

TABLE 4.4. Information on the selected $p\rho T$ data

Authors	Temperature range T/K	Pressure range p/MPa	Uncertainty			Number of data	
			ΔT/mK[a]	Δp[a]	$\Delta\rho$	Total	Selected
Tammann & Jellinghaus (1928)	259–273	49–147	···	···	±0.15%	257	28
Bridgman (1935)	253–268	98–490	···	···	±0.2%	129	22
Bridgman (1942)	348–448	980–3585	···	···	±0.5%	17	16
Vukalovich *et al.* (1961)	823–923	4.7–118	···	···	±0.2%	175	95
Vukalovich *et al.* (1962)	1022–1174	4.6–118	···	···	±0.25%	148	81
Rivkin & Akhundov (1962)	643–677	4.9–37	±15	±0.01%	±0.05%	298	162
Rivkin & Akhundov (1963)	647–723	4.7–59	±10	±0.01%	±0.05%	190	124
Rivkin & Troyanovskaya (1964)	643–653	9–27	±10	±0.01%	±0.05%	316	82
Rivkin *et al.* (1966)	646–648	14.6–23	±5	±0.01%	±0.04%	107	74
Grindley & Lind (1971)	298–423	100–800	±20	···	±0.02%	560	112
Kell (1975)	236–268	0.101 325	···	±0.01%	±0.05%	120	21
Kell & Whalley (1975)	273–423	0.5–103	±1	±0.01%	$\Delta\rho$[b]	596	574
Kell *et al.* (1978)	448–623	1.3–103	±1	±0.01%	$\Delta\rho$[c]	196	145
Hilbert *et al.* (1981)	293–873	10–400	±5	±0.01%	±0.2%	530	396
Hanafusa *et al.* (1984)	643–673	19.7–38.6	±5	±0.003 MPa	±0.04%	123	93
Kell *et al.* (1985)	648–773	21–103	±1	±0.01%	$\Delta\rho$[d]	587	131
Kell *et al.* (1989)	473–773	0.1–36	±2	±0.01%	±0.006 kg m^{-3}	630	509
Morita *et al.* (1989)	638–652	18.5–38	±4	±0.02%	±0.04%	93	90
Takenaka & Masui (1990)	273–358	0.101 325	···	···	±1 ppm	79	18[e,f]
Patterson & Morris (1994)	274–313	0.101 325	···	···	±(0.6–1.4) ppm	13[f]	...[g]
Masui *et al.* (1995)	273–358	0.101 325	···	···	±(0.9–1.3) ppm	2[f,h]	...[g]
Tanaka *et al.* (2001)	273–313	0.101 325	···	···	±(0.84–0.87) ppm	41	...[g]

[a]If no uncertainty values are given, then these uncertainties are taken into account in the uncertainty in ρ.
[b]$\Delta\rho = \pm(6 + 0.05\cdot(T/\mathrm{K} - 273\ \mathrm{K}) + p/\mathrm{MPa}) \times 10^{-4}$.
[c]$\Delta\rho = \pm(7 + 0.1\ p/\mathrm{MPa}) \times 10^{-5}\rho + 0.04\ \mathrm{kg\ m^{-3}}$; $T \geqslant 548$ K: $\Delta\rho = \pm 0.1\ \mathrm{kg\ m^{-3}}$.
[d]$\Delta\rho = \pm(7 + 0.1\ p/\mathrm{MPa}) \times 10^{-5}\rho + 0.04\ \mathrm{kg\ m^{-3}}$.
[e]Calculated from their $\rho(T)/\rho_{\max}$ equation, see text.
[f]The values correspond to VSMOW.
[g]These data were only available after the development of IAPWS-95 had been finished.
[h]In addition, a $\rho(T)$ equation is given valid for temperatures from 273.15 to 358.15 K.

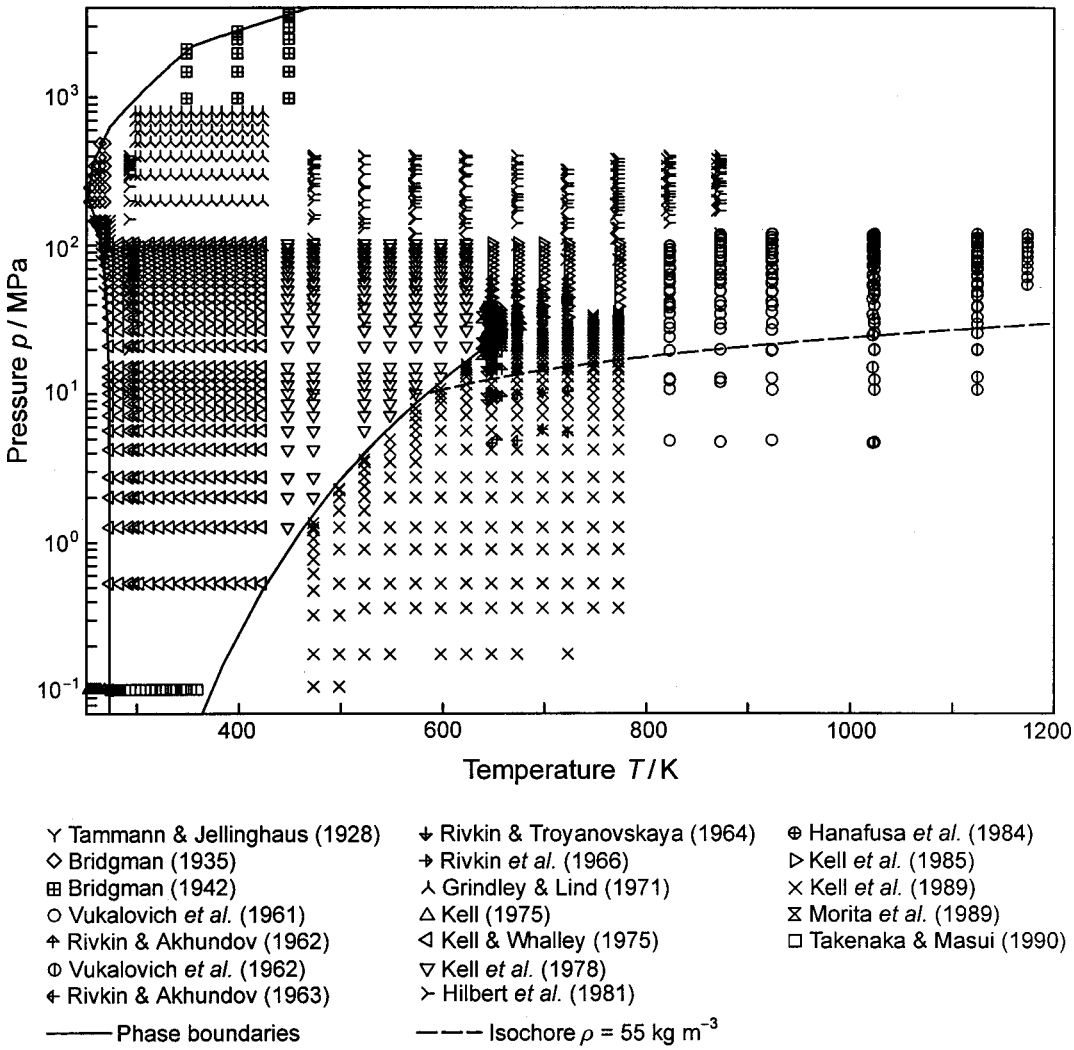

FIG. 4.1. Distribution of the selected $p\rho T$ data used to develop the residual part of IAPWS-95, Eq. (6.6), in a $p-T$ diagram. The isochore $\rho=55$ kg m^{-3} shows the upper density limit for the $p\rho T$ data used to develop the gas equation, Eq. (3.2).

are partly based on experimental data that were not considered accurate enough to be included in the selected data set for IAPWS-95, the IST-85 values [IAPWS (1994)] were also not used for the development of the IAPWS-95 formulation. For an investigation of the corresponding $p\rho T$ data at high temperatures and high pressures, see Sec. 7.2.1.5.

The tables in the following subsections contain information on experimental data used to develop the IAPWS-95 formulation and also on data that are considered to be accurate enough but were not yet available when IAPWS-95 was developed. Information on other experimental data, which are only used in comparisons with IAPWS-95 in Sec. 7, is only given in the text.

4.2.1. $p\rho T$ Data

Based on a comprehensive examination of the very great number of existing $p\rho T$ data, 2773 data points were finally selected. Figure 4.1 shows how these selected $p\rho T$ data cover the $p-T$ surface of water.

Table 4.4 summarizes the information on the selected $p\rho T$ data set where the measuring runs, published through 1990, were used to develop the IAPWS-95 formulation. In addition to the temperature and pressure range covered by each data set, the experimental uncertainties of the individual measured quantities T, p, and ρ are listed. These uncertainties were used in Eq. (5.8) to calculate the weighting factor when the coefficients of the residual part ϕ^r of IAPWS-95, Eq. (6.6), were fitted to the data.

Except for converting the original temperature values to ITS-90, all $p\rho T$ values of this data set were used as originally given by the original authors with the exception of the $p\rho T$ data measured by Grindley and Lind (1971); the reason for correcting the data of Grindley and Lind (1971) is as follows. For temperatures up to 423 K and pressures up to 100 MPa, the liquid region is covered by the very accurate data of Kell and Whalley (1975), see Fig. 4.1. For these temperatures and higher pressures, the liquid region is mainly covered by the $p\rho T$ data of Grindley and Lind (1971). Unfortunately, these two data sets do not fit smoothly

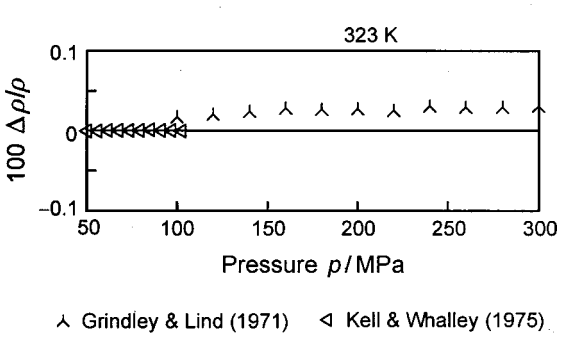

FIG. 4.2. Percentage density deviations $100\Delta\rho/\rho = 100(\rho_{exp} - \rho_{calc})/\rho_{exp}$ of experimental $p\rho T$ data of Grindley and Lind (1971) and Kell and Whalley (1975) from values calculated from a preliminary equation of state.

together as can be clearly seen in Fig. 4.2. Choosing the isotherm of 323 K as an example, Fig. 4.2 illustrates that at about 100 MPa the offset between these two data sets amounts to about 0.02% in density. Keeping in mind that Kell and Whalley's data have an uncertainty in density of less than $\pm 0.01\%$, such an offset made a simultaneous fit of an equation of state to both data sets impossible. A special analysis of the two data sets led to a reduction of Grindley and Lind's density values by 0.02%. Only in this way was it possible to represent consistently the high-pressure data of Grindley and Lind (1971) with the very accurate data of Kell and Whalley (1975).

In the gas phase, the low temperature and pressure range is completely covered by the data set of Kell *et al.* (1989). These data replace for the most part the data of Kell *et al.* (1985), since Kell *et al.*'s more recent data are more accurate. However, none of the equations of state is able to represent the data of Kell *et al.* (1989) for the lowest isotherms

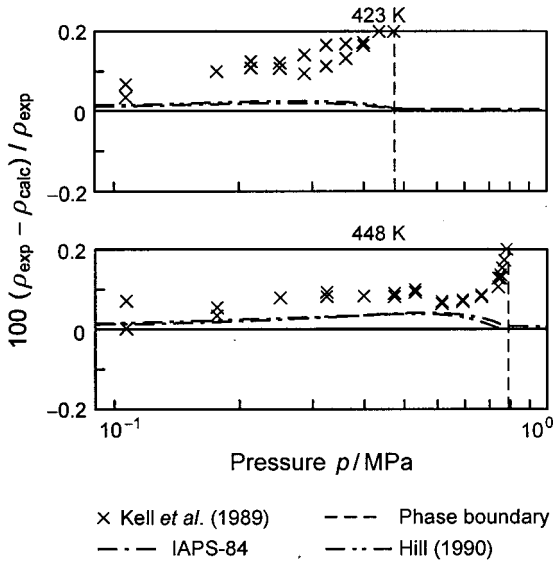

FIG. 4.3. Percentage density deviations between experimental $p\rho T$ data of Kell *et al.* (1989) and values calculated from a preliminary equation of state. The corresponding values from IAPS-84 and the equation of Hill (1990) are plotted for comparison.

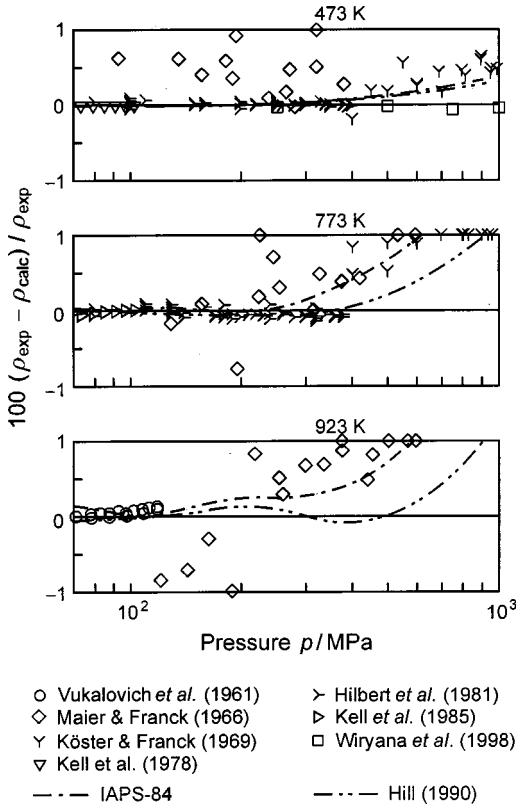

FIG. 4.4. Percentage density deviations between experimental $p\rho T$ data and values calculated from a preliminary equation of state. The corresponding values from IAPS-84 and the equation of Hill (1990) are plotted for comparison.

to within the given experimental uncertainty. This is illustrated by Fig. 4.3; for the isotherms 423 and 448 K, systematic deviations of up to 0.2% between the experimental and calculated values are exhibited by all three equations of state used for these investigations. Hill (1990) assumed adsorption and capillary effects as a source for these obviously systematic errors of the data. Consequently, for these two isotherms, the data of Kell *et al.* (1989) were not taken into account for developing IAPWS-95.

Figure 4.4 illustrates that the high-pressure $p\rho T$ data measured by Maier and Franck (1966) and by Köster and Franck (1969) are not consistent with the more recent data set of Franck's group, namely with the data of Hilbert *et al.* (1981). From the deviation diagram for the isotherm $T = 473\,\mathrm{K}$, it is clear that the data set of Hilbert *et al.* (1981) is confirmed at the lower pressure end by the data of Kell *et al.* (1978) and at the higher pressure end by the recent data of Wiryana *et al.* (1998). When using IAPS-84 and the equation of Hill (1990) as examples, the deviation diagram for $T = 773\,\mathrm{K}$ makes clear that these two equations of state are able to represent either the data of Hilbert *et al.* (1981) or of Maier and Franck (1966) and of Köster and Franck (1969), but not all three data sets. This can be seen in Fig. 4.4 for the 923 K isotherm for the equation of Hill (1990). Moreover, the scatter of the

data of Maier and Franck (1966) and of Köster and Franck (1969) reach up to ±1.5% in density, which underlines the assessment of these data. As a consequence of these factors, the data of Maier and Franck (1966) and of Köster and Franck (1969) were not included in the selected $p\rho T$ data set and IAPWS-95 was not fitted to these data. In contrast, these less accurate $p\rho T$ data were considered in establishing the Skeleton Tables IST-85 [IAPWS (1994)], for the consequences see Sec. 7.2.1.5.

The last four data sets listed in Table 4.4 cover high-precision measurements of the liquid density at a pressure of $p=0.101\,325$ MPa. At the Japanese National Research Laboratory of Metrology (NRLM), Takenaka and Masui (1990) measured dilatometrically the thermal expansion of purified Japanese tap water (JTW) at temperatures from 273.15 to 358.15 K. To obtain absolute density values, they related their thermal expansion measurements to the maximum density $\rho_{\max}$ on this isobar near 4 °C in the following way. Proceeding from the commonly accepted $\rho_{\max}$ value for Vienna Standard Mean Ocean Water (VSMOW) at that time, given by the BIPM (Bureau International des Poids et Mesures, France), and the known isotopic compositions of VSMOW and the JTW used, Takenaka and Masui transferred the $\rho_{\max}$ value of VSMOW to their JTW. [VSMOW's isotopic composition is documented by Gonfiantini (1978) and which is available from the International Atomic Energy Agency in Vienna.] In this way Takenaka and Masui (1990) obtained 79 density values of JTW in the temperature range mentioned above. Moreover, they fitted an $\rho(T)/\rho_{\max}$ equation to their data and give for this equation an uncertainty of about 1 ppm. We used this equation, however, not with their $\rho_{\max}$ value of JTW but with the one of VSMOW given by the BIPM as $\rho_{\max}=999.975\,\mathrm{kg\,m^{-3}}$ [Menaché and Girard (1973)]. In this way we determined VSMOW densities for every 5 K between 273.15 and 358.15 K and IAPWS-95 was fitted to these 18 VSMOW densities, see Table 4.4.

After the development process of IAPWS-95 had been completed, additional density measurements of VSMOW at $p=0.101\,325$ MPa were published. The liquid density measurements of Patterson and Morris (1994) were carried out at the CSIRO National Measurement Laboratory (Australia). By hydrostatic weighing they measured absolute densities at temperatures from 274.15 to 313.15 K. They give an uncertainty for their densities ranging from 0.6 ppm at 288.15 K to 1.4 ppm at 313.15 K. At NRLM, Masui *et al.* (1995) measured the absolute density of VSMOW at 289.15 K by hydrostatic weighing. Separately, they measured dilatometrically the thermal expansion of their VSMOW samples for temperatures from 273.15 to 358.15 K. Using the results of these measurements, they developed a $\rho(T)$ equation for the temperature range of their measurements; the measured absolute density at 289.15 K is given in the article by Masui *et al.* (1995/96). For this $\rho(T)$ equation, an uncertainty between 0.9 ppm at 273.15 K and 1.3 ppm at 358.15 K is claimed by the authors. Very recently, a Task Group, formed by the Working Group on Density of the Consultative Committee for Mass and Related Quantities, analyzed the density data at a pressure of 0.101 325 MPa measured in the three studies mentioned above, namely Takenaka and Masui (1990), Patterson and Morris (1994), Masui *et al.* (1995/96), and in addition the data of Watanabe (1991). As a result, this Task Group [Tanaka *et al.* (2001)] presented a new formula for the density–temperature relationship of VSMOW at 0.101 325 MPa in the temperature range from 273.15 to 313.15 K. [In the article of Tanaka *et al.* (2001), it is said that the density–temperature relationship and the corresponding density tables refer to SMOW (Standard Mean Ocean Water). However, from a note in this article it can be seen that VSMOW is meant; all the density measurements used to derive the density–temperature relationship given in this article are based on VSMOW.] Using this formula, they calculated a recommended table for the density of water in this range, which also contains the uncertainty estimation for each density value (tabulated every 1 K); the uncertainty was estimated to be between 0.84 and 0.87 ppm. The maximum density on this isobar was given as $(\rho_{\max}=999.974\,950 \pm 0.000\,84)\ \mathrm{kg\,m^{-3}}$ at a temperature of $(3.983\,035 \pm 0.000\,67)$ °C. All these more recent VSMOW densities have been included in the comparisons with those values calculated from IAPWS-95, see Sec. 7.2.1.2.

In the last few years, a relatively large number of measurements on mixtures have been carried out where one of the components is water. Besides the experimental data of the corresponding mixture, in most of the investigations measurements of pure water have also been made, mainly for calibration purposes. One typical example is the article by Abdulagatov *et al.* (1993). Those authors measured $p\rho T$ data of water–methane mixtures for temperatures between 523 and 653 K at pressures from 2 to 64 MPa. However, these data are of lower quality than those of other authors who measured only pure water in this region; for example, the scatter of Abdulagatov *et al.*'s data amounts to ±0.4% in density. Other similar cases of measurements on water, where the predominant portion of data has been taken in connection with measurements of mixtures, were also not taken into account for the selected $p\rho T$ data set; examples of such measurements are Kubota *et al.* (1987) and Yokoyama and Takahashi (1989).

Wiryana *et al.* (1998) reported $p\rho T$ data for temperatures from 353.15 to 473.15 K at pressures up to 3500 MPa. Although these data are not direct density measurements but were derived from their speed-of-sound measurements (see the second to the last paragraph of Sec. 4.3), these $p\rho T$ data can be used for extrapolation tests of IAPWS-95, see Sec. 7.2.1.2.

There are also $p\rho T$ data in the two metastable regions: subcooled liquid (metastable with respect to the solid) and superheated liquid (metastable with respect to the vapor). In the subcooled liquid there are two accurate $p\rho T$ data sets along the isobar $p=0.101\,325$ MPa. The data of Kell (1975), to which IAPWS-95 was fitted for $T<273.15$ K, cover temperatures from 236 to 268 K, see Table 4.4, and the data of Hare and Sorensen (1987) are in the temperature range from

240 to 268 K. In Sec. 7.3.2.1 these data are compared with the $p\rho T$ values calculated from IAPWS-95. References of further $p\rho T$ data on this isobar of the subcooled liquid can be taken from Fig. 7.49; these data show systematic deviations from the two data sets mentioned above. In the superheated liquid, there are two data sets to which IAPWS-95 was not fitted. The $p\rho T$ data of Chukanov *et al.* (1971) cover temperatures from 413 to 504 K at pressures from 0.06 to 4 MPa, while the data of Evstefeev *et al.* (1977) range from 508 to 571 K at pressures from 0.1 to 9.4 MPa; some of these data are in the stable liquid range of H_2O. Comparisons of these data with values from IAPWS-95 can be found in Sec. 7.3.2.2.

4.2.2. Second Virial Coefficients

The information on the second and third virial coefficients, B and C, of water vapor (steam) determined through 1989 was summarized by Sato *et al.* (1991). More recent experimental B values were determined by Hendl *et al.* (1997). However, the IAPWS-95 formulation was not fitted to any of these B and C data for reasons described in the following paragraphs. References regarding the experimental data of the second and third virial coefficient are given in Figs. 7.19 and 7.20.

Virial coefficients cannot be measured directly. In most cases they are determined from $p\rho T$ measurements and, more seldom, from measurements of the properties speed of sound, Joule–Thomson coefficient (isenthalpic throttling coefficient), and isothermal throttling coefficient. However, all experimental data sets on B and C mentioned above are based on $p\rho T$ measurements. Such values of the virial coefficients contain absolutely no additional information beyond the original $p\rho T$ data, and they are clearly more uncertain than the $p\rho T$ data themselves for the following reason. The B and C values considered here were obtained from correlation equations for the isothermal $p\rho T$ data by extrapolating to the density $\rho=0$; in this way, uncertainties of the $p\rho T$ data result in increased uncertainties of the second virial coefficients, so that the B values are more uncertain than the original $p\rho T$ data. This problem is even more pronounced for low temperatures, because in this range the isotherms are very short due to their upper pressure limit at the phase boundary (vapor pressure), see Fig. 4.1. In addition, at these low pressures and temperatures there are adsorption effects that tend to dominate over the nonideality effects. Therefore, virial coefficients derived from $p\rho T$ data at low temperatures and pressures have rather large uncertainties, and a fit of an equation of state to such B and C data may do more harm than good.

The most accurate $p\rho T$ data in the gas region of H_2O are without a doubt the data of Kell *et al.* (1989). Thus, the B data derived by Kell *et al.* (1989) from their $p\rho T$ data are the most accurate values of the second virial coefficient for the temperature range from 448 to 773 K, the upper temperature limit of Kell *et al.*'s $p\rho T$ data, see Table 4.4. Taking into account the difficulties in determining virial coefficients at low temperatures, Kell *et al.* (1989) limited their B values to 423 K, where their B value at 423 K is clearly more uncertain than for temperatures above 423 K, see Sec. 7.2.2. The $p\rho T$ data of Eubank *et al.* (1988) are clearly more uncertain than those of Kell *et al.* (1989) and are, therefore, also clearly outside the uncertainty of IAPWS-95 regarding the $p\rho T$ data in this range. However, due to their corrections for adsorption effects, the B values of Eubank *et al.* (1988) are the best second virial coefficients at 373, 403, and 423 K. The most recent B values of Hendl *et al.* (1997) are estimated to be less accurate than the data mentioned before for this temperature range. The high temperature region up to 1173 K is covered by the second virial coefficients of Vukalovich *et al.* (1967). The article of Le Fevre *et al.* (1975) contains tabulated B values which are not measurements (although often quoted as being such), but they were calculated from an equation for the second virial coefficient. For temperatures from 293 to 413 K this equation was fitted to $[B-T(\mathrm{d}B/\mathrm{d}T)]$ values derived from isothermal throttling experiments [mainly $\delta_{T,0}$ data of Wormald (1964) which are identical to that of McGlashan and Wormald (2000)] and for temperatures from 423 to 1173 K it was fitted to B values derived from $p\rho T$ data. This equation is less accurate for temperatures below 450 K and particularly below 348 K; in this low temperature region, based on our assessment, this equation yields B values that are systematically too high.

Based on all the facts discussed above, the IAPWS-95 formulation was not fitted to any second virial coefficients with the exception of a few very high-temperature B values calculated from the gas equation, Eq. (3.2), for details see Sec. 4.10. Nevertheless, in Sec. 7.2.2 second and third virial coefficients calculated from IAPWS-95 will be compared with the experimental B and C values described above.

4.3. Speeds of Sound

Due to the relatively high accuracy of the experimental data of the (isentropic) speed of sound w of H_2O, this property provides a very sensitive test of derivatives in the course of developing an equation of state. Table 4.5 lists information on the selected speed of sound data used to fit the IAPWS-95 formulation. Figure 4.5 shows the distribution of these selected w data in a $p-T$ diagram. From Figs. 4.1 and 4.5, it can be seen that in the gas region there are two data sets, the $p\rho T$ data of Kell *et al.* (1989) and the w data of Novikov and Avdonin (1968). The doubts regarding Kell *et al.*'s data on the isotherms 423 and 448 K, mentioned in Sec. 4.2.1, are confirmed by the speed of sound data in this region.

Of special importance are the measurements of the speed of sound in the liquid phase at ambient pressure. These data were measured with very good agreement by two groups of experimenters, namely by Del Grosso and Mader (1972) and by Fujii and Masui (1993). These high-precision speed-of-sound data, which have absolute uncertainties of only $\pm 0.015\ \mathrm{m\,s^{-1}}$ corresponding to relative uncertainties of about ± 10 ppm, serve as calibration points for many pieces of equipment to measure the speed of sound of liquid water.

TABLE 4.5. Information on the selected data for the speed of sound w

Authors	Temperature range T/K	Pressure range p/MPa	Uncertainty ΔT/mK[a]	Uncertainty Δp[a]	Uncertainty Δw	Number of data Total	Number of data Selected
Wilson (1959)	283–364	0.1–97	±1	···	±0.05%	88	32
Holton *et al.* (1968)	323	103–983	±20	···	±0.2%	34	26
Novikov & Avdonin (1968)	423–583	0.2–9.7	···	···	±0.5%	99	59
Del Grosso & Mader (1972)	273–368	0.1013	±1	···	±0.015 ms^{-1}	148	148
Alexandrov & Larkin (1976)	373–647	0.1–50	···	···	±0.05%	195	61
Alexandrov & Kochetov (1979)	373–423	6–99	···	···	±0.05%	60	14
Alexandrov & Kochetov (1980)	473–647	50–99	···	···	±0.25%	37	30
Mamedov (1979)	273–623	5–71	···	···	±0.5%	83	83
Petitet *et al.* (1983)	253–296	0.1–461	···	···	±0.05%	105	67
Petitet *et al.* (1986)	509–967	50–300	±1000	···	±0.5%	73	44
Fujii & Masui (1993)	293–348	0.1013	···	···	±0.015 ms^{-1}	41	41
Fujii (1994)	303–323	0.1–200	±5	±0.01%	±0.005%	47	47
Wiryana *et al.* (1998)	353–473	250–3500	···	···	±1%[b]	42	···[c]

[a]If no uncertainty values are given, then these uncertainties are taken into account in the uncertainty in speed of sound.
[b]For pressures up to 1000 MPa, estimated by ourselves.
[c]These data were only available after the development of IAPWS-95 had been finished.

Unfortunately, there are no accurate speed-of-sound data for the critical region. The decrease of the speed of sound to very small values when approaching the critical point is nearly impossible to measure because frequency-dependent dispersion effects become significant close to the critical point. The w data closest to the critical point of water were measured by Erokhin and Kal'yanov (1979), (1980). However, for reasons mentioned above, these data do not approach the critical point very closely, and consequently the smallest values of these speed-of-sound data are on the order

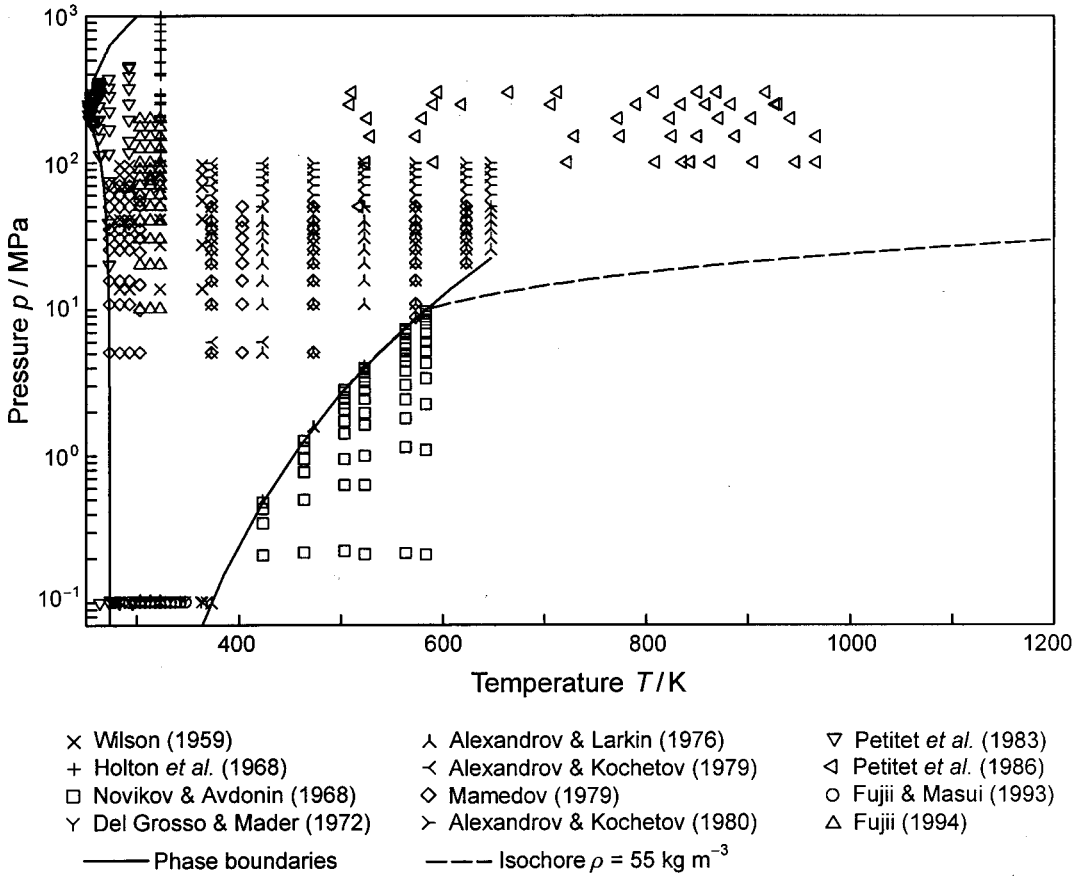

FIG. 4.5. Distribution of the selected data of the speed of sound used to develop the residual part of IAPWS-95, Eq. (6.6), in a $p-T$ diagram. The isochore ρ=55 kg m^{-3} shows the upper density limit for the w data used to develop the gas equation, Eq. (3.2).

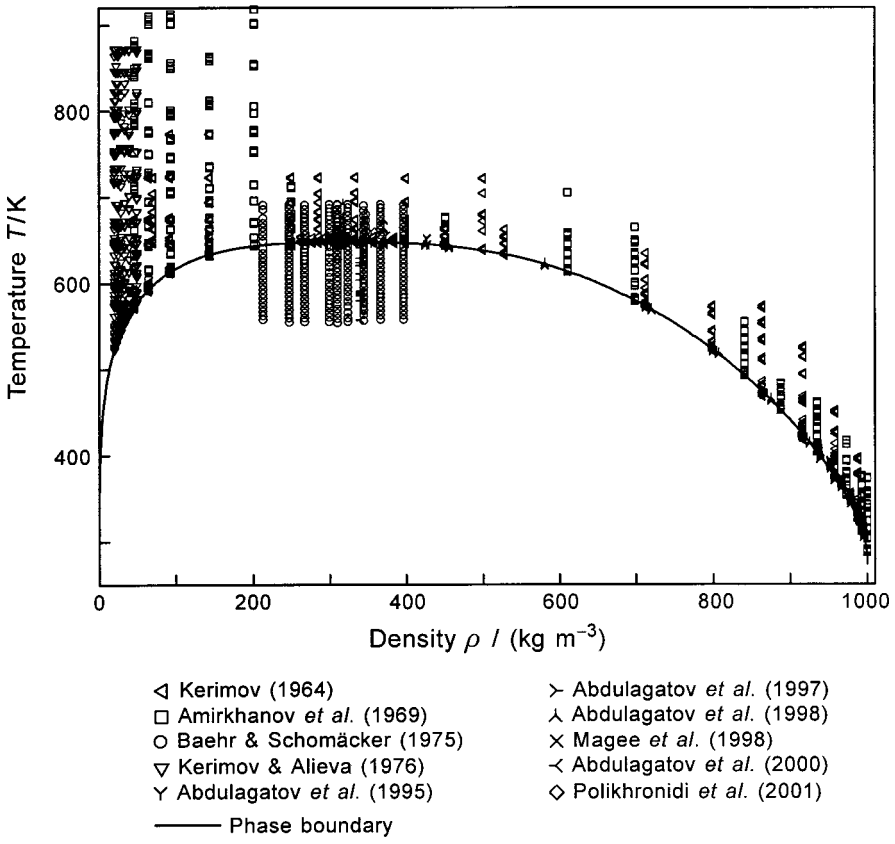

FIG. 4.6. Distribution of experimental data of the isochoric heat capacity in a $T-\rho$ diagram. For densities up to 200 kg m^{-3}, the data extend to temperatures up to about 1000 K.

of 300 m s^{-1}. Thus, equations of state for water are, with respect to the critical region, experimentally more determined by $p\rho T$ data than by speed-of-sound data. Therefore, the w data of Erokhin and Kal'yanov (1979), (1980) were only used for comparison purposes (see Sec. 7.2.3) and not for the development of the IAPWS-95 formulation.

Wiryana *et al.* (1998) reported speed-of-sound data for H_2O at temperatures between 353.15 and 473.15 K at pressures up to 3500 MPa measured with a diamond-anvil high-pressure cell. For their temperature range, these w data fill the gap in the selected data for pressures between 100 and 1000 MPa, see Fig. 4.5; for their estimated uncertainty see Table 4.5. Moreover, since these data extend to pressures which are 3.5 times as high as IAPWS-95's range of validity for pressure (1000 MPa), these data are useful for extrapolation tests of IAPWS-95, see Sec. 7.2.3.

As with the $p\rho T$ data, there are speed-of-sound data in the metastable regions of subcooled liquid and superheated liquid. The w data in the subcooled liquid are only on the isobar $p = 0.101\,325$ MPa and seem to be inconsistent with the accurate $p\rho T$ data in this metastable region. The references to these data can be taken from Fig. 7.50; IAPWS-95 was not fitted to these data. In the superheated liquid there are the data of Evstefeev *et al.* (1979), which cover a temperature range from 423 to 573 K at pressures from 0.1 to 9.9 MPa. The comparison with these data, to which IAPWS-95 was not fitted, is given in Sec. 7.3.2.2.

4.4. Isochoric Heat Capacities

Between 1962 and 2001, a great number of data of the isochoric heat capacity c_v for H_2O were measured at the Dagestan Scientific Center of the Russian Academy of Sciences. Information on the c_v data published through 1975 can be found in the article by Sato *et al.* (1991); in this period of time, the only data set not measured at the Dagestan Scientific Center is that of Baehr and Schomäcker (1975). The more recent c_v data sets are those of Abdulagatov *et al.* (1995), Abdulagatov *et al.* (1998), Magee *et al.* (1998), Abdulagatov *et al.* (2000), and Polikhronidi *et al.* (2001). Figure 4.6 illustrates that these c_v data cover the entire density region from about 20 to 1000 kg m^{-3} for temperatures up to about 70–100 K above the saturation temperature, and for densities up to 200 kg m^{-3} also to temperatures up to about 1000 K (not shown in Fig. 4.6).

The positive feature of the Dagestan data is that they include the immediate vicinity of the critical point and illustrate experimentally the strong increase of c_v in the critical region. Unfortunately, these data are clearly more uncertain than estimated by the authors. There are considerable inconsistencies of up to 20% between the c_v data sets of the different papers, but inconsistencies of up to 5% and more can also be observed within the same data set; for details see Sec. 7.2.4. Such inconsistencies are visible in the older data and also in the more recent data. Therefore, we decided not to fit

TABLE 4.6. Information on the selected data for the specific isochoric heat capacity

Authors	Temperature range T/K	Density range ρ/(kg m^{-3})	Uncertainty ΔT/mK[a]	Uncertainty $\Delta\rho$[a]	Uncertainty Δc_v	Number of data Total	Number of data Selected
Baehr & Schomäcker (1975)	649–691	213–396	···	±0.3%	±5%	414	113[b]
Magee *et al.* (1998)	304.5–413.5	935–996	···	···	±0.3%	278	···[c]

[a]The uncertainties in ΔT are taken into account in the uncertainty in isochoric heat capacity.
[b]Only data from the single-phase region were selected.
[c]These data were only available after the development of IAPWS-95 had been finished.

the IAPWS-95 formulation to any of the Dagestan data. Thus, IAPWS-95 was only fitted to those c_v data of Baehr and Schomäcker (1975) which cover the single-phase region; data from the two-phase region were not taken into account. Information on these c_v data and the most recent c_v measurements of Magee *et al.* (1998) is summarized in Table 4.6. Section 7.2.4 presents examples of comparisons between the experimental c_v data mentioned above and the corresponding values calculated from IAPWS-95.

In the last few years, the group at the Dagestan Scientific Center has also published c_v data for mixtures where H_2O is one of the components, e.g., Abdulagatov and Dvoryanchikov (1993) and Abdulagatov *et al.* (1997). These papers also contain a few c_v data for pure water, which are, however, sometimes republications of older measurements. The article of Abdulagatov and Dvoryanchikov (1993), for example, contains c_v data for H_2O which were previously published by Amirkhanov *et al.* (1969).

4.5. Isobaric Heat Capacities

This section describes both the situation regarding the data of the specific isobaric heat capacity in the ideal-gas state c_p° and regarding the experimental data of the specific isobaric heat capacity c_p of H_2O (in the real-fluid state). The knowledge of the c_p° behavior is necessary for the development of any equation of state that covers caloric properties.

4.5.1. Data of the Specific Isobaric Heat Capacity in the Ideal-Gas State

According to Eq. (5.4), knowledge of the specific isobaric heat capacity in the ideal-gas state, c_p°, forms the basis for the description of the ideal-gas part of the Helmholtz free energy. Such c_p° data are usually calculated from statistical mechanical models with the aid of spectroscopic data.

Table 4.7 lists in its upper part information on those c_p° data sets obtained within (about) the last 20 yr from such statistical mechanical models. The c_p° data set that is most widely used is that of Woolley (1980), which covers temperatures up to 4000 K. In order to extend the c_p° data of H_2O up to 10 000 K, Woolley modified his statistical mechanical model (e.g., inclusion of centrifugal effects, modifications of rotational and vibrational cutoff effects). Depending on the kind of modification, Woolley (1987) published two different c_p° data sets called ''1982 version'' and ''1984 version.'' The fourth c_p° data set based on a statistical mechanical model was reported by Gurvich *et al.* (1989); these data extend up to 20 000 K. The c_p° data set based on the most recent statistical mechanical model is that of Vidler and Tennyson (2000).

The lower part of Table 4.7 contains information on a well-known correlation equation for the c_p° values of H_2O and on c_p° values published in the most recent editions of two well-known tables for caloric data in the ideal-gas state, the TRC Tables (1988) and the NIST-JANAF Tables [Chase (1998)]. The c_p° equation developed by Cooper (1982) was fitted to Woolley's data of 1980 for temperatures from 130 to 2000 K. Cooper's equation, given as Eq. (5.5), represents the c_p° data of Woolley (1980) very well. This c_p° equation was adopted for the ideal-gas part of IAPWS-95, see Sec. 5.2. The c_p° values given in the TRC Tables (1988) are based on the c_p° data ''1984 version'' of Woolley (1987), where, for $T > 1000$ K, the c_p° values are not only printed at every 1000 K as in Woolley's article but also intermediate values are listed. In contrast to the TRC Tables, the c_p° values given in the NIST-JANAF Tables [Chase (1998)] are based again on the c_p° data of Woolley (1980).

In Fig. 4.7 the seven c_p° data sets defined in Table 4.7 are plotted as percentage deviations in comparison with the c_p° values from the ideal-gas part of IAPWS-95, Eq. (6.5), which corresponds to the c_p° equation of Cooper (1982), Eq. (5.5). The upper deviation diagram covers temperatures up to 3000 K, while the temperature range of the lower diagram extends to 1273 K corresponding to the range of validity of IAPWS-95. From the upper diagram, it can be seen that the three c_p° data sets of Woolley are not consistent with each other; even the ''1982 version'' and the ''1984 version'' c_p° data of Woolley (1987) are not in agreement. Unfortunately,

TABLE 4.7. Information on data sets for the isobaric heat capacity of water in the ideal-gas state

Source	Number of data	Temperature range T/K
c_p° data calculated from statistical mechanical models		
Woolley (1980)	259	10–4000
Woolley (1987), 1982 version	18	200–10 000
Woolley (1987), 1984 version	18	200–10 000
Gurvich *et al.* (1989)	101	100–20 000
Vidler & Tennyson (2000)	38	100–6 000
c_p° values represented by a correlation equation and by well-known tables		
Equation of Cooper (1982)		130–2 000
TRC Tables (1988)	30	0–5 000
NIST-JANAF Tables [Chase (1998)]	62	0–6 000

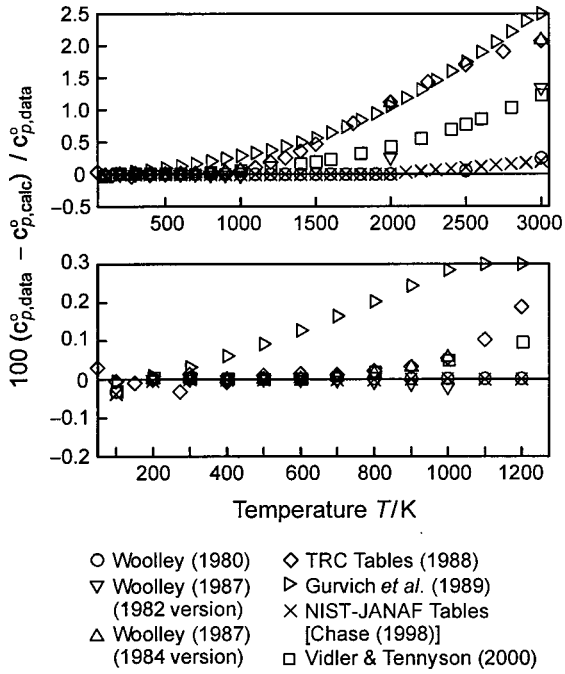

FIG. 4.7. Percentage deviations between the data of the isobaric heat capacity in the ideal-gas state c_p° from statistical mechanical models and from property tables, respectively, and values calculated from the ϕ° equation of IAPWS-95, Eq. (6.5).

he does not give any uncertainty values for his c_p° data, neither for the data published in 1980 nor in 1987, nor does he make any statement as to which of the two data sets of 1987 might be the more accurate. The c_p° data of Gurvich (1989) also differ considerably from the other data sets. The exact agreement of the values from the TRC Tables (1988) with the ''1984 version'' data of Woolley (1987) and, for temperatures to 2000 K, of the values from the NIST-JANAF Tables [Chase (1998)] with the data of Woolley (1980) show that the values from these tables are based on the corresponding Woolley data and are not independent results. The article of Vidler and Tennyson (2000) reports that up to 1000 K their c_p° data are ''in complete agreement'' with those of the NIST-JANAF Tables [Chase (1998)]. However, this is not completely correct (see the lower diagram of Fig. 4.7 at 900 and 1000 K), but above 1000 K these data are in rather good agreement with the ''1982 version'' of Woolley (1987), see the upper diagram of Fig. 4.7.

All wide-range equations of state for H_2O developed after 1980 (see Table 1.1) are based on the c_p° data of Woolley (1980); this is also true for the IAPWS-95 formulation. The lower diagram of Fig. 4.7 shows that, within the range of validity of IAPWS-95, the greatest difference between the ''1984 version'' c_p° data of Woolley (1987) and the values from IAPWS-95 is 0.19% at 1200 K, while at this temperature the data of Vidler and Tennyson (2000) deviate from IAPWS-95 by 0.09%.

4.5.2. Experimental Data of the Specific Isobaric Heat Capacity

Nearly all the data for the isobaric heat capacity c_p for water are based on measurements of Sirota's group in the former Soviet Union in the period from 1956 to 1970. Since then, only two further c_p data sets have been published that were used for fitting the IAPWS-95 formulation. These are the measurements of Angell *et al.* (1982), who investigated subcooled liquid water at ambient pressure, and the high-pressure c_p data measured by Czarnota (1984). The data of Czarnota (1984) have not yet been confirmed by other experimenters. Recently, Archer and Carter (2000) published c_p measurements for subcooled liquid water, which cover almost the same region as the data of Angell *et al.* (1982). Table 4.8 gives details on the selected experimental c_p data sets, and Fig. 4.8 presents in a $p-T$ diagram the distribution

TABLE 4.8. Information on the selected data for the specific isobaric heat capacity c_p

Authors	Temperature range T/K	Pressure range p/MPa	Uncertainty ΔT/mK[a]	Uncertainty Δp[a]	Uncertainty Δc_p	Number of data Total	Number of data Selected
Sirota & Timrot (1956)	487–653	2–12	±20	···	±2%	62	62
Sirota (1958)	587–827	2–15	±20	···	±2%	29	29
Sirota & Mal'tsev (1959)	572–774	29–49	±10	···	±1%	230	172
Sirota & Mal'tsev (1960)	736–872	29–49	±10	···	±0.6%	26	26
Sirota & Mal'tsev (1962a)	577–775	12–27	±10	···	±0.6%	252	250
Sirota & Mal'tsev (1962b)	620–868	6–22	±10	···	±1%	44	44
Sirota *et al.* (1963)	613–875	59–78	±10	···	±0.5%	58	58
Sirota & Grishkov (1966)	453–968	39–98	±100	···	±1%	60	60
Sirota *et al.* (1966)	587–872	12–69	±10	···	±2%	138	138
Sirota & Grishkov (1968)[b]	277–306	29–98	±5	···	±0.3%	18	18
Sirota *et al.* (1970)	272–306	20–98	±5	···	±0.3%	51	51
Angell *et al.* (1982)	236–290	0.1	···	···	±3%	31	30
Czarnota (1984)	299, 300	1.3–103	···	···	±6%	9	9
Archer & Carter (2000)	236–285	0.1	···	···	±(0.3%–1%)	13	···[c]

[a]If no uncertainty values are given, then these uncertainties are taken into account in the uncertainty in isobaric heat capacity.
[b]Preliminary report, for the final data see Sirota *et al.* (1970).
[c]These data were only available after the IAPWS-95 formulation had been developed.

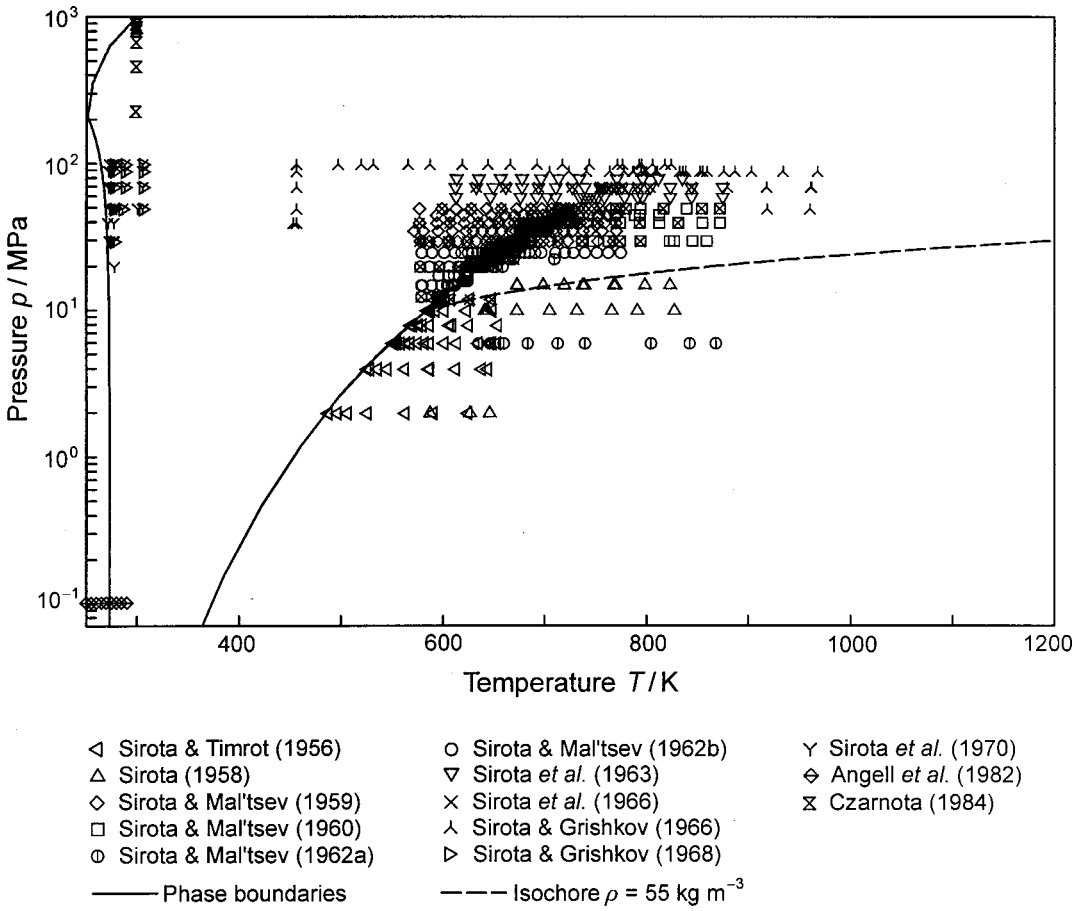

FIG. 4.8. Distribution of the selected data of the isobaric heat capacity used to develop the residual part of IAPWS-95, Eq. (6.6), in a $p-T$ diagram. The isochore $\rho=55$ kg m^{-3} shows the upper density limit for the c_p data used to develop the gas equation, Eq. (3.2).

of the c_p data used to develop IAPWS-95. In the following, additional information on the selected data sets is given and further data sets are discussed.

Levelt Sengers *et al.* (1983) carried out investigations regarding the behavior of several properties in the critical region of H_2O. They concluded that the values of the isobaric heat capacity measured by Sirota and Mal'tsev (1962a) are not sufficiently consistent with the $p\rho T$ data in the critical region. To overcome these inconsistencies, Levelt Sengers *et al.* (1983) proposed to reduce the temperature values of the c_p data of the four near-critical isobars ($p=22.561$ MPa, $p=23.536$ MPa, $p=24.517$ MPa, and $p=26.968$ MPa) by 0.05 K. Our own investigations supported this procedure, so we have included these c_p data corrected in the way proposed by Levelt Sengers *et al.* (1983).

Angell *et al.* (1982) did not report experimental uncertainties for their c_p data in the subcooled liquid at $p=0.101\,325$ MPa, but gave a value of $\pm1\%$ for the reproducibility of their data. Based on the scatter of their data and the description of the measurements, we estimated the experimental uncertainty to be less than $\pm3\%$ in c_p, see Table 4.8. This table also shows that the more recent c_p data of Archer and Carter (2000) for $p=0.101\,325$ MPa cover practically the same temperature range as the data of Angell *et al.* (1982). Archer and Carter (2000) give experimental uncertainties for their c_p data of $\pm0.3\%$ at 285 K increasing to about $\pm1\%$ at 236 K. The comparisons between these two data sets, carried out in Sec. 7.3.2.1, show that there are systematic differences between them. Except for the lowest temperature, where the difference amounts to about 5%, the maximum difference between the two data sets is about 3.2%. Archer and Carter (2000) suggest that the calibration of Angell *et al.*'s (1982) differential scanning calorimeter was in error.

In their review article, Sato *et al.* (1991) list information on isobaric heat capacity data measured by Philippi (1987) and classify these data into the best category (category A). However, in addition to the c_p data, which were derived (as is always done) from the originally measured $\Delta h-\Delta T$ data, Philippi (1987) also gave the corresponding information on these directly measured data, see Table 4.9. Thus, we used his measurements not as c_p but as Δh data, see Sec. 4.6. Since the corresponding paper published in English by Ernst and Philippi (1990) presents only the c_p data and offers no information to determine the corresponding enthalpy differences, we only refer to Philippi (1987) with regard to the Δh data. Although the c_p data given in both publications [(Philippi (1987) and Ernst and Philippi (1990)] were not

TABLE 4.9. Information on the selected data of the caloric properties enthalpy difference Δh, Joule–Thomson coefficient μ, and isothermal throttling coefficient δ_T

Authors	Property	Temperature range T/K	Pressure range p/MPa	Uncertainty			Number of data	
				ΔT/mK	Δp	Δy[a]	Total	Selected
Philippi (1987)	Δh	300–670	20–50	±3	±0.01%	±3%	235	235
Castro-Gomez *et al.* (1990)	Δh	328–455	0.7–11.9	±2	±0.01%	±1%	49	49
Ertle (1979)	μ	430–1073	0.1–5	±10	±0.01%	±4%	272	234
Ertle (1979)	δ_T	620–1073	0.1–5	±10	±0.01%	±4%	180	180

[a] y corresponds to (h_2-h_1), μ, and δ_T.

used to develop IAPWS-95, a comparison between these data and IAPWS-95 is shown in Sec. 7.2.5.

Wiryana *et al.* (1998) reported c_p data for temperatures from 353.15 to 473.15 K and pressures up to 3500 MPa. However, these data are not direct measurements of the isobaric heat capacity, but were derived from their speed-of-sound measurements (see the second to the last paragraph of Sec. 4.3). For this derivation, they used not only the equation of state of Saul and Wagner (1989) and IAPS-84 but also the experimental $p\rho T$ data of Maier and Franck (1966) and Köster and Franck (1969) (which we have not included in the selected $p\rho T$ data set, see the discussion in Sec. 4.2.1). On this basis, it is very difficult to estimate the uncertainty of Wiryana *et al.*'s c_p data. Nevertheless, in Sec. 7.2.5 these c_p data are compared with values extrapolated from IAPWS-95.

4.6. Enthalpy Differences

In contrast to the experimental data for the isobaric heat capacity, there are only a few measuring runs of enthalpy differences Δh. One characteristic feature of such measurements is that the data of several authors cannot be compared with each other since the authors normally measure different enthalpy differences; such measurements can only be compared with values calculated from an equation of state. This problem is commonly overcome by dividing the measured (small) enthalpy difference by the corresponding temperature difference and leads then to the known method of determining isobaric heat capacities. The transition from the difference quotient $(\Delta h/\Delta T)_p$ (which corresponds to the quantity measured) to the differential quotient $c_p=(\partial h/\partial T)_p$ is not a problem as long as the temperature differences are not too large and as long as the c_p behavior is sufficiently linear in the temperature range considered. If these preconditions are not sufficiently well met, then the fitting of the equation of state directly to the measured enthalpy differences proves to be the more correct procedure.

Since the older measurements of enthalpy differences do not exhibit the required quality, only the data of Philippi (1987) were used to fit IAPWS-95, see also the remarks in Sec. 4.5, and the data of Castro-Gomez *et al.* (1990); from Philippi's data only those taken with the ''second'' calorimeter were selected. Table 4.9 gives information on these two measuring runs of the enthalpy differences. Figure 4.9 illustrates the distribution of these Δh data in a $p-T$ diagram. It can be seen that the Δh data of Castro-Gomez *et al.* (1990) are in that part of the liquid region where only the $p\rho T$ data of Kell and Whalley (1975) exist.

4.7. Joule–Thomson Coefficient

Measurements of the Joule–Thomson coefficient $[\mu=(\partial T/\partial p)_h]$, which is also called the isenthalpic throttling coefficient, are inherently less accurate than other caloric properties. In particular, experimental data of the Joule–Thomson coefficient do not yield any relevant additional information if measurements of other caloric properties (e.g., c_p and w) exist. For this reason, only the μ data of the gas region measured by Ertle (1979) were used for fitting IAPWS-95. Information on this measuring run is given in Table 4.9, and the distribution of these data on the $p-T$ surface is shown in Fig. 4.9.

In this range of state, Ertle's μ data border on the range of the $p\rho T$ data of Kell *et al.* (1989). Based on the relation

$$\lim_{\rho\to 0}\mu=\left(T\frac{dB}{dT}-B\right)\frac{1}{c_p}, \tag{4.1}$$

the μ data of the gas region also influence an equation of state regarding its second virial coefficient behavior in such regions where no $p\rho T$ data exist.

4.8. Isothermal Throttling Coefficient

In principle, the statement made on the quality of experimental data of the Joule–Thomson coefficient (see Sec. 4.7) is also valid for the data of the isothermal throttling coefficient $[\delta_T=(\partial h/\partial p)_T]$. Due to the relation

$$\delta_T=-\mu c_p, \tag{4.2}$$

measurements of the isothermal throttling coefficient have a similar influence on the behavior of an equation of state regarding the second virial coefficient B as the μ data. Only the δ_T data of Ertle (1979) were used to fit IAPWS-95. Table 4.9 lists information on the used δ_T data measured by Ertle (1979) and Fig. 4.9 shows the distribution of these data in a $p-T$ diagram; the δ_T data are located at almost the same $p-T$ points as the μ data for temperatures above 550 K. Both data sets, the μ and δ_T data, were not used to optimize the structure of IAPWS-95 but only to fit its coefficients after the structure had been found, for details see Sec. 5.5.2.

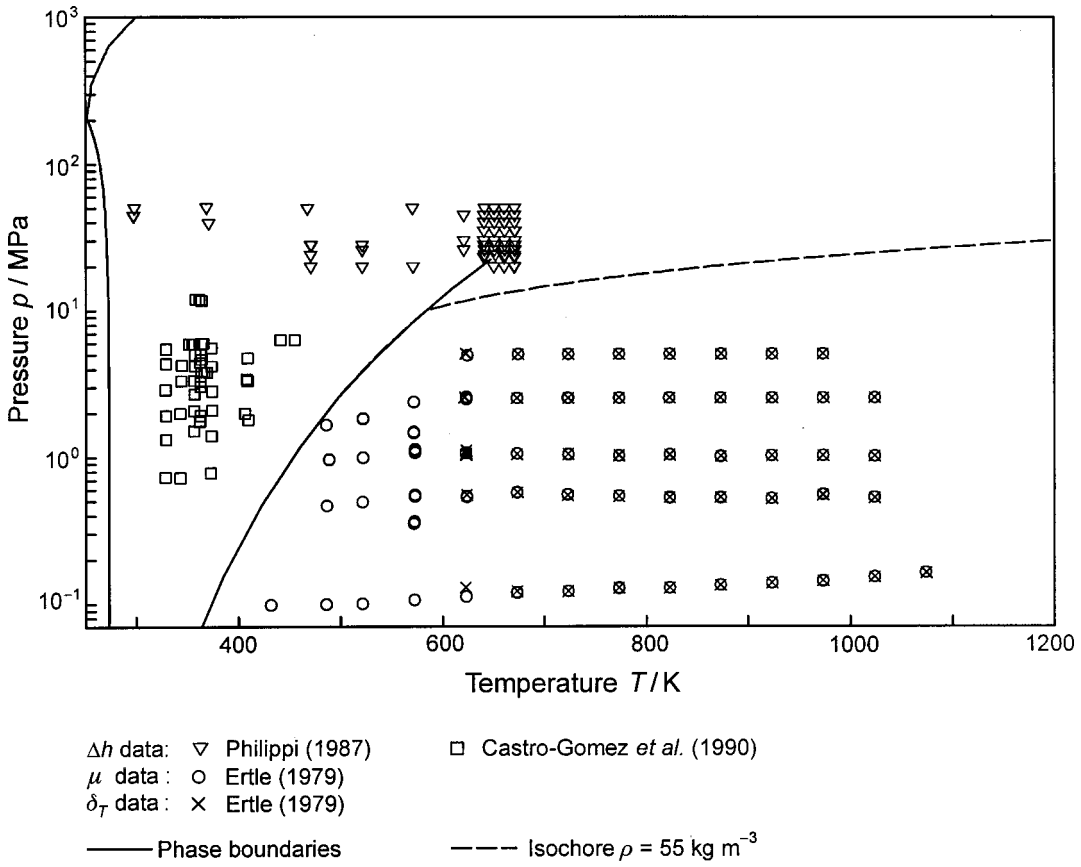

FIG. 4.9. Distribution of the selected data of the three properties enthalpy difference, Joule–Thomson coefficient, and isothermal throttling coefficient used to develop the residual part of IAPWS-95, Eq. (6.6), in a $p-T$ diagram. The isochore ρ=55 kg m^{-3} shows the upper density limit for the μ and δ_T data used to develop the gas equation, Eq. (3.2).

Very recently, McGlashan and Wormald (2000) reported measurements of the isothermal throttling coefficient. These data, which are the same as given in the Ph. D. thesis of Wormald (1964), cover a temperature range from 313 to 413.19 K at very low pressures up to 82 kPa. By extrapolating these isothermal δ_T data to zero pressure, the authors also obtained data for the quantity $\delta_{T,0}=B-T(\mathrm{d}B/\mathrm{d}T)$, the isothermal throttling coefficient at zero pressure. For these $\delta_{T,0}$ data, estimates of their uncertainties are given by McGlashan and Wormald (2000). For the main measuring range from 333 to 413 K, these uncertainties extend from 0.8% to 1.4% with increasing temperature. In contrast to the $\delta_{T,0}$ data, no uncertainties are given for the directly measured δ_T data. However, one can assume that the uncertainties of the δ_T data must be smaller than those of the extrapolated $\delta_{T,0}$ data. Comparisons with the δ_T and $\delta_{T,0}$ data of McGlashan and Wormald (2000) are presented in Sec. 7.2.7.

4.9. Hugoniot-Curve Data and Derived $p\rho T$ Data

One method used to demonstrate the extrapolation behavior of an equation of state at extreme pressures and temperatures is examination of how well it represents shock-wave measurements of the Hugoniot curve. Based on the conservation relations for mass, momentum, and energy across the shock wave, such measurements result in the Hugoniot relation

$$h-h_{0\mathrm{H}}=0.5(p-p_{0\mathrm{H}})\left[\frac{1}{\rho}+\frac{1}{\rho_{0\mathrm{H}}}\right]. \qquad (4.3)$$

The evaluation of this relation yields data for the enthalpy h as a function of pressure p and density ρ at shock-wave pressures up to tens of GPa and temperatures of several thousand Kelvins; the index 0H corresponds to the initial state prior to the release of the shock wave. Although it is not yet clear whether these measurements describe equilibrium states at all, comparisons with such $p\rho h$ data are the only experimental information to test the extrapolation capability of an equation of state to these extreme conditions of pressure and temperature.

For water, such shock-wave measurements meeting the Hugoniot relation, Eq. (4.3), were carried out by Walsh and Rice (1957), Lyzenga *et al.* (1982), and Mitchell and Nellis (1982). The corresponding $p\rho h$ data extend to pressures beyond 80 000 MPa. These data were not taken into account for the development of the IAPWS-95 formulation, because their use would have resulted in nonlinear relations which require iterative solutions of temperature. However, such an

approach implies the risk of distorting the experimental information given by the Hugoniot data because the determined temperature belonging to the $p\rho h$ data cannot be checked due to the absence of other $p\rho T$ data under these extreme conditions. Nevertheless, based on the relation

$$dT = \frac{1}{c_p}\left[dh - \left(v - T\left(\frac{\partial v}{\partial T}\right)_p \right) dp \right] \tag{4.4}$$

and estimates for c_p and the derivative $(\partial v/\partial T)_p$, Rice and Walsh (1957) determined the temperature T for their Hugoniot–$p\rho h$ data [Walsh and Rice (1957)]. We strongly recommend against use of these $p\rho T$ data. Based on our experience, the fit of an equation of state to these $p\rho T$ data yields a totally incorrect plot of the Hugoniot curve, for further details see Sec. 7.3.3.1. As mentioned above, IAPWS-95 was not directly fitted to the Hugoniot–$p\rho h$ data, but the high-pressure high-temperature behavior defined by these data was indirectly taken into account, see Sec. 4.11. In Sec. 7.3.3.1, IAPWS-95 is compared with the Hugoniot-curve data.

4.10. Calculated Data for the Gas Region

As mentioned at the beginning of Sec. 3, to support the development of a wide-range equation it has been necessary to include input data of several properties calculated from a specially developed gas equation, particularly if such data are not available from direct measurements. Thus, such ''synthetic'' data were calculated from Eq. (3.2), namely 75 data points for each of the properties density ($p\rho T$ data), specific isochoric heat capacity, and speed of sound. These data cover the temperature range from 273 to 1073 K at pressures up to 5 MPa. Based on the existing data situation for H_2O, the use of these data helped to prevent a wide-range equation of state consisting of numerous complex functional forms from behaving unphysically for various properties in certain parts of the gas region; for example, the heat capacity of the saturated vapor and the second and third virial coefficient at low temperatures.

In addition, when using the gas equation, Eq. (3.2), to calculate synthetic $p\rho T$ data for the range of state in which experimental data for the Joule–Thomson coefficient and isothermal throttling coefficient exist [Eq. (3.2) was fitted to these μ and δ_T data], the experimental information based on the μ and δ_T data could be incorporated in the linear fitting procedure as part of optimizing the structure of IAPWS-95, not just in the nonlinear fitting of the coefficients, see Sec. 5.5.2.

In order to improve the behavior of IAPWS-95 regarding the representation of the so-called ''ideal curves'' (see Sec. 7.3.3.2), ten values of the second virial coefficient $B(T)$ in the temperature range from 6000 to 15 000 K were calculated from Eq. (3.2). These high-temperature virial coefficients formed the only data for the second virial coefficient used to develop IAPWS-95.

4.11. Data for Special Applications

In this section, three further synthetic data sets used to develop IAPWS-95 are described. Two of these data sets cover thermal properties ($p\rho T$ data) and were ''produced'' to influence the extrapolation behavior of IAPWS-95. The third data set consists of data for the isochoric heat capacity in the critical region, and was intended to support the development of IAPWS-95 regarding this difficult region.

The entire development process of IAPWS-95 was started by establishing preliminary wide-range equations of state in the following way. The equations were fitted only to $p\rho T$ data of the gas region [determined from the gas equation, Eq. (3.2)] and to the selected experimental $p\rho T$ data of the entire fluid region including the $p_\sigma \rho' \rho'' T$ data in the saturation state (see Tables 4.4 and 4.1). In this way, in the ''difficult'' parts of the entire thermodynamic surface (e.g., critical region, subcooled liquid) the preliminary equations of state were not (negatively) influenced by data of properties other than the very accurate $p\rho T$ data. The aim of establishing such an equation was to achieve a reasonable description of the high-pressure and high-temperature range, where few if any reliable experimental data exist.

In this way we succeeded in determining preliminary equations that showed a physically meaningful behavior when we calculated simultaneously the Hugoniot curve and the $p\rho T$ behavior in the high-pressure high-temperature range, for further details see Sec. 7.3.3.1. In order to ensure that the positive behavior that had been achieved at this stage of development could be retained in the following generations of equations, 50 $p\rho T$ data were calculated from the respective preliminary equations in the temperature range from 555 to 5300 K at densities from 1500 to 2500 kg m^{-3} to support the behavior of the Hugoniot curve. Further, 120 $p\rho T$ data were calculated from these preliminary equations for temperatures between 448 and 1273 K and densities from 1000 to 2500 kg m^{-3} to ensure that IAPWS-95 did not produce any crossing of isotherms or even a bending of isotherms in the extrapolation range at pressures up to 100 000 MPa. In the final stage of the equation development leading to IAPWS-95, any of the preliminary equations could be used to calculate the 170 synthetic $p\rho T$ data, because all these equations yielded basically the same reasonable $p\rho T$ surface in this high-pressure high-temperature region. Thus, the 170 synthetic $p\rho T$ data can also be calculated from the final equation, the IAPWS-95 formulation itself.

The behavior of caloric properties in the critical region of water is covered insufficiently by existing experimental data. On the one hand, the experimental data near the critical point were not free of systematic errors so that these data had to be adjusted using the ''revised and extending scaled equation'' of Levelt Sengers *et al.* (1983), and therefore considerable corrections in the temperature values given by the experimenters for their data were made. This is the case for the isochoric heat capacity data of Amirkhanov *et al.* (1969) and the speed of sound data of Erokhin and Kal'yanov (1979), (1980). Thus, the real information content of these data is

questionable, see also Secs. 4.3 and 4.4. On the other hand, the measurements of reliable caloric data end far before the range of interest in the critical region; this is the case for the c_v data of Baehr and Schomäcker (1975).

Nevertheless, in order to achieve a consistent description of the critical region it was necessary to calculate synthetic c_v values in the near-critical region using suitable equations from the literature. When IAPWS-95 was being developed, the scaled equation developed by Luettmer-Strathmann (1992) was the obvious choice for this procedure; this equation corresponds to a parametric crossover model. For the critical region and a greater range outside the critical region, namely for temperatures from 628 to 800 K ($T_c = 647.096$ K) and densities from 115 to 635 kg m^{-3} ($\rho_c = 322$ kg m^{-3}), Luettmer-Strathmann fitted the coefficients of her equation to $p\rho T$, c_v, c_p, and $p_\sigma \rho' \rho'' T$ data calculated from the equation of state of Saul and Wagner (1989), taking into account the temperature conversion to ITS-90 temperatures.

Besides the crossover equation of Luettmer-Strathmann (1992), c_v values were also calculated from the equation of state of Hill (1990). This was done because Hill's equation yields better results for the extended critical region than Luettmer-Strathmann's equation. The reason for this is that, in the transition region between the critical and extended critical region, Hill's equation is better than that of Saul and Wagner (1989) on which Luettmer-Strathmann's equation was based.

After careful investigation of Hill's and Luettmer-Strathmann's equations in the critical and extended critical region, the following input data for the development of IAPWS-95 were used: 176 c_v values along seven isochores in the critical region for temperatures between 646.24 and 654.92 K and densities from 267 to 400 kg m^{-3} calculated as follows: The equation of Luettmer-Strathmann (1992) was used to calculate the c_v values for $T \leqslant 648$ K, while for $T > 648$ K the values were determined from the equation of Hill (1990). When calculating these synthetic c_v data, we made allowance for the fact that the two equations and IAPWS-95 are based on different critical parameters and different temperature scales.

5. Details of the Development of the IAPWS-95 Formulation

The new equation of state for ordinary water substance is an empirical description of the Helmholtz free energy. For the development of such empirical formulations, the application of linear optimization procedures and nonlinear multiproperty fitting algorithms is state-of-the-art. Although this strategy has already been presented in the literature [e.g., Setzmann and Wagner (1989), (1991), Wagner and de Reuck (1996), and Span (2000)], this section summarizes the basic elements of this strategy along with the special features necessary when developing the new equation of state for H_2O.

5.1. Basic Structure of an Equation of State Explicit in the Helmholtz Free Energy

The equation of state described in this article is a fundamental equation explicit in the Helmholtz free energy f with the independent variables density ρ and temperature T. The function $f(\rho,T)$ is commonly split into a part f° that represents the properties of the ideal gas at given T and ρ and a part f^r that takes into account the residual fluid behavior. This convention can be written as

$$f(\rho,T) = f^\circ(\rho,T) + f^r(\rho,T). \tag{5.1}$$

Usually, the Helmholtz free energy is used in its dimensionless form $\phi = f/(RT)$ so that Eq. (5.1) becomes

$$\phi(\delta,\tau) = \phi^\circ(\delta,\tau) + \phi^r(\delta,\tau), \tag{5.2}$$

where $\delta = \rho/\rho_c$ is the reduced density and $\tau = T_c/T$ is the inverse reduced temperature with ρ_c and T_c the critical density and the critical temperature, respectively.

Since the Helmholtz free energy as a function of density and temperature is one of the four fundamental forms of an equation of state, all thermodynamic properties of a pure substance can be obtained by combining derivatives of Eq. (5.2). For the relations between Eq. (5.2) and its derivatives and the thermodynamic properties considered in this paper, see Table 6.3.

5.2. The Equation for the Helmholtz Free Energy of the Ideal Gas

The Helmholtz free energy of the ideal gas is given by

$$f^\circ(\rho,T) = h^\circ(T) - RT - Ts^\circ(\rho,T). \tag{5.3}$$

For the ideal gas, the enthalpy h° is a function of temperature only, and the entropy s° depends on temperature and density. Both properties can be derived from an equation for the ideal-gas heat capacity $c_p^\circ(T)$. When c_p° is inserted into the expression for $h^\circ(T)$ and $s^\circ(\rho,T)$ in Eq. (5.3), one obtains

$$f^\circ(\rho,T) = \left(\int_{T_0}^{T} c_p^\circ \mathrm{d}T + h_0^\circ \right) - RT - T\left[\int_{T_0}^{T} \frac{c_p^\circ - R}{T} \mathrm{d}T - R \ln\left(\frac{\rho}{\rho_0^\circ}\right) + s_0^\circ \right], \tag{5.4}$$

where all variables with the subscript "0" refer to an arbitrary reference state.

In order to obtain the equation for $f^\circ(\rho,T)$ and $\phi^\circ(\delta,\tau)$, the well-established equation of Cooper (1982) was used for the isobaric heat capacity in the ideal-gas state, $c_p^\circ(T)$. This equation, which is a sum of so-called "Planck–Einstein" functions, is:

$$\frac{c_p^\circ}{R} = b_0 + \sum_{i=1}^{5} b_i \frac{(\beta_i/T)^2 e^{-\beta_i/T}}{[1 - e^{-\beta_i/T}]^2} \quad . \tag{5.5}$$

Cooper determined the coefficients b_0, b_i, and the exponents β_i by nonlinear least-squares fitting to the c_p° values of Woolley (1980), where he took into account only the data for temperatures between 130 and 2000 K. After rearranging the coefficients and exponents, namely $n_3^\circ = b_0 - 1$, and for $i=1$ to 5 $n_{i+3}^\circ = b_i$ and $\gamma_{i+3}^\circ = \beta_i / T_c$, one obtains from Eq. (5.5)

$$\frac{c_p^\circ}{R} = 1 + n_3^\circ + \sum_{i=4}^{8} n_i^\circ \frac{(\gamma_i^\circ \tau)^2 e^{-\gamma_i^\circ \tau}}{[1 - e^{-\gamma_i^\circ \tau}]^2} \tag{5.6}$$

with $\tau = T_c/T$. Equations (5.5) and (5.6) represent the c_p° values of Woolley (1980) very accurately. The values of the coefficients of Eq. (5.6) are given in Table 6.1. In the temperature range from 250 to 2000 K, the deviations in c_p°/R between the values of Woolley (1980) and the values from Eqs. (5.5) and (5.6) are less than 0.0005%, and from 140 to 240 K they do not exceed 0.001%.

After inserting $c_p^\circ(T)$ according to Eq. (5.6) in Eq. (5.4), working out the integrations and proceeding to the dimensionless form of the Helmholtz free energy in the ideal-gas state ϕ° [see Eq. (5.2)], one obtains the final ϕ° equation, given as Eq. (6.5).

5.3. Basic Statements for Fitting and Optimizing the Structure of an Equation for the Residual Part of the Helmholtz Free Energy

While statistical thermodynamics can predict the behavior of fluids in the ideal-gas state with high accuracy, no physically founded equation is known which accurately describes the real thermodynamic behavior of fluids in the whole fluid region. Thus, for this purpose an equation for the residual fluid behavior, in this case for the residual part of the Helmholtz free energy ϕ^r, must be determined in an empirical way where, as a matter of course, as much physical understanding as possible is taken into account. Since the Helmholtz free energy itself is not accessible to direct measurements, it is necessary to determine the unknown mathematical structure and the unknown coefficients of the residual part of the dimensionless Helmholtz free energy from properties for which experimental data are available.

In this context, the following steps for the development of the final form of an equation for ϕ^r must be performed:

(1) selection of the final data set, see Secs. 2–4;
(2) weighting of the data;
(3) precorrelation of auxiliary quantities;
(4) linear least squares fitting in connection with the structure optimization method; and
(5) nonlinear least squares fitting.

In this section, basic statements on items (2)–(5) are made.

5.3.1. Fitting an Equation for ϕ^r to Data

If a certain functional form has been selected for $\phi^r(\delta, \tau, \overline{n})$, data for J different properties z_j (e.g., pressure p, speed of sound w, ...) can be used to determine the unknown coefficients n_i (expressed as the vector $\overline{n}$) by minimizing the following sum of squares:

$$\chi^2 = \sum_{j=1}^{J} \chi_j^2 = \sum_{j=1}^{J} \sum_{m=1}^{M_j} [[z_{exp} - z_{calc}(x_{exp}, y_{exp}, \overline{n})]^2]_{j,m} \cdot \sigma_{tot,m}, \tag{5.7}$$

where M_j is the number of data points used for the jth property, z_{exp} is the experimental value for any property z, and z_{calc} is the value for the property calculated from the equation for ϕ with the parameter vector $\overline{n}$ at x_{exp} and y_{exp}. The measured independent variables x and y may vary for the different properties of z, but usually one of them corresponds to temperature T, while the other corresponds to density ρ or pressure p [e.g., $p(T,\rho)$ or $w(T,\rho)$]. When data sets of different properties are used for the development of a correlation equation, then the residuum $\Delta z = (z_{exp} - z_{calc})$ of Eq. (5.7) is reduced with a suitable measure for the uncertainty of the data point considered. According to the Gaussian error propagation formula, the uncertainty of a measured data point is given by

$$\sigma_{exp}^2 = \left[\frac{\partial \Delta z}{\partial x}\right]_{y,z}^2 \sigma_x^2 + \left[\frac{\partial \Delta z}{\partial y}\right]_{x,z}^2 \sigma_y^2 + \left[\frac{\partial \Delta z}{\partial z}\right]_{x,y}^2 \sigma_z^2, \tag{5.8}$$

where σ_x, σ_y, and σ_z are the isolated uncertainties of the single variables x, y, and z, respectively. The partial derivatives of Δz have to be calculated from a preliminary equation of state.

In order to have an additional influence on the data set, a weighting factor f_{wt} is introduced. The total variance σ_{tot}^2 of a data point used in Eq. (5.7) is defined as

$$\sigma_{tot}^2 = \sigma_{exp}^2 / f_{wt}^2. \tag{5.9}$$

In this way, weighting factors $f_{wt} > 1$ increase the influence of a data point with respect to the sum of squares and weighting factors $f_{wt} < 1$ reduce it. Usually f_{wt} is equal to one and σ_{tot}^2 is equal to σ_{exp}^2. However, in some cases different weighting factors are used to compensate for effects caused by the structure of the data set.

The determination of $\overline{n}$ by minimizing χ^2 for data of more than one property is called ''multiproperty fitting.'' This problem leads to a linear system of normal equations if each of the properties z depends on the same independent variables as the function used (for example, T and ρ for the Helmholtz free energy) and if the relations between z and the function or its derivatives is linear for all properties considered. Data for such properties are called ''linear data.'' For functions in terms of the Helmholtz free energy, examples of such properties are $p(T,\rho)$ and $c_v(T,\rho)$, see Table 5.1. If one or both of these conditions is not fulfilled [for instance, for $h(T,p)$, $w(T,p)$, $c_p(T,p)$,..., see also Sec. 5.3.2], those data are called ''nonlinear data'' and more complicated and time-consuming nonlinear algorithms must be used to minimize the sum of squares, Eq. (5.7). Table 5.1 lists all sums of

TABLE 5.1. Contribution of the several linear, nonlinear, and linearized data to the weighted sum of squares for the fitting and optimization process

j	Type of data	Weighted sum of squares	
		Linear data	
1	$p(\rho,T)$	$\chi_1^2=\sum_{m=1}^{M}\left[\frac{p-\rho RT}{\rho^2 RT}-\rho_c^{-1}\phi_\delta^r\right]_m^2\cdot\sigma_m^{-2}$	(5.10)
2	$c_v(\rho,T)$	$\chi_2^2=\sum_{m=1}^{M}\left[\frac{c_v}{R}+\tau^2(\phi_{\tau\tau}^\circ+\phi_{\tau\tau}^r)\right]_m^2\cdot\sigma_m^{-2}$	(5.11)
3	$B(T)$	$\chi_3^2=\sum_{m=1}^{M}\left[B\cdot\rho_c-\lim_{\rho\to 0}\phi_\delta^r\right]_m^2\cdot\sigma_m^{-2}$	(5.12)
		Nonlinear data	
4	$w(p,T)$	$\chi_4^2=\sum_{m=1}^{M}\left[\frac{w^2}{RT}-1-2\delta\phi_\delta^r-\delta^2\phi_{\delta\delta}^r+\frac{(1+\delta\phi_\delta^r-\delta\tau\phi_{\delta\tau}^r)^2}{\tau^2(\phi_{\tau\tau}^\circ+\phi_{\tau\tau}^r)}\right]_m^2\cdot\sigma_m^{-2}$	(5.13)
5	$c_p(p,T)$	$\chi_5^2=\sum_{m=1}^{M}\left[\frac{c_p}{R}+\tau^2(\phi_{\tau\tau}^\circ+\phi_{\tau\tau}^r)-\frac{(1+\delta\phi_\delta^r-\delta\tau\phi_{\delta\tau}^r)^2}{1+2\delta\phi_\delta^r+\delta^2\phi_{\delta\delta}^r}\right]_m^2\cdot\sigma_m^{-2}$	(5.14)
6	$h_2(p_2,T_2)-h_1(p_1,T_1)$	$\chi_6^2=\sum_{m=1}^{M}\left[\frac{h_2}{RT_2}-\frac{h_1}{RT_1}-[\tau(\phi_\tau^\circ-\phi_\tau^r)+\delta\phi_\delta^r]_2+[\tau(\phi_\tau^\circ-\phi_\tau^r)+\delta\phi_\delta^r]_1\right]_m^2\cdot\sigma_m^{-2}$	(5.15)
7	$\mu(p,T)$	$\chi_7^2=\sum_{m=1}^{M}\left[\mu R\rho+\frac{(\delta\phi_\delta^r+\delta^2\phi_{\delta\delta}^r+\delta\tau\phi_{\delta\tau}^r)}{(1+\delta\phi_\delta^r-\delta\tau\phi_{\delta\tau}^r)^2-\tau^2(\phi_{\tau\tau}^\circ+\phi_{\tau\tau}^r)(1+2\delta\phi_\delta^r+\delta^2\phi_{\delta\delta}^r)}\right]_m^2\cdot\sigma_m^{-2}$	(5.16)
8	$\delta_T(p,T)$	$\chi_8^2=\sum_{m=1}^{M}\left[\delta_T\rho-1+\frac{1+\delta\phi_\delta^r-\delta\tau\phi_{\delta\tau}^r}{1+2\delta\phi_\delta^r+\delta^2\phi_{\delta\delta}^r}\right]_m^2\cdot\sigma_m^{-2}$	(5.17)
9	$p_\sigma(T)$	$\chi_9^2=\sum_{m=1}^{M}\left[\frac{p_{\sigma,m}-p_\sigma}{RT_c\rho_c}\right]_m^2\cdot\sigma_m^{-2}$	(5.18)
10	$\rho'(T)$	$\chi_{10}^2=\sum_{m=1}^{M}\left[\frac{\rho'_m-\rho'}{\rho_c}\right]_m^2\cdot\sigma_m^{-2}$	(5.19)
11	$\rho''(T)$	$\chi_{11}^2=\sum_{m=1}^{M}\left[\frac{\rho''_m-\rho''}{\rho_c}\right]_m^2\cdot\sigma_m^{-2}$	(5.20)
12	$u'_2(T_2)-u'_1(T_1)$	$\chi_{12}^2=\sum_{m=1}^{M}\left[\frac{u'_2}{RT_2}-\frac{u'_1}{RT_1}-[\tau(\phi_\tau^\circ+\phi_\tau^r)]_2+[\tau(\phi_\tau^\circ+\phi_\tau^r)]_1\right]_m^2\cdot\sigma_m^{-2}$	(5.21)
13	$u''(T)-u'(T)$	$\chi_{13}^2=\sum_{m=1}^{M}\left[\frac{u''-u'}{RT}-\tau\left[\ln\frac{\delta''}{\delta'}+\phi_\tau^r(\delta'',\tau)-\phi_\tau^r(\delta',\tau)\right]\right]_m^2\cdot\sigma_m^{-2}$	(5.22)
		Linearized data	
4*	$w(\rho^p,T)$	$\chi_{4*}^2=\sum_{m=1}^{M}\left[\frac{w^2}{RT}-\gamma^p\cdot(1+2\delta\phi_\delta^r+\delta^2\phi_{\delta\delta}^r)\right]_m^2\cdot\sigma_m^{-2}$	(5.23)
5*	$c_p(\rho^p,T)$	$\chi_{5*}^2=\sum_{m=1}^{M}\left[\frac{c_p}{R}+\tau^2(\phi_{\tau\tau}^\circ+\phi_{\tau\tau}^r)-\epsilon^p\right]_m^2\cdot\sigma_m^{-2}$	(5.24)
6*	$h_2(\rho_2^p,T_2)-h_1(\rho_1^p,T_1)$	$\chi_{6*}^2=\sum_{m=1}^{M}\left[\frac{h_2}{RT_2}-\frac{h_1}{RT_1}-[\tau(\phi_\tau^\circ-\phi_\tau^r)+\delta\phi_\delta^r]_2+[\tau(\phi_\tau^\circ-\phi_\tau^r)+\delta\phi_\delta^r]_1\right]_m^2\cdot\sigma_m^{-2}$	(5.25)

TABLE 5.1. Contribution of the several linear, nonlinear, and linearized data to the weighted sum of squares for the fitting and optimization process—Continued

12*	$u_2'(\rho_2'^{\,p},T_2)-u_1'(\rho_1'^{\,p},T_1)$	$\chi^2_{12*}=\sum_{m=1}^{M}\left[\frac{u_2'}{RT_2}-\frac{u_1'}{RT_1}-[\tau(\phi_\tau^\circ+\phi_\tau^r)]_2+[\tau(\phi_\tau^\circ+\phi_\tau^r)]_1\right]_m^2\cdot\sigma_m^{-2}$	(5.26)
13*	$u''(\rho''^{\,p},T)-u'(\rho'^{\,p},T)$	$\chi^2_{13*}=\sum_{m=1}^{M}\left[\frac{u''-u'}{RT}-\tau\left[\ln\frac{\delta''}{\delta'}+\phi_\tau^r(\delta'',\tau)-\phi_\tau^r(\delta',\tau)\right]\right]_m^2\cdot\sigma_m^{-2}$	(5.27)
14	$p(\rho'^{\,p},T)$	$\chi^2_{14}=\sum_{m=1}^{M}\left[\frac{p_\sigma-\rho' RT}{(\rho')^2RT}-\rho_c^{-1}\phi_\delta^r(\delta',\tau)\right]_m^2\cdot\sigma_m^{-2}$	(5.28a)
15	$p(\rho''^{\,p},T)$	$\chi^2_{15}=\sum_{m=1}^{M}\left[\frac{p_\sigma-\rho'' RT}{(\rho'')^2RT}-\rho_c^{-1}\phi_\delta^r(\delta'',\tau)\right]_m^2\cdot\sigma_m^{-2}$	(5.28b)
16	Maxwell criterion	$\chi^2_{16}=\sum_{m=1}^{M}\left[\frac{p_\sigma}{RT}\cdot\left[\frac{1}{\rho''}-\frac{1}{\rho'}\right]-\ln\left[\frac{\rho'}{\rho''}\right]-[\phi^r(\delta',\tau)-\phi^r(\delta'',\tau)]\right]_m^2\cdot\sigma_m^{-2}$	(5.28c)

Explanations

For the relations between the several properties and ϕ° and ϕ^r and their derivatives see Table 6.3.
For the weighted sum of squares the following abbreviations and definitions are used:

$$(1)\quad \phi_\delta^r=\left[\frac{\partial\phi^r}{\partial\delta}\right]_\tau,\ \phi_{\delta\delta}^r=\left[\frac{\partial^2\phi^r}{\partial\delta^2}\right]_\tau,\ \phi_\tau^r=\left[\frac{\partial\phi^r}{\partial\tau}\right]_\delta,\ \phi_{\tau\tau}^r=\left[\frac{\partial^2\phi^r}{\partial\tau^2}\right]_\delta,\ \phi_{\delta\tau}^r=\left[\frac{\partial^2\phi^r}{\partial\delta\partial\tau}\right],\ \phi_\tau^\circ=\left[\frac{\partial\phi^\circ}{\partial\tau}\right]_\delta,\ \phi_{\tau\tau}^\circ=\left[\frac{\partial^2\phi^\circ}{\partial\tau^2}\right]_\delta. \tag{5.29}$$

(2) The weight σ_m corresponds to the quantity σ_{tot} according to Eq. (5.9).
(3) The subscript p means precorrelated. The precorrelation factors γ^p and ϵ^p are defined by the relations:

$$\gamma^p=\frac{c_p(\rho^p,T)}{c_v(\rho^p,T)} \tag{5.30}$$

$$\epsilon^p=c_p-c_v=\left[\frac{(1+\delta\phi_\delta^r-\delta\tau\phi_{\delta\tau}^r)^2}{1+2\,\delta\phi_\delta^r+\delta^2\phi_{\delta\delta}^r}\right]_{\tau,\delta^p} \tag{5.31}$$

All precorrelated quantities are calculated from a preliminary equation of state.

squares of the linear and nonlinear data used for the development of IAPWS-95. The total sum of squares is obtained as given by Eq. (5.7).

5.3.2. Basic Statements for Optimizing the Mathematical Form of ϕ^r

Since the functional form of an equation for the residual part of the Helmholtz free energy is not initially known, a suitable mathematical structure must be established before any coefficients n_i can be fitted to the data. In the past, the structure of most correlation equations was determined subjectively, based on the experience of the correlator or by trial and error. To improve this situation, we developed different optimization strategies [Wagner (1974), Ewers and Wagner (1982), Setzmann and Wagner (1989), and Tegeler *et al.* (1999)] that introduce objective criteria for the selection of the mathematical structure of such equations of state.

The entire strategy of the structure optimization of an equation of state consists of two basic steps:

(1) Formulation of a comprehensive set of mathematical functions of the reduced density and inverse reduced temperature which is used as a ''bank of terms.''
(2) From this bank of terms, the structure-optimization method determines with mathematical statistical and stochastic methods the best combination of a certain number of terms.

For developing IAPWS-95, a modified form of the structure-optimization method developed by Setzmann and Wagner (1989) was used. This method only works with linear data, see Sec. 5.3.1. Thus, to take into account the optimization process, at least partly, the experimental information of the nonlinear data, the nonlinear relations between these properties, and the derivatives of ϕ° and ϕ^r were linearized. The results of this linearization for the sums of squares of those nonlinear properties considered to be important for the development of IAPWS-95 are given by Eqs. (5.23)–(5.28) listed in Table 5.1. In the following an example of such a linearization is shown for the property speed of sound w.

According to the relation between the property $z=w$ and the derivatives of ϕ° and ϕ^r given in Table 6.3 the sum of squares [see Eq. (5.7)] for fitting an equation for ϕ^r to M experimental data of w (w is the jth property considered in the entire multiproperty fitting process) reads:

$$\chi_j^2=\sum_{m=1}^{M}\left[\frac{w^2}{RT}-1-2\,\delta\phi_\delta^{\mathrm{r}}-\delta^2\phi_{\delta\delta}^{\mathrm{r}}+\frac{(1+\delta\phi_\delta^{\mathrm{r}}-\delta\tau\phi_{\delta\tau}^{\mathrm{r}})^2}{\tau^2(\phi_{\tau\tau}^{\circ}+\phi_{\tau\tau}^{\mathrm{r}})}\right]_m^2\cdot\sigma_{\mathrm{tot},m}^{-2}. \tag{5.32}$$

This type of sum of squares leads to a nonlinear system of normal equations when determining the coefficients $\overline{n}$ in the equation for $\phi^{\mathrm{r}}(\delta,\tau,\overline{n})$. However, the structure optimization method used here cannot cope with such a nonlinear system. A further difficulty arises because the speed of sound is measured as a function of pressure and temperature, and not density and temperature, which are the variables of the equation for ϕ^{r}. Thus, the sum of squares according to Eq. (5.32) is implicitly nonlinear. As shown by Schmidt and Wagner (1985), this implicitly nonlinear relation can be linearized by using the following sum of least squares:

$$\chi_j^2=\sum_{m=1}^{M}\left[\frac{w^2}{RT}-\gamma^{\mathrm{p}}\cdot(1+2\,\delta\phi_\delta^{\mathrm{r}}+\delta^2\phi_{\delta\delta}^{\mathrm{r}})\right]_m^2\cdot\sigma_{\mathrm{tot},m}^{-2} \tag{5.33}$$

with the so-called precorrelation factor γ^{p} according to

$$\gamma^{\mathrm{p}}=\frac{c_p(\rho^{\mathrm{p}},T)}{c_v(\rho^{\mathrm{p}},T)}. \tag{5.33a}$$

The density ρ^{p} and the precorrelation factor γ^{p} have to be precalculated by a preliminary equation of state.

Because the linearizations of the nonlinear sums of squares require precalculations with preliminary equations of state, the entire process of optimizing the structure of the ϕ^{r} equation is a recursive process, see Sec. 5.5.

In this work, a modified form of the structure-optimization method developed by Setzmann and Wagner (1989) was used to determine a suitable mathematical structure of IAPWS-95. The modifications relate to both the stochastic and the deterministic part of the original algorithm. More importantly, however, are the changes mentioned in the next paragraph with regard to the handling of different functional forms in the bank of terms.

A sophisticated correlation equation for the residual part of the Helmholtz free energy consists of an extensive sum of terms. Hence, the mathematical form of a single term can be associated with different functional groups ranging from simple polynomials in the reduced density δ and the inverse reduced temperature τ to complicated exponential expressions [see the bank of terms, Eq. (5.41)]. During our work on the reference equation of state for carbon dioxide [Span and Wagner (1996)] additional limitations with respect to the number of terms belonging to certain functional groups turned out to be useful and the optimization algorithm was modified to allow such limitations; for further details see Span (2000).

5.4. Functional Forms for ϕ^{r} and the Bank of Terms

For the development of a suitable form of the equation for the residual part ϕ^{r} of IAPWS-95, the composition of the comprehensive set of functional forms for the bank of terms is of great importance. The starting point for the investigated functional forms was our experience with the development of wide-range equations of state of reference quality for oxygen, water, methane, and carbon dioxide [Schmidt and Wagner (1985), Saul and Wagner (1989), Setzmann and Wagner (1991), and Span and Wagner (1996)]. A great number of investigations were necessary in order to find out the applicability of the several functional forms in view of the requirements for establishing the new equation of state for water. Finally, the bank of terms was composed of four different functional forms.

5.4.1. Polynomial Terms

Polynomial terms have been part of all previous wide-range equations of state. They are a part of our bank of terms in the following form:

$$\phi_i^{\mathrm{r}}=n_i\delta^{d_i}\tau^{t_i} \tag{5.34}$$

with $\delta=\rho/\rho_{\mathrm{c}}$ and $\tau=T_{\mathrm{c}}/T$. In order for the new equation of state to achieve good extrapolation, the values of the density exponents d_i were limited to the range from 1 to 5 with integral step sizes. This limitation is particularly important when extrapolating to high densities. For the same reason, the values of the temperature exponents t_i were limited to a small range as well. Moreover, the temperature exponent t_i of the polynomial term with the highest density exponent d_i (the leading term when extrapolating the equation to high densities) should be between $0<t_i\leqslant 1$; for further details and discussion of these considerations see Span and Wagner (1997). Based on these considerations, the entire range for the temperature exponents of the polynomial terms was selected to be from -0.5 to 1 with a step size of 0.125. With this small step size, which was used for the first time in this work, a sufficiently large selection of these functional terms was available despite the small range for t_i.

5.4.2. Polynomial Terms in Combination with Exponential Functions

The mathematical structure of polynomial terms in combination with exponential functions is illustrated by the equation

$$\phi_i^{\mathrm{r}}=n_i\delta^{d_i}\tau^{t_i}e^{-\delta^{c_i}}. \tag{5.35}$$

Terms of this type with $c_i=2$ are known as Benedict, Webb, and Rubin (BWR)-type terms, see Benedict *et al.* (1940). In an extended form, namely with density exponents up to $c_i=6$, these terms are nowadays considered to be the standard functional forms of modern wide-range equations of state. Shortly after starting the development of the new equation of state, we recognized that those terms of Eq. (5.35) with $c_i=5$ were hardly ever selected by the structure-optimization procedure if at the same time corresponding terms with the density exponent $c_i=6$ had been contained in the set of functions. Thus, during the development of the ϕ^{r} equation these terms were omitted from the bank of terms.

In order to avoid unwanted influences of the polynomial terms coupled with the exponential functions when extrapolating IAPWS-95, for the temperature exponents t_i in Eq. (5.35) only values $t_i \geqslant 1$ were used in the bank of terms.

5.4.3. Modified Gaussian Bell-Shaped Terms

Gaussian bell-shaped terms were previously used by Haar *et al.* (1982) for the IAPS-84 formulation [Kestin and Sengers (1986)], namely in the form:

$$\phi_i^{\mathrm{r}} = n_i \delta^{d_i} e^{-\alpha_i(\delta-\epsilon_i)^2-\beta_i(\tau-\gamma_i)^2}. \tag{5.36}$$

In IAPS-84 these terms proved to be less successful. For the reference equation of state for methane, Setzmann and Wagner (1991) modified these terms in two respects:

(1) The Gaussian functions [the exponential part of Eq. (5.36)] were not only combined with a polynomial in the reduced density δ, but also in the inverse reduced temperature τ.
(2) The adjustable parameters α_i, ϵ_i, β_i, and γ_i must be determined extremely carefully, because the effect of these terms is very sensitive to their values.

Thus, the modified Gaussian bell-shaped terms used in the bank of terms for the ϕ^{r} equation have the following structure:

$$\phi_i^{\mathrm{r}} = n_i \delta^{d_i} \tau^{t_i} e^{-\alpha_i(\delta-\epsilon_i)^2-\beta_i(\tau-\gamma_i)^2}. \tag{5.37}$$

Due to the strong sensitivity of these terms to the values of the parameters in the Gaussian exponential function, these parameters could not be determined automatically in the optimization and nonlinear fitting process. Therefore, these values were determined based on comprehensive precalculations and subsequent checking by nonlinearly fitting a maximum of two of them at the same time. If in this step an improvement in the combination of the parameters could be achieved, correspondingly varied combinations were included in the bank of terms for the next optimization step. This recursive procedure was repeated until a further modification of the parameters no longer produced a reduction of the sum of squares.

The incorporation of the modified Gaussian bell-shaped terms according to Eq. (5.37) had a significantly positive influence on the representation of the thermal properties in the critical region. After using these terms, the difficulties in covering the $p\rho T$ data in the entire critical region were overcome. A further important advantage of using these terms in the right way was the clear improvement in representing the caloric properties in the critical region, even though this improvement only covers reduced temperatures $T/T_{\mathrm{c}} < \approx 0.997$. When nearing the critical temperature, the equations—also with this functional type—were not able to follow the course of the experimental data of the isochoric heat capacity. Thus, a functional form had to be included into the bank of terms which could model the steep increase of c_v and the steep decrease of w when approaching the critical temperature.

5.4.4. Nonanalytical Terms

In contrast to water, there are reliable measurements of the isochoric heat capacity for carbon dioxide that clearly extend closer to the critical point than for other substances. Since these data could not be represented by equations of state which consist of functional forms described in Secs. 5.4.1–5.4.3, Span and Wagner (1996) developed special nonanalytical terms for the reference equation of state for CO_2. This type of term was also used for IAPWS-95 and is briefly described in the following, for further details see Span and Wagner (1996) and Span (2000).

According to Table 6.3, the relations between both the isochoric heat capacity c_v and the speed of sound w and the derivatives of the ideal-gas part ϕ° and the residual part ϕ^{r} of the dimensionless Helmholtz free energy ϕ read:

$$\frac{c_v}{R} = -\tau^2(\phi^\circ_{\tau\tau} + \phi^{\mathrm{r}}_{\tau\tau}), \tag{5.38}$$

$$\frac{w^2}{RT} = \underbrace{1 + 2\delta\phi^{\mathrm{r}}_\delta + \delta^2\phi^{\mathrm{r}}_{\delta\delta}}_{\sim\left(\frac{\partial p}{\partial \rho}\right)_T} - \overbrace{\frac{(1+\delta\phi^{\mathrm{r}}_\delta - \delta\tau\phi^{\mathrm{r}}_{\delta\tau})^2}{\underbrace{\tau^2(\phi^\circ_{\tau\tau}+\phi^{\mathrm{r}}_{\tau\tau})}_{-\frac{c_v}{R}}}}^{\sim\left(\frac{\partial p}{\partial T}\right)_\rho^2}, \tag{5.39}$$

where R corresponds to the specific gas constant. The quantities τ and δ used as subscripts indicate the corresponding derivative of ϕ° and ϕ^{r}, see Eq. (5.29) in Table 5.1. From Eq. (5.38) it can be seen that a divergence of c_v can be achieved when the second derivative $\phi^{\mathrm{r}}_{\tau\tau}$ becomes infinite at the critical point. (Producing a singular behavior of c_v at the critical point by making $\phi^{\mathrm{r}}_{\tau\tau}$ infinite at this point is just a mathematical tool to produce the strong increase of c_v when approaching the critical point. From very accurate and internally consistent $p\rho T$ measurements in the immediate vicinity of the critical point of SF_6 and CO_2 [Wagner *et al.* (1992), Kurzeja *et al.* (1999), Kurzeja *et al.* (2002), and Kurzeja and Wagner (2002)], it can be concluded that on earth (which means under gravity) c_v remains finite at the critical point.) Then, according to Eqs. (5.38) and (5.39), at the critical point c_v would have a singularity and w would become zero because $(\partial p/\partial T)_\rho$ has a finite value and $(\partial p/\partial \rho)_T$ also becomes zero.

Thus, the nonanalytical terms were required to fulfill the following three conditions:

(1) The derived values for $\phi^{\mathrm{r}}_{\tau\tau}$ must be finite everywhere except at the critical point.
(2) Singular behavior of the other second derivatives and all derivatives with respect to δ must be avoided everywhere. However, there are no further restrictions on the behavior of these derivatives—the *complete* equation of state has to be designed to behave in a special way and

not just one term in the equation. (Meanwhile this assumption has proved to be erroneous, see the discussion in Sec. 6.4.2.)

(3) Within the δ, τ surface of the critical region, the maximum of $\phi^{r}_{\tau\tau}$ should follow the course of the saturated vapor and saturated liquid curves in order to avoid unreasonable c_v maxima in the single-phase region near the phase boundary.

Taking these conditions into account, the nonanalytical terms to be included into the bank of terms use the following form:

$$\phi^{r}_{i} = n_i \Delta^{b_i} \delta \psi, \tag{5.40}$$

with

$$\Delta = \theta^2 + B_i[(\delta - 1)^2]^{a_i},$$

$$\theta = (1 - \tau) + A_i[(\delta - 1)^2]^{1/(2\beta_i)},$$

$$\psi = e^{-C_i(\delta - 1)^2 - D_i(\tau - 1)^2}.$$

The exponential function ψ damps the influence of this expression outside the critical region. The distance function Δ raised to the noninteger power b_i introduces the nonanalytical behavior and should ensure that the maximum in c_v follows the phase boundary. Finally, the reduced density in the product of ϕ^{r} guarantees a physically correct behavior in the low-density limit.

Besides the coefficients n_i, Eq. (5.40) introduces seven ''internal'' parameters ($A_i, B_i, C_i, D_i, a_i, b_i, \beta_i$) for each of the terms i; in principle, these parameters can be included into a nonlinear fit of the entire equation. However, because these parameters are highly correlated, a simultaneous nonlinear fit turned out to be very difficult. Thus, except for A_i and β_i, the values of these parameters were determined by a method similar to the one used for the exponents of the Gaussian bell-shaped terms, see Sec. 5.4.3. The parameters A_i and β_i of the function θ were determined at the very beginning in the following way: the value for β_i was preselected so that it had a value near that of the critical exponent corresponding to the renormalization group theory and obeyed certain relationships with the parameters a_i and b_i, for details see Span and Wagner (1996). Then, A_i was determined so that the function θ of Eq. (5.40) represents the phase boundary defined by the experimental $p_\sigma \rho' \rho'' T$ data in the critical region as well as possible. The effectiveness of this form of terms was already increased by preinvestigations with different combinations of values for the parameters within the structure-optimization process so that we could avoid refitting the parameters nonlinearly in the final stages of the development of the new equation of state.

5.4.5. Bank of Terms

Based on the general functional forms discussed in Secs. 5.4.1–5.4.4, and as a result of comprehensive preinvestigations regarding the ranges of exponents and other parameters, the general expression for the bank of terms for the residual part ϕ^{r} of the dimensionless Helmholtz free energy equation consisted of 745 terms and was of the following form:

$$\phi^{r} = \sum_{i=1}^{5} \sum_{j=-4}^{8} n_{ij} \delta^i \tau^{j/8} + e^{-\delta} \sum_{i=1}^{15} \sum_{j=1}^{16} n_{ij} \delta^i \tau^j + e^{-\delta^2} \sum_{i=1}^{12} \sum_{j=1}^{10} n_{ij} \delta^i \tau^j + e^{-\delta^3} \sum_{i=1}^{5} \sum_{j=10}^{23} n_{ij} \delta^i \tau^j + e^{-\delta^4} \sum_{i=1}^{9} \sum_{j=10}^{20} n_{ij} \delta^{2i} \tau^j + e^{-\delta^6} \sum_{i=3}^{7} \sum_{j=12}^{25} n_{ij} \delta^i \tau^{2j}$$

TABLE 5.2. Parameters of the modified Gaussian bell-shaped terms according to Eq. (5.37) which are contained in the bank of terms, Eq. (5.41)

i	d_i	t_i	α_i	β_i	γ_i	ϵ_i
1	1	0	10	150	1.21	1
2	1	1	10	150	1.21	1
3	1	2	10	150	1.21	1
4	1	3	10	150	1.21	1
5	1	4	10	150	1.21	1
6	2	0	15	150	1.21	1
7	2	1	15	150	1.21	1
8	2	2	15	150	1.21	1
9	2	3	15	150	1.21	1
10	2	4	15	150	1.21	1
11	3	0	20	150	1.21	1
12	3	1	20	150	1.21	1
13	3	2	20	150	1.21	1
14	3	3	20	150	1.21	1
15	3	4	20	150	1.21	1
16	1	0	10	200	1.23	1
17	1	1	10	200	1.23	1
18	1	2	10	200	1.23	1
19	1	3	10	200	1.23	1
20	1	4	10	200	1.23	1
21	2	0	15	200	1.23	1
22	2	1	15	200	1.23	1
23	2	2	15	200	1.23	1
24	2	3	15	200	1.23	1
25	2	4	15	200	1.23	1
26	3	0	20	200	1.23	1
27	3	1	20	200	1.23	1
28	3	2	20	200	1.23	1
29	3	3	20	200	1.23	1
30	3	4	20	200	1.23	1
31	1	0	10	250	1.25	1
32	1	1	10	250	1.25	1
33	1	2	10	250	1.25	1
34	1	3	10	250	1.25	1
35	1	4	10	250	1.25	1
36	2	0	15	250	1.25	1
37	2	1	15	250	1.25	1
38	2	2	15	250	1.25	1
39	2	3	15	250	1.25	1
40	2	4	15	250	1.25	1
41	3	0	20	250	1.25	1
42	3	1	20	250	1.25	1
43	3	2	20	250	1.25	1
44	3	3	20	250	1.25	1
45	3	4	20	250	1.25	1

$$+\sum_{i=1}^{45} n_i \delta^{d_i} \tau^{t_i} e^{-\alpha_i(\delta-\epsilon_i)^2-\beta_i(\tau-\gamma_i)^2}$$

$$+\sum_{i=1}^{1}\sum_{j=1}^{4}\sum_{k=1}^{3}\sum_{l=1}^{1}\sum_{m=1}^{3} n_{ijklm}\Delta^{b_j}\delta\psi, \qquad (5.41)$$

with

$$\Delta=\theta^2+B_k[(\delta-1)^2]^{a_i},$$

$$\theta=(1-\tau)+A[(\delta-1)^2]^{1/(2\beta)},$$

$$\psi=e^{-C_l(\delta-1)^2-D_m(\tau-1)^2}.$$

The parameters d_i, t_i, α_i, β_i, γ_i, and ϵ_i of the 45 Gaussian bell-shaped terms according to Eq. (5.37) are listed in Table 5.2. The parameters a_i, b_i, B_k, C_l, D_m, A, and β of the 36 nonanalytical terms corresponding to Eq. (5.41) are given in Table 5.3. The bank of terms given by Eq. (5.41) contains all terms from which the final equation of state for H_2O, the IAPWS-95 formulation, has been determined by the structure-optimization procedure, see Secs. 5.3.2 and 5.5.

TABLE 5.3. Parameters of the nonanalytical terms according to Eq. (5.40) which are contained in the bank of terms, Eq. (5.41)

i,j,k,l,m	a_i	b_i	B_k	C_l	D_m	A	β
1	3.5	0.8	24	0.2	700	0.32	0.3
2		0.85	28		800		
3		0.9	32		900		
4		0.95					

5.5. Determination of the Final Form of the IAPWS-95 Formulation

After the following three main tasks had been completed, the final form of IAPWS-95 could be developed:

(i) setting up the selected set of experimental data;
(ii) description of several auxiliary equations for calculating further data; and
(iii) considerations of functional forms and setting up the bank of terms for the structure-optimization procedure (see Sec. 5.3.2)

5.5.1. Summarizing Information on the Sorts of Data Used

Information on the data used to develop the IAPWS-95 formulation is summarized in Table 5.4. Details are given for the individual types of data with their independent variables. The majority of the data are directly based on measurements, but there are also so-called synthetic data calculated from corresponding auxiliary equations or from preliminary equations of state obtained during the process of developing IAPWS-95. The values of some independent variables had to be precorrelated from preliminary equations of state in order to be able to use these data in the *linear* structure optimization to determine the optimum functional structure of IAPWS-95, for details see Secs. 5.3.2 and 5.5.2. Those variables for which the values were precorrelated are marked by the superscript p.

5.5.2. Iterative Process of the Development of the IAPWS-95 Formulation

Based on the data set of which certain details are summarized in Table 5.4, the development of IAPWS-95 occurred using an iterative process. As illustrated in Fig. 5.1, this iterative process can be summarized as follows:

(1) The selected data (experimental and synthetic data, see Secs. 2 and 4) for the single-phase region and the vapor–liquid phase boundary formed the starting point of the cycle of development.

(2) Using a preliminary equation of state, or, for the thermal properties on the vapor–liquid phase boundary, the auxiliary equations (2.5)–(2.7), the nonlinear data are linearized by calculating the density ρ^p and the precorrelation factors γ^p and ϵ^p.

(3) Then all data, the original and the precorrelated data, are weighted (calculation of σ_m^2 for the sums of squares given in Table 5.1) with a preliminary equation of state.

(4) Based on the linear and linearized data (see the penultimate column of Table 5.4), the modified structure-optimization procedure of Setzmann and Wagner (1989), see also Sec. 5.3.2, yields an interim equation of state with an optimized functional structure containing, for example, 56 terms. The structure-optimization procedure works on the basis of the bank of terms, Eq. (5.41), consisting of 745 terms. By modifying the original Setzmann and Wagner method, see Sec. 5.3.2, it was possible to limit the number of terms belonging to certain functional groups of the bank of terms. In the case of IAPWS-95, the following limitations were preselected: In order to assist the extrapolation capability, the maximum number of polynomial terms was limited to 12. The number of Gaussian bell-shaped terms and nonanalytical terms were limited to six and two, respectively, in order to avoid intercorrelations in the near-critical region. The maximum total number of terms to be selected by the structure-optimization procedure was set to 58, for further details see Pruß and Wagner (1995b). The interim equation of state with the functional structure found in this way is then nonlinearly fitted to all original data, linear and nonlinear (but not to the linearized data), see the last column of Table 5.4.

(5) The optimized interim equation of state obtained in step 4 is then used to recalculate the precorrelated densities ρ^p and the precorrelation factors γ^p and ϵ^p, and for all data the weight σ_m^2 as well.

(6) Without any changes in the data set, this iteration cycle is repeated until the linearly optimized equation cannot be further improved by fitting this equation nonlinearly to the selected data set (consisting of linear and nonlinear data). Usually, 2–4 iteration cycles are needed to obtain such a result. However, if the data set is changed (e.g., change in weighting factors or in the data set itself), then the iteration process starts again from the beginning. More than 100 such iteration cycles were performed before the final form of IAPWS-95 was determined.

TABLE 5.4. Summarizing information on the selected data used in the linear optimization procedure and in the nonlinear fitting process when developing the IAPWS-95 formulation

Type of data[a]	Contribution to the sum of squares according to	For details see	Number of data: Linear structure optimization	Number of data: Nonlinear fitting
$p(\rho,T)$	Eq. (5.10)	Table 4.4	2773	2773
$p(\rho,T)$	Eq. (5.10)	Sec. 4.10	75	75
$p(\rho,T)$	Eq. (5.10)	Sec. 4.11	170	170
Phase-equilibrium condition	Eqs. (5.28a) to (5.28c)	Table 4.1	218	⋯
$p_\sigma(T)$	Eq. (5.18)	Table 4.1	⋯	109
$\rho'(T)$	Eq. (5.19)	Table 4.1	⋯	109
$\rho''(T)$	Eq. (5.20)	Table 4.1	⋯	35
$B(T)$	Eq. (5.12)	Sec. 4.10	10	10
$c_v(\rho,T)$	Eq. (5.11)	Table 4.6	113	113
$c_v(\rho,T)$	Eq. (5.11)	Sec. 4.10	75	75
$c_v(\rho,T)$	Eq. (5.11)	Sec. 4.11	176	176
$c_p(\rho^{\mathrm{p}},T,\epsilon^{\mathrm{p}})$	Eq. (5.24)	Table 4.8	947	⋯
$c_p(p,T)$	Eq. (5.14)	Table 4.8	⋯	947
$c'_p(\rho'^{\mathrm{p}},T,\epsilon^{\mathrm{p}})$	Eq. (5.24)	Table 4.3	36	⋯
$c'_p(T)$	Eq. (5.14)	Table 4.3	⋯	36
$c''_p(\rho''^{\mathrm{p}},T,\epsilon^{\mathrm{p}})$	Eq. (5.24)	Table 4.3	36	⋯
$c''_p(T)$	Eq. (5.14)	Table 4.3	⋯	36
$w(\rho^{\mathrm{p}},T,\gamma^{\mathrm{p}})$	Eq. (5.23)	Table 4.5	652	⋯
$w(p,T)$	Eq. (5.13)	Table 4.5	⋯	652
$w(\rho^{\mathrm{p}},T,\gamma^{\mathrm{p}})$	Eq. (5.23)	Sec. 4.10	75	⋯
$w(p,T)$	Eq. (5.13)	Sec. 4.10	⋯	75
$w'(\rho'^{\mathrm{p}},T,\gamma^{\mathrm{p}})$	Eq. (5.23)	Table 4.3	108	⋯
$w'(T)$	Eq. (5.13)	Table 4.3	⋯	108
$w''(\rho''^{\mathrm{p}},T,\gamma^{\mathrm{p}})$	Eq. (5.23)	Table 4.3	50	⋯
$w''(T)$	Eq. (5.13)	Table 4.3	⋯	50
$\Delta h(\rho^{\mathrm{p}},T)$	Eq. (5.25)	Table 4.9	284	⋯
$\Delta h(p,T)$	Eq. (5.15)	Table 4.9	⋯	284
$\Delta u'(\rho_2'^{\mathrm{p}},T_2,\rho_1'^{\mathrm{p}},T_1)$	Eq. (5.26)	Table 4.2	74	⋯
$\Delta u'(T_2,T_1)$	Eq. (5.21)	Table 4.2	⋯	74
$[u''-u'](\rho''^{\mathrm{p}},\rho'^{\mathrm{p}},T)$	Eq. (5.27)	Table 4.2	75	⋯
$[u''-u'](T)$	Eq. (5.22)	Table 4.2	⋯	75
$\mu(p,T)$	Eq. (5.16)	Table 4.9	⋯	234
$\delta_T(p,T)$	Eq. (5.17)	Table 4.9	⋯	180
	Total number of data points:		5947	6396

[a]The superscript p at some independent variables means ''precorrelated value,'' for details see Sec. 5.3.2.

Figure 5.1 is specially designed for the development of IAPWS-95 based on the data set described in Table 5.4. If, for example, for other substances, other types of data should be taken into account, such data can easily be included in this scheme of development; examples for such data might be third virial coefficients, internal energies of the single-phase region, linearized data of the Joule–Thomson coefficient, etc.

By carrying out steps 1–6 mentioned above, the final equation of state for H_2O, the IAPWS-95 formulation, was determined. All the numerical information on IAPWS-95 necessary to use this new standard equation is summarized in Sec. 6.

6. The IAPWS-95 Formulation

This section presents the new international standard equation of state for H_2O, the ''IAPWS Formulation 1995 for the Thermodynamic Properties of Ordinary Water Substance for General and Scientific Use'' referred to in the following as the IAPWS-95 formulation or IAPWS-95 for short. All numerical details needed for the use of IAPWS-95 are given, and statements on the range of validity and estimates of uncertainty are made. In this respect, this section essentially corresponds to the content of the IAPWS release on this

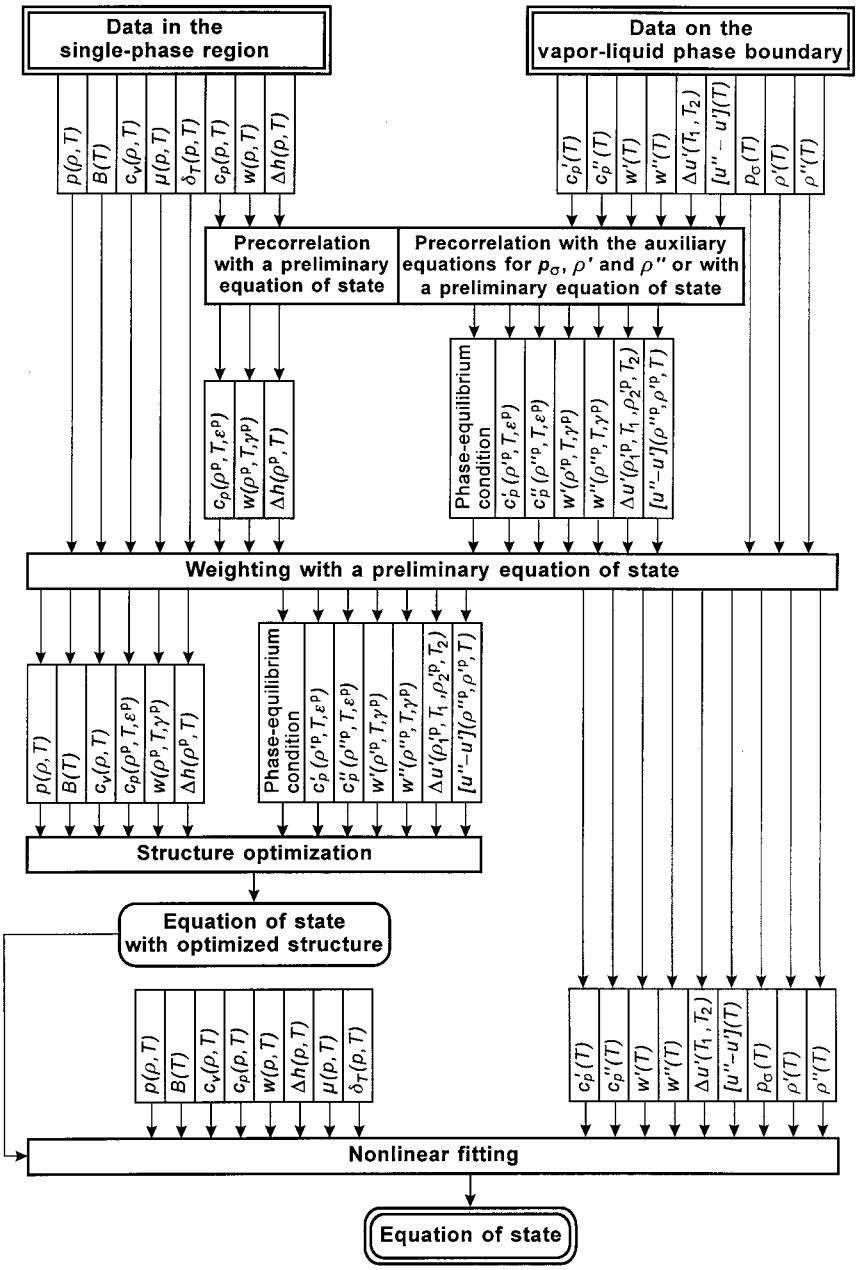

FIG. 5.1. Scheme of one step of the entire iteration cycle to develop the residual part ϕ^r of IAPWS-95, Eq. (6.6).

formulation [IAPWS (1996)] and gives some further information. Details of the development of the IAPWS-95 formulation are summarized in Sec. 5.

6.1. Reference Constants

The so-called reference constants needed for evaluating the IAPWS-95 formulation are:

$$T_c = 647.096 \ \text{K}, \tag{6.1}$$

$$\rho_c = 322 \ \text{kg m}^{-3}, \tag{6.2}$$

$$R = 0.461\,518\,05 \ \text{kJ kg}^{-1}\,\text{K}^{-1}. \tag{6.3}$$

The values for the critical temperature T_c and the critical density ρ_c are identical to those given in Eqs. (2.2a) and (2.2c). The value of the specific gas constant R is derived from values of the molar gas constant R_m [Taylor *et al.* (1969)] and the molar mass M [Kell (1977)], which differ slightly from the accepted values of these quantities at the time when the IAPWS-95 formulation was developed and from the current values $R_m = 8.314\,472 \ \text{J mol}^{-1}\,\text{K}^{-1}$ [Mohr and Taylor (1999)] and $M = 18.015\,268 \ \text{g mol}^{-1}$. This value for M results from the molar masses of the stable isotopes of hydrogen and oxygen given by Audi and Wapstra (1993) and the isotopic composition of VSMOW. (As a result of a recent investigation carried out by Harvey (1998), IAPWS recommends that VSMOW be used as the standard definition of

''ordinary water substance'' [IAPWS (2001)]. The isotopic composition of VSMOW is documented by Gonfiantini (1978) and is also given in the IAPWS guideline [IAPWS (2001)]; samples of VSMOW are available from the International Atomic Energy Agency (IAEA) in Vienna, Austria. Although IAPWS-95 is not based on the current M value for VSMOW, one may say that IAPWS-95 is not in conflict with this value. The only property which is measured so accurately that the value of the molar mass is indeed of importance is the liquid density at atmospheric pressure. The highly accurate measurements of this quantity are represented by IAPWS-95 to within their experimental uncertainties, see Sec. 7.2.1.2.) The use of the current values for R_m and M would yield a specific gas constant which is greater than the value given in Eq. (6.3) by $5.6 \times 10^{-6}\,\mathrm{kJ\,kg^{-1}\,K^{-1}}$. Density in the ideal-gas limit calculated from Eq. (6.4) is therefore off by 6 ppm. However, since the value of R in Eq. (6.3) has been used in determining the coefficients in the residual part ϕ^r, Eq. (6.6), then this value of R must be used in obtaining property values from the IAPWS-95 formulation, Eq. (6.4).

By using the *specific* gas constant, Eq. (6.4) corresponds to a mass-based formulation. In order to convert values of specific properties to molar properties, the most recent value for the molar mass of VSMOW must be used; at present it is the M value given above.

6.2. Numerical Description of the IAPWS-95 Formulation

The IAPWS-95 formulation is a fundamental equation for the specific Helmholtz free energy f. This equation is expressed in dimensionless form, $\phi = f/(RT)$, and is separated into two parts, an ideal-gas part ϕ° and a residual part ϕ^r, so that:

$$\frac{f(\rho,T)}{RT} = \phi(\delta,\tau) = \phi^\circ(\delta,\tau) + \phi^r(\delta,\tau), \qquad (6.4)$$

where $\delta = \rho/\rho_c$ and $\tau = T_c/T$ with T_c, ρ_c, and R given by Eqs. (6.1)–(6.3).

The equation for the ideal-gas part ϕ° of the dimensionless Helmholtz free energy has been obtained from the equation for the specific isobaric heat capacity in the ideal-gas state c_p°, Eq. (5.6), which was developed by Cooper (1982); for details see Sec. 5.2. The corresponding equation for ϕ° reads:

$$\phi^\circ = \ln\delta + n_1^\circ + n_2^\circ\tau + n_3^\circ \ln\tau + \sum_{i=4}^{8} n_i^\circ \ln[1 - e^{-\gamma_i^\circ \tau}], \qquad (6.5)$$

for the definition of δ and τ see Eq. (6.4). The coefficients of Eq. (6.5) are listed in Table 6.1.

The form of the residual part ϕ^r of the dimensionless Helmholtz free energy is as follows:

TABLE 6.1. Coefficients of Eq. (6.5)[a]

i	n_i°	γ_i°	i	n_i°	γ_i°
1	−8.320 446 482 01	⋯	5	0.973 15	3.537 342 22
2	6.683 210 526 8	⋯	6	1.279 50	7.740 737 08
3	3.006 32	⋯	7	0.969 56	9.244 377 96
4	0.012 436	1.287 289 67	8	0.248 73	27.507 510 5

[a]The values of the coefficients n_3° to n_8° and γ_i° are also valid for Eq. (5.6).

$$\phi^r = \sum_{i=1}^{7} n_i \delta^{d_i}\tau^{t_i} + \sum_{i=8}^{51} n_i \delta^{d_i}\tau^{t_i} e^{-\delta^{c_i}} + \sum_{i=52}^{54} n_i \delta^{d_i}\tau^{t_i} e^{-\alpha_i(\delta-\epsilon_i)^2 - \beta_i(\tau-\gamma_i)^2} + \sum_{i=55}^{56} n_i \Delta^{b_i}\delta\psi \qquad (6.6)$$

with

$$\Delta = \theta^2 + B_i[(\delta-1)^2]^{a_i},$$
$$\theta = (1-\tau) + A_i[(\delta-1)^2]^{1/(2\beta_i)},$$
$$\psi = e^{-C_i(\delta-1)^2 - D_i(\tau-1)^2},$$

for the definition of δ and τ see Eq. (6.4). The coefficients and exponents of Eq. (6.6) are listed in Table 6.2; for the determination of these values see Sec. 5.5.

All thermodynamic properties can be derived from Eq. (6.4) by using the appropriate combinations of the ideal-gas part ϕ°, Eq. (6.5), and the residual part ϕ^r, Eq. (6.6), of the dimensionless Helmholtz free energy, and the derivatives of ϕ° and ϕ^r. Relations between thermodynamic properties and ϕ° and ϕ^r and their derivatives are summarized in Table 6.3. All required derivatives of the ideal-gas part and of the residual part of the dimensionless Helmholtz free energy are explicitly given in Tables 6.4 and 6.5, respectively.

Since the 5th International Conference on the Properties of Steam in London in 1956, the specific internal energy and the specific entropy of the saturated liquid at the triple point have been arbitrarily set equal to zero. Thus, at the triple-point temperature $T_t = 273.16\,\mathrm{K}$:

$$u_t' = 0, \quad s_t' = 0. \qquad (6.7)$$

The coefficients n_1° and n_2° in Eq. (6.5) have been adjusted to meet this condition. Consequently, after calculating for T_t the saturated liquid density ρ_t' via the phase-equilibrium condition [see Eqs. (6.9a)–(6.9c)], Eq. (6.4) yields for the specific enthalpy of the saturated liquid at the triple point:

$$h_t' = 0.611\,872 \ \ \mathrm{J\,kg^{-1}}. \qquad (6.8)$$

In the liquid–water region, small changes in density along an isotherm cause large changes in pressure. For this reason, due to an accumulation of small errors, a particular computer code may fail to return the zeros in Eq. (6.7) for the saturated liquid at the triple-point temperature. In order to avoid this, it is advisable to readjust the constants n_1° and n_2° in Eq. (6.5) by imposing the condition $u_t' = 0$, $s_t' = 0$ with the desired accuracy.

TABLE 6.2. Coefficients and exponents of Eq. (6.6)

i	c_i	d_i	t_i	n_i
1	⋯	1	−0.5	$0.125\,335\,479\,355\,23\times10^{-1}$
2	⋯	1	0.875	$0.789\,576\,347\,228\,28\times10^{1}$
3	⋯	1	1	$-0.878\,032\,033\,035\,61\times10^{1}$
4	⋯	2	0.5	0.318 025 093 454 18
5	⋯	2	0.75	−0.261 455 338 593 58
6	⋯	3	0.375	$-0.781\,997\,516\,879\,81\times10^{-2}$
7	⋯	4	1	$0.880\,894\,931\,021\,34\times10^{-2}$
8	1	1	4	−0.668 565 723 079 65
9	1	1	6	0.204 338 109 509 65
10	1	1	12	$-0.662\,126\,050\,396\,87\times10^{-4}$
11	1	2	1	−0.192 327 211 560 02
12	1	2	5	−0.257 090 430 034 38
13	1	3	4	0.160 748 684 862 51
14	1	4	2	$-0.400\,928\,289\,258\,07\times10^{-1}$
15	1	4	13	$0.393\,434\,226\,032\,54\times10^{-6}$
16	1	5	9	$-0.759\,413\,770\,881\,44\times10^{-5}$
17	1	7	3	$0.562\,509\,793\,518\,88\times10^{-3}$
18	1	9	4	$-0.156\,086\,522\,571\,35\times10^{-4}$
19	1	10	11	$0.115\,379\,964\,229\,51\times10^{-8}$
20	1	11	4	$0.365\,821\,651\,442\,04\times10^{-6}$
21	1	13	13	$-0.132\,511\,800\,746\,68\times10^{-11}$
22	1	15	1	$-0.626\,395\,869\,124\,54\times10^{-9}$
23	2	1	7	−0.107 936 009 089 32
24	2	2	1	$0.176\,114\,910\,087\,52\times10^{-1}$
25	2	2	9	0.221 322 951 675 46
26	2	2	10	−0.402 476 697 635 28
27	2	3	10	0.580 833 999 857 59
28	2	4	3	$0.499\,691\,469\,908\,06\times10^{-2}$
29	2	4	7	$-0.313\,587\,007\,125\,49\times10^{-1}$
30	2	4	10	−0.743 159 297 103 41
31	2	5	10	0.478 073 299 154 80
32	2	6	6	$0.205\,279\,408\,959\,48\times10^{-1}$
33	2	6	10	−0.136 364 351 103 43
34	2	7	10	$0.141\,806\,344\,006\,17\times10^{-1}$
35	2	9	1	$0.833\,265\,048\,807\,13\times10^{-2}$
36	2	9	2	$-0.290\,523\,360\,095\,85\times10^{-1}$
37	2	9	3	$0.386\,150\,855\,742\,06\times10^{-1}$
38	2	9	4	$-0.203\,934\,865\,137\,04\times10^{-1}$
39	2	9	8	$-0.165\,540\,500\,637\,34\times10^{-2}$
40	2	10	6	$0.199\,555\,719\,795\,41\times10^{-2}$
41	2	10	9	$0.158\,703\,083\,241\,57\times10^{-3}$
42	2	12	8	$-0.163\,885\,683\,425\,30\times10^{-4}$
43	3	3	16	$0.436\,136\,157\,238\,11\times10^{-1}$
44	3	4	22	$0.349\,940\,054\,637\,65\times10^{-1}$
45	3	4	23	$-0.767\,881\,978\,446\,21\times10^{-1}$
46	3	5	23	$0.224\,462\,773\,320\,06\times10^{-1}$
47	4	14	10	$-0.626\,897\,104\,146\,85\times10^{-4}$
48	6	3	50	$-0.557\,111\,185\,656\,45\times10^{-9}$
49	6	6	44	−0.199 057 183 544 08
50	6	6	46	0.317 774 973 307 38
51	6	6	50	−0.118 411 824 259 81

i	c_i	d_i	t_i	n_i	α_i	β_i	γ_i	ϵ_i
52	⋯	3	0	$-0.313\,062\,603\,234\,35\times10^{2}$	20	150	1.21	1
53	⋯	3	1	$0.315\,461\,402\,377\,81\times10^{2}$	20	150	1.21	1
54	⋯	3	4	$-0.252\,131\,543\,416\,95\times10^{4}$	20	250	1.25	1

i	a_i	b_i	B_i	n_i	C_i	D_i	A_i	β_i
55	3.5	0.85	0.2	−0.148 746 408 567 24	28	700	0.32	0.3
56	3.5	0.95	0.2	0.318 061 108 784 44	32	800	0.32	0.3

TABLE 6.3. Relations of thermodynamic properties to the ideal-gas part ϕ°, Eq. (6.5), and the residual part ϕ^r, Eq. (6.6), of the dimensionless Helmholtz free energy and their derivatives[a]

Property	Relation
Pressure $p=\rho^2(\partial f/\partial\rho)_T$	$\dfrac{p(\delta,\tau)}{\rho RT}=1+\delta\phi^r_\delta$
Entropy $s=-(\partial f/\partial T)_\rho$	$\dfrac{s(\delta,\tau)}{R}=\tau(\phi^\circ_\tau+\phi^r_\tau)-\phi^\circ-\phi^r$
Internal energy $u=f+Ts$	$\dfrac{u(\delta,\tau)}{RT}=\tau(\phi^\circ_\tau+\phi^r_\tau)$
Enthalpy $h=u+pv$	$\dfrac{h(\delta,\tau)}{RT}=1+\tau(\phi^\circ_\tau+\phi^r_\tau)+\delta\phi^r_\delta$
Gibbs free energy $g=h-Ts$	$\dfrac{g(\delta,\tau)}{RT}=1+\phi^\circ+\phi^r+\delta\phi^r_\delta$
Isochoric heat capacity $c_v=(\partial u/\partial T)_\rho$	$\dfrac{c_v(\delta,\tau)}{R}=-\tau^2(\phi^\circ_{\tau\tau}+\phi^r_{\tau\tau})$
Isobaric heat capacity $c_p=(\partial h/\partial T)_p$	$\dfrac{c_p(\delta,\tau)}{R}=-\tau^2(\phi^\circ_{\tau\tau}+\phi^r_{\tau\tau})+\dfrac{(1+\delta\phi^r_\delta-\delta\tau\phi^r_{\delta\tau})^2}{1+2\delta\phi^r_\delta+\delta^2\phi^r_{\delta\delta}}$
Saturated liquid heat capacity $c_\sigma(T)=(\partial h/\partial T)_p+T(\partial p/\partial T)_\rho$ $\cdot(\mathrm{d}p_\sigma/\mathrm{d}T)/(-\rho^2(\partial p/\partial\rho)_T)\big\vert_{\rho=\rho'}$	$\dfrac{c_\sigma(\tau)}{R}=-\tau^2(\phi^\circ_{\tau\tau}+\phi^r_{\tau\tau})+\dfrac{1+\delta'\phi^r_\delta-\delta'\tau\phi^r_{\delta\tau}}{1+2\delta'\phi^r_\delta+\delta'^2\phi^r_{\delta\delta}}$ $\cdot\left[(1+\delta'\phi^r_\delta-\delta'\tau\phi^r_{\delta\tau})-\dfrac{\rho_c}{R\delta'}\dfrac{\mathrm{d}p_\sigma}{\mathrm{d}T}\right]$ [b]
Speed of sound $w=(\partial p/\partial\rho)_s^{1/2}$	$\dfrac{w^2(\delta,\tau)}{RT}=1+2\delta\phi^r_\delta+\delta^2\phi^r_{\delta\delta}-\dfrac{(1+\delta\phi^r_\delta-\delta\tau\phi^r_{\delta\tau})^2}{\tau^2(\phi^\circ_{\tau\tau}+\phi^r_{\tau\tau})}$
Joule–Thomson coefficient $\mu=(\partial T/\partial p)_h$	$\mu R\rho=\dfrac{-(\delta\phi^r_\delta+\delta^2\phi^r_{\delta\delta}+\delta\tau\phi^r_{\delta\tau})}{(1+\delta\phi^r_\delta-\delta\tau\phi^r_{\delta\tau})^2-\tau^2(\phi^\circ_{\tau\tau}+\phi^r_{\tau\tau})(1+2\delta\phi^r_\delta+\delta^2\phi^r_{\delta\delta})}$
Isothermal throttling coefficient $\delta_T=(\partial h/\partial p)_T$	$\delta_T\rho=1-\dfrac{1+\delta\phi^r_\delta-\delta\tau\phi^r_{\delta\tau}}{1+2\delta\phi^r_\delta+\delta^2\phi^r_{\delta\delta}}$
Isentropic temperature-pressure coefficient $\beta_s=(\partial T/\partial p)_s$	$\beta_s\rho R=\dfrac{1+\delta\phi^r_\delta-\delta\tau\phi^r_{\delta\tau}}{(1+\delta\phi^r_\delta-\delta\tau\phi^r_{\delta\tau})^2-\tau^2(\phi^\circ_{\tau\tau}+\phi^r_{\tau\tau})(1+2\delta\phi^r_\delta+\delta^2\phi^r_{\delta\delta})}$
Second virial coefficient $B(T)=\lim_{\rho\to0}(\partial(p/(\rho RT))/\partial\rho)_T$	$B(\tau)\rho_c=\lim_{\delta\to0}\phi^r_\delta(\delta,\tau)$
Third virial coefficient $C(T)=\lim_{\rho\to0}\left[\frac{1}{2}(\partial^2(p/(\rho RT))/\partial\rho^2)_T\right]$	$C(\tau)\rho_c^2=\lim_{\delta\to0}\phi^r_{\delta\delta}(\delta,\tau)$

[a] $\phi^r_\delta=\left[\dfrac{\partial\phi^r}{\partial\delta}\right]_\tau$, $\phi^r_{\delta\delta}=\left[\dfrac{\partial^2\phi^r}{\partial\delta^2}\right]_\tau$, $\phi^r_\tau=\left[\dfrac{\partial\phi^r}{\partial\tau}\right]_\delta$, $\phi^r_{\tau\tau}=\left[\dfrac{\partial^2\phi^r}{\partial\tau^2}\right]_\delta$, $\phi^r_{\delta\tau}=\left[\dfrac{\partial^2\phi^r}{\partial\delta\partial\tau}\right]$, $\phi^\circ_\tau=\left[\dfrac{\partial\phi^\circ}{\partial\tau}\right]_\delta$, $\phi^\circ_{\tau\tau}=\left[\dfrac{\partial^2\phi^\circ}{\partial\tau^2}\right]_\delta$.

[b] $\dfrac{\mathrm{d}p_\sigma}{\mathrm{d}T}=\dfrac{\rho''\cdot\rho'}{\rho''-\rho'}R\left[\ln\left(\dfrac{\rho''}{\rho'}\right)+\phi^r(\tau,\delta'')-\phi^r(\tau,\delta')-\tau(\phi^r_\tau(\tau,\delta'')-\phi^r_\tau(\tau,\delta'))\right]$.

Besides the single-phase region, the IAPWS-95 formulation, Eq. (6.4), also covers the vapor–liquid phase boundary. The calculation of properties along this phase boundary is based on the phase-equilibrium condition, which, in connection with Eq. (6.6), reads:

$$\frac{p_\sigma}{RT\rho'}=1+\delta'\phi^r_\delta(\delta',\tau), \tag{6.9a}$$

$$\frac{p_\sigma}{RT\rho''}=1+\delta''\phi^r_\delta(\delta'',\tau), \tag{6.9b}$$

$$\frac{p_\sigma}{RT}\left(\frac{1}{\rho''}-\frac{1}{\rho'}\right)-\ln\left(\frac{\rho'}{\rho''}\right)=\phi^r(\delta',\tau)-\phi^r(\delta'',\tau). \tag{6.9c}$$

TABLE 6.4. The ideal-gas part ϕ°, Eq. (6.5), of the dimensionless Helmholtz free energy and its derivatives[a]

$$\phi^\circ = \ln\delta + n_1^\circ + n_2^\circ\tau + n_3^\circ \ln\tau + \sum_{i=4}^{8} n_i^\circ \ln(1-e^{-\gamma_i^\circ\tau})$$

$$\phi_\delta^\circ = 1/\delta + 0 + 0 + 0 + 0$$

$$\phi_{\delta\delta}^\circ = -1/\delta^2 + 0 + 0 + 0 + 0$$

$$\phi_\tau^\circ = 0 + 0 + n_2^\circ + n_3^\circ/\tau + \sum_{i=4}^{8} n_i^\circ\gamma_i^\circ[(1-e^{-\gamma_i^\circ\tau})^{-1} - 1]$$

$$\phi_{\tau\tau}^\circ = 0 + 0 + 0 - n_3^\circ/\tau^2 - \sum_{i=4}^{8} n_i^\circ(\gamma_i^\circ)^2 e^{-\gamma_i^\circ\tau}(1-e^{-\gamma_i^\circ\tau})^{-2}$$

$$\phi_{\delta\tau}^\circ = 0 + 0 + 0 + 0 + 0$$

[a] $\phi_\delta^\circ = \left[\frac{\partial\phi^\circ}{\partial\delta}\right]_\tau$, $\phi_{\delta\delta}^\circ = \left[\frac{\partial^2\phi^\circ}{\partial\delta^2}\right]_\tau$, $\phi_\tau^\circ = \left[\frac{\partial\phi^\circ}{\partial\tau}\right]_\delta$, $\phi_{\tau\tau}^\circ = \left[\frac{\partial^2\phi^\circ}{\partial\tau^2}\right]_\delta$, $\phi_{\delta\tau}^\circ = \left[\frac{\partial^2\phi^\circ}{\partial\delta\partial\tau}\right]$.

These equations represent the equality of pressure, temperature, and specific Gibbs free energy (Maxwell criterion) in the coexisting vapor and liquid phases; for an explanation of the quantities ϕ_δ^r see the footnote of Table 6.5. For a given saturation temperature, after iterative solution of Eqs. (6.9a)–(6.9c), Eq. (6.4) yields the thermal saturation properties p_σ, ρ', and ρ''. Then, all the other saturation properties can be derived from Eq. (6.4). In this way, the properties calculated on the vapor–liquid phase boundary are thermodynamically consistent with the properties of the single-phase region.

Moreover, Eq. (6.4) meets the conditions at the critical point, i.e., it reproduces the critical parameters T_c, p_c, and ρ_c according to Eqs. (2.2a)–(2.2c) and yields zero for the first and second partial derivative of pressure with respect to density at the critical point.

6.3. Basic Information on the Application of the IAPWS-95 Formulation

In this subsection brief statements on the range of validity, estimates of uncertainty, and computer-program verification of IAPWS-95, Eq. (6.4), are made. Comprehensive comparisons of IAPWS-95 with experimental data and other equations of state are shown in Sec. 7.

6.3.1. Range of Validity

As a result of comprehensive tests carried out by IAPWS, the following statements on the validity of IAPWS-95 can be made:

(1) The formulation is valid in the entire stable fluid region of H_2O from the melting curve [see Eqs. (2.16)–(2.19)] to 1273 K at pressures up to 1000 MPa; the lowest temperature on the melting curve is 251.165 K (at 209.9 MPa). Figure 6.1 illustrates the range of validity of IAPWS-95 in a $p-T$ diagram. In this entire region, Eq. (6.4) represents the experimental data available at the time the release on IAPWS-95 [IAPWS (1996)] was prepared (except for a very few data points) to within their uncertainties. Although Eq. (6.4) is also in satisfactory agreement with the experimental data in the critical region, the equation has some unsatisfactory features in the immediate vicinity of the critical point. These features involve second order and higher derivatives of the dimensionless Helmholtz free energy and properties obtained from them. Specifically, the isothermal compressibility $[\kappa_T = \rho^{-1}(\partial\rho/\partial p)_T]$, and the specific isobaric heat capacity c_p exhibit unphysical behavior (indentations) which occurs in a region from T_c to 5 K above T_c for densities $\pm 0.5\%$ from ρ_c. (The value of 5 K is given in the release on IAPWS-95 [IAPWS (1996)]. However, comprehensive investigations carried out after 1996 showed that the temperature range where this weakness occurs noticeably extends only from T_c to 2 K above T_c [see Figs. 6.11 and 6.12].) In addition, within a temperature range from 20 mK below T_c up to T_c, the isochoric heat capacity c_v exhibits a maximum and the speed of sound w exhibits a minimum not at the saturation temperature T_σ of the corresponding isochore (as it should be) but in the single-phase region up to 2.5 mK above T_σ. Details of this behavior, which is of no relevance for the vast majority of applications of IAPWS-95, are given in Sec. 6.4.

(2) In the stable fluid region, the IAPWS-95 formulation can also be extrapolated beyond the limits given under item (1). Tests showed that Eq. (6.4) behaves reasonably when extrapolated to pressures up to about 100 GPa and temperatures up to about 5000 K. This holds at least for the density and enthalpy of undissociated H_2O. In the gas region at pressures below the triple-point pressure, Eq. (6.4) behaves reasonably when extrapolated to the sublimation curve [see Eq. (2.21)] for temperatures down to 200 K. Due to the extremely low densities in this region which go down to about $10^{-6}\,\mathrm{kg\,m^{-3}}$, attention must be paid to numerical problems.

(3) As far as can be tested with experimental data, the formulation behaves reasonably when extrapolated into the metastable regions. Equation (6.4) represents the currently available experimental data for the subcooled liquid and for the superheated liquid to within the experimental uncertainty. In the case of the subcooled vapor, no experimental data are available. In this region, for pressures below 10 MPa, Eq. (6.4) produces reasonable values close to the saturated vapor line. For calculations further away from the saturated vapor line, the gas equation, Eq. (3.2), should be used instead of Eq. (6.4). For further details, see Sec. 7.3.2.

6.3.2. Estimates of Uncertainty

Estimates have been made of the uncertainty of the density, speed of sound, and isobaric heat capacity when calculated from the IAPWS-95 formulation, Eq. (6.4). These estimates were derived from comparisons with the various sets of experimental data together with the assessment of the Working Group on Thermophysical Properties of Water and Steam of IAPWS.

For the single-phase region, these tolerances are indicated in Figs. 6.1–6.3, which give the estimated uncertainties in various areas. As used here, ''tolerance'' means the range of

TABLE 6.5. The residual part ϕ^r, Eq. (6.6), of the dimensionless Helmholtz free energy and its derivatives[a]

$$\phi^r = \sum_{i=1}^{7} n_i \delta^{d_i} \tau^{t_i} + \sum_{i=8}^{51} n_i \delta^{d_i} \tau^{t_i} e^{-\delta^{c_i}} + \sum_{i=52}^{54} n_i \delta^{d_i} \tau^{t_i} e^{-\alpha_i(\delta-\epsilon_i)^2 - \beta_i(\tau-\gamma_i)^2} + \sum_{i=55}^{56} n_i \Delta^{b_i} \delta\psi$$

with $\Delta = \theta^2 + B_i[(\delta-1)^2]^{a_i}$

$\theta = (1-\tau) + A_i[(\delta-1)^2]^{1/(2\beta_i)}$

$\psi = e^{-C_i(\delta-1)^2 - D_i(\tau-1)^2}$

$$\phi^r_\delta = \sum_{i=1}^{7} n_i d_i \delta^{d_i-1} \tau^{t_i} + \sum_{i=8}^{51} n_i e^{-\delta^{c_i}} [\delta^{d_i-1} \tau^{t_i} (d_i - c_i \delta^{c_i})]$$
$$+ \sum_{i=52}^{54} n_i \delta^{d_i} \tau^{t_i} e^{-\alpha_i(\delta-\epsilon_i)^2 - \beta_i(\tau-\gamma_i)^2} \left[\frac{d_i}{\delta} - 2\alpha_i(\delta-\epsilon_i) \right]$$
$$+ \sum_{i=55}^{56} n_i \left[\Delta^{b_i} \left(\psi + \delta \frac{\partial\psi}{\partial\delta} \right) + \frac{\partial \Delta^{b_i}}{\partial\delta} \delta\psi \right]$$

$$\phi^r_{\delta\delta} = \sum_{i=1}^{7} n_i d_i (d_i - 1) \delta^{d_i-2} \tau^{t_i} + \sum_{i=8}^{51} n_i e^{-\delta^{c_i}} [\delta^{d_i-2} \tau^{t_i} ((d_i - c_i \delta^{c_i})(d_i - 1 - c_i \delta^{c_i}) - c_i^2 \delta^{c_i})]$$
$$+ \sum_{i=52}^{54} n_i \tau^{t_i} e^{-\alpha_i(\delta-\epsilon_i)^2 - \beta_i(\tau-\gamma_i)^2} \cdot [-2\alpha_i \delta^{d_i} + 4\alpha_i^2 \delta^{d_i} (\delta-\epsilon_i)^2 - 4 d_i \alpha_i \delta^{d_i-1} (\delta-\epsilon_i) + d_i (d_i - 1) \delta^{d_i-2}]$$
$$+ \sum_{i=55}^{56} n_i \left[\Delta^{b_i} \left(2 \frac{\partial\psi}{\partial\delta} + \delta \frac{\partial^2\psi}{\partial\delta^2} \right) + 2 \frac{\partial \Delta^{b_i}}{\partial\delta} \left(\psi + \delta \frac{\partial\psi}{\partial\delta} \right) + \frac{\partial^2 \Delta^{b_i}}{\partial\delta^2} \delta\psi \right]$$

$$\phi^r_\tau = \sum_{i=1}^{7} n_i t_i \delta^{d_i} \tau^{t_i-1} + \sum_{i=8}^{51} n_i t_i \delta^{d_i} \tau^{t_i-1} e^{-\delta^{c_i}} + \sum_{i=52}^{54} n_i \delta^{d_i} \tau^{t_i} e^{-\alpha_i(\delta-\epsilon_i)^2 - \beta_i(\tau-\gamma_i)^2} \left[\frac{t_i}{\tau} - 2\beta_i(\tau-\gamma_i) \right]$$
$$+ \sum_{i=55}^{56} n_i \delta \left[\frac{\partial \Delta^{b_i}}{\partial\tau} \psi + \Delta^{b_i} \frac{\partial\psi}{\partial\tau} \right]$$

$$\phi^r_{\tau\tau} = \sum_{i=1}^{7} n_i t_i (t_i - 1) \delta^{d_i} \tau^{t_i-2} + \sum_{i=8}^{51} n_i t_i (t_i - 1) \delta^{d_i} \tau^{t_i-2} e^{-\delta^{c_i}}$$
$$+ \sum_{i=52}^{54} n_i \delta^{d_i} \tau^{t_i} e^{-\alpha_i(\delta-\epsilon_i)^2 - \beta_i(\tau-\gamma_i)^2} \left[\left(\frac{t_i}{\tau} - 2\beta_i(\tau-\gamma_i) \right)^2 - \frac{t_i}{\tau^2} - 2\beta_i \right]$$
$$+ \sum_{i=55}^{56} n_i \delta \left[\frac{\partial^2 \Delta^{b_i}}{\partial\tau^2} \psi + 2 \frac{\partial \Delta^{b_i}}{\partial\tau} \frac{\partial\psi}{\partial\tau} + \Delta^{b_i} \frac{\partial^2\psi}{\partial\tau^2} \right]$$

$$\phi^r_{\delta\tau} = \sum_{i=1}^{7} n_i d_i t_i \delta^{d_i-1} \tau^{t_i-1} + \sum_{i=8}^{51} n_i t_i \delta^{d_i-1} \tau^{t_i-1} (d_i - c_i \delta^{c_i}) e^{-\delta^{c_i}}$$
$$+ \sum_{i=52}^{54} n_i \delta^{d_i} \tau^{t_i} e^{-\alpha_i(\delta-\epsilon_i)^2 - \beta_i(\tau-\gamma_i)^2} \left[\frac{d_i}{\delta} - 2\alpha_i(\delta-\epsilon_i) \right] \left[\frac{t_i}{\tau} - 2\beta_i(\tau-\gamma_i) \right]$$
$$+ \sum_{i=55}^{56} n_i \left[\Delta^{b_i} \left(\frac{\partial\psi}{\partial\tau} + \delta \frac{\partial^2\psi}{\partial\delta\partial\tau} \right) + \delta \frac{\partial \Delta^{b_i}}{\partial\delta} \frac{\partial\psi}{\partial\tau} + \frac{\partial \Delta^{b_i}}{\partial\tau} \left(\psi + \delta \frac{\partial\psi}{\partial\delta} \right) + \frac{\partial^2 \Delta^{b_i}}{\partial\delta\partial\tau} \delta\psi \right]$$

Derivatives of the distance function Δ^{b_i}:

$$\frac{\partial \Delta^{b_i}}{\partial\delta} = b_i \Delta^{b_i-1} \frac{\partial\Delta}{\partial\delta}$$

$$\frac{\partial^2 \Delta^{b_i}}{\partial\delta^2} = b_i \left\{ \Delta^{b_i-1} \frac{\partial^2\Delta}{\partial\delta^2} + (b_i - 1) \Delta^{b_i-2} \left(\frac{\partial\Delta}{\partial\delta} \right)^2 \right\}$$

$$\frac{\partial \Delta^{b_i}}{\partial\tau} = -2\theta b_i \Delta^{b_i-1}$$

Derivatives of the exponential function ψ:

$$\frac{\partial\psi}{\partial\delta} = -2C_i(\delta-1)\psi$$

$$\frac{\partial^2\psi}{\partial\delta^2} = \{2C_i(\delta-1)^2 - 1\} 2C_i \psi$$

$$\frac{\partial\psi}{\partial\tau} = -2D_i(\tau-1)\psi$$

TABLE 6.5. The residual part ϕ^r, Eq. (6.6), of the dimensionless Helmholtz free energy and its derivatives[a]—Continued

$$\frac{\partial^2\Delta^{b_i}}{\partial\tau^2}=2b_i\Delta^{b_i-1}+4\theta^2b_i(b_i-1)\Delta^{b_i-2} \qquad \frac{\partial^2\psi}{\partial\tau^2}=\{2D_i(\tau-1)^2-1\}2D_i\psi$$

$$\frac{\partial^2\Delta^{b_i}}{\partial\delta\partial\tau}=-A_ib_i\frac{2}{\beta_i}\Delta^{b_i-1}(\delta-1)[(\delta-1)^2]^{1/(2\beta_i)-1}-2\theta b_i(b_i-1)\Delta^{b_i-2}\frac{\partial\Delta}{\partial\delta} \qquad \frac{\partial^2\psi}{\partial\delta\partial\tau}=4C_iD_i(\delta-1)(\tau-1)\psi$$

with $$\frac{\partial\Delta}{\partial\delta}=(\delta-1)\left\{A_i\theta\frac{2}{\beta_i}[(\delta-1)^2]^{1/(2\beta_i)-1}+2B_ia_i[(\delta-1)^2]^{a_i-1}\right\}$$

$$\frac{\partial^2\Delta}{\partial\delta^2}=\frac{1}{(\delta-1)}\frac{\partial\Delta}{\partial\delta}+(\delta-1)^2\left\{4B_ia_i(a_i-1)[(\delta-1)^2]^{a_i-2}+2A_i^2\left(\frac{1}{\beta_i}\right)^2\left\{[(\delta-1)^2]^{1/(2\beta_i)-1}\right\}^2\right.$$
$$\left.+A_i\theta\frac{4}{\beta_i}\left(\frac{1}{2\beta_i}-1\right)[(\delta-1)^2]^{1/(2\beta_i)-2}\right\}$$

[a] $\phi^r_\delta=\left[\frac{\partial\phi^r}{\partial\delta}\right]_\tau$, $\phi^r_{\delta\delta}=\left[\frac{\partial^2\phi^r}{\partial\delta^2}\right]_\tau$, $\phi^r_\tau=\left[\frac{\partial\phi^r}{\partial\tau}\right]_\delta$, $\phi^r_{\tau\tau}=\left[\frac{\partial^2\phi^r}{\partial\tau^2}\right]_\delta$, $\phi^r_{\delta\tau}=\left[\frac{\partial^2\phi^r}{\partial\delta\partial\tau}\right]$.

possible values as judged by IAPWS, and no statistical significance can be attached to it. With regard to the uncertainty for the speed of sound and the specific isobaric heat capacity (see Figs. 6.2 and 6.3), it should be noted that the uncertainties for these properties increase drastically when approaching the critical point. (Over wide ranges of state, the uncertainty of IAPWS-95 in the isobaric heat capacity is considered to be smaller than the uncertainty of the experimental c_p data, see Sec. 7.2.5. This attribute of IAPWS-95 is due to the very accurate $p\rho T$ data and speeds of sound on which IAPWS-95 is based.) The statement ''no definitive uncertainty estimates possible'' for the high-pressure region in Figs. 6.2 and 6.3 is based on the lack of experimental data in this region. (After the adoption of the release on the IAPWS-95 formulation [IAPWS (1996)], Wiryana *et al.* (1998) reported speed-of-sound data for temperatures between 351 and 473 K at pressures up to 3500 MPa. In the pressure range up to 1000 MPa, which is in the region with the statement ''no definitive uncertainty estimates possible''

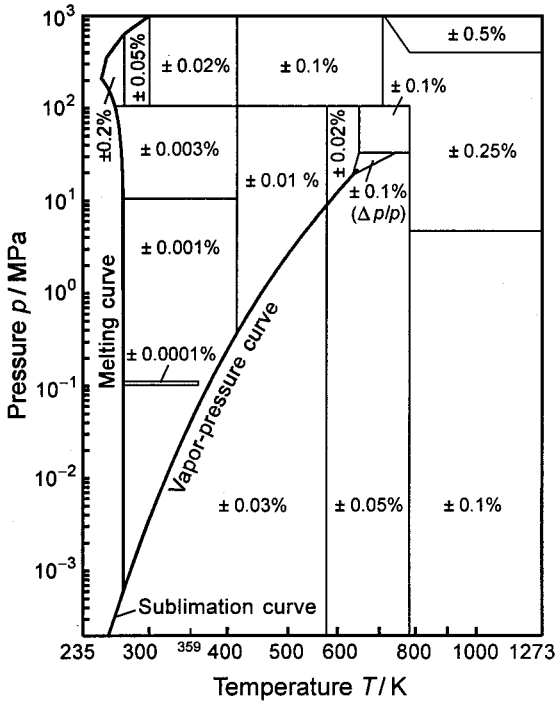

FIG. 6.1. Percentage uncertainties in density estimated for IAPWS-95, Eq. (6.4). In the enlarged critical region (triangle), the uncertainty is given as percentage uncertainty in pressure. This region is bordered by the two isochores 527 and 144 kg m^{-3} and by the 30 MPa isobar. The positions of the lines separating the uncertainty regions are approximate.

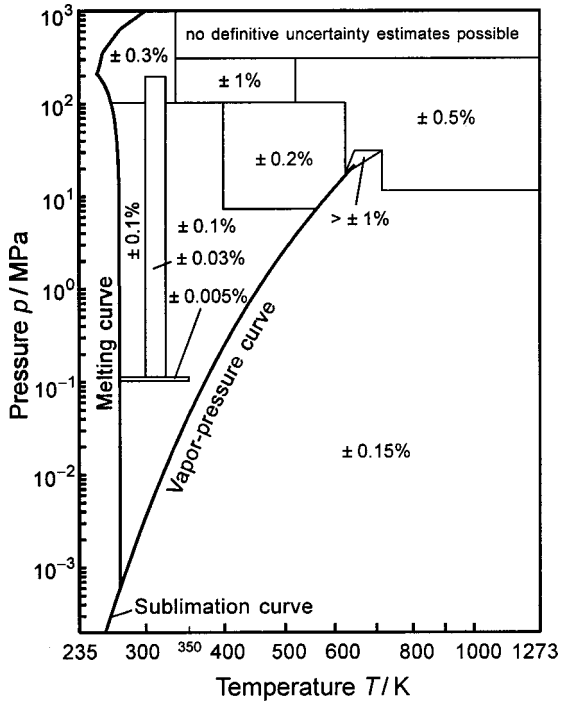

FIG. 6.2. Percentage of uncertainties in speed of sound estimated for IAPWS-95, Eq. (6.4). For the uncertainty in the triangle around the critical point, see the text; for the definition of this region, see Fig. 6.1. The positions of the lines separating the uncertainty regions are approximate.

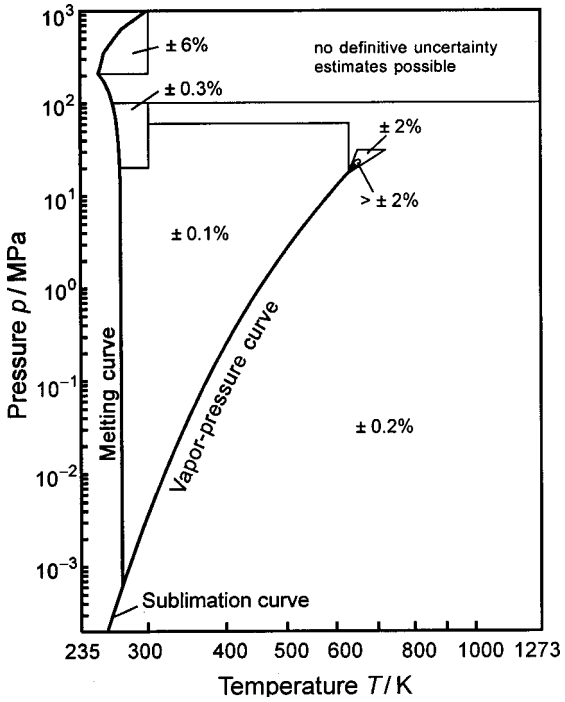

FIG. 6.3. Percentage uncertainties in specific isobaric heat capacity estimated for IAPWS-95, Eq. (6.4). For the uncertainty in the immediate vicinity of the critical point, see the text; for the definition of the triangle around the critical point, see Fig. 6.1. The positions of the lines separating the uncertainty regions are approximate.

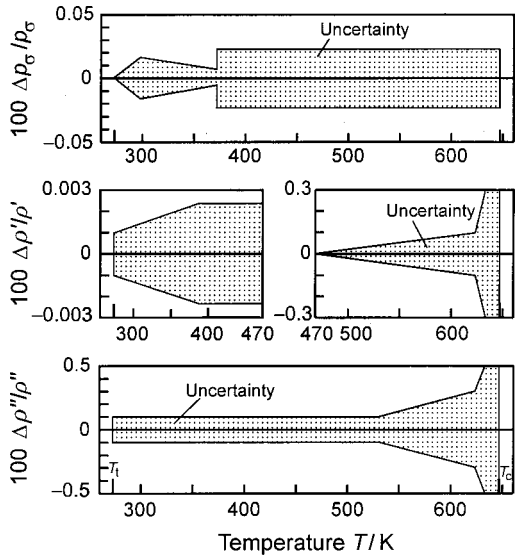

FIG. 6.4. Percentage uncertainties in vapor pressure $100\Delta p_\sigma / p_\sigma$, in saturated liquid density $100\Delta\rho'/\rho'$, and in saturated vapor density $100\Delta\rho''/\rho''$ estimated for IAPWS-95, Eq. (6.4).

in Fig. 6.2, Wiryana *et al.*'s *w* data are represented by IAPWS-95 to within ±1%, for details see Sec. 7.2.3. Most likely, the region described by the statement ''no definitive uncertainty estimates possible'' could be shifted to temperatures above 473 K.) For a statement regarding the uncertainty of enthalpy, see Sec. 8.

For the saturation properties, the estimates of the uncertainties of vapor pressure, saturated liquid density, and saturated vapor density are shown in Fig. 6.4.

6.3.3. Computer-Program Verification

To assist the user in computer-program verification of IAPWS-95, Eq. (6.4), Table 6.6 contains values of the ideal-gas part ϕ° and the residual part ϕ^r of the dimensionless Helmholtz free energy together with the corresponding derivatives. These values were calculated for two combinations of temperature and density; one $T-\rho$ point is in the ''normal'' fluid region and the other one is in the critical region. Moreover, values for the most relevant thermodynamic properties can be compared with the corresponding values listed in the thermodynamic property tables, Tables 13.1 and 13.2, given in the Appendix. The values for the saturated vapor and saturated liquid along the vapor–liquid phase boundary given in Table 13.1 have been calculated from Eq. (6.4) by applying the phase-equilibrium condition [see the corresponding comment in context with Eqs. (6.9a)–(6.9c)] and not by using the auxiliary equations for the saturation properties given in Sec. 2.3. Users who require more significant figures for their computer-program verification should refer directly to the release on IAPWS-95 [IAPWS (1996)]. Information about available computer codes based on IAPWS-95 is given on the IAPWS website http://www.iapws.org/newform.htm

6.4. Features of the Nonanalytical Terms Used for IAPWS-95

As mentioned briefly in Sec. 6.3.1, there are certain problems with the nonanalytical terms used in IAPWS-95 [terms $i=55$ and $i=56$ in Eq. (6.6)]. These problems relate more to scientific considerations regarding the functional forms of IAPWS-95 than to practical consequences. Thus, those readers who are less interested in these basic considerations may turn to the conclusions given in Sec. 6.4.4.

6.4.1. Positive Features of the Nonanalytical Terms

For a very near-critical isochore, Fig. 7.29 illustrates that IAPWS-95, Eq. (6.4), is basically able to follow the steep increase of the data of the isochoric heat capacity when approaching the saturation temperature (phase boundary) extremely close to the critical temperature. With the help of Fig. 6.5, it is shown that this positive feature of IAPWS-95 is produced by the new nonanalytical terms. For the critical isochore, the figure presents the isochoric heat capacity calculated from three equations of state which differ clearly regarding their functional structure. The equation of Saul and Wagner (1989) does not contain modified Gaussian bell-shaped terms, the interim equation of state contains such terms but no nonanalytical terms and the IAPWS-95 formulation contains, in addition to Gaussian bell-shaped terms, special nonanalytical terms according to Eq. (5.40). It can be

TABLE 6.6. Values for the ideal-gas part ϕ°, Eq. (6.5), and for the residual part ϕ^r, Eq. (6.6), of the dimensionless Helmholtz free energy together with the corresponding derivatives[a] for two combinations of temperature and density

$T=500$ K, $\rho=838.025$ kg m^{-3}	
$\phi^\circ = 0.204\,797\,734\times10^{1}$	$\phi^r = -0.342\,693\,206\times10^{1}$
$\phi^\circ_\delta = 0.384\,236\,747$	$\phi^r_\delta = -0.364\,366\,650$
$\phi^\circ_{\delta\delta} = -0.147\,637\,878$	$\phi^r_{\delta\delta} = 0.856\,063\,701$
$\phi^\circ_\tau = 0.904\,611\,106\times10^{1}$	$\phi^r_\tau = -0.581\,403\,435\times10^{1}$
$\phi^\circ_{\tau\tau} = -0.193\,249\,185\times10^{1}$	$\phi^r_{\tau\tau} = -0.223\,440\,737\times10^{1}$
$\phi^\circ_{\delta\tau} = 0$	$\phi^r_{\delta\tau} = -0.112\,176\,915\times10^{1}$
$T=647$ K, $\rho=358$ kg m^{-3}	
$\phi^\circ = -0.156\,319\,605\times10^{1}$	$\phi^r = -0.121\,202\,657\times10^{1}$
$\phi^\circ_\delta = 0.899\,441\,341$	$\phi^r_\delta = -0.714\,012\,024$
$\phi^\circ_{\delta\delta} = -0.808\,994\,726$	$\phi^r_{\delta\delta} = 0.475\,730\,696$
$\phi^\circ_\tau = 0.980\,343\,918\times10^{1}$	$\phi^r_\tau = -0.321\,722\,501\times10^{1}$
$\phi^\circ_{\tau\tau} = -0.343\,316\,334\times10^{1}$	$\phi^r_{\tau\tau} = -0.996\,029\,507\times10^{1}$
$\phi^\circ_{\delta\tau} = 0$	$\phi^r_{\delta\tau} = -0.133\,214\,720\times10^{1}$

[a]For the abbreviated notation of the derivatives of ϕ° and ϕ^r see the footnotes of Tables 6.4 and 6.5, respectively.

seen that wide-range equations of state without the modified Gaussian bell-shaped terms (here, the Saul and Wagner equation of state) are not able to follow the increase of the c_v data for temperatures $(T-T_c)<\approx5.5$ K, or expressed more generally in reduced temperatures, for $T/T_c<\approx1.01$. The IAPWS-95-like equation with Gaussian bell-shaped terms but without nonanalytical terms only fails for $(T-T_c)<\approx2.2$ K corresponding to $T/T_c<\approx1.003$. However, with the nonanalytical terms IAPWS-95 is indeed able to yield the required steep increase of the isochoric heat capacity in the near-critical region. Thus, Fig. 6.5 illustrates very clearly the improvement achieved by the Gaussian bell-shaped terms and in particular by the nonanalytical terms.

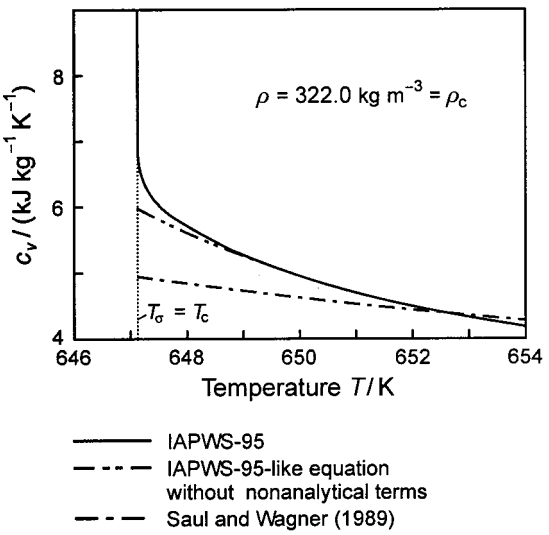

FIG. 6.5. Isochoric heat capacity in the critical region as a function of temperature (on the critical isochore of the single-phase region) calculated from IAPWS-95, Eq. (6.4), an IAPWS-95-like equation but without nonanalytical terms, and the equation of Saul and Wagner (1989).

In order to demonstrate the capability of IAPWS-95 to represent a very steep increase of the isochoric heat capacity in the temperature range $(T-T_c)$ of a few hundredths of a Kelvin, Fig. 6.6 shows, as a function of density, c_v values calculated from two other equations of state at the critical temperature T_c and for a temperature $T=T_c+0.05$ K. Both the IAPWS-95 formulation and the crossover equation of Kostrowicka Wyczalkowska *et al.* (2000) yield a completely

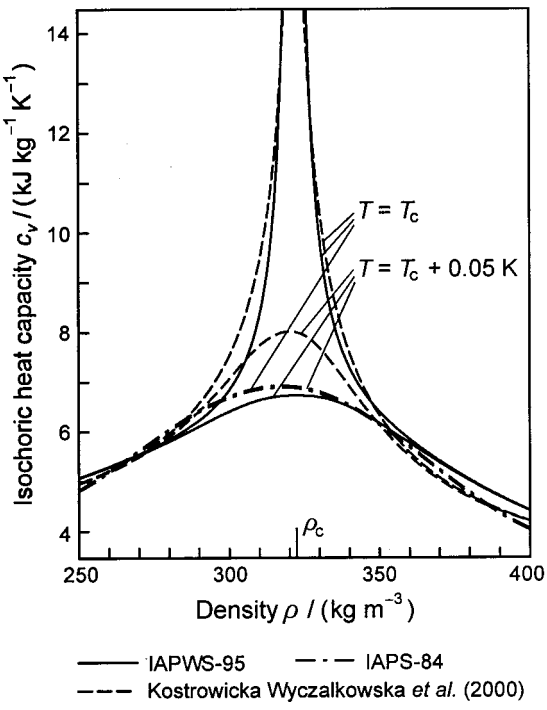

FIG. 6.6. Isochoric heat capacity in the critical region as a function of density on two isotherms calculated from IAPWS-95, Eq. (6.4), IAPS-84, and the crossover equation of Kostrowicka Wyczalkowska *et al.* (2000).

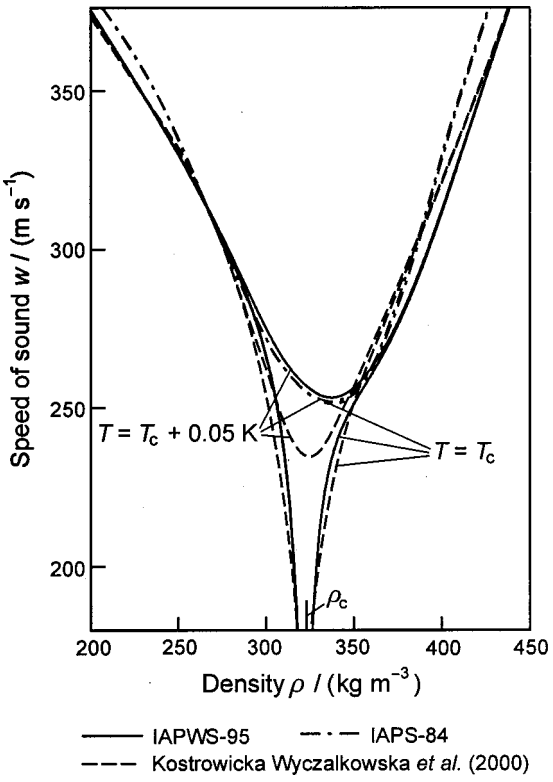

FIG. 6.7. Speed of sound in the critical region as a function of density on two isotherms calculated from IAPWS-95, Eq. (6.4), IAPS-84, and the crossover equation of Kostrowicka Wyczalkowska *et al.* (2000).

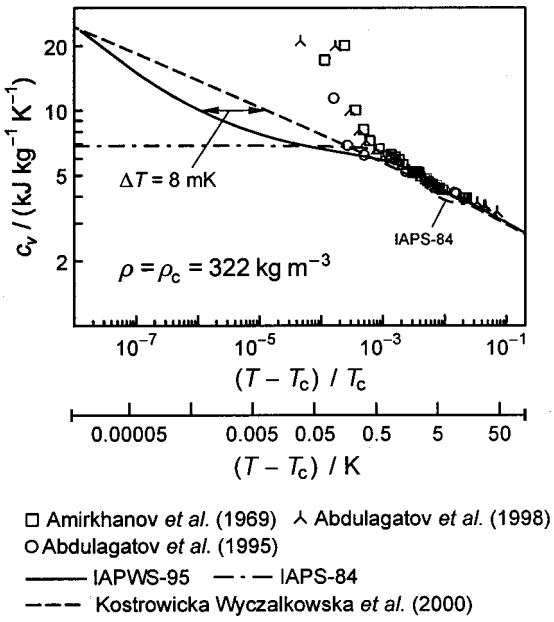

FIG. 6.8. Isochoric heat capacity along the critical isochore of the single-phase region in a double logarithmic diagram calculated from IAPWS-95, Eq. (6.4), IAPS-84, and the crossover equation of Kostrowicka Wyczalkowska *et al.* (2000). Experimental data from the isochore $\rho = 316.84$ kg m^{-3} are plotted for comparison.

different course for the two isotherms $T = T_c + 0.05$ K and $T = T_c$ (both equations yield an infinite c_v value for $T = T_c$ at $\rho = \rho_c$), whereas IAPS-84 does not show any difference between the isotherms $T = T_c + 0.05$ K and $T = T_c$. However, it can also be seen that IAPWS-95 and the crossover equation yield a rather different kind of increase of c_v for the critical temperature when approaching the critical density.

Figure 6.7 shows the speed of sound w plotted as a function of density for two isotherms, namely for the critical temperature $T = T_c$ and the temperature $T = T_c + 0.05$ K. The corresponding plots of w have been calculated from IAPWS-95, IAPS-84, and the crossover equation of Kostrowicka Wyczalkowska *et al.* (2000). IAPS-84 yields practically the same values for the isotherm $T = T_c + 0.05$ K and for the critical isotherm, where the smallest speed-of-sound value amounts to about $w = 250$ m s^{-1}. In contrast, the IAPWS-95 formulation and the crossover equation of Kostrowicka Wyczalkowska *et al.* (2000) yield very small values of w for $T = T_c$ when approaching the critical density ρ_c (with $w = 0$ at the critical point). Thus, IAPWS-95 yields the required strong decrease in the speed of sound when approaching the critical point, even though its critical isotherm in the $w-\rho$ diagram shows a certain oscillation for $\rho > \rho_c$.

An important advantage for practical applications of this kind of nonanalytical terms in a wide-range equation of state is that, in contrast to crossover and other scaled equations, no transformation of the independent variables has to be made: the distance function Δ, see Eq. (6.6), directly contains δ and τ, the reduced density and inverse reduced temperature, like all the other terms of IAPWS-95. Compared to scaled equations like that of Kostrowicka Wyczalkowska *et al.* (2000) or that of Levelt Sengers *et al.* (1983) used in the equation of Hill (1990), this feature drastically simplifies the evaluation of IAPWS-95.

6.4.2. Weaknesses of the Nonanalytical Terms

Besides the significant improvement of the capability of IAPWS-95 for representing caloric properties in the critical region, such terms also have some basic weaknesses which are discussed in this section.

Limiting behavior. Equations of state containing the kind of nonanalytical terms presented in Sec. 5.4.4 still have certain weaknesses in the limiting behavior when approaching the critical point. As an example, Fig. 6.8 shows c_v in a double logarithmic plot versus $[(T-T_c)/T_c]$ for $\rho = \rho_c = 322$ kg m^{-3} as calculated from IAPWS-95, the crossover equation of Kostrowicka Wyczalkowska *et al.* (2000), and IAPS-84. For comparison, the experimental data along the isochore $\rho = 316.84$ kg m^{-3} are also plotted. In this diagram, the density difference between the calculated c_v values and the experimental data does not matter, because the difference between the critical temperature $T_c = 647.096$ K and the saturation temperature $T_\sigma(\rho = 316.84\,\text{kg m}^{-3}) = 647.095$ K is only 1 mK. It can be seen that IAPWS-95 does not yield a straight line in this diagram (as it should for $\rho = \rho_c$), but sags below the line beginning at about $(T-T_c) = 0.5$ K. Although the c_v data are represented within their experimental uncertainties, the results from IAPWS-95 are for $(T-T_c) = 0.5$ K

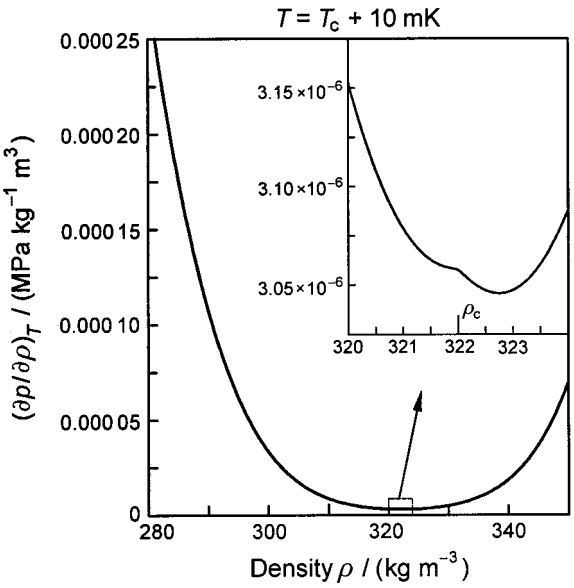

FIG. 6.9. Partial derivative of pressure with respect to density at constant temperature as a function of density calculated from IAPWS-95, Eq. (6.4), along the isotherm $T=T_c+10\,\mathrm{mK}$. The enlarged section shows a small range around the critical density.

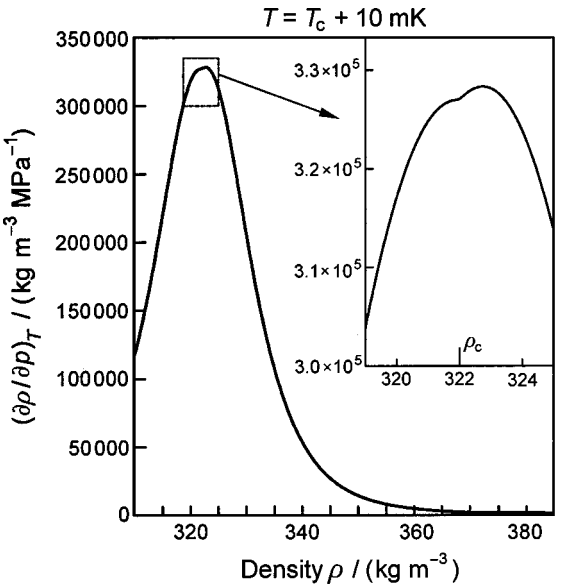

FIG. 6.10. Partial derivative of density with respect to pressure at constant temperature as a function of density calculated from IAPWS-95, Eq. (6.4), along the isotherm $T=T_c+10\,\mathrm{mK}$. The enlarged section shows a small range around the critical density.

to $(T-T_c)=8\times10^{-6}\,\mathrm{K}$ systematically below the c_v values from the crossover equation of Kostrowicka Wyczalkowska *et al.* (2000). In this diagram, the maximum distance in $(T-T_c)/T_c$ between the two equations occurs at $c_v=10\,\mathrm{kJ\,kg^{-1}\,K^{-1}}$, corresponding to a temperature difference of about -0.008 K. In contrast to this very good agreement, the c_v data point of Abdulagatov *et al.* (1995) in this region lies about 0.095 K above the crossover equation, which illustrates the experimental situation in this region. Figure 6.8 also shows that the previous scientific standard equation IAPS-84 already exhibits such an oscillating behavior at $(T-T_c)\approx13\,\mathrm{K}$ and yields c_v values that are much too small very near and at T_c.

Derivatives $(\partial p/\partial\rho)_T$ and $(\partial\rho/\partial p)_T$, isothermal compressibility, and isobaric heat capacity. A second problem is linked to the derivatives of Eq. (5.40) with respect to density. When using these kinds of nonanalytical terms, it was assumed that a continuous plot of derivatives which do not diverge are sufficient; possible physically incorrect contributions have to be compensated by other terms in the multiparameter equation of state in this case. However, at the critical isochore, Eq. (5.40) results in changes of higher derivatives with respect to density which are small and continuous but so rapid that even Gaussian bell-shaped terms cannot compensate for this effect.

The basic problem is the derivative $(\partial p/\partial\rho)_T$, which is related to the derivatives $(\partial\phi^r/\partial\rho)_T$ and $(\partial^2\phi^r/\partial\rho^2)_T$. Figure 6.9 illustrates the behavior of IAPWS-95 for $(\partial p/\partial\rho)_T$ for the isotherm $T=T_c+10\,\mathrm{mK}$. The main figure shows this derivative for the density range between 280 and 360 $\mathrm{kg\,m^{-3}}$, while the enlarged section shows it around the critical density $\rho_c=322\,\mathrm{kg\,m^{-3}}$. This enlarged section illustrates a physically incorrect shape (indentation) at $\rho=\rho_c$, where there is, however, no discontinuity. This "indentation," which occurs only at near-critical temperatures, is so small, as are the absolute values of this derivative, that it has absolutely no effect on the representation of the $p\rho T$ data. This statement is also valid for substances for which the $p\rho T$ measurements in the critical region are clearly more accurate than those for H_2O, for example, for CO_2, see Span and Wagner (1996). The main reason for this negligible influence is that the representation of the $p\rho T$ data depends not on this derivative itself but on the integrated property, the pressure.

In contrast to the thermal properties, the indentation in the derivative $(\partial p/\partial\rho)_T$ directly affects the isothermal compressibility and the isobaric heat capacity via the reciprocal derivative $(\partial\rho/\partial p)_T$, which has very large values in the critical region. Figure 6.10 shows the plot of this derivative for the temperature $T=T_c+10\,\mathrm{mK}$ and presents this derivative for a greater density range as well as for a small section around the indentation. Logically, the indentation occurs once again at the critical density ρ_c. According to the definition of the isothermal compressibility, namely

$$\kappa_T=\rho^{-1}(\partial\rho/\partial p)_T, \tag{6.10}$$

it is obvious that this property shows the same behavior as the derivative $(\partial\rho/\partial p)_T$ regarding the occurrence of the indentation. It is therefore not necessary to illustrate this effect in a $\kappa_T-\rho$ diagram.

The connection between the isobaric heat capacity c_p, the isochoric heat capacity c_v, and the two derivatives $(\partial p/\partial T)_\rho$ and $(\partial p/\partial\rho)_T$ is given by the relation

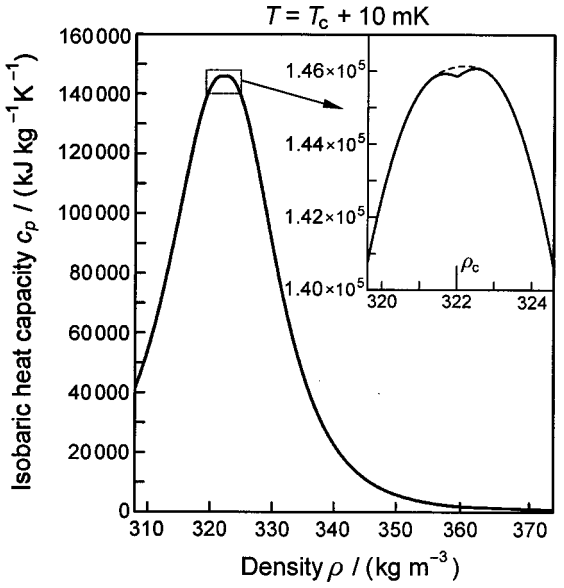

FIG. 6.11. Isobaric heat capacity as a function of density calculated from IAPWS-95, Eq. (6.4), along the isotherm $T=T_c+10$ mK. The enlarged section shows a small region around the critical density.

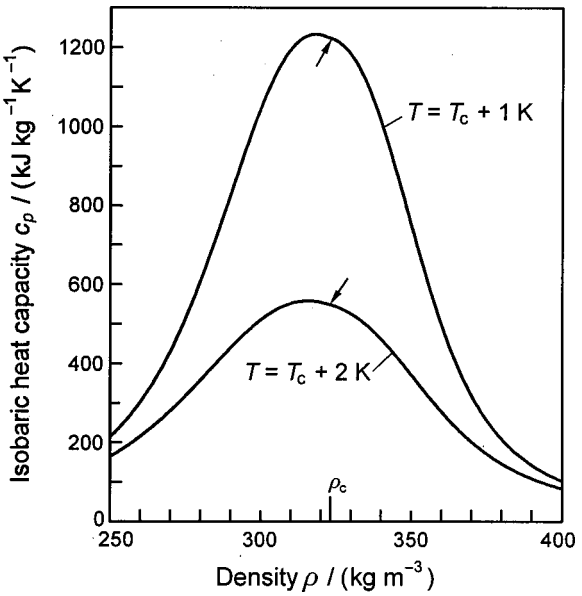

FIG. 6.12. Isobaric heat capacity as a function of density calculated from IAPWS-95, Eq. (6.4), along the two isotherms $T=T_c+1$ K and $T=T_c+2$ K. The arrows mark the locations where the indentations occur, see text.

$$\frac{c_p}{R}=\underbrace{-\tau^2(\phi^{\circ}_{\tau\tau}+\phi^{r}_{\tau\tau})}_{\frac{c_v}{R}}+\underbrace{\overbrace{\frac{(1+\delta\phi^{r}_{\delta}-\delta\tau\phi^{r}_{\delta\tau})^2}{1+2\delta\phi^{r}_{\delta}+\delta^2\phi^{r}_{\delta\delta}}}^{\sim\left(\frac{\partial p}{\partial T}\right)^2_{\rho}}}_{-\left(\frac{\partial p}{\partial \rho}\right)}, \tag{6.11}$$

see Table 6.3. Equation (6.11) indicates that, in the critical region, c_p is proportional to the derivative $(\partial\rho/\partial p)_T=(\partial p/\partial\rho)_T^{-1}$ because this derivative grows much faster when approaching the critical point than c_v, and $(\partial p/\partial T)_\rho$ changes its value only slightly around the critical density. Thus, c_p behaves similarly to the derivative $(\partial\rho/\partial p)_T^{-1}$ regarding the indentation, see Fig. 6.10. Nevertheless, due to the importance of c_p, the weakness of the nonanalytical terms regarding this property in the critical region is explicitly illustrated in Figs. 6.11 and 6.12. These figures show c_p versus density, Fig. 6.11 for $T=T_c+10$ mK with an enlarged section around the indentation, and Fig. 6.12 for $T=T_c+1$ K and $T=T_c+2$ K.

Looking at the enlarged section of Fig. 6.11, everything would be fine if the c_p curve did not show such an indentation but rather followed the dashed line. The difference between the solid line (behavior of IAPWS-95) and a physically reasonable course without such an indentation (dashed line) of this isotherm at ρ_c amounts to about 0.2% of the c_p value in this region. Such a difference is, however, at least 2 orders of magnitude smaller than the estimated uncertainty of IAPWS-95 in c_p in this immediate vicinity of the critical point. When comparing the c_p curves in Figs. 6.11 and 6.12, it can be seen that the indentation diminishes rather rapidly with increasing temperature differences $(T-T_c)$; for $(T-T_c)\approx 2$ K it is practically gone.

Isochoric heat capacity and speed of sound extremely near the phase boundary. According to item (3) before Eq. (5.40), within the δ–τ surface of the critical region, the maximum of $\phi^{r}_{\tau\tau}$ has to follow the course of the saturated vapor and liquid line in order to avoid unreasonable c_v maxima and w minima in the single-phase region close to the phase boundary. The first sum of the Δ function in Eq. (5.40) is responsible for meeting this requirement, which models the course of the phase boundary in the critical region. Thus, the two parameters A_i and β_i must to be determined in such a way that the phase boundary modeled by this function is in agreement with the phase boundary defined by the experimental $p_\sigma\rho'\rho''T$ data. Since one of the two parameters, namely β_i, must fulfill some relations with regard to the parameters a_i and b_i of Eq. (5.40), the variability in this function is given only by the parameter A_i, which means that the first sum of the Δ function is not very flexible. Thus, it is not easy to model this function correctly, or at least in such a way that the ''phase boundary of this function'' lies *within* the real phase boundary defined by the experimental data. Here, for IAPWS-95 the modeling of the first sum of the Δ function has not been as successful as for our reference equation of state for CO_2, which also contains such nonanalytical terms [see Span and Wagner (1996)]. In the following, the weaknesses of IAPWS-95 in this regard are discussed.

Figure 6.13 shows the isochoric heat capacity calculated from IAPWS-95 in the gas region when approaching the saturated vapor line. The figure presents the results for seven gas isochores between $\rho=302$ and $\rho=314$ kg m^{-3} ($\rho_c=322$ kg m^{-3}). It can be seen that IAPWS-95 yields the maxima of c_v not at the saturated vapor line (as it should be)

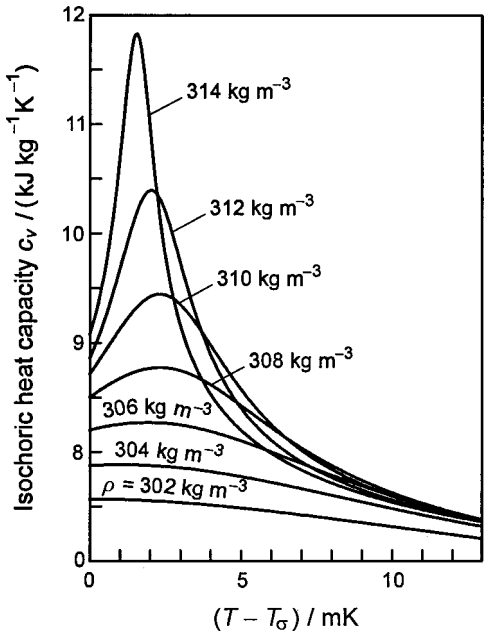

FIG. 6.13. Isochoric heat capacity along several near-critical isochores $\rho < \rho_c$ (gas region) calculated from IAPWS-95, Eq. (6.4), in a small temperature range above the saturation temperature.

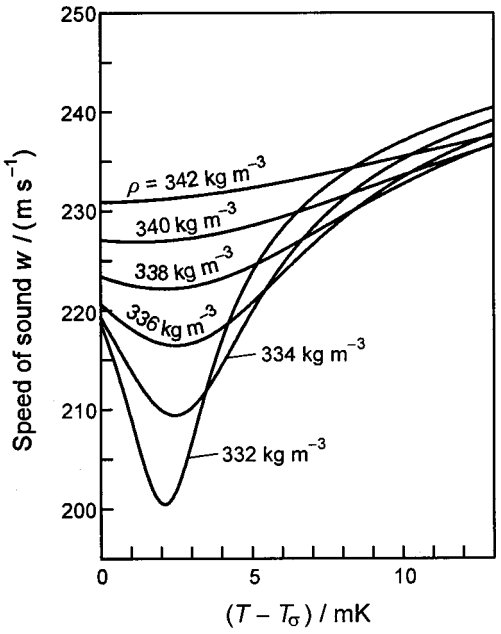

FIG. 6.14. Speed of sound along several near-critical isochores $\rho > \rho_c$ (liquid region) calculated from IAPWS-95, Eq. (6.4), in a small temperature range above the saturation temperature.

but up to 2.5 mK before the saturated vapor line, which corresponds to the y axis $[(T-T_\sigma)=0]$ in Fig. 6.13. Although a temperature difference of $(T-T_\sigma)=2.5$ mK is clearly within the uncertainty of the $c_v''-T$ curve (expressed in temperature, this uncertainty is estimated to be definitely greater than 25 mK in this region), the occurrence of such maxima in the single-phase region rather than at the saturated vapor line shows an incorrect behavior of IAPWS-95 in this respect. An analogous behavior of IAPWS-95 can be observed in the liquid region when approaching the saturated liquid line. This weakness of IAPWS-95 disappears in the gas region for $\rho \leqslant 302$ kg m^{-3} (see Fig. 6.13) and in the liquid region for $\rho \geqslant 342$ kg m^{-3}, which means for densities about 6% smaller or greater than the critical density.

Analogous to the maxima in c_v along isochores when approaching the vapor–liquid phase boundary, IAPWS-95 yields minima for the speed of sound w along isochores not at the saturation temperature T_σ (as it should be) but up to 2.5 mK above T_σ. Figure 6.14 illustrates this incorrect behavior of IAPWS-95 in the liquid region when approaching the saturated liquid line. This weakness disappears for the same densities as mentioned above for c_v.

Using the example of the isochoric heat capacity along the vapor–liquid saturation curve, Fig. 6.15 shows c_v'' and c_v' as a function of density calculated from IAPWS-95. It can be seen that IAPWS-95 is basically able to yield the steep increase of c_v along the phase boundary when approaching the critical density. A certain weakness is the oscillating course of the saturated vapor and liquid line (in c_v) instead of a smooth increase. However, without the nonanalytical terms, IAPWS-95 (or any other analytical wide-range equation of state) would yield a course of c_v'' and c_v' corresponding to the dashed-dotted line in Fig. 6.15. Figure 6.16 shows the corresponding behavior of IAPWS-95 with regard to the speed of sound along the saturated vapor and liquid line. IAPWS-95 yields the strong decrease of w'' and w' when approaching the critical density, but with the weakness of an oscillation at about $w=220$ m s^{-1}. Thus, the following conclusion can be drawn: while the nonanalytical terms are not perfect, they

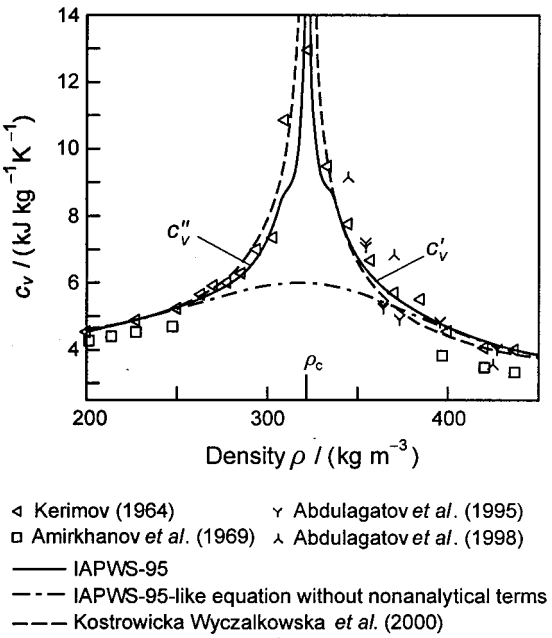

FIG. 6.15. Isochoric heat capacity along the vapor–liquid phase boundary as a function of density calculated from IAPWS-95, an IAPWS-95-like equation without nonanalytical terms, and the crossover equation of Kostrowicka Wyczalkowska *et al.* (2000). Experimental data are plotted for comparison.

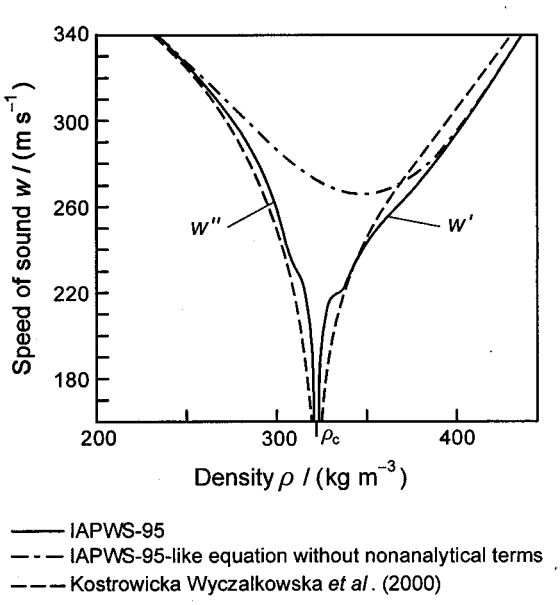

FIG. 6.16. Speed of sound along the vapor–liquid phase boundary as a function of density calculated from IAPWS-95, an IAPWS-95-like equation without nonanalytical terms, and the crossover equation of Kostrowicka Wyczalkowska *et al.* (2000).

help considerably to model the strong increase of the isochoric heat capacity and the strong decrease of the speed of sound in the critical region.

6.4.3. Nonanalytical Terms Proposed by Kiselev and Friend

Being aware of the problems of IAPWS-95 with physically incorrect limiting behavior when approaching the critical point, Kiselev and Friend (1999) developed a crossover formalism for the thermodynamic surface of pure fluids that can be used for multiparameter equations of state. They applied their idea to IAPWS-95 and replaced the two nonanalytical terms in Eq. (6.4) with a modification of the so-called kernel term developed by Chen *et al.* (1990) in the context of their crossover theory based on the renormalized Landau expansion of the Helmholtz free energy. This kernel term, depending directly on density and temperature, contains a crossover function Y that is implicitly defined by a set of four equations with six universal and six substance-specific parameters; the substance-specific parameters were fitted by Kiselev and Friend to the experimental data of H_2O in the critical region.

Kiselev and Friend (1999) showed that, with such a kernel term, the physically incorrect behavior of Eq. (6.4) regarding the caloric properties in a small part of the critical region could be avoided. However, this advantage has a price: the complexity of the entire multiparameter equation has clearly increased. The following items are examples of this complexity, for further details see Span (2000):

(i) for the evaluation of the kernel term, the equations defining the crossover function Y must be solved iteratively;

(ii) due to the implicit nature of the kernel term, the calculation of thermodynamic properties becomes rather complicated; and

(iii) the kernel term in Kiselev and Friend's modified version of Eq. (6.4) contributes to all derivatives of the dimensionless Helmholtz free energy.

Even if the contributions according to item (iii) are small, they are certainly not completely negligible. Thus, such a kernel term should not simply be added to an existing equation, but should be fitted together with all the other coefficients of the equation. In order to obtain optimum results, such a kernel term should even be included in the entire process of optimizing the functional form of an equation of state, see Sec. 5.5.2. However, based on the structure-optimization methods existing at present, these demands make the development of such a complex equation of state practically impossible.

Whatever one does to improve the representation of the caloric properties in the critical region in connection with a wide-range equation of state, the corresponding terms should not be much more complex than the terms $i=55$ and 56 in Eq. (6.6).

6.4.4. Summary of the Advantages and Weaknesses of the Nonanalytical Terms in IAPWS-95

The advantages and weaknesses of the nonanalytical terms [terms $i=55$ and $i=56$ in Eq. (6.6)] of IAPWS-95 discussed in Secs. 6.4.1 and 6.4.2 can be summarized as follows:

(i) In contrast to all the analytical wide-range equations of state for H_2O, IAPWS-95 is able to follow the steep increase of the isochoric heat capacity and the strong decrease of the speed of sound when approaching the critical point.

(ii) This desirable behavior has been achieved by incorporating two special nonanalytical terms without any transformation of the independent variables δ and τ, resulting in a relatively simple (in comparison with scaled and crossover equations) and easily programmable structure of IAPWS-95.

(iii) This relatively simple form of the nonanalytical terms has been achieved at the expense of a behavior which is physically incorrect in some features very close to the critical point. It results in one indentation of the derivative $(\partial p/\partial \rho)_T$ at the critical density on each isotherm in the immediate vicinity of the critical point. This indentation occurs at densities about $\pm 0.5\%$ around the critical density ρ_c at temperatures from the critical temperature T_c up to about 2 K above T_c. In the same region, this indentation in $(\partial p/\partial \rho)_T$ produces a corresponding indentation in the isothermal compressibility and in the isobaric heat capacity. Although this indentation is without any doubt a physically incorrect feature, it has practically no effect on the application of IAPWS-95. Nevertheless, in this region derivatives of κ_T and c_p [e.g., $(\partial c_p/\partial \rho)_T$] should not be calculated, but such derivatives are not usually needed.

(iv) Within a temperature range from 20 mK below T_c up to T_c (corresponding to saturation densities $\pm 6\%$ around ρ_c), the isochoric heat capacity c_v calculated from IAPWS-95 exhibits a maximum and the speed of sound w exhibits a

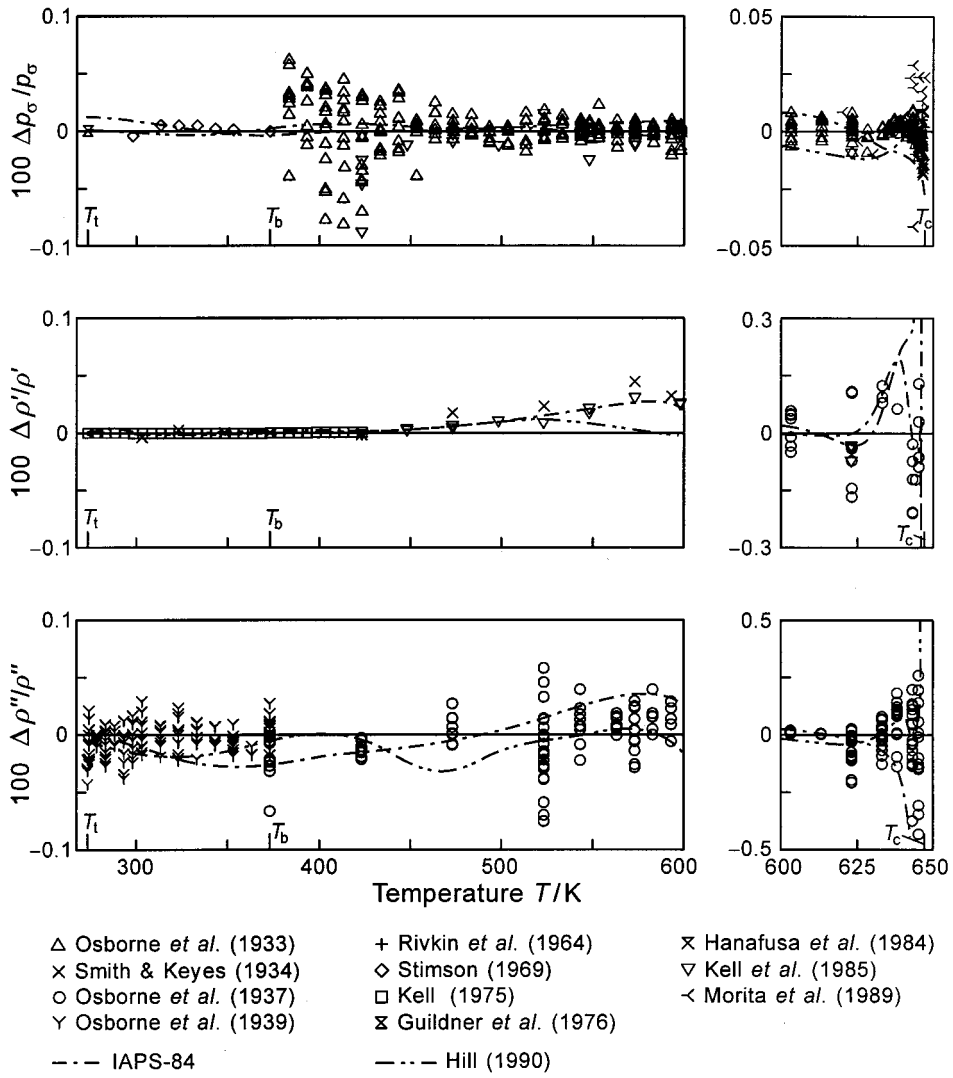

FIG. 7.1. Percentage deviations of the experimental data of the vapor pressure p_σ, the saturated liquid density ρ', and the saturated vapor density ρ'' from the corresponding values calculated from IAPWS-95, Eq. (6.4). Values calculated from IAPS-84 and the equation of Hill (1990) are plotted for comparison: $100\Delta p_\sigma/p_\sigma = 100(p_{\sigma,\mathrm{exp}} - p_{\sigma,\mathrm{calc}})/p_{\sigma,\mathrm{exp}}$, $100\Delta\rho'/\rho' = 100(\rho'_{\mathrm{exp}} - \rho'_{\mathrm{calc}})/\rho'_{\mathrm{exp}}$, $100\Delta\rho''/\rho'' = 100(\rho''_{\mathrm{exp}} - \rho''_{\mathrm{calc}})/\rho''_{\mathrm{exp}}$.

minimum away from the saturation temperature T_σ of the corresponding isochore (the extrema should be directly at T_σ) but in the single-phase region up to 2.5 mK above T_σ. However, this physically incorrect behavior has practically no effect because it is clearly within the uncertainty of IAPWS-95 with respect to c_v and w along the saturated vapor and saturated liquid line in this very near-critical region. Nevertheless, in this region derivatives of c_v and w [e.g., $(\partial c_v/\partial T)_\rho$] should not be calculated, but such derivatives are not usually needed.

In our experience, the described deficiencies of IAPWS-95 regarding some caloric properties in a small part of the critical region have no effects on the practical use of IAPWS-95. However, for users who must avoid these problems, use of the crossover equation of Kostrowicka Wyczalkowska *et al.* (2000) is recommended.

7. Comparison of the IAPWS-95 Formulation with Experimental Data and Values from Other Equations of State

In this section, the quality of the IAPWS-95 formulation is discussed based on comparisons with the selected experimental data used to develop IAPWS-95 (see Sec. 4) and when necessary with further experimental data. Most figures also show results of the previous scientific standard equation IAPS-84 [Haar *et al.* (1984), Kestin and Sengers (1986)] and of the equation of state of Hill (1990); for a brief description of these two equations see Sec. 1.2. Since both previous equations were developed on the IPTS-68 temperature scale, all temperatures were converted to the IPTS-68 scale before values were calculated from these equations. Comparisons with the experimental data of the various properties in the

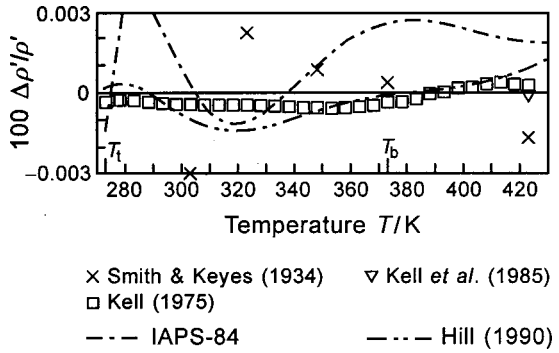

FIG. 7.2. Percentage deviations $100\Delta\rho'/\rho' = 100(\rho'_{exp} - \rho'_{calc})/\rho'_{exp}$ between experimental data of the saturated liquid density ρ' and values calculated from IAPWS-95, Eq. (6.4). Values calculated from IAPS-84 and the equation of Hill (1990) are plotted for comparison.

critical region are not summarized in a special critical-region section but are given for each property in its subsection. When such comparisons for the critical region are made, the values from the crossover equation of Kostrowicka Wyczalkowska *et al.* (2000) are also included in the corresponding figures.

7.1. The Vapor–Liquid Phase Boundary

7.1.1. Thermal Properties at Saturation

Figure 7.1 shows the deviations of the selected experimental data for the vapor pressure p_σ and the saturated liquid and vapor density, ρ' and ρ'', from the corresponding values calculated with IAPWS-95, Eq. (6.4); for comparison purposes the values calculated from IAPS-84 and from the equation of Hill (1990) are also given. For all three equations of state, the saturation properties p_σ, ρ', and ρ'' were calculated via the phase-equilibrium condition, Eqs. (6.9a)–(6.9c). In order to take into account that the scatter of the ρ' and ρ'' data increases for temperatures above 600 K, different deviation scales have been used for the temperatures below and above 600 K. IAPWS-95 represents all the selected thermal saturation data to within the uncertainties given in Table 2.1. From the deviation diagram of the saturated liquid density, it can be seen that for temperatures between 550 and 600 K the ρ' values from IAPWS-95 are slightly systematically below the experimental data by about -0.05% (but still within the experimental uncertainty). This deviation is caused by the fact that IAPWS-95 was also fitted to the $p\rho T$ data of Kell *et al.* (1978), which cover the homogeneous liquid region up to near the saturated liquid line (see Sec. 7.2.1.2). As can be seen from Fig. 2.2, the auxiliary equation for ρ', Eq. (2.6), represents the experimental data of this region without such systematic deviations. This is, however, a slight overfitting because Eq. (2.6) did not have, of course, the experimental information from the homogeneous liquid region. Thus, it follows that IAPS-84, which represents the ρ' data without such systematic deviations, is not able to represent the mentioned $p\rho T$ data of Kell *et al.* (1978) to within their uncertainty.

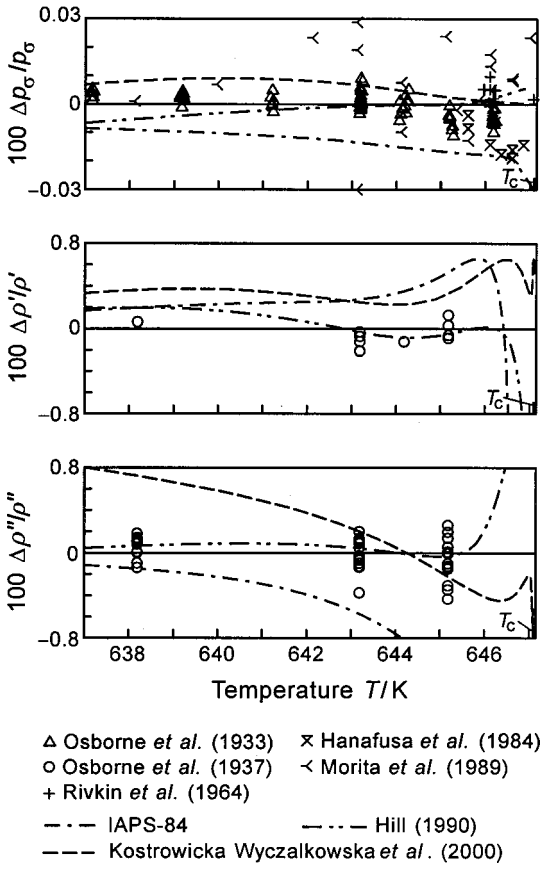

FIG. 7.3. Percentage deviations of the experimental data of the vapor pressure p_σ, the saturated liquid density ρ', and the saturated vapor density ρ'' from the corresponding values calculated from IAPWS-95, Eq. (6.4), for the temperature range from 10 K below the critical temperature up to T_c. Values calculated from IAPS-84, the equation of Hill (1990), and the crossover equation of Kostrowicka Wyczalkowska *et al.* (2000) are plotted for comparison. $100\Delta p_\sigma/p_\sigma = 100(p_{\sigma,exp} - p_{\sigma,calc})/p_{\sigma,exp}$, $100\Delta\rho'/\rho' = 100(\rho'_{exp} - \rho'_{calc})/\rho'_{exp}$, $100\Delta\rho''/\rho'' = 100(\rho''_{exp} - \rho''_{calc})/\rho''_{exp}$.

In the discussions throughout Sec. 7.1, the homogeneous liquid region is referred to quite often, because many experimental saturation data are not mutually consistent. The first example of this is given in the following.

Figure 7.2 illustrates that, in contrast to IAPS-84 and Hill's equation of state, IAPWS-95 is able to represent the ρ' data of Kell (1975) to within their experimental uncertainty ($\Delta\rho' = \pm 0.0004\%$ at $T = 277\,K$ to $\Delta\rho' = \pm 0.0012\%$ at $T = 423\,K$) without significant oscillations. However, the nearly constant deviation of Kell's data from the ρ' values of IAPWS-95 up to the normal boiling temperature T_b could not be avoided, since otherwise the correct representation of the second derivatives $(\partial^2\rho/\partial p^2)_T$ and $(\partial^2\rho/\partial p\,\partial T)$ of Eq. (6.4) in the liquid region would have suffered, see Sec. 7.3.1.

Behavior in the critical region. In order to show how the IAPWS-95 formulation behaves in the critical region for the thermal saturation properties, a comparison with the experimental data is given for temperatures from $(T_c - 10\,K)$ to T_c in Fig. 7.3. Besides IAPS-84 and the equation of Hill (1990), in the critical region of the vapor–liquid phase boundary, the values from the crossover equation of Kostrowicka Wycza-

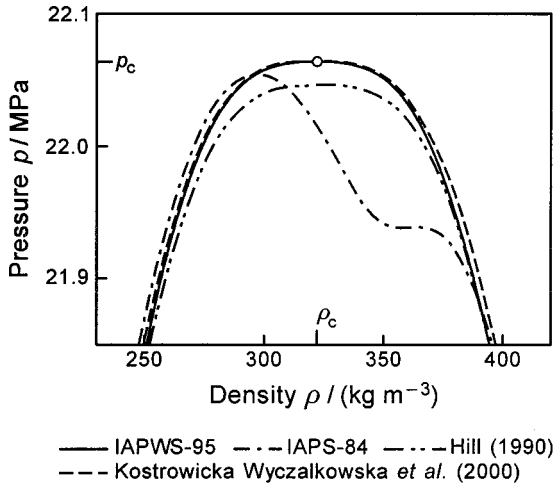

FIG. 7.4. The vapor–liquid phase boundary in the critical region of the $p-\rho$ diagram calculated from IAPWS-95, Eq. (6.4), IAPS-84, the equation of Hill (1990), and the crossover equation of Kostrowicka Wyczalkowska *et al.* (2000).

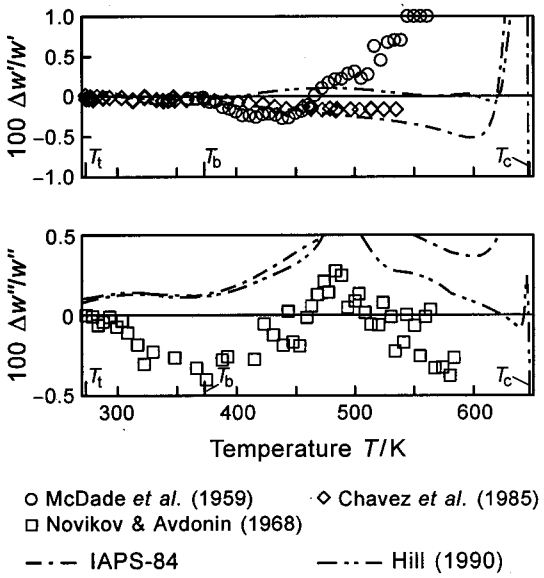

FIG. 7.5. Percentage deviations of the experimental data of the speed of sound of the saturated liquid w' and the speed of sound of the saturated vapor w'' from the corresponding values calculated from IAPWS-95, Eq. (6.4). Values calculated from IAPS-84 and the equation of Hill (1990) are plotted for comparison: $100\Delta w'/w' = 100(w'_{exp} - w'_{calc})/w'_{exp}$, $100\Delta w''/w'' = 100(w''_{exp} - w''_{calc})/w''_{exp}$.

lkowska *et al.* (2000) are also plotted for comparison purposes. It can be seen that IAPWS-95 represents the experimental data of all three properties, namely p_σ, ρ', and ρ'', very well to within their scatter, which means without any systematic trend up to the critical temperature. This behavior is a clear improvement in comparison with the previous standard IAPS-84, which shows systematically increasing deviations from the experimental data when approaching the critical temperature T_c. This weakness of IAPS-84 is even more apparent in Fig. 7.4; see further below. Except for the region very close to T_c (see Fig. 7.4), the equation of Hill (1990) covers the thermal saturation properties for temperatures shown in Fig. 7.3 well. The crossover equation of Kostrowicka Wyczalkowska *et al.* (2000) represents the experimental data of the vapor pressure to within the experimental uncertainty of $\pm 0.025\%$ valid for the data of Osborne *et al.* (1933). In contrast, the representation of the saturation densities is clearly unsatisfactory. While the values of the saturated liquid density calculated from the crossover equation are still mostly within the experimental uncertainty (but biased above the experimental data), clearly systematic deviations occur for the saturated vapor density; for temperatures below 642 K, these deviations are clearly outside the experimental uncertainty of about $\pm 0.3\%$ claimed by Osborne *et al.* (1937) for their measurements (see Table 2.1). From all three deviation diagrams of Fig. 7.3, it can be seen that the thermal saturation properties of the critical region are clearly better covered by the IAPWS-95 formulation than by the crossover equation of Kostrowicka Wyczalkowska *et al.* (2000).

Figure 7.4 shows the absolute plot of the vapor–liquid phase boundary in a pressure–density diagram calculated from the four equations of state discussed here; the plotted phase boundaries cover a temperature range from T_c to 1 K below T_c. It can be seen that IAPS-84 yields a fundamentally incorrect plot in this part of the critical region. This figure also illustrates that the phase boundary calculated from the equation of Hill (1990) ends at a temperature that is too low. The simple reason for this behavior is that the critical point of Hill's equation does not correspond to the critical parameters later agreed on by IAPWS [IAPWS (1992)]. Moreover, this absolute $p-\rho$ diagram shows that IAPWS-95 and the crossover equation of Kostrowicka Wyczalkowska *et al.* (2000) yield basically the same shape of the phase boundary when approaching the critical point.

7.1.2. Speeds of Sound at Saturation

The only experimental speeds of sound on the saturated liquid line w' used for developing IAPWS-95 are the data of Chavez *et al.* (1985), see Table 4.3. Figure 7.5 shows a comparison of these w' data with the values calculated from IAPWS-95, Eq. (6.4). For temperatures above 420 K, the data of Chavez *et al.* (1985) are systematically up to 0.13% below the values calculated from IAPWS-95; this deviation is outside the experimental uncertainty of $\pm 0.05\%$ claimed by the authors. Several attempts to represent the w' data to within the given uncertainty failed, since otherwise the representation of the other properties on the saturated liquid line would have been worsened. Moreover, an improved representation of the w' data would have resulted in an oscillating behavior of the calculated values of the enthalpy h' on the saturated liquid line that would have clearly exceeded the tolerances of the IST-85 values [IAPWS (1994)], see Sec. 7.1.5. This conclusion is confirmed by the behavior of IAPS-84. As can be seen in this figure, IAPS-84 follows Chavez *et al.*'s data up to 480 K, but for higher temperatures

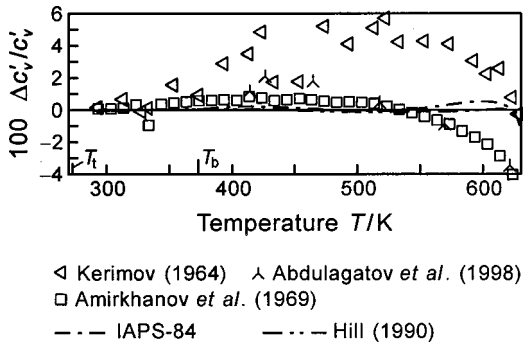

FIG. 7.6. Percentage deviations $100\Delta c'_v/c'_v = 100(c'_{v,\mathrm{exp}} - c'_{v,\mathrm{calc}})/c'_{v,\mathrm{exp}}$ between experimental data of the isochoric heat capacity of the saturated liquid c'_v and values calculated from IAPWS-95, Eq. (6.4). Values calculated from IAPS-84 and the equation of Hill (1990) are plotted for comparison.

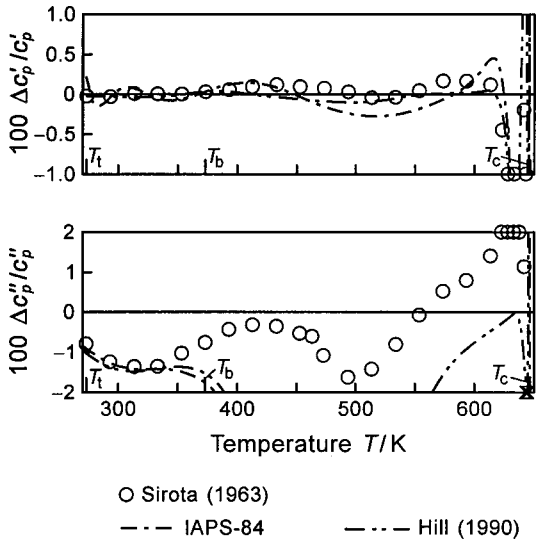

FIG. 7.7. Percentage deviations of the experimental data of the isobaric heat capacity of the saturated liquid c'_p and the isobaric heat capacity of the saturated vapor c''_p from the corresponding values calculated from IAPWS-95, Eq. (6.4). Values calculated from IAPS-84 and the equation of Hill (1990) are plotted for comparison: $100\Delta c'_p/c'_p = 100(c'_{p,\mathrm{exp}} - c'_{p,\mathrm{calc}})/c'_{p,\mathrm{exp}}$, $100\Delta c''_p/c''_p = 100(c''_{p,\mathrm{exp}} - c''_{p,\mathrm{calc}})/c''_{p,\mathrm{exp}}$.

IAPS-84 yields values up to 0.13% below the experimental data. In this temperature range, IAPS-84 shows a clearly oscillating behavior with regard to the h' values and has difficulties in remaining within the IST-85 tolerances, see Fig. 7.9. Nevertheless, a final assessment of the w' data of Chavez *et al.* (1985) can only be made by remeasuring the caloric properties at saturation.

The upper diagram of Fig. 7.5 also contains the w' data of McDade *et al.* (1959), which were not used to fit IAPWS-95. These data are represented to within their relatively large experimental uncertainty of $\Delta w' = \pm 1\%$. However, for temperatures above 500 K, these data are no longer consistent with the speed-of-sound data of the homogeneous liquid region.

Novikov and Avdonin (1968) give for their speed-of-sound data w'' on the saturated vapor line uncertainties of $\Delta w'' = \pm 1\%$. From the lower diagram of Fig. 7.5 it can be seen that the w'' data are represented to within this uncertainty by all three equations of state, but the best representation has been achieved by IAPWS-95. This observation is in agreement with the representation of the speed-of-sound data in the homogeneous gas region near the saturated vapor line, see Sec. 7.2.3.

7.1.3. Isochoric Heat Capacities at Saturation

Since the data sets of the isochoric heat capacities at saturation, measured by experimenters at the Dagestan Scientific Center of the Russian Academy of Sciences, are unfortunately not very consistent with each other (see the discussion in Sec. 7.2.4), these data were not used to develop the IAPWS-95 formulation; for more details about these data see Sec. 4.1.2.

As an example, Fig. 7.6 shows percentage deviations between the experimental isochoric heat capacities of the saturated liquid c'_v (from the single-phase region) and corresponding values calculated from IAPWS-95; the figure covers the temperature range up to 630 K, for the critical region see Fig. 6.15. The differences between the three data sets are obvious; the deviations of the c'_v data of Amirkhanov *et al.* (1969) from the values calculated with IAPWS-95 remain within $\pm 1\%$ for temperatures up to 573 K. On the other hand, there is an excellent agreement between IAPWS-95 and the equation of Hill (1990); the differences in c'_v between the two equations remain within $\pm 0.15\%$ in the entire temperature range covered by Fig. 7.6. Both equations are very well determined by the accurate $p\rho T$ data on and around the saturated liquid line. In this respect, the isochoric heat capacity is, outside the critical region, not a "difficult" property for good equations of state. It is estimated that, outside the critical region, the uncertainty of IAPWS-95 in c'_v is less than $\pm 0.5\%$.

7.1.4. Isobaric Heat Capacities at Saturation

The only measuring runs which exist for H_2O for the isobaric heat capacity on the saturated liquid and saturated vapor line are the c'_p and c''_p data of Sirota (1963) which he derived from his c_p data of the homogeneous liquid and vapor. Figure 7.7 shows the representation of Sirota's c'_p and c''_p data by IAPWS-95, Eq. (6.4). It can be seen that, particularly for c''_p, the data are clearly better represented by IAPWS-95 than by IAPS-84 and by the equation of Hill (1990). This improved behavior was achieved by including these data into the fit of IAPWS-95, although the behavior of Eq. (6.4) regarding the caloric properties along the vapor–liquid phase boundary was essentially already fixed by fitting to the u' and u'' values (see Table 5.4). The effectiveness of this measure is mainly based on the fact that, for fitting IAPWS-95 to the data of c'_p and c''_p, the phase-equilibrium condition was applied in the direct nonlinear way, see Sec. 5.5.2 and particularly Eqs. (5.18) to (5.20) in Table 5.1 and

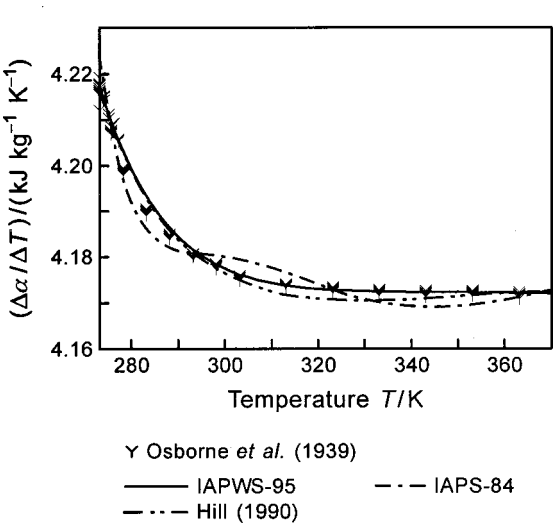

FIG. 7.8. The caloric difference quantity $\Delta\alpha$ related to ΔT (with $\Delta T = 1$ K) as a function of temperature calculated from IAPWS-95, Eq. (6.4), IAPS-84, and the equation of Hill (1990). The experimental data $\Delta\alpha/\Delta T$ of Osborne *et al.* (1939) are plotted for comparison.

Fig. 5.1. Due to the strongly increasing uncertainty in density, the fit to the c_p' and c_p'' data was not performed for temperatures $T > 628$ K.

7.1.5. The Caloric Difference Property $\Delta\alpha$ and the Enthalpies at Saturation

The importance of the caloric property α for the determination of the enthalpy h, the internal energy u, and the entropy s on the vapor–liquid phase boundary has been described in Sec. 2. In Fig. 7.8 the $(\Delta\alpha/\Delta T)$ values are plotted for the temperature range up to 370 K, which is covered by Osborne *et al.*'s (1939) more precise data. The experimental uncertainty of these data corresponds to approximately the scatter of the data. It can be seen that IAPWS-95 follows the experimental data very smoothly, while IAPS-84 shows larger systematic oscillations. The upper diagram of Fig. 7.9 presents the percentage deviations of the experimental $\Delta\alpha$ data in comparison with those calculated from IAPWS-95, Eq. (6.4). In contrast to IAPS-84 and the equation of Hill (1990), IAPWS-95 is able to reproduce the $\Delta\alpha$ data within the experimental uncertainty without significant oscillations; IAPWS-95 represents these $\Delta\alpha$ data practically as well as the auxiliary equation for this quantity, Eq. (2.9), see Fig. 2.3.

Figure 7.9 also shows that IAPWS-95 represents the enthalpies on the saturated liquid and vapor line, h' and h'', according to the international skeleton table values IST-85 [IAPWS (1994)] very well, i.e., without any oscillations and clearly within the tolerances of IST-85. According to IAPWS (1994), these IST-85 values for h' and h'' were calculated from Eqs. (2.10) and (2.11) so that the very good agreement of IAPWS-95 with these IST-85 values means that IAPWS-95 is not only in good agreement with the international saturation equations for the thermal properties, Eqs. (2.5)–(2.7), but also with the corresponding saturation equations for the caloric properties, Eqs. (2.9)–(2.15).

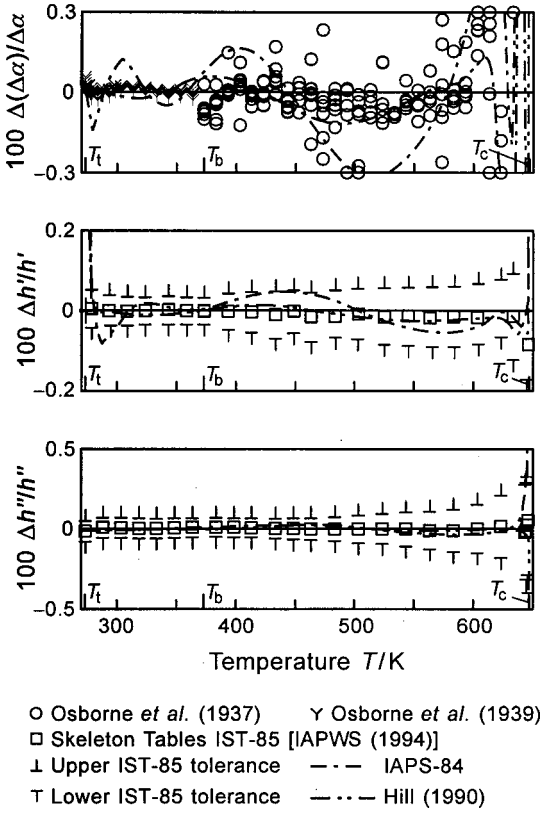

FIG. 7.9. Percentage deviations of the experimental data of the caloric difference quantity $\Delta\alpha$ and values of the Skeleton Tables IST-85 with their tolerances [IAPWS (1994)] of the enthalpy of the saturated liquid h' and the enthalpy of the saturated vapor h'' from the corresponding values calculated from IAPWS-95, Eq. (6.4). Values calculated from IAPS-84 and the equation of Hill (1990) are plotted for comparison: $100\Delta(\Delta\alpha)/\Delta\alpha = 100(\Delta\alpha_{\text{exp}} - \Delta\alpha_{\text{calc}})/\Delta\alpha_{\text{exp}}$, $100\Delta h'/h' = 100(h'_{\text{table}} - h'_{\text{calc}})/h'_{\text{table}}$, $100\Delta h''/h'' = 100(h''_{\text{table}} - h''_{\text{calc}})/h''_{\text{table}}$.

7.2. The Representation of Properties in the Single-Phase Region

7.2.1. $p\rho T$ Data

The $p\rho T$ data used to develop the IAPWS-95 formulation cover a temperature range from 253 to 1174 K, see Fig. 4.1 and Table 4.4. These data lie on 55 isotherms, of which 30 representative isotherms have been selected to illustrate the quality of IAPWS-95 in representing the $p\rho T$ data. The comparisons are discussed for increasing temperatures where specific temperature regions are summarized in the following subsections.

7.2.1.1. Temperature Range $T < 273.16$ K. It is well known that for H_2O there is a small part of the liquid region with temperatures less than the temperature of the triple point, $T_t = 273.16$ K; this region is bordered by the melting–pressure curves of the ice modifications I, III, and V, see Fig. 2.1. Figure 7.10 shows that IAPWS-95, Eq. (6.4), represents the experimental $p\rho T$ data to within $\pm 0.1\%$ in density for temperatures between 253.15 and 263.15 K and to within $\pm 0.2\%$ in density for $T = 268$ K. The equation of Hill

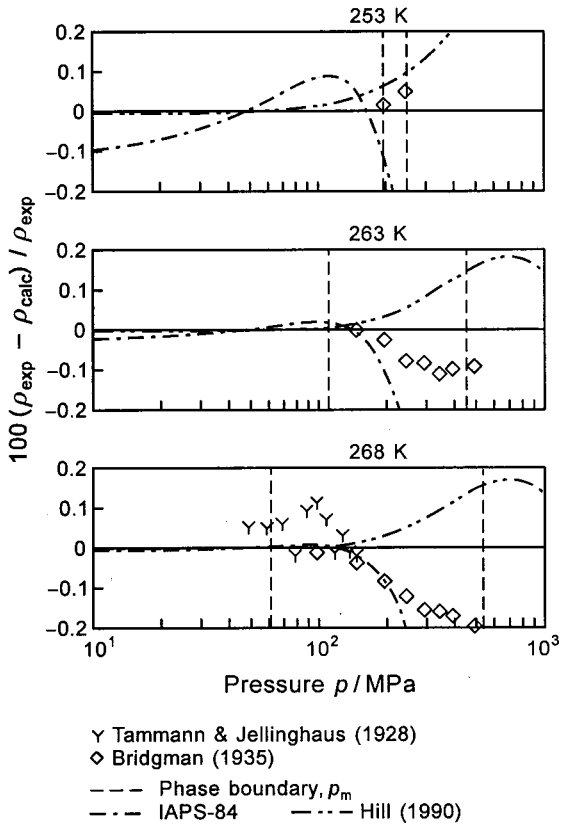

FIG. 7.10. Percentage density deviations between experimental $p\rho T$ data and values calculated from IAPWS-95, Eq. (6.4). Values calculated from IAPS-84 and the equation of Hill (1990) are plotted for comparison. The stable liquid region is bordered by the two phase-boundary lines of the melting pressure p_m.

(1990) shows somewhat greater deviations and IAPS-84 clearly deviates more from the experimental data.

7.2.1.2. Temperature Range 273.16 K≤T<643.15 K. Figure 7.11 presents comparisons between the experimental $p\rho T$ data and those values calculated from IAPWS-95, Eq. (6.4), for temperatures from 273.16 to 643.15 K. These isotherms cover both the gas region ($p<p_\sigma$) and the liquid region ($p>p_\sigma$). These two regions are separated by the phase boundary at $p=p_\sigma$, which can be seen in these diagrams for $p_\sigma \geqslant 0.1$ MPa. This means that the diagrams show the gas region only for $T \geqslant 393.15$ K whereas the selected $p\rho T$ data only exist for $T \geqslant 473.15$ K at $p \geqslant 0.1$ MPa, see also Fig. 4.1.

In the gas region, the data situation was clearly improved by the $p\rho T$ data of Kell *et al.* (1989). This fact can be clearly seen in Fig. 4.1 and the characteristic points of this data set are discussed in Sec. 4.2.1. In contrast to IAPS-84 and the equation of Hill (1990), IAPWS-95 represents these data to within their experimental uncertainty of ± 0.006 kg m^{-3} given by Kell *et al.* (1989). To give an example, this absolute uncertainty value corresponds to a percentage uncertainty in density of $\pm 0.025\%$ for the isotherm $T=548$ K at a pressure of $p=5$ MPa. The data set of Kell *et al.* (1989) extends to temperatures of 773 K; for the deviation diagrams regarding these data for $T>423$ K see Fig. 7.17.

There are very accurate $p\rho T$ data in the liquid region for temperatures from 273 to 423 K at pressures up to 100 MPa. The representation of these data by IAPWS-95 is illustrated in Fig. 7.12 with a suitable deviation scale. Thus, for Fig. 7.11, only the $p\rho T$ data of the liquid region for pressures between 100 and 1000 MPa are discussed.

It can be seen that IAPWS-95 and the equation of Hill (1990) are able to very well represent the high-pressure data measured by Grindley and Lind (1971) at temperatures between 298 and 423 K. For these two equations the deviations in density remain essentially within $\pm 0.02\%$, while they increase up to $\pm 0.2\%$ for IAPS-84. In Sec. 4.2.1, the inconsistency between the high-pressure data sets of Maier and Franck (1966), Köster and Franck (1969), and Hilbert *et al.* (1981) was discussed. The exclusion of the first two data sets from the selected data explains why IAPWS-95 represents the high-pressure data of Hilbert *et al.* (1981) clearly better than the other two equations of state plotted in these diagrams. Moreover, the fact that there are no essential inconsistencies in the high-pressure range of the selected $p\rho T$ data set has clearly improved the extrapolation behavior of IAPWS-95. This fact should be kept in mind when discussing the systematic deviations of the IST-85 values in the high-temperature high-pressure range, see Sec. 7.2.1.5.

Liquid range (T≤423.15 K, p≤100 MPa) covered by very accurate data. In order to illustrate the high quality of IAPWS-95 in representing the $p\rho T$ data in the liquid region for temperatures not greater than 423.15 K and pressures up to 100 MPa, Fig. 7.12 shows the corresponding deviation diagrams in high resolution. The representation of this part of the liquid region by IAPWS-95 is essentially based on the very accurate $p\rho T$ data of Kell and Whalley (1975). The experimental uncertainty of these data is $\pm 0.001\%$ in density at low pressures and up to $\pm 0.003\%$ at pressures up to 100 MPa. The IAPWS-95 formulation is able to represent the data to within these very small uncertainty values. This attribute of IAPWS-95 is very important for calibration purposes at higher pressures, and means a clear improvement in comparison with IAPS-84. Hill's equation also represents these data well; very small deviations appear only near $p=100$ MPa.

Highly accurate data of liquid densities at p=0.101 325 MPa. For a pressure of 0.101 325 MPa at temperatures from 273.15 to 358.15 K, there are highly accurate liquid density data of H_2O corresponding to an isotopic composition of VSMOW. The data are based on the BIPM value for the maximum density on this isobar and the measurements of thermal expansion carried out by Takenaka and Masui (1990) at the Japanese National Research Laboratory of Metrology (NRLM); for further details see Sec. 4.2.1. These data of metrological quality were of great importance for modeling IAPWS-95 in this part of the liquid region. Figure 7.13 shows that IAPWS-95 is indeed able to represent Takenaka's and Masui's densities to within the given experimental uncertainty of ± 1 ppm. The IAPWS-95 formulation is the only

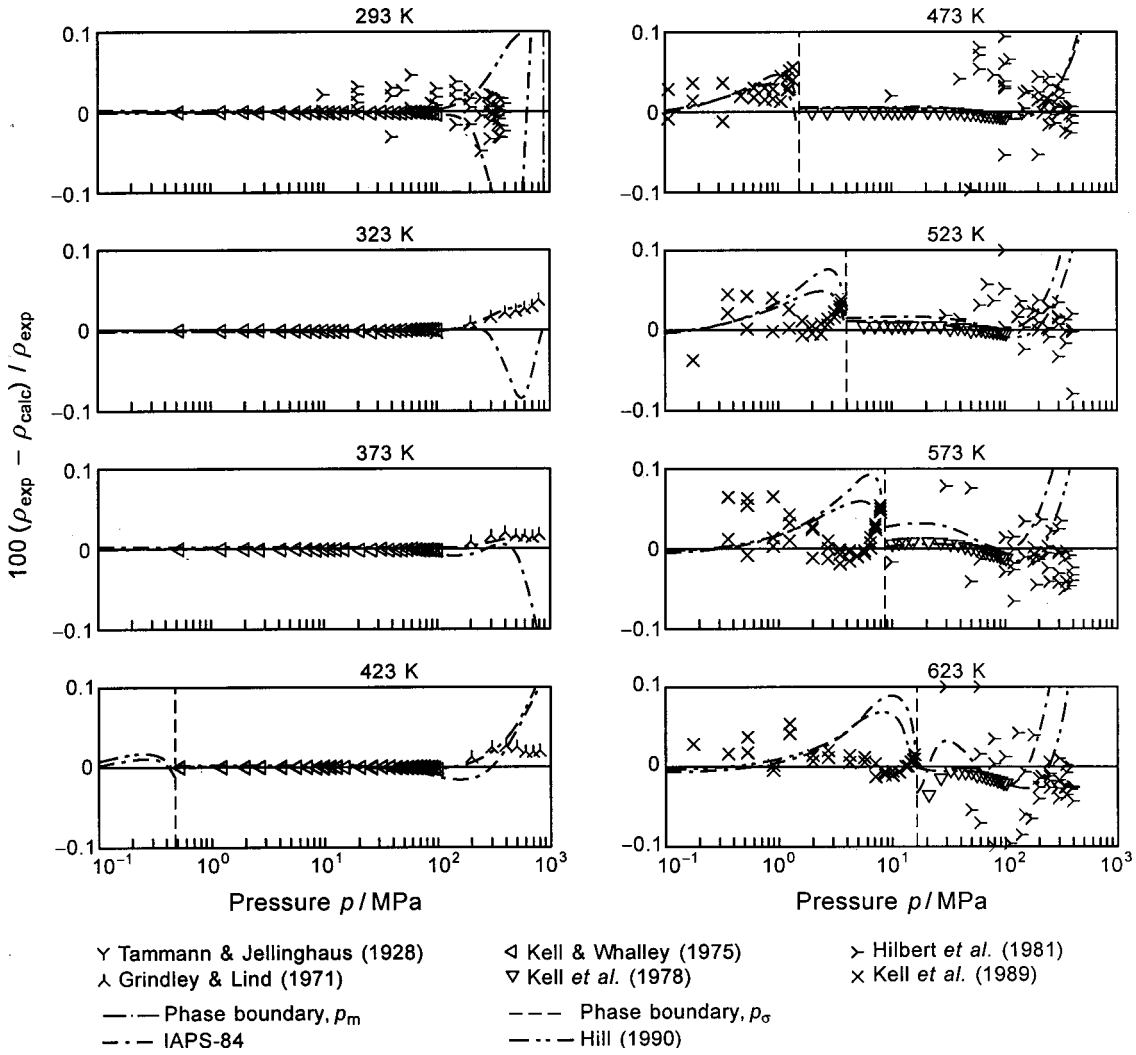

FIG. 7.11. Percentage density deviations between experimental $p\rho T$ data and values calculated from IAPWS-95, Eq. (6.4). Values calculated from IAPS-84 and the equation of Hill (1990) are plotted for comparison.

wide-range equation of state for H_2O which has such a quality in the liquid region at ambient pressure. The densities of Kell (1975), to which IAPWS-95 was not fitted, are included in Fig. 7.13 for comparison because they were the most accurate liquid densities for this isobar before Takenaka and Masui (1990) reported their values.

After the development of IAPWS-95 was finished, new liquid density measurements of metrological quality have been published for VSMOW at $p=0.101\,325$ MPa. These are the densities of Patterson and Morris (1994) measured at the CSIRO Australian National Measurement Laboratory and the measurements of Masui *et al.* (1995) carried out at NRLM; for details of these measurements see Sec. 4.2.1. Masui *et al.* (1995) also reported a $\rho(T)$ equation which represents their measurements very accurately. From this equation, we calculated 18 density values for temperatures from 273.15 to 358.15 K. As described in Sec. 4.2.1, for the isobar $p=0.101\,325$ MPa and temperatures from 273.15 to 313.15 K an internationally agreed set of densities was very recently adopted by a Task Group formed by the Working Group of Density of the Consultative Committee for Mass and Related Quantities, see Tanaka *et al.* (2001).

All these liquid–density data of metrological quality at $p=0.101\,325$ MPa are plotted in Fig. 7.14 in comparison with the values calculated from IAPWS-95. It can be seen that IAPWS-95 represents both the internationally agreed values of Tanaka *et al.* (2001) and the data of Takenaka and Masui (1990) to within ± 1 ppm; only the value of Tanaka *et al.* (2001) at $T=313.15$ K is with -1.1 ppm slightly outside the ± 1 ppm band. The value for the maximum density along this isobar determined from IAPWS-95 amounts to $\rho_{max}=999.9749\,\mathrm{kg\,m^{-3}}$, which agrees almost exactly with the value $\rho_{max}=999.974\,950\,\mathrm{kg\,m^{-3}}$ given by Tanaka *et al.* (2001); for the temperature of this ρ_{max} value and its uncertainty see Sec. 4.2.1. Thus, Fig. 7.14 confirms very clearly that the IAPWS-95 formulation produces accurate densities for VSMOW, even though the molar mass on which IAPWS-95 is based is not identical to that of VSMOW, see Sec. 6.1.

Extrapolation behavior of IAPWS-95. Recently, Wiryana

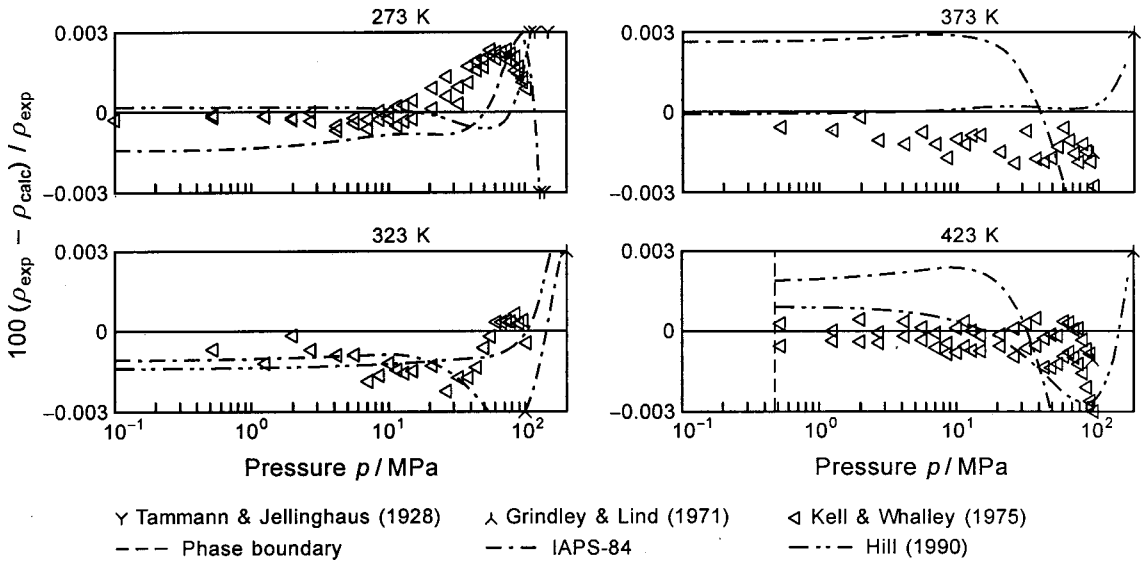

FIG. 7.12. Percentage density deviations between very accurate experimental $p\rho T$ data and values calculated from IAPWS-95, Eq. (6.4). Values calculated from IAPS-84 and the equation of Hill (1990) are plotted for comparison.

et al. (1998) reported $p\rho T$ data for temperatures from 353.15 to 473.15 K at pressures up to 3500 MPa. Although these data are not direct density measurements but were derived from their speed-of-sound measurements (see Sec. 4.2.1), they can be used to test the extrapolation behavior of IAPWS-95 at pressures up to 3.5 times its range of validity (1000 MPa). Figure 7.15 shows a comparison between Wiryana *et al.*'s $p\rho T$ data and the values calculated from IAPWS-95. The maximum deviation is about 0.2% and occurs at $T=473.15\,\mathrm{K}$ and $p=3500\,\mathrm{MPa}$. At this $p\rho T$ point, the deviations of IAPS-84 and the equation of Hill (1990) are slightly greater than 1%. This test shows the very good extrapolation capability of IAPWS-95, at least for the thermal properties in this temperature range.

7.2.1.3. Critical Region 643.15 K≤T<663.15 K. Figure 7.16 presents comparisons between the experimental $p\rho T$ data of the critical region and those values calculated from IAPWS-95, Eq. (6.4), covering a temperature range from 646.15 to 653.15 K ($T_c=647.096\,\mathrm{K}$) at densities from 0 to 500 $\mathrm{kg\,m^{-3}}$ ($\rho_c=322\,\mathrm{kg\,m^{-3}}$); the density range clearly exceeds the critical region. As usual, for this region with very large values of $(\partial\rho/\partial p)_T$, the comparisons are not presented as density deviations but as pressure deviations. Besides IAPS-84 and the equation of Hill (1990), values from the crossover equation of Kostrowicka Wyczalkowska *et al.* (2000) are plotted for comparison. It can be seen that IAPWS-95 represents the $p\rho T$ data on the near-critical isotherms to within the scatter of the data of about ±0.05% in pressure. The critical isotherm is excellently covered. The slight systematic peak of the data for $T=647.3\,\mathrm{K}$ and $T=648\,\mathrm{K}$ at about $\rho=370\ \mathrm{kg\,m^{-3}}$ is obviously an artifact of the data; none of the equations is able to follow this oscillation. For the density range of about ±25% around the critical density, the crossover equation of Kostrowicka Wyczalkowska *et al.* (2000) shows very good behavior as well, but outside this density range its deviations increase quite rap-

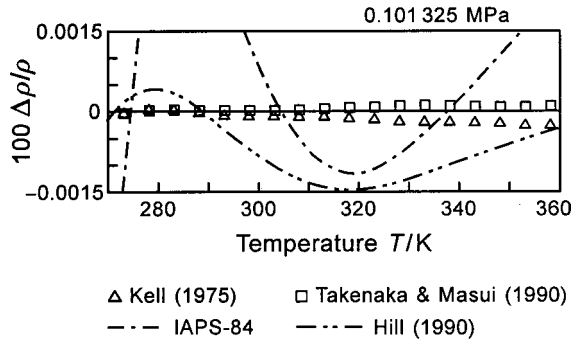

FIG. 7.13. Percentage density deviations $100\Delta\rho/\rho=100(\rho_{exp}-\rho_{calc})/\rho_{exp}$ between highly accurate experimental $p\rho T$ data along the isobar $p=0.101\,325\,\mathrm{MPa}$ and values calculated from IAPWS-95, Eq. (6.4). Values calculated from IAPS-84 and the equation of Hill (1990) are plotted for comparison.

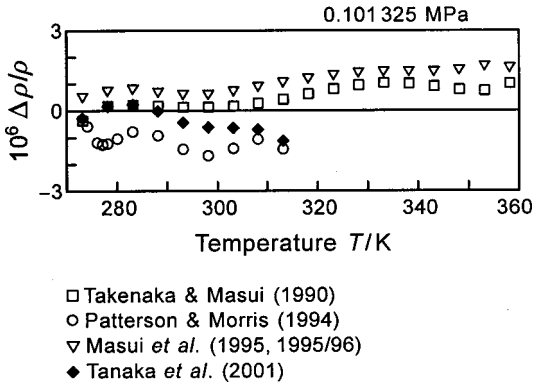

FIG. 7.14. Parts-per-million density deviations $10^6\Delta\rho/\rho=10^6(\rho_{exp}-\rho_{calc})/\rho_{exp}$ between highly accurate experimental $p\rho T$ data along the isobar $p=0.101\,325\,\mathrm{MPa}$ and values calculated from IAPWS-95, Eq. (6.4).

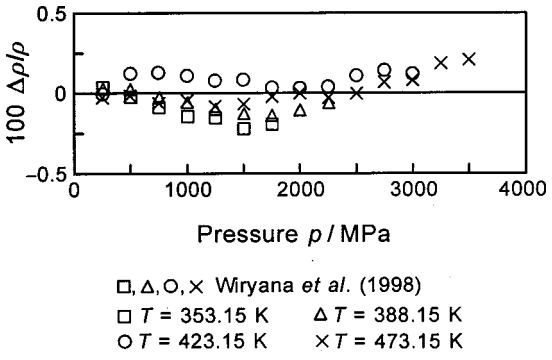

FIG. 7.15. Percentage density deviations $100\Delta\rho/\rho = 100(\rho_{exp} - \rho_{calc})/\rho_{exp}$ between the $p\rho T$ data of Wiryana *et al.* (1998) for temperatures from 353.15 to 473.15 K and values calculated with IAPWS-95, Eq. (6.4). For the pressures above 1000 MPa, IAPWS-95 was correspondingly extrapolated.

idly; the deviations are only plotted within the range of validity of this equation. The equation of Hill (1990) also represents the data very well, whereas IAPS-84 yields an oscillating course in this density range.

7.2.1.4. Temperature Range 663.15≤T<1273.15 K. The representation of the experimental $p\rho T$ data of the high-temperature range by IAPWS-95, Eq. (6.4), and by the other equations of state is summarized in Fig. 7.17 for six representative isotherms between 673 and 1123 K. It can be seen that the temperature region up to 773 K is still quite well covered by the $p\rho T$ data, which are represented by IAPWS-95 roughly to within ±0.1% in density (except for the isotherm $T = 673$ K near its inflection point). Besides the $p\rho T$ data of Hilbert *et al.* (1981), which extend to 873 K, the temperature range from 823 to 1174 K is covered only by the data of Vukalovich *et al.* (1962), see also Fig. 4.1. While Hilbert *et al.*'s data are still mostly represented by IAPWS-95 to within ±0.1% in density, there are systematic deviations from the data of Vukalovich *et al.* (1962) that extend up to 0.35% in density at 923 K. A better representation of these data would have made the extrapolation capability worse. The values from IAPS-84 and from the equation of Hill are plotted for comparison.

7.2.1.5. Comparison with the IAPS Skeleton Table Values at High Pressures and High Temperatures. In the past, knowledge of the thermodynamic properties of H_2O was summarized in a set of skeleton steam tables whose values had been found by critical evaluation of experimental data with respect to their estimated uncertainties in connection with statistical methods. In this way, Sato *et al.* (1988) established the "IAPS Skeleton Tables 1985 for the Thermodynamic Properties of Ordinary Water Substance," referred to

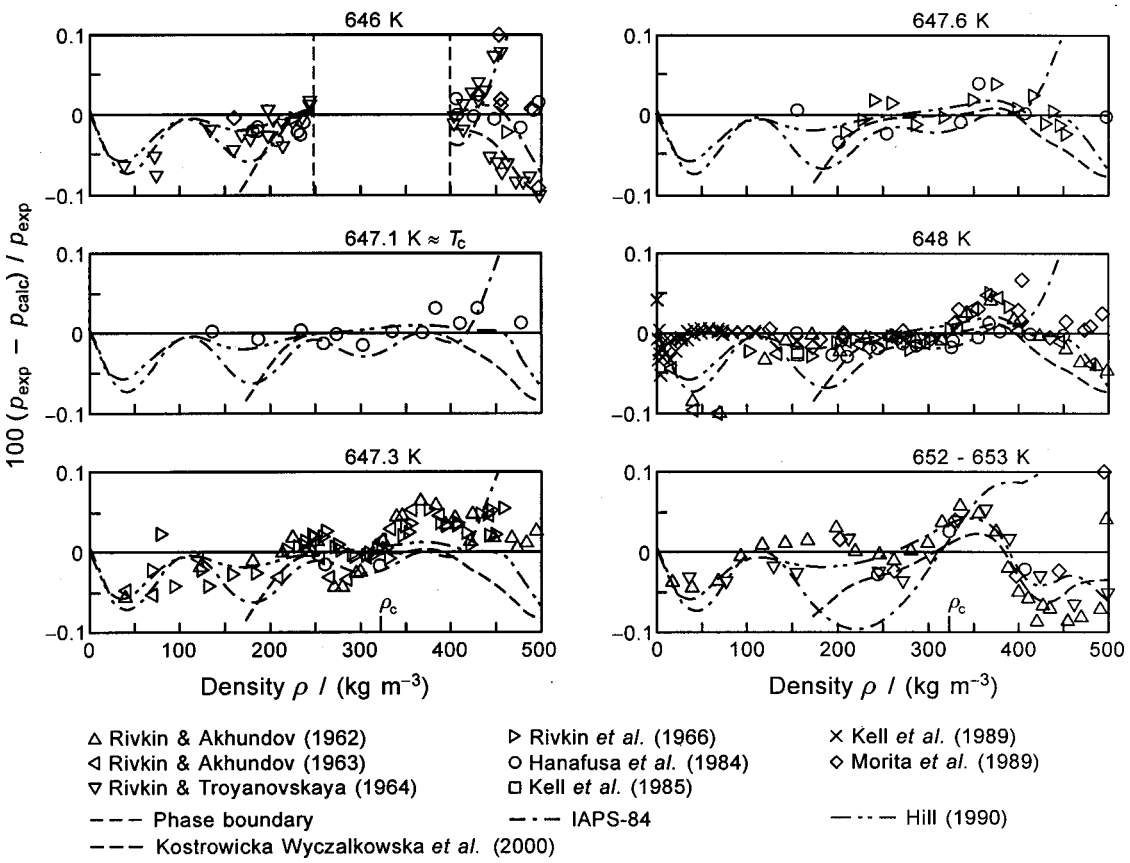

FIG. 7.16. Percentage pressure deviations between experimental $p\rho T$ data in the critical region and values calculated from IAPWS-95, Eq. (6.4); the density range of the diagrams clearly exceeds the critical region. Values calculated from IAPS-84, the equation of Hill (1990), and the crossover equation of Kostrowicka Wyczalkowska *et al.* (2000) are plotted for comparison; values from the crossover equation are only shown within its range of validity.

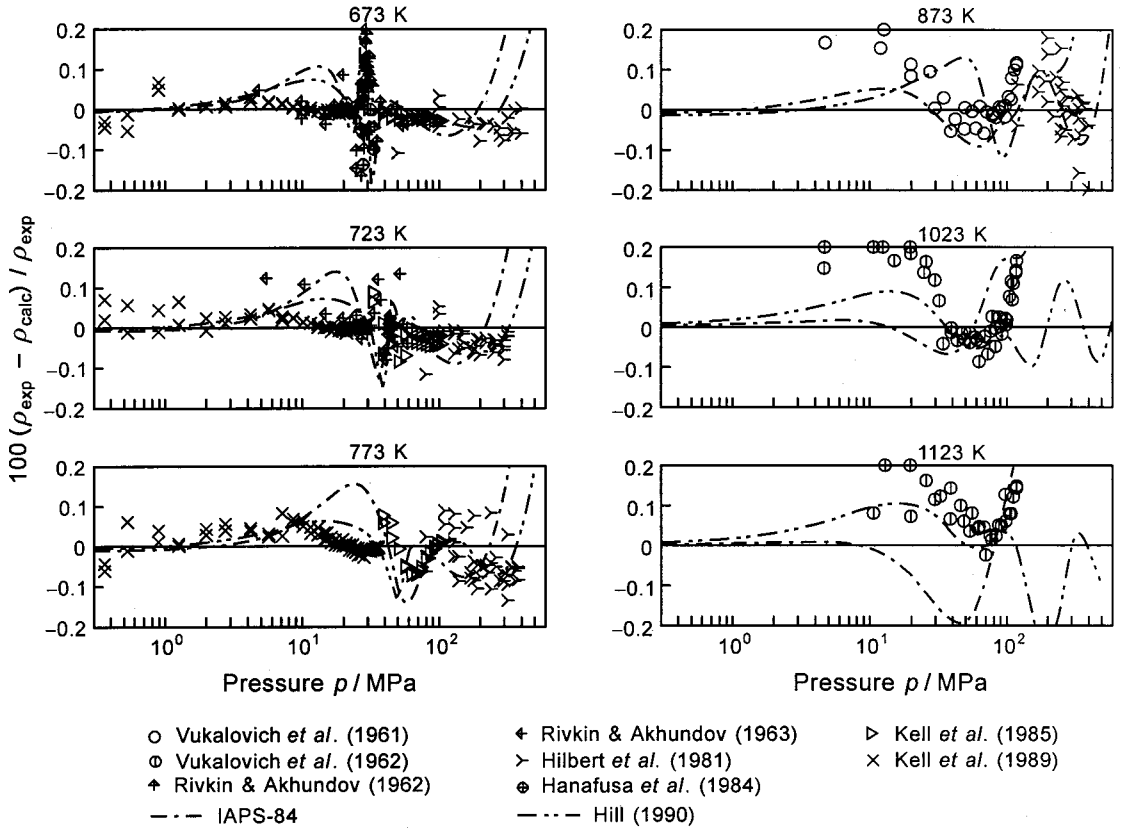

FIG. 7.17. Percentage density deviations between experimental $p\rho T$ data and values calculated from IAPWS-95, Eq. (6.4). Values calculated from IAPS-84 and the equation of Hill (1990) are plotted for comparison.

as IST-85 in the following. IST-85 contains values for the specific volume and specific enthalpy that were originally based on the temperature scale IPTS-68; a revised release [IAPWS (1994)] provides the values corresponding to the current temperature scale ITS-90.

The IAPWS task group for evaluating the IAPWS-95 formulation ascertained that, in the high-temperature high-pressure range, the IST-85 values of the specific volume exhibit systematically positive deviations from the corresponding values of IAPWS-95, Eq. (6.4). For temperatures from 573 to 1073 K and pressures greater than 200 MPa, there are ranges of pressure where the deviations of the IST-85 values exceed their tolerances. Figure 7.18 illustrates this situation for three high-temperature isotherms. It can be seen that the IST-85 values are clearly influenced by the $p\rho T$ data sets of Maier and Franck (1966) and of Köster and Franck (1969) which are not consistent with the data set of Hilbert *et al.* (1981), see the discussion in Sec. 4.2.1 in context with Fig. 4.4. Hilbert *et al.*'s $p\rho T$ data have uncertainties of less than $\pm 0.2\%$ in density and are therefore five times more accurate than the other two data sets. Moreover, Fig. 4.4 shows that Hilbert *et al.*'s data are confirmed at lower pressures by the data of Kell *et al.* (1978) and at higher pressures by the recent data of Wiryana *et al.* (1998). Thus, it can be concluded that the IST-85 values are misguided in this high-temperature high-pressure range by the $p\rho T$ data of Maier and Franck (1966) and of Köster and Franck (1969). Although there are no $p\rho T$ data of Hilbert *et al.* (1981) for $T > 873$ K, the course of IAPWS-95 in the high-temperature high-pressure range is guided by the data of Hilbert *et al.* (1981).

In general, it can be stated that the thermodynamic surface of water (or of any other substance) can be much better defined by an accurate wide-range equation of state, such as IAPWS-95, than by any skeleton table, such as IST-85; an equation of state contains much more thermodynamic information than one can take into account when establishing skeleton tables.

7.2.2. Second and Third Virial Coefficients

As discussed in detail in Sec. 4.2.2, the IAPWS-95 formulation was not fitted to experimental values of the second virial coefficient B (neither, of course, to the third virial coefficient C). Nevertheless, in the following the B and C values calculated from IAPWS-95, Eq. (6.4), are compared with the experimental data sets for the second and third virial coefficients. The outer diagram of Fig. 7.19 shows the second virial coefficient B versus temperature T as calculated from IAPWS-95, IAPS-84, and the equation of Hill (1990); since the virial equation of Hill and MacMillan (1988) is very often used in context with virial coefficients of H_2O,

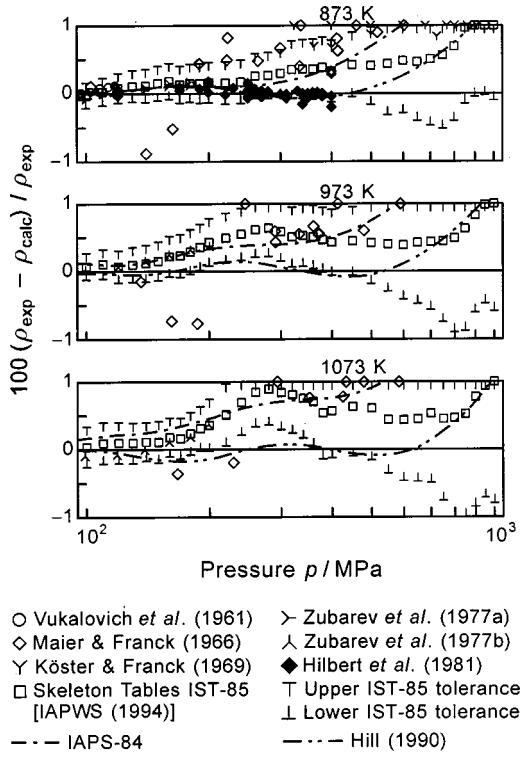

FIG. 7.18. Percentage density deviations of experimental $p\rho T$ data and values of the Skeleton Tables IST-85 [IAPWS (1994)] together with their tolerances from values calculated with IAPWS-95, Eq. (6.4). Values calculated from IAPS-84 and the equation of Hill (1990) are plotted for comparison.

values from this equation and the experimental B values are also plotted. For temperatures down to 275 K, all four equations yield a very similar plot of B, whereas for very low temperatures the equation of Hill (1990) does not go asymptotically to minus infinity but yields again increasing B values. The inner diagram of Fig. 7.19 presents the absolute deviations between experimental second virial coefficients and the corresponding values calculated from IAPWS-95. It can be seen that the most reliable experimental B values, namely the data of Eubank *et al.* (1988) at 373, 403, and 423 K and of Kell *et al.* (1989) for temperatures from 448 to 723 K, are very well represented by IAPWS-95 to within 1–3 $\mathrm{cm^3\,mol^{-1}}$. For temperatures above 723 up to 1173 K, IAPWS-95 represents the B values of Vukalovich *et al.* (1967) to within 2 $\mathrm{cm^3\,mol^{-1}}$; this temperature range is not covered by the inner deviation diagram of Fig. 7.19. For temperatures above the normal boiling temperature T_b, all four equations represent the most accurate B data [Eubank *et al.* (1988) and Kell *et al.* (1989)] similarly well, where, however, the equation of Hill and MacMillan (1988) remains below the data for temperatures above 550 K; this is of importance when discussing the representation of the data of the third virial coefficients C at about T_c. All three equations, IAPS-84, Hill (1990), and Hill and MacMillan (1988), exhibit clearly increasing deviations from the IAPWS-95 values (zero line) for temperatures below about 350 K because these equations were either fitted to B values calculated from the correlation equation for the second virial coefficient developed by Le Fevre *et al.* (1975) or in the case of Hill and MacMillan (1988) to the data of the isothermal throttling coefficient at zero-density limit (see Sec. 7.2.7). For temperatures below 423 K, Le Fevre *et al.*'s equation was exclusively fitted to experimental B values derived from measurements of the isothermal throttling coefficient; we estimate that these B values [see Le Fevre (1975)] exhibit systematic trends to higher B values.

The third virial coefficient C calculated from the four equations of state is plotted in Fig. 7.20. The C data, which are also based on $p\rho T$ data extrapolated to $\rho\rightarrow 0$, are still more uncertain than the B data; thus, the data of the third virial coefficient were not used to fit IAPWS-95 either. Figure 7.20 shows the absolute course of the C values calculated from the four equations for temperatures from 300 to 2000 K; the experimental data are plotted for comparison. The inner diagram of Fig. 7.20 shows an enlarged section for temperatures from 500 to 1500 K. It can be seen that only the equation of Hill and MacMillan agrees with the C data for temperatures from 625 to 750 K; all three wide-range equations of state [IAPS-84, IAPWS-95, and Hill (1990)] are not able to cover these data. The virial equation of Hill and MacMillan (1988) was fitted to the B and C values discussed here, and the requirement to cover these C data leads to B values from this equation which are in this range systematically slightly lower than those of the wide-range equations. Moreover, starting at about 550 K but more clearly for temperatures between 648 and 748 K at pressures above 4 MPa, this equation cannot represent the very accurate $p\rho T$ data of Kell *et al.* (1989) to within their uncertainty. This confirms our decision not to fit IAPWS-95 to the experimental data of the virial coefficients.

According to theoretical considerations, the third virial coefficient should reach a maximum at about the critical temperature. A qualitatively correct plot of the third virial coefficient at high temperatures is a prerequisite of an equation of state for it to yield a reasonable Joule inversion curve, see Colina and Olivera-Fuentes (2001). The Joule inversion curve is far outside the range of validity of IAPWS-95 and the other two wide-range equations of state. Its representation is therefore a good extrapolation test, see Sec. 7.3.3.

From the inner diagram of Fig. 7.20, it can be seen that, of the three wide-range equations of state, only IAPWS-95 meets this criterion. IAPS-84 and the equation of Hill (1990) yield a maximum in $C(T)$ only at temperatures $T>3T_c$.

7.2.3. Speed of Sound

Figure 4.5 shows the distribution of the experimental data of the speed of sound w used to develop the IAPWS-95 formulation, see also Table 4.5. In the following, these data are compared with the corresponding w values calculated from the IAPWS-95 formulation, Eq. (6.4), and from the other three equations of state mentioned at the beginning of

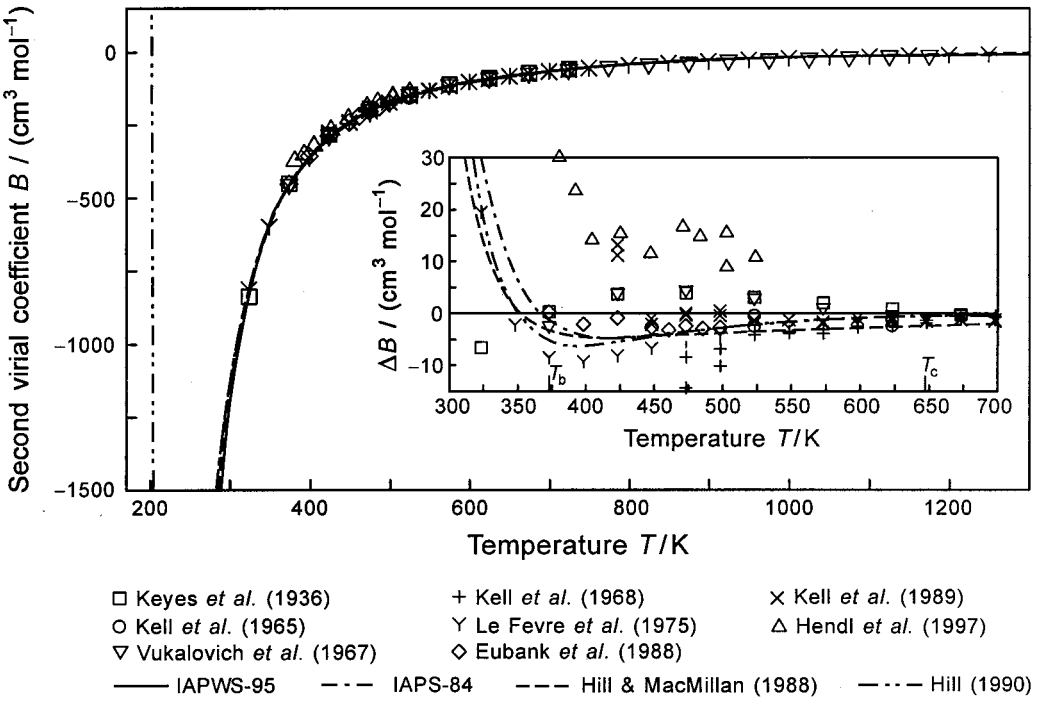

FIG. 7.19. Second virial coefficient B as a function of temperature as calculated from IAPWS-95, Eq. (6.4); the experimental data are plotted for comparison. The inner diagram shows absolute deviations $\Delta B = B_{exp} - B_{calc}$ between experimental B data and values calculated from IAPWS-95. In both diagrams, B values calculated from IAPS-84, the equation of state of Hill (1990), and the virial equation of Hill and MacMillan (1988) are plotted for comparison.

Sec. 7. Since the selected data summarized in Table 4.5 do not cover the critical region, the data sets of Erokhin and Kal'yanov (1979), (1980) are used for comparisons in the critical region but also outside the critical region.

The percentage deviation diagrams of Fig. 7.21, with deviation scales between $\pm 0.3\%$ and $\pm 1\%$, cover a temperature range from 252 to 873 K. In the two diagrams below 273 K, the stable liquid region is only located in the small range between the two-phase-boundary lines corresponding to the melting pressure. IAPWS-95 is able to represent these low-temperature speed-of-sound data to within $\pm 0.25\%$, while the w values from IAPS-84 deviate by more than 10% and those from the equation of Hill (1990) by about 1%. For the isotherms up to $T = 474$ K, the vast majority of the w data is represented by IAPWS-95 with deviations of less than $\pm 0.1\%$. In particular, the measurements of the speed of sound in the liquid phase at temperatures up to 330 K and pressures up to 100 MPa are better covered by IAPWS-95 than by IAPS-84 and Hill's equation. The very accurate w data of Fujii (1994) on the three isotherms 303, 313 (not shown), and 323 K at pressures from 10 to 200 MPa are represented to within $\pm 0.025\%$, which is also not achieved by the two other equations.

The representation of the gas-region speed-of-sound data of Novikov and Avdonin (1968) within $\pm 0.2\%$ by IAPWS-95 is consistent with the representation of the w'' data of these authors along the saturated vapor line, see Fig. 7.5 and the discussion in Sec. 7.1.2.

From the isotherms 423–596 K, it can be seen that, near the phase boundary, the w values from IAPWS-95 remain above the liquid-region data (but within their experimental uncertainty). This behavior was accepted since IAPWS-95 would have otherwise yielded values of w' that were too low

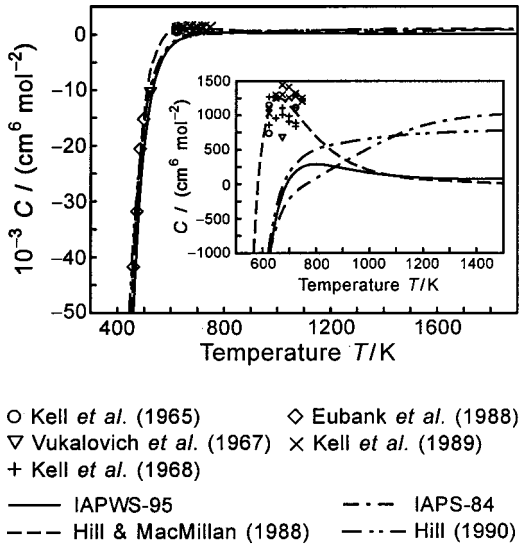

FIG. 7.20. Third virial coefficient C as a function of temperature as calculated from IAPWS-95, Eq. (6.4); the experimental data are plotted for comparison. The inner diagram shows an enlarged section of the plot of C around its maximum. In both diagrams C values calculated from IAPS-84, the equation of state of Hill (1990), and the virial equation of Hill and MacMillan (1988) are plotted for comparison.

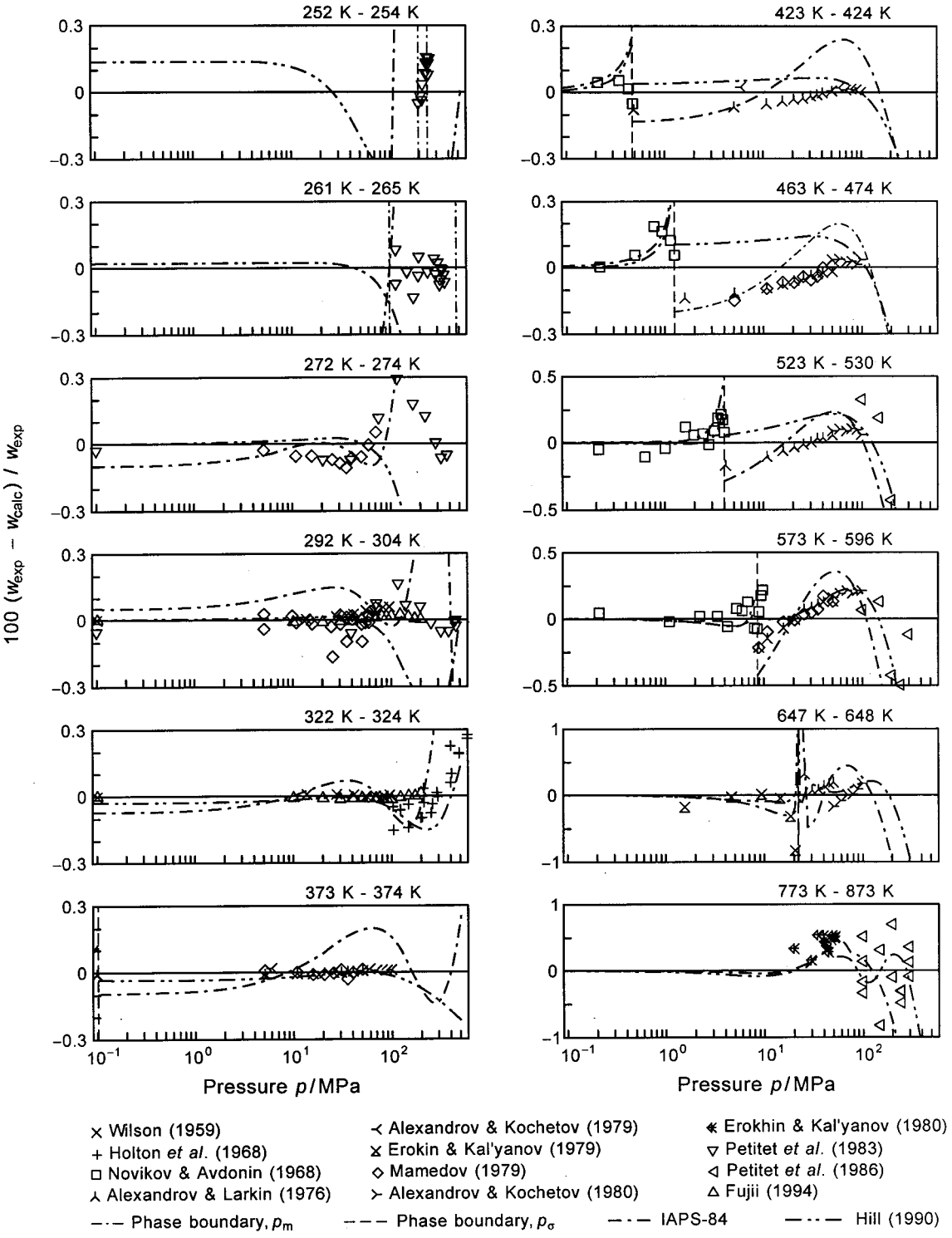

FIG. 7.21. Percentage deviations between experimental data of the speed of sound w and values calculated from IAPWS-95, Eq. (6.4). Values calculated from IAPS-84 and the equation of Hill (1990) are plotted for comparison. In the first two diagrams, the stable liquid region is bordered by the two phase-boundary lines of the melting pressure p_m.

and would also have had difficulties with the enthalpies h' along the saturated liquid line at these temperatures, see the discussion in Sec. 7.1.2. Obviously, there are some inconsistencies between the w data in this region and the corresponding $p\rho T$ data. This conclusion is supported by the plot of w values calculated from the equation of Hill (1990). IAPS-84 was forced to better fit the w data near the phase boundary, but then has the difficulties mentioned above and also has problems in the liquid region at about 60 MPa. In the diagram for the temperatures between 647 and 648 K, the data

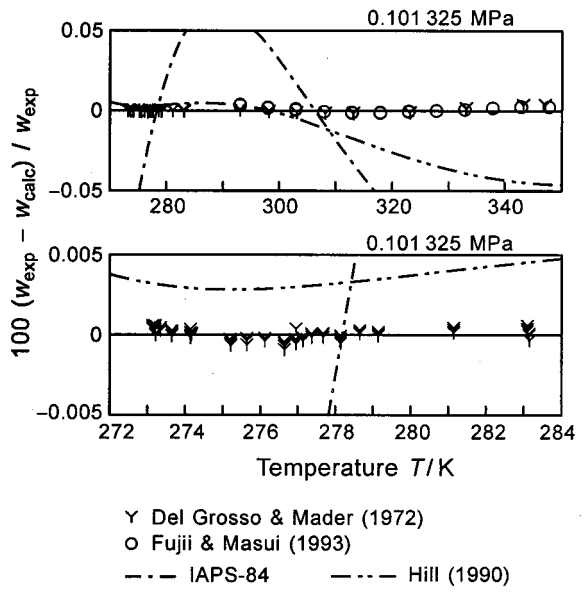

FIG. 7.22. Percentage deviations between very accurate experimental data of the speed of sound w along the isobar $p=0.101\,325$ MPa and values calculated from IAPWS-95, Eq. (6.4). Values calculated from IAPS-84 and the equation of Hill (1990) are plotted for comparison.

of Erokhin and Kal'yanov (1979) for $p>20.63$ MPa were omitted because the critical region is discussed below. The diagrams for $T>648$ K show that this region is not very well covered by the selected experimental speeds of sound. From the data of Petitet *et al.* (1986), which extend to temperatures of 968 K, only those data up to 873 K are compared in Fig. 7.21. However, the deviations of their data above 873 K look very similar.

Similar to the $p\rho T$ measurements on liquid water at ambient pressure, there are very accurate speed-of-sound data at $p=0.101\,325$ MPa measured by Del Grosso and Mader (1972) and by Fujii and Masui (1993). The upper diagram of Fig. 7.22 illustrates that the IAPWS-95 formulation is able to cover these data sets with a maximum deviation of about $\pm 0.003\%$. The lower diagram shows that, for temperatures up to $T=284$ K, the w data of Del Grosso and Mader (1972) are represented by IAPWS-95 to within $\pm 0.001\%$, which is within the experimental uncertainty of these data. IAPS-84 and Hill's equation do not achieve this accuracy.

There are no accurate speed-of-sound data for the critical region close to the critical point. The strong decrease of the speed of sound to very small values when approaching the critical point can hardly be measured for water (frequency-dependent dispersion effects). The w data closest to the critical point were reported by Erokhin and Kal'yanov (1979), (1980). However, even these data remain relatively far away from the critical point, and consequently the smallest values of these speed-of-sound data are on the order of 300 m s^{-1}. Nevertheless, in order to illustrate how IAPWS-95 behaves in the critical region with regard to the speed of sound, Fig. 7.23 shows absolute w values calculated from IAPWS-95, from the equation of Hill (1990) and, within its range of validity, also from the crossover equation of Kostrowicka Wyczalkowska *et al.* (2000); for comparison the diagram also contains the experimental data of Erokhin and Kal'yanov (1980). It can be seen that IAPWS-95 represents this part of the critical region well where the temperature goes down to $T=648.196$ K (1.1 K above T_c). Due to the steep slope of the isotherms near their minima, it is a matter of course that the differences in w between the experimental data and the values from any equation of state increase correspondingly. The deviation diagrams on the left of Fig. 7.24, which correspond to the pressure range of Fig. 7.23, show that the maximum differences between the experimental data and the values from IAPWS-95 amount to about 4% at $T=648.196$ K and less than 2% on the two other isotherms. From Figs. 7.23 and 7.24, it can be seen that IAPWS-95 and Hill's equation agree, on average, better with each other than with the experimental data. Both equations are determined more by the reliable $p\rho T$ data in this region and less by the w data of Erokhin and Kal'yanow (1980), which do not agree so well with the $p\rho T$ data. The right-hand side of Fig. 7.24 illustrates that outside the closest pressure range around the minima of the speed of sound the deviations in w between the experimental data and the values from IAPWS-95 go down to $\pm 0.5\%$ and less.

Due to its nonanalytical terms [$i=55$ and 56 in Eq. (6.6)], IAPWS-95, is able to yield the steep decrease of the speed of sound when approaching the critical point, see Fig. 6.7 in Sec. 6.4.1. However, IAPWS-95 also has certain weaknesses in representing the speed of sound in the critical region, namely extremely near the phase boundary (within 2.5 mK above the saturation temperature) for densities about 6% around the critical density and along the phase boundary for densities about 4.5% around the critical density; for details see the discussion in connection with Figs. 6.14 and 6.16 in Sec. 6.4.2.

Wiryana *et al.* (1998) reported speed-of-sound data of H_2O at temperatures between 353.15 and 473.15 K at pressures up to 3500 MPa, see Sec. 4.3. A comparison between these data and w values calculated with IAPWS-95 is presented in Fig. 7.25. It can be seen that within its range of validity (1000 MPa) IAPWS-95 represents the data with deviations less than 1%, while in the pressure range from 1000 to 3500 MPa where IAPWS-95 was extrapolated, the maximum deviation does not exceed 2%. When IAPS-84 and the equation of Hill (1990) are extrapolated correspondingly, IAPS-84 exhibits deviations of more than 10% at temperatures of 353.15 and 388.15 K, while the maximum deviation of Hill's equation is about 9% at $T=473.15$ K.

7.2.4. Isochoric Heat Capacity

Figure 4.6 shows that the available experimental data for the isochoric heat capacity c_v cover the density range from 20 to 1000 kg m^{-3}. Due to the relatively large uncertainties and inconsistencies of the c_v data measured at the Dagestan Scientific Center of the Russian Academy of Sciences, from the totality of nearly 3400 data points of the isochoric heat

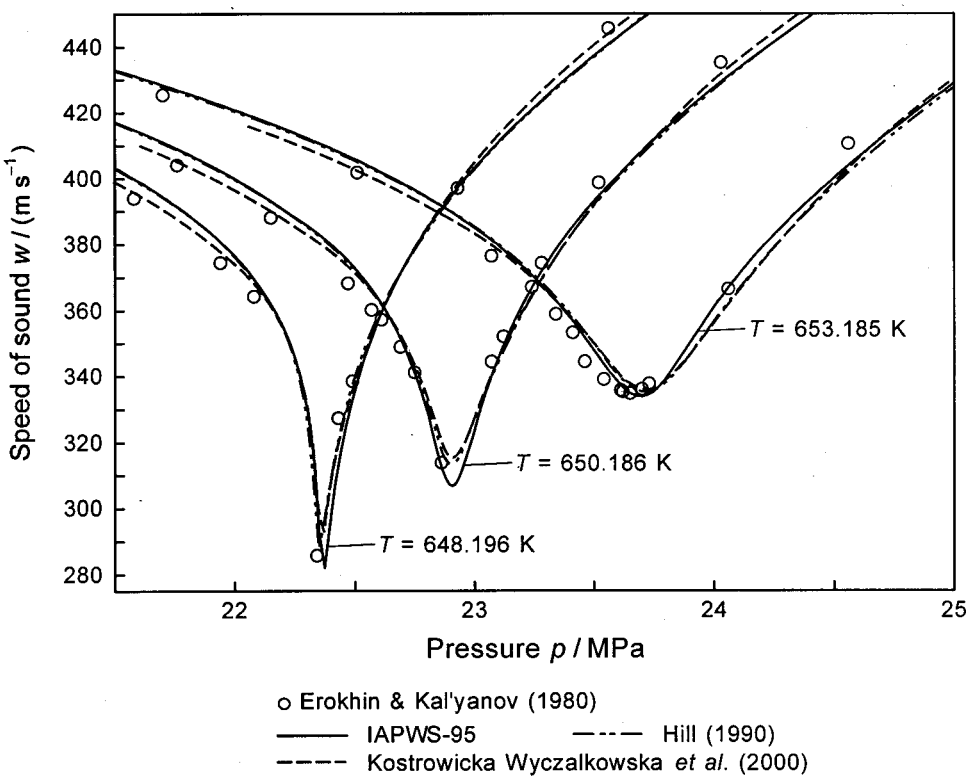

FIG. 7.23. Speed of sound in the critical region as a function of pressure on three isotherms as calculated from IAPWS-95, the equation of Hill (1990), and the crossover equation of Kostrowicka Wyczalkowska *et al.* (2000); values from the crossover equation are only shown within its range of validity. The experimental data of Erokhin and Kal'yanov (1980) are plotted for comparison.

capacity, the IAPWS-95 formulation was fitted only to those 113 c_v data of Baehr and Schomäcker (1975) that are in the single-phase region, see also Table 4.6. Therefore, the following comparisons with the c_v data are more a discussion of the data situation and give an impression of how IAPWS-95 represents the c_v surface without being fitted to accurate c_v data. The conclusion drawn from the comparisons is representative for the entire range of the c_v data shown in Fig. 4.6. For comparison purposes, besides the c_v values from the IAPWS-95 formulation, Eq. (6.4), most of the figures also contain the corresponding values from the other three equations of state mentioned at the beginning of Sec. 7.

Starting at low densities, Fig. 7.26 shows for the range near $\rho=50$ kg m^{-3} how IAPWS-95 predicts c_v values in comparison with the experimental data. The absolute c_v-T diagram illustrates inconsistencies (unnatural indentation) in the data set of Kerimov and Alieva (1975) at temperatures between 645 and 725 K. From the percentage deviation diagram of Fig. 7.26, it can be seen that the differences between the data of Kerimov and Alieva (1975) and of Amirkhanov *et al.* (1969) amount to 5% and the data of Kerimov (1964) deviate from the other two data sets by up to 15%. It is interesting to see that the equations of Hill (1990) and IAPWS-95 yield nearly the same c_v values in this region and, as can be seen in the following figures, in the entire region considered here except for the critical region.

For three characteristic isochores between about 200 and 400 kg m^{-3} covered by the c_v measurements of Baehr and Schomäcker (1975), Fig. 7.27 presents percentage deviations between the experimental data and the values calculated from IAPWS-95; the deviation scale corresponds to the uncertainty of the data. While IAPWS-95 and the equation of Hill (1990) represent the experimental data to within their uncertainty, IAPS-84 exhibits weaknesses when approaching the phase boundary from the single-phase region. The experimental isochore that is closest to the critical isochore ($\rho_c=322$ kg m^{-3}) is $\rho=323.8$ kg m^{-3}; this isochore is also very well represented by IAPWS-95. Nevertheless, from the deviation diagrams on the right of the phase boundary, it can be seen that the crossover equation of Kostrowicka Wyczalkowska *et al.* (2000) and Hill's equation represent the experimental data closest to the phase boundary better than IAPWS-95, see also Fig. 7.28 (top). Since the values from IAPS-84 oscillate very strongly near the phase boundary, these values were omitted in this region. Although IAPWS-95 was not fitted to the c_v data of Baehr and Schomäcker (1975) in the two-phase region (left of the phase boundary in Fig. 7.27), data in this region are also very well covered by IAPWS-95. We believe that c_v values within the two-phase region can be more accurately calculated than measured, except very close to the critical point. This basic statement applies to all equations of state that accurately represent the thermal saturation properties and the internal en-

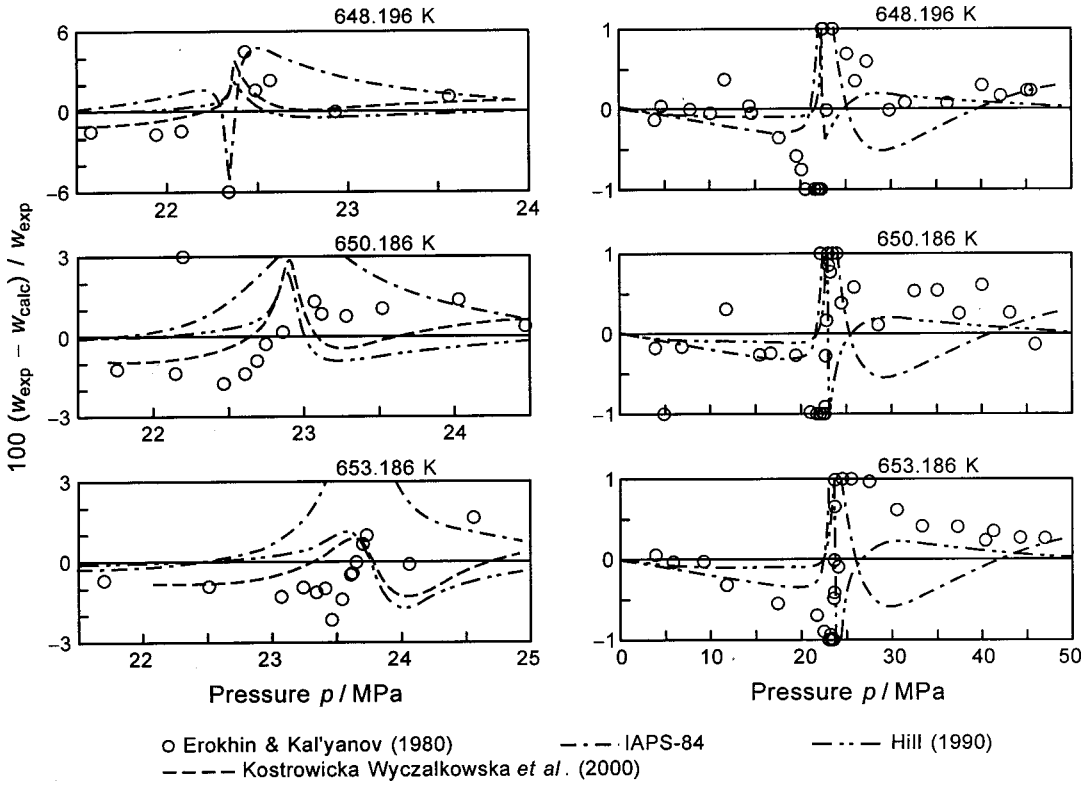

FIG. 7.24. Percentage deviations between experimental data of the speed of sound w and values calculated from IAPWS-95, Eq. (6.4). Values calculated from IAPS-84, the equation of Hill (1990), and the crossover equation of Kostrowicka Wyczalkowska *et al.* (2000) are plotted for comparison; the crossover equation is only shown in the diagrams on the left and only within its range of validity. The diagrams on the left correspond to the same isotherms and the same pressure range as given in Fig. 7.23. The diagrams on the right, which have a deviation scale of ±1%, cover a greater pressure range.

ergies of vaporization. This is the reason why IAPWS-95, the Hill equation, and IAPS-84 yield nearly the same c_v values within the two-phase region (the crossover equation is only valid for temperatures above 630 K).

There are two density regions where the c_v data of Baehr and Schomäcker (1975) and of three groups of authors at the Dagestan Scientific Center overlap, namely for $\rho \approx 310\ \mathrm{kg\,m^{-3}}$ and $\rho \approx 344\ \mathrm{kg\,m^{-3}}$ ($\rho_c = 322\ \mathrm{kg\,m^{-3}}$). Figure 7.28 presents deviation diagrams for these two isochores. The upper diagrams mainly contain the data of Baehr and Schomäcker (1975), which do not extend very close to the phase boundary (saturation temperature). The lower diagrams present the inner temperature range around the phase boundary covered by the c_v data of the Dagestan Scientific Center; there is also one c_v data point of Baehr and Schomäcker (1975) in the two-phase region at about 643 K. One can see from the upper diagrams that the data of Polikhronidi *et al.* (2001) and of Abdulagatov *et al.* (1998) deviate systematically from those of Baehr and Schomäcker (1975), namely in the two-phase region between 7% and 12% and in the single-phase region by about 5%. From the lower diagrams it can be seen that in the two-phase region, and in the single-phase region as well, the data sets of Kerimov (1964), Abdulagatov *et al.* (1998), and of Polikhronidi *et al.* (2001) are not very consistent with each other; even the two more recent data sets differ by up to 8% in the two-phase region. These diagrams also show that IAPS-84 was misled by the old data of Kerimov (1964), and that the difference between IAPWS-95 and the crossover equation of Kostrowicka Wyczalkowska *et al.* (2000) is not too large.

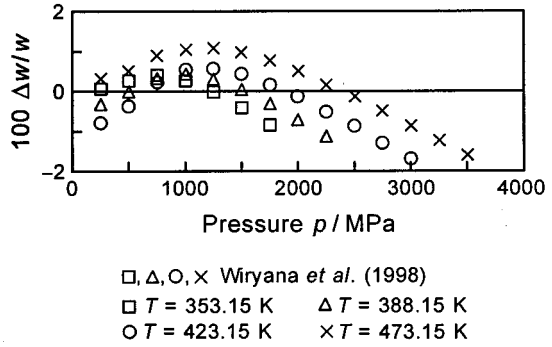

FIG. 7.25. Percentage deviations $100\Delta w/w = 100(w_{exp} - w_{calc})/w_{exp}$ between the experimental data of the speed of sound w of Wiryana *et al.* (1998) for temperatures from 353.15 to 473.15 K and values calculated with IAPWS-95, Eq. (6.4). For the pressures above 1000 MPa, IAPWS-95 was extrapolated.

The isochore $\rho = 316.84\ \mathrm{kg\,m^{-3}}$ is the one closest to the critical density ($\rho_c = 322\ \mathrm{kg\,m^{-3}}$) that is covered by experimental data up to very near the saturation temperature $T_\sigma = 647.095$ K ($T_c = 647.096$ K). For this isochore, Fig. 7.29 illustrates by an absolute $c_v - T$ diagram that IAPWS-95 is able to follow the steep increase of the c_v data when approaching the saturation temperature T_σ (phase boundary),

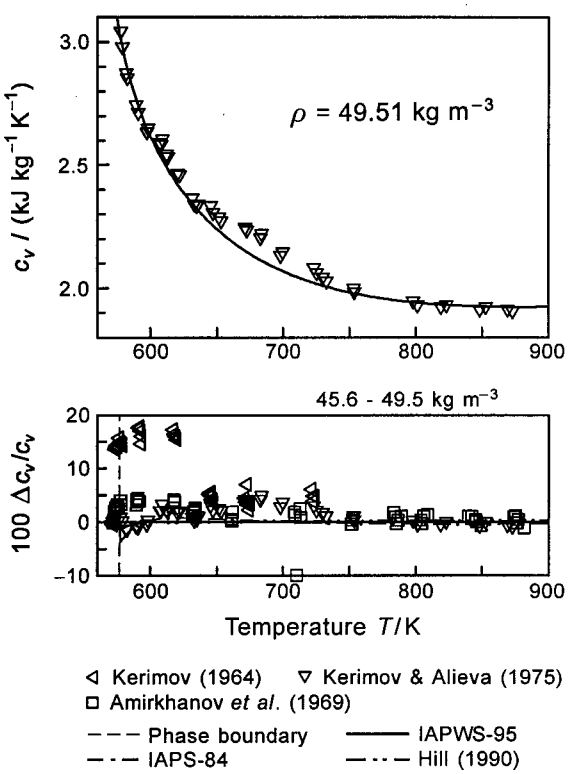

FIG. 7.26. Comparison between experimental data of the isochoric heat capacity c_v and values calculated from IAPWS-95, Eq. (6.4), IAPS-84, and the equation of Hill (1990). (Upper diagram) Absolute plot of c_v as a function of temperature for the isochore $\rho = 49.51\ \mathrm{kg\,m^{-3}}$; (Lower diagram) Percentage deviations $100\Delta c_v/c_v = 100(c_{v,\mathrm{exp}} - c_{v,\mathrm{calc}})/c_{v,\mathrm{exp}}$ for the density range given.

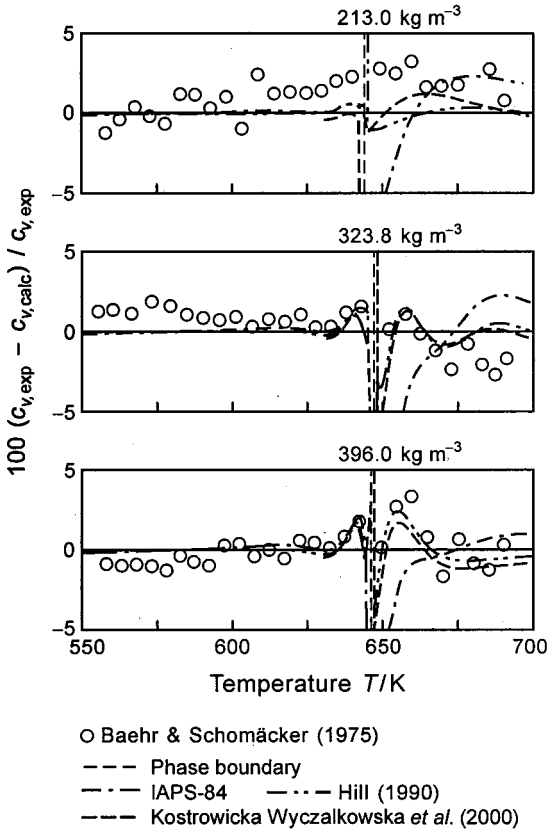

FIG. 7.27. Percentage deviations between experimental data of the isochoric heat capacity c_v in the extended critical region and values calculated from IAPWS-95, Eq. (6.4). Values calculated from IAPS-84, the equation of Hill (1990), and the crossover equation of Kostrowicka Wyczalkowska *et al.* (2000) are plotted for comparison; values of the crossover equation are only shown within its range of validity. Since IAPS-84 oscillates very strongly near the phase boundary, the corresponding lines were omitted in this region.

see also the diagram in the upper right corner of this figure. However, compared with the crossover equation of Kostrowicka Wyczalkowska *et al.* (2000) the shape of the isochore calculated from IAPWS-95 does not have such a steady curvature; very close to T_σ the slope of IAPWS-95 is too steep and further away from T_σ it is too flat. Nevertheless, as shown for the c_v point of Abdulagatov *et al.* (1995) with $c_v = 6.883\ \mathrm{kJ\,kg^{-1}\,K^{-1}}$, the difference between IAPWS-95 and the crossover equation amounts to -8.4% in c_v corresponding to -0.13 K or -0.02% in temperature. This means that such differences are well within the experimental uncertainty. Thus, such differences in c_v must not be overrated if they occur in regions with a steep slope of the isochoric heat capacity. One can also see from the small diagram in the upper right corner of this figure that the differences in temperature between IAPWS-95 and the crossover equation of Kostrowicka Wyczalkowska *et al.* (2000) practically vanish; for example, at $c_v = 18\ \mathrm{kJ\,kg^{-1}\,K^{-1}}$ the difference between IAPWS-95 and the crossover equation is about -0.04 mK. This difference is well within the scatter of the data with respect to temperature.

Figure 7.30 presents c_v along the isochore $\rho \approx 344\ \mathrm{kg\,m^{-3}} = 1.07\,\rho_c$. The diagram on the left covers a greater temperature range that also includes a part of the data of Baehr and Schomäcker (1975), while the diagram on the right shows the temperature range a few Kelvin around the saturation temperature T_σ, which is dominated by the data of Kerimov (1964) and of Abdulagatov *et al.* (1998). As one can see, IAPWS-95 is also able to follow the steep increase of the c_v data when approaching the saturation temperature from the two-phase region. Again, close to T_σ, the slope of the IAPWS-95 line is first too flat and then too steep, see the diagram on the right. This diagram also clearly shows that IAPS-84 yields the jump in c_v in the wrong place; this behavior is based on the poor representation of the densities of the saturated vapor and liquid in this near-critical region, see Fig. 7.4.

Although the IAPWS-95 formulation is generally able to yield reasonable c_v values in most of the critical region, IAPWS-95 has certain weaknesses in representing the isochoric heat capacity, in particular extremely near the phase boundary (within 2.5 mK above the saturation temperature) for densities about 6% around the critical density and along the phase boundary for densities about 4.5% around the critical density; for details see the discussion in connection with Figs. 6.13 and 6.15 in Sec. 6.4.2.

In Fig. 7.31, experimental c_v data at higher densities are

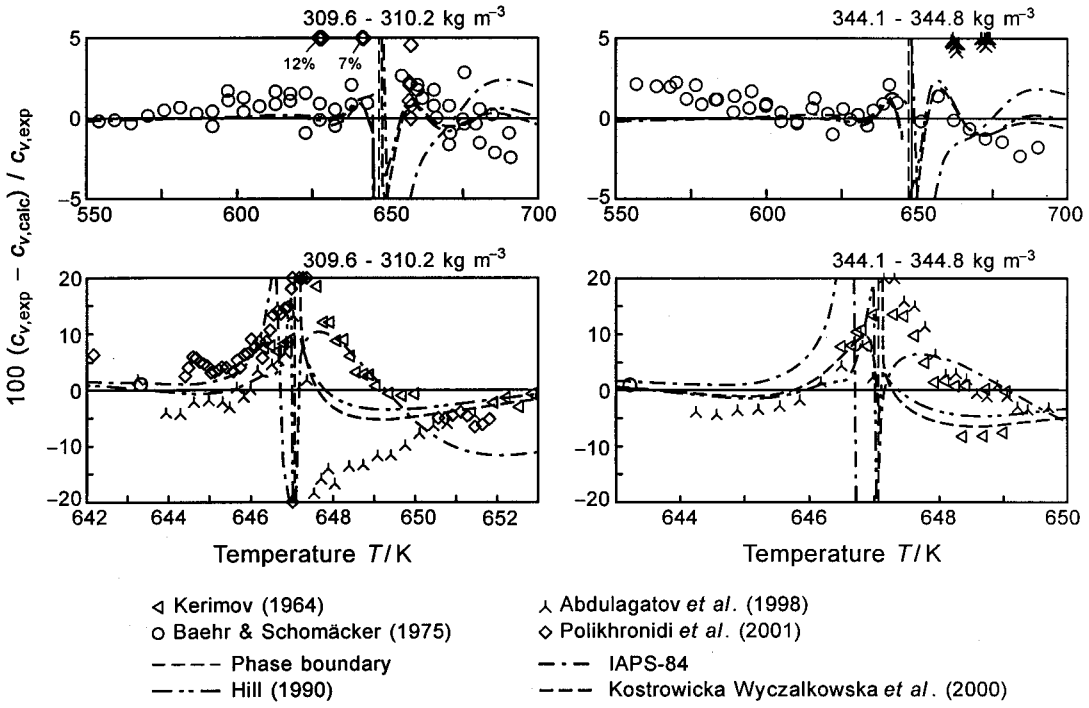

FIG. 7.28. Percentage deviations between experimental data of the isochoric heat capacity c_v in the extended critical region and values calculated from IAPWS-95, Eq. (6.4). Values calculated from IAPS-84, the equation of Hill (1990), and the crossover equation of Kostrowicka Wyczalkowska *et al.* (2000) are plotted for comparison; values of the crossover equation are only shown within its range of validity. The upper diagrams, which cover a greater temperature range, only contain the data of Baehr and Schomäcker (1975). The lower diagrams show a small temperature range around T_σ and contain all data available in this region.

compared with the corresponding c_v values calculated from IAPWS-95, where two typical examples have been selected. For the density $\rho \approx 712.6$ kg m^{-3}, the upper deviation diagram shows two data sets measured at the Dagestan Scientific Center; the data of Kerimov (1964) exhibit systematic deviations from the values of IAPWS-95 of about +2.5% while the data of Abdulagatov *et al.* (1997) lie, within their scatter of about ±2%, around the values from IAPWS-95. From the lower diagram, one can see that the recent data of Magee *et al.* (1998) are represented to within their scatter of about ±0.5% whereas the data of Kerimov (1964) lie about 2% higher. Altogether, the c_v data measured by Magee *et al.* (1998), deviate from IAPWS-95 on average between −0.5% and −1% for $\rho \leqslant 967$ kg m^{-3} and by ±0.5% for $\rho \geqslant 977$ kg m^{-3}; for the density and temperature range covered by Magee *et al.*'s data see Table 4.6.

Based on the detailed investigation of the IAPWS-95 formulation with regard to the representation of the isochoric heat capacity, we believe that the IAPWS-95 formulation describes the c_v surface outside the immediate critical region more accurately than the existing experimental data do. This statement is based on the fact that first, IAPWS-95 was not fitted to any c_v data [except for the 113 c_v data of Baehr and Schomäcker (1975), see Table 4.6], second, the way in which the best data of the Dagestan Scientific Center and the data of Magee *et al.* (1998) are represented, and third, on the very good agreement between the c_v values from IAPWS-95 and from the equation of Hill (1990). In the region limited by a pressure of 400 MPa and a temperature of 800 K, which is comprehensively covered by accurate $p\rho T$ data (see Fig. 4.1), the differences in c_v between the two equations of state are less than ±0.5% (not counting the critical region of course). Therefore, we estimate that in this range the uncertainty of the IAPWS-95 formulation in c_v is less than ±0.75%.

7.2.5. Isobaric Heat Capacity

The distribution of the experimental data for the isobaric heat capacity c_p used to develop the IAPWS-95 formulation is shown in Fig. 4.8, see also Table 4.8. In the following, these experimental data are compared with the corresponding values calculated from the IAPWS-95 formulation, Eq. (6.4), and from the other three equations of state mentioned at the beginning of Sec. 7.

For six characteristic isobars at pressures below 15 MPa, Fig. 7.32 presents comparisons between the experimental c_p data and the c_p values calculated from IAPWS-95 where the data are only in the gas phase (except for $p = 14.7$ MPa). From the deviation diagrams, it can be seen that IAPWS-95 represents the data to within their experimental uncertainty given in Table 4.8. IAPS-84 and the equation of Hill (1990) behave very similarly except for pressures below 10 MPa when approaching the phase boundary. While in this region the deviations between the data and IAPWS-95 do not exceed 2%, the two other equations clearly yield lower c_p val-

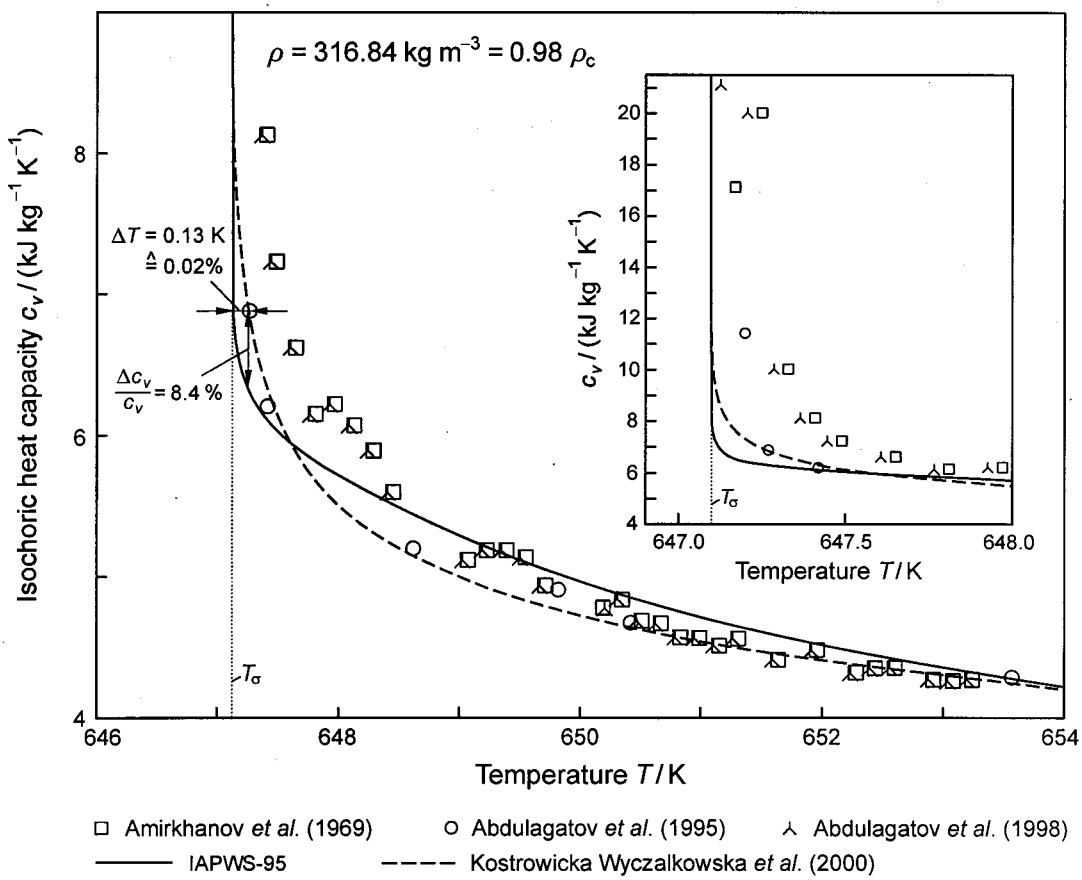

FIG. 7.29. Isochoric heat capacity in the near-critical region along a subcritical isochore as a function of temperature (near-critical temperature range, $T > T_\sigma$, single-phase region) as calculated from IAPWS-95, Eq. (6.4), and from the crossover equation of Kostrowicka Wyczalkowska *et al.* (2000). The inner diagram shows a smaller temperature range in higher resolution and extends to higher c_v values. The experimental data are plotted for comparison.

ues, which deviate from the experimental data by up to −4%. On the other hand, a still better representation of these data of Sirota and Timrot (1956) by IAPWS-95 was not possible without a significant deterioration in the representation of the $p\rho T$ data and the speeds of sound in this region.

Figure 7.33 illustrates the problem described above more clearly by plotting the absolute course of c_p along some isobars and along the saturated vapor line for temperatures from the triple point to 600 K. For IAPWS-95, this figure shows the good consistency between the representation of the c_p data of Sirota and Timrot (1956) in the single-phase region near the saturated vapor line and the c_p'' data of Sirota (1963) along the saturated vapor line. Except for temperatures $T < 370$ K, IAPS-84 and Hill's equation are not able to follow the c_p'' data along the phase boundary, see also Fig. 7.7. The c_p data point of Sirota and Timrot (1956) closest to the phase boundary is in the two-phase region for these equations.

The experimental c_p data in the critical region are compared with the values calculated from the IAPWS-95 formulation in Fig. 7.34 by a $c_p - \rho$ diagram along four isobars and in Fig. 7.35 by percentage deviation diagrams for the same isobars; values calculated from IAPS-84, the equation of Hill (1990), and the crossover equation of Kostrowicka Wyczalkowska *et al.* (2000) are plotted for comparison. Before discussing the representation of these data by IAPWS-95 and the other equations of state, we give a brief comment on this "difficult" region. There are two basic reasons why the total experimental uncertainty in c_p rises drastically in the critical region. First, due to the strong increase of the isobaric heat capacity in this region (see Fig. 7.34), experimental uncertainties in temperature and pressure have a very strong effect on the uncertainty in c_p. For the same reason, relatively large differences in c_p between the several equations of state would result in relatively small differences when expressed in density or in temperature. The second reason is based on the experimental procedure to determine isobaric heat capacities. Usually, with flow calorimeters, enthalpy differences and corresponding temperature differences are measured. Due to the strong increase of c_p in the critical region and the strong change of the slope of the isobars near their maximum in a $c_p - \rho$ diagram, the exact assignment of the measured difference quotient $(\Delta h/\Delta T)_p$ to the isobaric heat capacity defined by the differential quotient $c_p = (\partial h/\partial T)_p$ is a considerable source of error. Moreover, uncertainties in temperature or problems with its stability strongly affect the

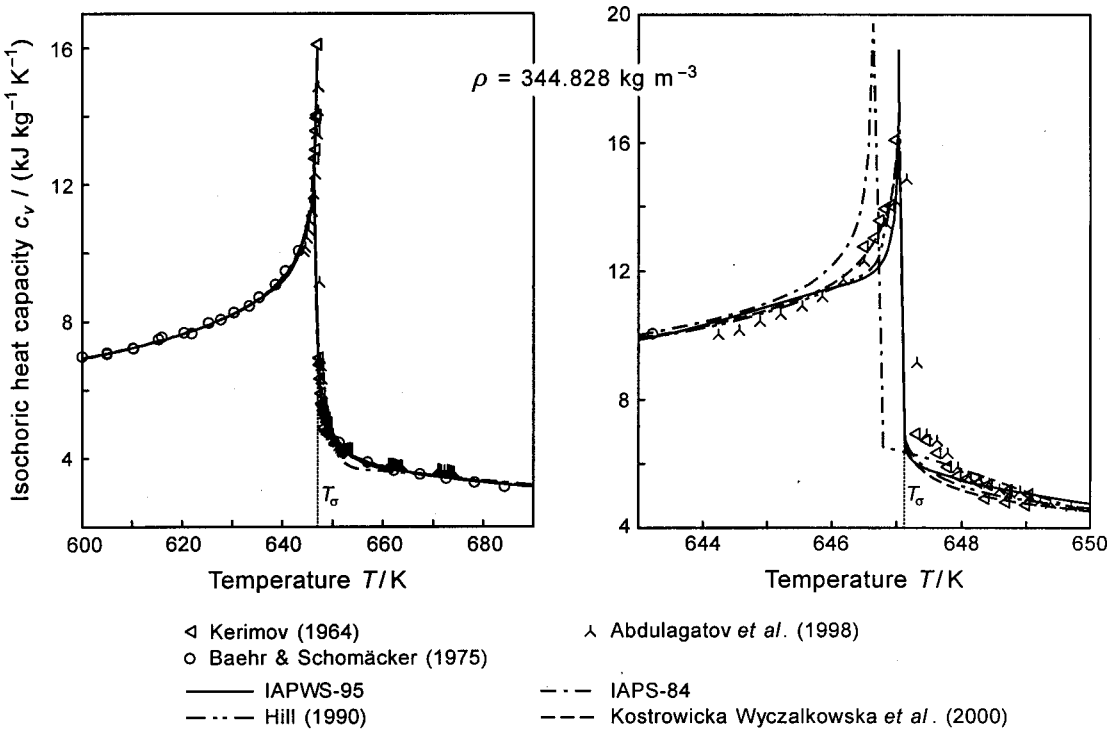

FIG. 7.30. Isochoric heat capacity in the critical region along a supercritical isochore as a function of temperature as calculated from IAPWS-95, Eq. (6.4). Experimental data and values calculated from IAPS-84, the equation of Hill (1990), and the crossover equation of Kostrowicka Wyczalkowska *et al.* (2000) are plotted for comparison. The diagrams also cover the two-phase region ($T<T_\sigma$), where the left side shows a greater temperature range around T_σ and the right side a smaller one with higher resolution in temperature.

uncertainty in c_p. In this difficult region, the IAPWS-95 formulation still represents the data within the experimental uncertainty, but one can see from Fig. 7.35 that the crossover equation and Hill's equation are clearly closer to the experimental c_p data in this near-critical region. Outside the density region shown in Fig. 7.35, the deviations again diminish to about 0.2% and less, for example along the isobar $p = 24.517$ MPa. In this pressure range, namely on the isobars 20, 23, 24, 26, and 28 MPa, there are also experimental c_p data of Ernst and Philippi (1990), which cover the density range from 100 to 1000 kg m^{-3}. For densities greater than 550 kg m^{-3}, these data do not deviate from the values of IAPWS-95 by more than $\pm 0.5\%$, and in most cases the deviation lies within $\pm 0.3\%$.

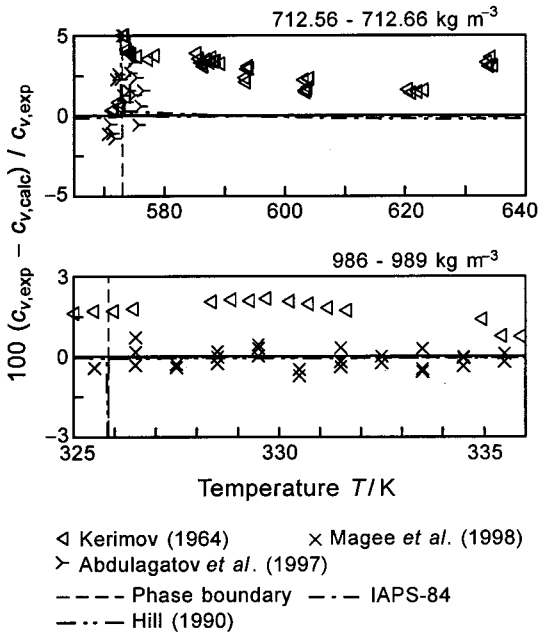

FIG. 7.31. Percentage deviations between experimental data of the isochoric heat capacity c_v and values calculated from IAPWS-95, Eq. (6.4). Values calculated from IAPS-84 and the equation of Hill (1990) are plotted for comparison.

However, very close to the critical point IAPWS-95 yields an unnatural indentation in the plot of c_p isotherms or isobars over density, for details see the discussion in connection with Figs. 6.9–6.12 in Sec. 6.4.2.

The corresponding comparisons for five representative supercritical isobars from about 30 to 100 MPa are presented in Fig. 7.36, which also includes the extended critical region. Besides the data of Sirota's group, this figure also contains c_p data of Ernst and Philippi (1990). In contrast to Fig. 7.32, the percentage deviations are again plotted versus density; in this way, the region around the critical density is stretched much more than when plotted over temperature. It can be seen that in the extended critical region the deviations between the c_p data and the values from IAPWS-95 remain within $\pm 2\%$ for the isobar $p = 29.42$ MPa and within $\pm 1\%$ and less for the isobars up to $p = 68.65$ MPa. It is not surprising that the crossover equation of Kostrowicka Wyczalkowska *et al.* (2000) covers the c_p data in the extended critical region on average better than IAPWS-95, but attention

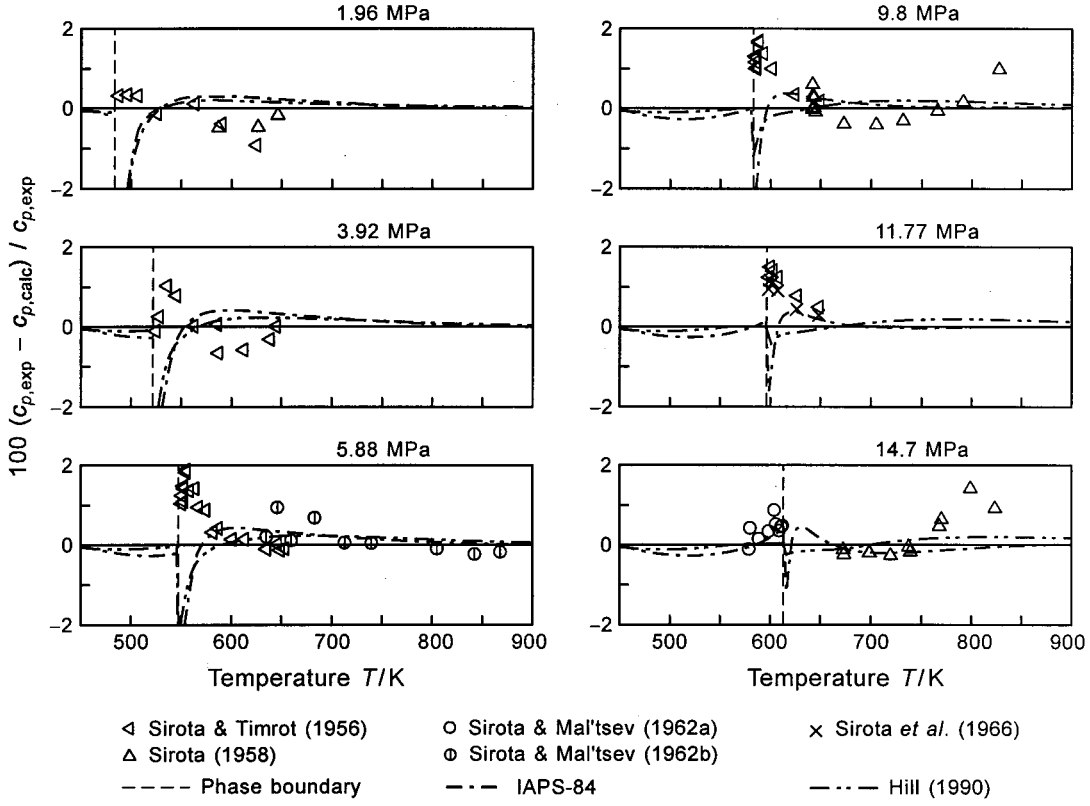

FIG. 7.32. Percentage deviations between experimental data of the isobaric heat capacity c_p and values calculated from IAPWS-95, Eq. (6.4). Values calculated from IAPS-84 and the equation of Hill (1990) are plotted for comparison.

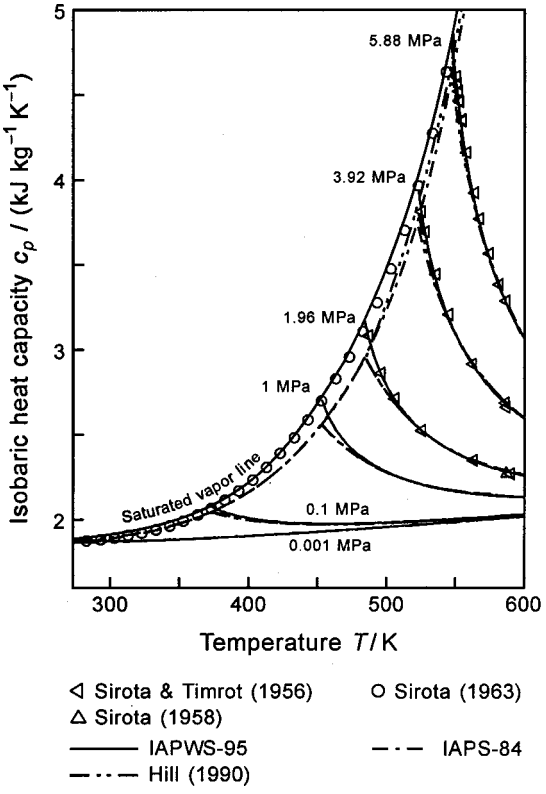

FIG. 7.33. Isobaric heat capacity as a function of temperature as calculated from IAPWS-95, Eq. (6.4), along a part of the saturated-vapor line and in the gas region. Experimental data and values calculated from IAPS-84 and the equation of Hill (1990) are plotted for comparison.

should be paid to the limited range of validity for which its line is drawn; for example, for $p = 68.65$ MPa the range of validity extends from about 314 to 543 kg m^{-3}. Outside the extended critical region, the deviations between the data and IAPWS-95 are less than $\pm 0.5\%$, even for the highest density at and above $\rho = 1000$ kg m^{-3}.

Along the isotherm $T = 300$ K, there are high-pressure c_p data reported by Czarnota (1984) that cover a pressure range from 224 to 1033 MPa. In Fig. 7.37, these data are compared with the values from IAPWS-95 and from the other two equations of state. Both IAPWS-95 and the equation of Hill (1990) represent the data to within $\pm 6\%$, corresponding to the estimated uncertainty for these data. The two data points at and above 1000 MPa are already in the metastable part (subcooled liquid) of the two-phase liquid–solid region. The deviation of the data point near 200 MPa of about -5% is most probably based on the uncertainty of the measurement; here, all three equations of state yield nearly the same c_p value and, moreover, this deviation is not supported by the more recent data of Wiryana *et al.* (1998), see below. IAPS-84 shows strongly increasing deviations of up to almost -100% near 1000 MPa.

Wiryana *et al.* (1998) reported c_p data for temperatures from 353.15 to 473.15 K and pressures up to 3500 MPa. Although these data are not direct measurements of the isobaric heat capacity but were derived from their speed-of-sound measurements (see Sec. 4.5.2), Fig. 7.38 shows a com-

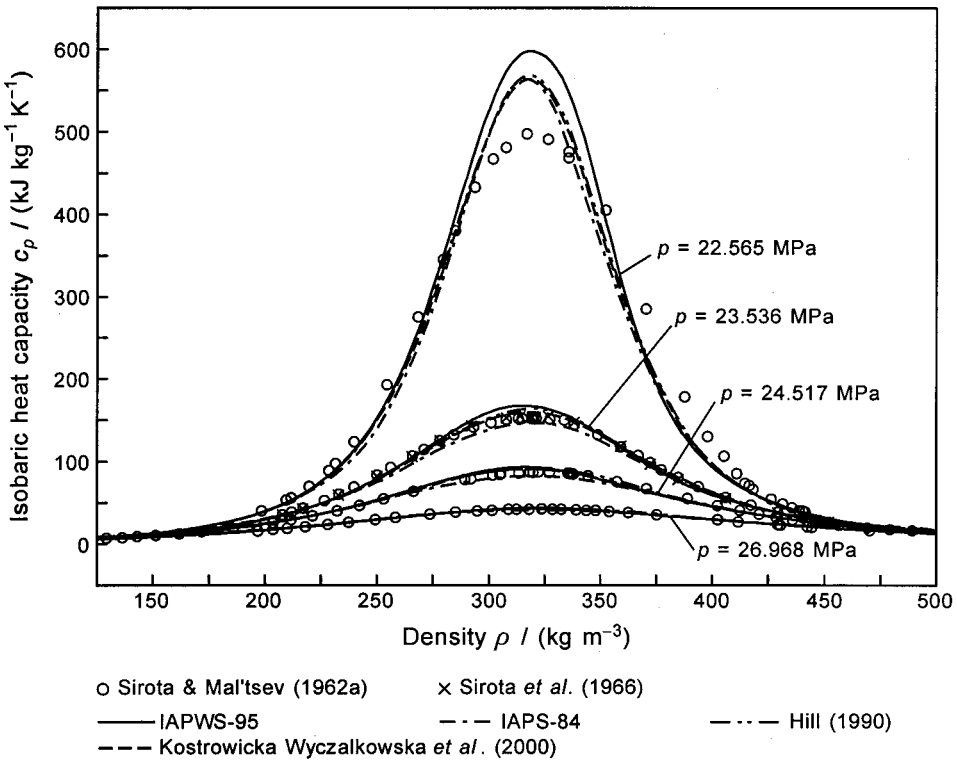

FIG. 7.34. Isobaric heat capacity in the critical region as a function of density on four isobars as calculated from IAPWS-95, Eq. (6.4). Experimental data and values calculated from IAPS-84, the equation of Hill (1990), and the crossover equation of Kostrowicka Wylczalkowska *et al.* (2000) are plotted for comparison. The density range shown extends beyond the critical region.

parison between Wiryana *et al.*'s c_p data and values calculated from IAPWS-95. It can be seen that for pressures up to 1000 MPa, i.e., within the range of validity of IAPWS-95, the deviations of the c_p data remain within 3.5%, which is probably well within the uncertainty of the data. In the extrapolation range for pressures up to 3500 MPa, the maximum deviations of the data from the values calculated with IAPWS-95 are 11.4%. Due to the way in which Wiryana *et al.* (1998) obtained these c_p data, we believe that the systematic trend between the c_p data and the values from IAPWS-95, shown in Fig. 7.38, is mainly due to the uncertainty of the data.

From the statements on the uncertainty of the IAPWS-95 formulation in c_p made in Sec. 6.3.2 and from its compari-

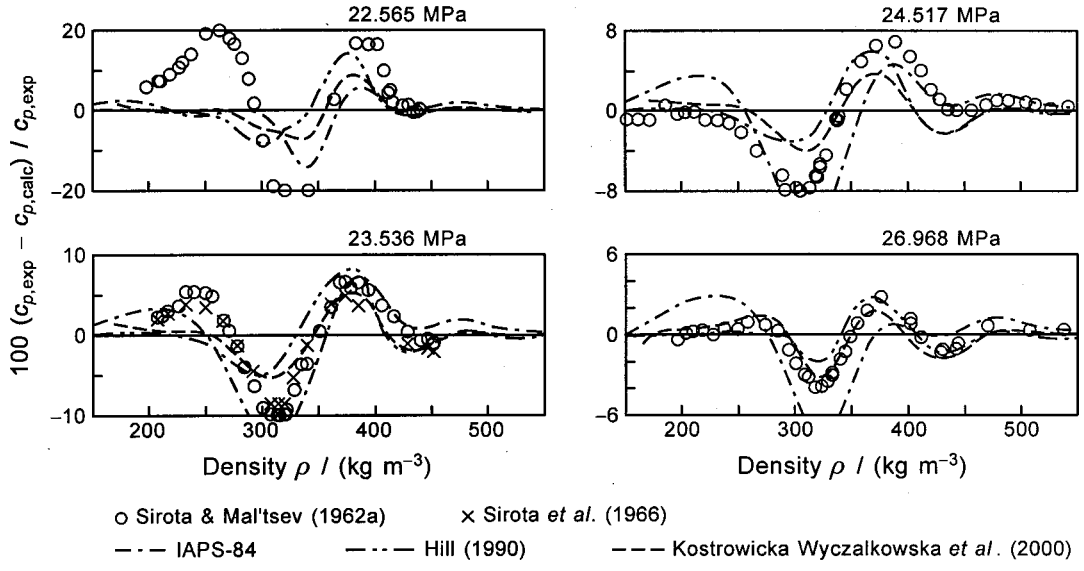

FIG. 7.35. Percentage deviations between experimental data of the isobaric heat capacity c_p and values calculated from IAPWS-95, Eq. (6.4). Values calculated from IAPS-84 and the equation of Hill (1990) are plotted for comparison. The diagrams correspond to the same pressures and about the same density range as covered by Fig. 7.34.

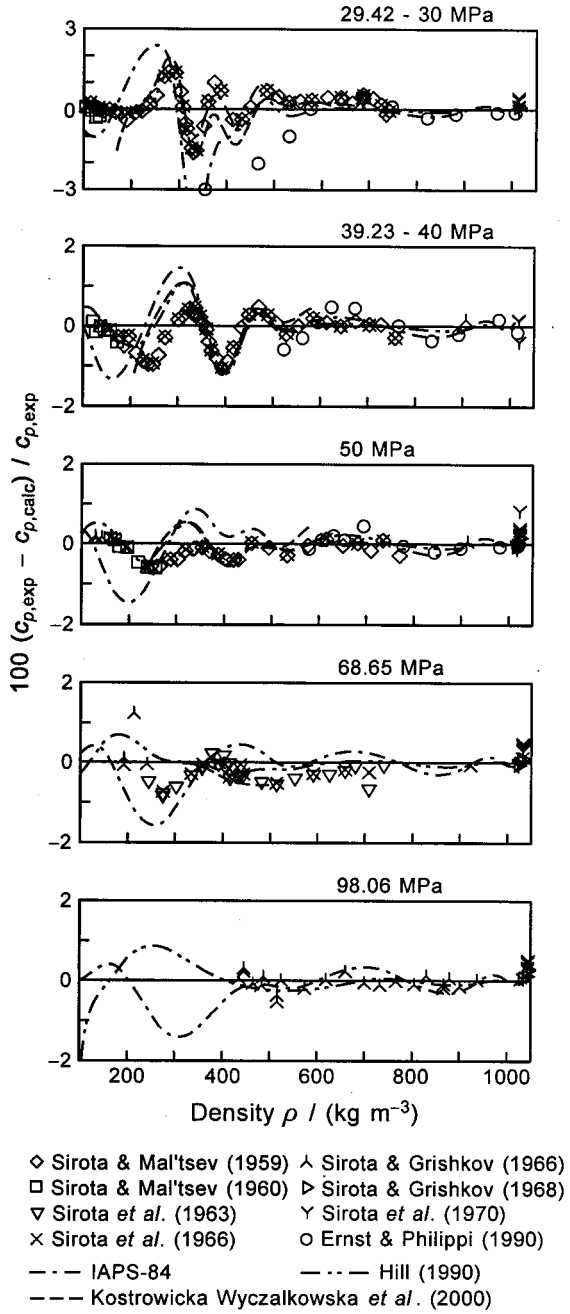

FIG. 7.36. Percentage deviations between experimental data of the isobaric heat capacity c_p in the extended critical region and values calculated from IAPWS-95, Eq. (6.4). Values calculated from IAPS-84, the equation of Hill (1990), and the crossover equation of Kostrowicka Wyczalkowska *et al.* (2000) are plotted for comparison; the crossover equation is only shown within its range of validity. The two lowest diagrams and the density range of all diagrams extend beyond the extended critical region.

sons with the experimental c_p data carried out in this section, it follows that, except for the critical region, IAPWS-95 is considered to be more accurate than the experimental c_p data. This behavior is based on the fact that IAPWS-95 is very well guided by highly accurate $p\rho T$ data for temperatures up to 800 K and pressures up to 100 MPa and also by accurate speed-of-sound data. Therefore, it is not surprising that IAPWS-95 and the equation of Hill (1990) agree with

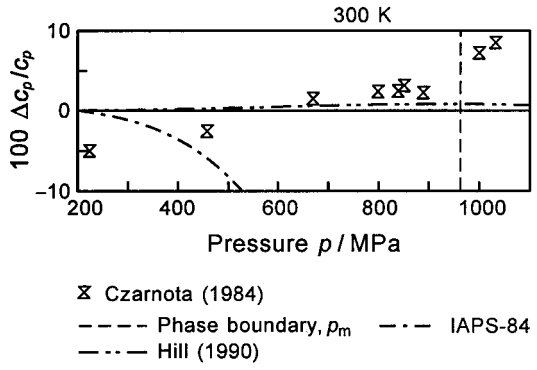

FIG. 7.37. Percentage deviations $100\Delta c_p/c_p = 100(c_{p,\mathrm{exp}} - c_{p,\mathrm{calc}})/c_{p,\mathrm{exp}}$ between experimental data of the isobaric heat capacity c_p measured by Czarnota (1984) and values calculated from IAPWS-95, Eq. (6.4). Values calculated from IAPS-84 and the equation of Hill (1990) are plotted for comparison. The two data points right of the phase boundary are in the liquid–solid metastable region.

each other regarding the c_p representation in this region. Both equations agree within $\pm 0.1\%$ in c_p for temperatures up to 800 K and pressures up to 60 MPa (except for the region near the phase boundary and in the critical region), and for pressures up to 100 MPa the differences do not exceed $\pm 0.25\%$. For this pressure range and temperatures up to 1273 K, the differences remain within $\pm 0.8\%$, and only for higher pressures do the c_p values calculated from these two equations differ by up to $\pm 2\%$.

7.2.6. Enthalpy Differences

Information on the two data sets of enthalpy differences measured by Philippi (1987) and Castro-Gomez *et al.* (1990), which were used to develop the IAPWS-95 formulation, is given in Table 4.9 and Fig. 4.9. In Fig. 7.39, these Δh data are compared with the corresponding Δh values calculated from IAPWS-95, Eq. (6.4), along three isobars that are representative of the range of the measurements. The data

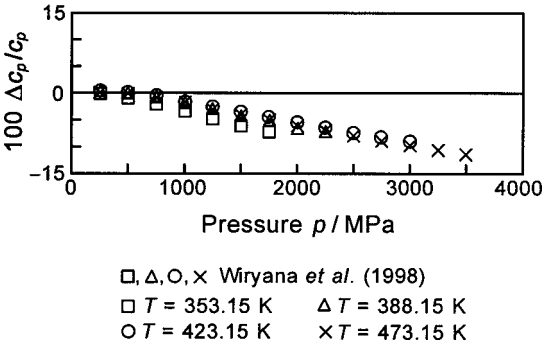

FIG. 7.38. Percentage deviations $100\Delta c_p/c_p = 100(c_{p,\mathrm{exp}} - c_{p,\mathrm{calc}})/c_{p,\mathrm{exp}}$ between the data of the isobaric heat capacity c_p of Wiryana *et al.* (1998) for temperatures from 353.15 to 473.15 K and values calculated with IAPWS-95, Eq. (6.4). For the pressures above 1000 MPa, IAPWS-95 was extrapolated correspondingly.

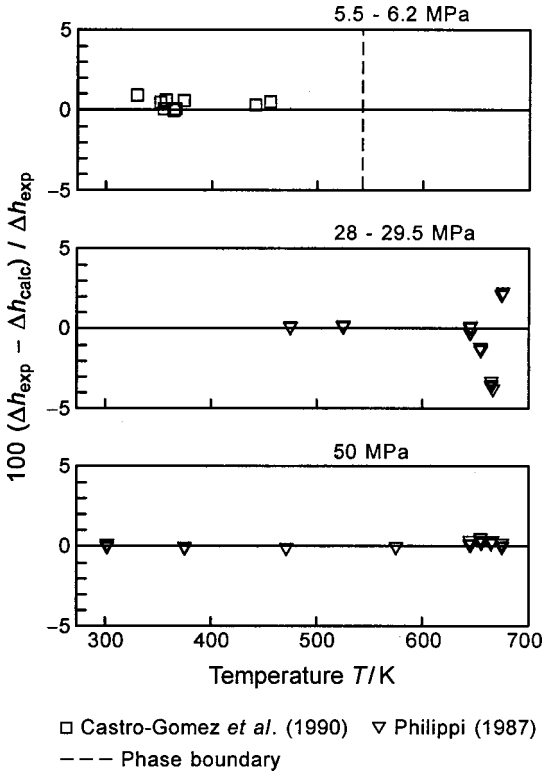

FIG. 7.39. Percentage deviations between experimental data of the enthalpy differences Δh and values calculated from IAPWS-95, Eq. (6.4).

points, which correspond to isobaric enthalpy differences $\Delta h = h_2(p,T_2) - h_1(p,T_1)$, are plotted in these percentage deviation diagrams at the end point of the measurement, i.e., at the temperature T_2. In the case of difference quantities such as Δh, the corresponding properties calculated from other equations of state cannot be plotted as lines in such diagrams. Therefore, these special deviation diagrams do not contain comparisons with the corresponding values from IAPS-84 and the equation of Hill (1990). However, such comparisons were carried out separately and a corresponding statement is given below.

Figure 7.39 shows that the Δh data can be represented by IAPWS-95 to within the experimental uncertainty (see Table 4.9). For the data of Castro-Gomez *et al.* (1990), this means a representation within their scatter of $\Delta(\Delta h) = \pm 1\%$. Outside the critical region, the data of Philippi (1987) do not deviate from IAPWS-95 by more than $\pm 1\%$; in the extended critical region, the deviations increase to $\pm 4\%$ (see, for example, the deviation diagram for pressures between 28 and 29.5 MPa) and in the critical region for pressures between 22.5 and 24.1 MPa (not shown) at temperatures between 651 and 664 K, deviations of up to 35% occur. The clearly increasing deviations in the critical region are due to the fact that the measured quantity $(\Delta h/\Delta T)_p$ rises very strongly, and therefore the experimental uncertainties in temperature have a very strong effect on the uncertainty of $(\Delta h/\Delta T)_p$; see also the corresponding statement on the isobaric heat capacity in the preceding section. Except for the extended critical region, IAPS-84 and the equation of Hill (1990) yield very similar deviations $\Delta(\Delta h)$ to IAPWS-95. In the investigated pressure range from 0.5 to 50 MPa at temperatures from 273.15 to 700 K, the difference between IAPWS-95 and Hill's equation is less than $\pm 0.12\%$ in the gas region and at supercritical pressures (except for the extended critical region) and less than $\pm 0.25\%$ in the liquid region.

7.2.7. Joule–Thomson and Isothermal Throttling Coefficient

The Joule–Thomson coefficient $[\mu = (\partial T/\partial p)_h]$, which is sometimes also called the isenthalpic throttling coefficient, is coupled with the isothermal throttling coefficient $[\delta_T = (\partial h/\partial p)_T]$ via the isobaric heat capacity c_p, namely $\delta_T = -\mu \cdot c_p$. Due to this close relation between μ and δ_T, one can expect that the two properties are similarly represented by an equation of state. Therefore, the representation of μ and δ_T by the IAPWS-95 formulation, Eq. (6.4), is jointly discussed in this section.

For the reasons given in Secs. 4.7 and 4.8, only the μ and δ_T data of Ertle (1979) that are in the gas region were included in the data set used to develop IAPWS-95; information on these measuring runs is given in Table 4.9 and Fig. 4.9.

Comparisons between the data of the Joule–Thomson coefficient and the corresponding μ values calculated from IAPWS-95 are presented in Fig. 7.40 for six representative isotherms. One can see that IAPWS-95 represents the μ data to within their experimental uncertainty of $\pm 4\%$; this is also true for IAPS-84 and the equation of Hill (1990), which go approximately through the mean values of the scatter of the data for temperatures up to 673 K. Since, however, the representation of the data within their scatter without a systematic trend led to a clear deterioration in representing the very accurate $p\rho T$ data of Kell *et al.* (1989) in this temperature range, we did not force a better representation of Ertle's μ data by IAPWS-95 at these temperatures. The deviation diagram for temperatures in the range of 571–573 K shows a peak in the deviations between IAPWS-95 and the two other equations of state in the liquid range at about 60 MPa. This behavior is caused by the zero crossing of μ at this pressure (from positive to negative μ values).

For temperatures above 800 K, all three equations, but particularly IAPWS-95, exhibit a parallel offset compared with the mean values of the scatter of the data. During the development of IAPWS-95, a reduction in this systematic offset was attempted. However, such an ''improvement'' resulted in a clear deterioration of the extrapolation capability of IAPWS-95. The maximum in the second virial coefficient B at a reasonable temperature, which is very important for good extrapolation behavior of an equation of state (see Sec. 7.3.3.2), could only be achieved when this offset was accepted. This decision was confirmed by the (successful) attempt to make IAPWS-95 yield a maximum in the third virial coefficient at about the critical temperature, see Fig. 7.20 and the corresponding statements in Sec. 7.2.2. This is a further indication that the μ data of Ertle (1979) are not more accurate than defined by the given uncertainty of $\pm 4\%$ and

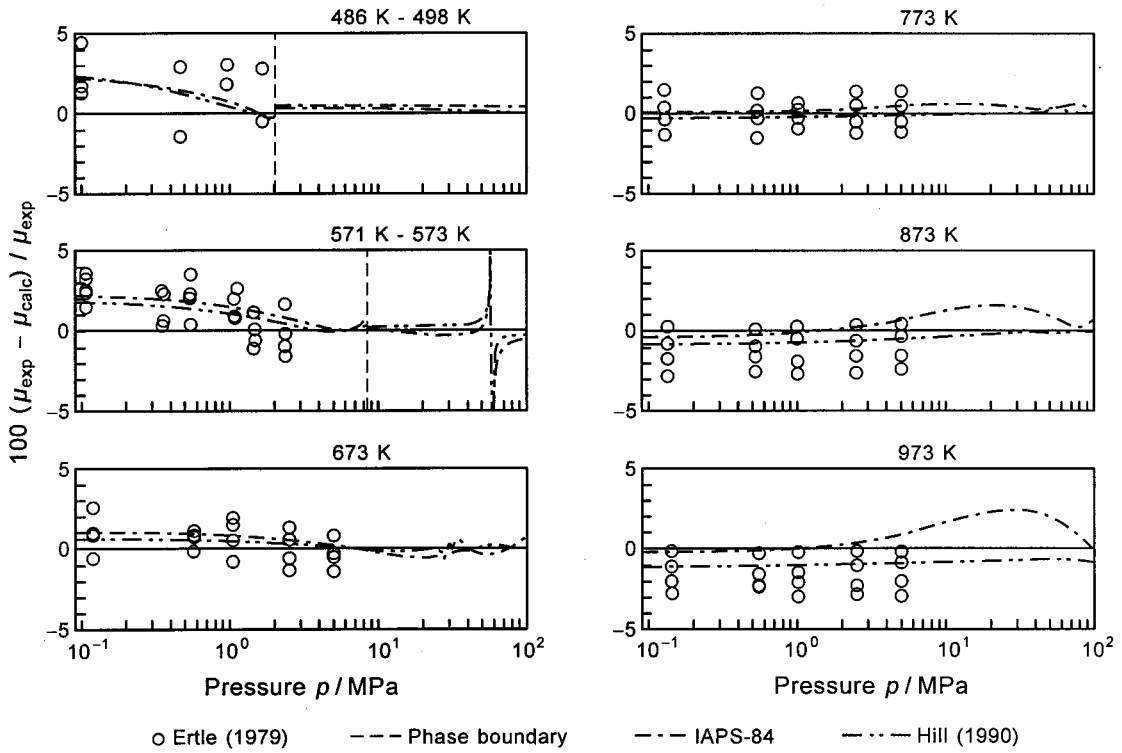

FIG. 7.40. Percentage deviations between experimental data of the Joule–Thomson coefficient μ and values calculated from IAPWS-95, Eq. (6.4). Values calculated from IAPS-84 and the equation of Hill (1990) are plotted for comparison.

one should not try to represent them to within their scatter.

Figure 7.41 presents comparisons between the experimental data of the isothermal throttling coefficient and the δ_T values from IAPWS-95 along four representative isotherms; altogether the measurements of Ertle (1979) cover a temperature range from 621 to 1073 K. The comparisons are very similar to those of the Joule–Thomson coefficient data and the statements made for Fig. 7.40 are also true here. The peak in the deviations between IAPWS-95 and the other two equations at $T=673$ K and 28 MPa is not based on a zero crossing of δ_T (as for μ at 572 K), but are caused by a very strong increase and decrease of c_p in this small pressure region ($\delta_T=-\mu\cdot c_p$); the δ_T values of the three equations of state differ correspondingly along this sharp peak of δ_T.

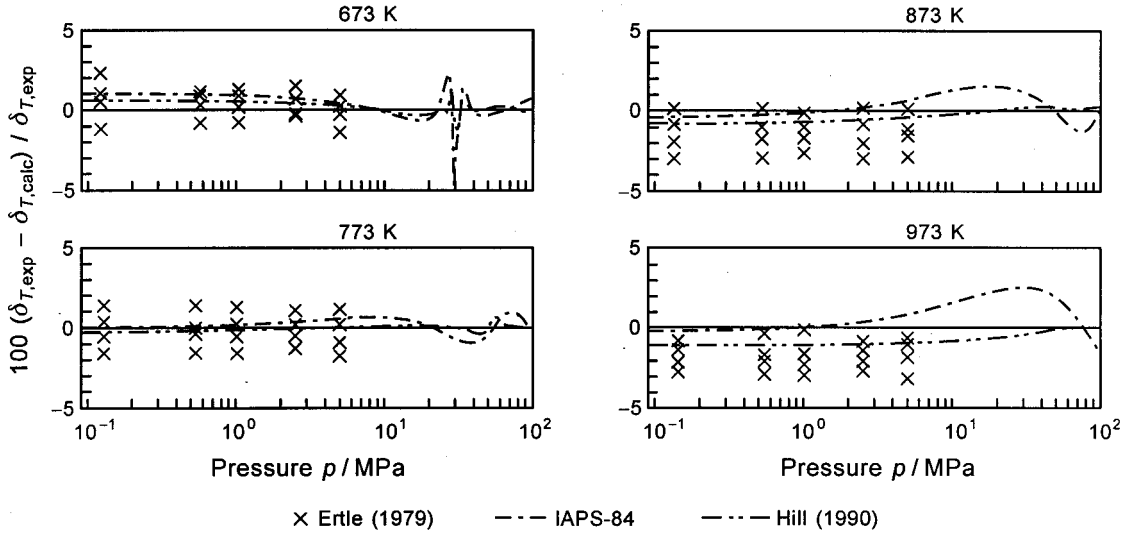

FIG. 7.41. Percentage deviations between experimental data of the isothermal throttling coefficient δ_T of Ertle (1979) and values calculated from IAPWS-95, Eq. (6.4). Values calculated from IAPS-84 and the equation of Hill (1990) are plotted for comparison.

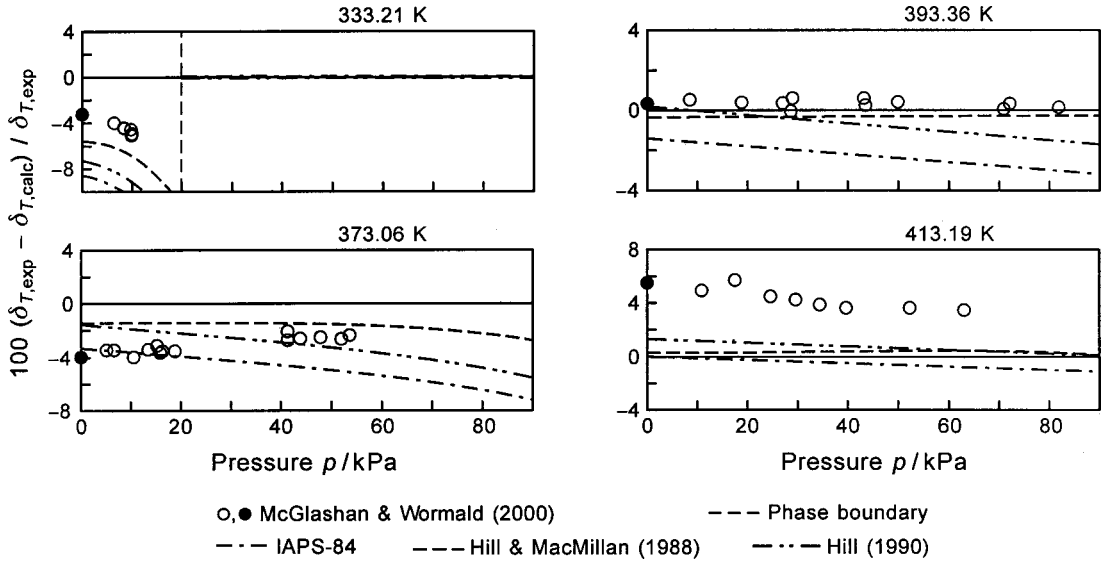

FIG. 7.42. Percentage deviations between experimental data of the isothermal throttling coefficient δ_T of McGlashan and Wormald (2000) and values calculated from IAPWS-95, Eq. (6.4). Values calculated from IAPS-84, the equation of Hill (1990), and the virial equation of Hill and MacMillan (1988) are plotted for comparison. The data shown as solid circles are $\delta_{T,0}$ data extrapolated by McGlashan and Wormald from their δ_T data to zero pressure. Note that the pressure unit is kPa.

Very recently, measurements of the isothermal throttling coefficient δ_T and of $\delta_{T,0}$ at zero pressure were reported by McGlashan and Wormald (2000). On 12 isotherms, these data cover a temperature range from 313 to 413 K at very low pressures of up to 82 kPa; for further details see Sec. 4.8. For four representative isotherms, Fig. 7.42 shows the deviations of these δ_T data from values calculated with IAPWS-95. Again, this figure also contains the δ_T values from IAPS-84 and the equation of Hill (1990) for comparison. Since in the context of properties of H_2O in the diluted gas region the virial equation of Hill and MacMillan (1988) is often used (see also Sec. 7.2.2), δ_T values from this equation are also plotted. When keeping in mind the statements made in Sec. 4.8 on the experimental uncertainty of these data, it can be seen in Fig. 7.42 that in the greatest part of the measuring range neither IAPWS-95 nor any of the three other equations are able to represent the data to within the uncertainties derived from the statements made by McGlashan and Wormald (2000). There are systematic deviations of the data from values calculated with IAPWS-95, which go from negative to positive with increasing temperature. In the course of this trend, very good agreement is exhibited on the isotherm $T=393.36\,\mathrm{K}$. For $T=413.19\,\mathrm{K}$ the four equations agree very well with each other, but the δ_T data deviate considerably from the average of the values of the equations. For the uncertainty of the solid $\delta_{T,0}$ point at this temperature, McGlashan and Wormald give a value of only $\pm 1.4\%$, but they do not exclude systematic errors.

Figure 7.43 presents absolute deviations of the data of McGlashan and Wormald (2000) for the isothermal throttling coefficient at zero pressure $\delta_{T,0}$ from the corresponding values calculated with IAPWS-95 and with the three other equations. Besides the $\delta_{T,0}$ data themselves, where $\delta_{T,0}=B-T(\mathrm{d}B/\mathrm{d}T)$, this figure also contains the range of their uncertainty. It can be seen that, except for $T=383.26\,\mathrm{K}$ and $T=393.36\,\mathrm{K}$, IAPWS-95 is not able to represent the $\delta_{T,0}$ data to within the uncertainty claimed by McGlashan and Wormald (2000). In particular, the differences at the temperatures 363, 373, 403, and 413 K are not fully explainable, because the best data of the second virial coefficient in the temperature range from 373 to 473 K [Eubank *et al.* (1988) and Kell *et al.* (1989)] are represented to within their uncertainty, see Fig. 7.19. The equation that covers the $\delta_{T,0}$ data best is the virial equation of Hill and MacMillan (1988). Nevertheless, it still cannot meet about half of the data within their uncertainty. Based on this entire investigation, it seems as if the experimental data for the isothermal throttling coefficient at

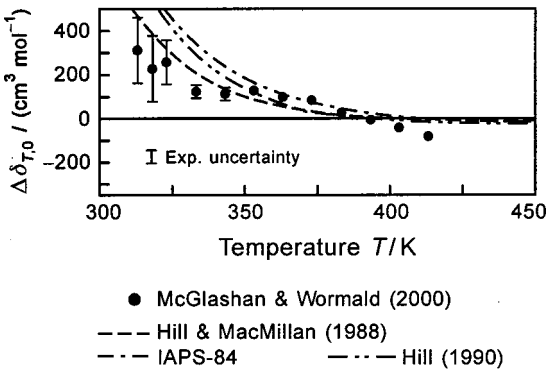

FIG. 7.43. Absolute deviations $\Delta\delta_{T,0}=(\delta_{T,0,\mathrm{exp}}-\delta_{T,0,\mathrm{calc}})$ between experimental data of the isothermal throttling coefficient at zero pressure $\delta_{T,0}$ of McGlashan and Wormald (2000) and values calculated from IAPWS-95, Eq. (6.4). Values calculated from IAPS-84, the equation of Hill (1990), and the virial equation of Hill and MacMillan (1988) are plotted for comparison. For those data for which no uncertainties (estimated by the experimenters) are plotted, the uncertainty range corresponds to the size of the symbols.

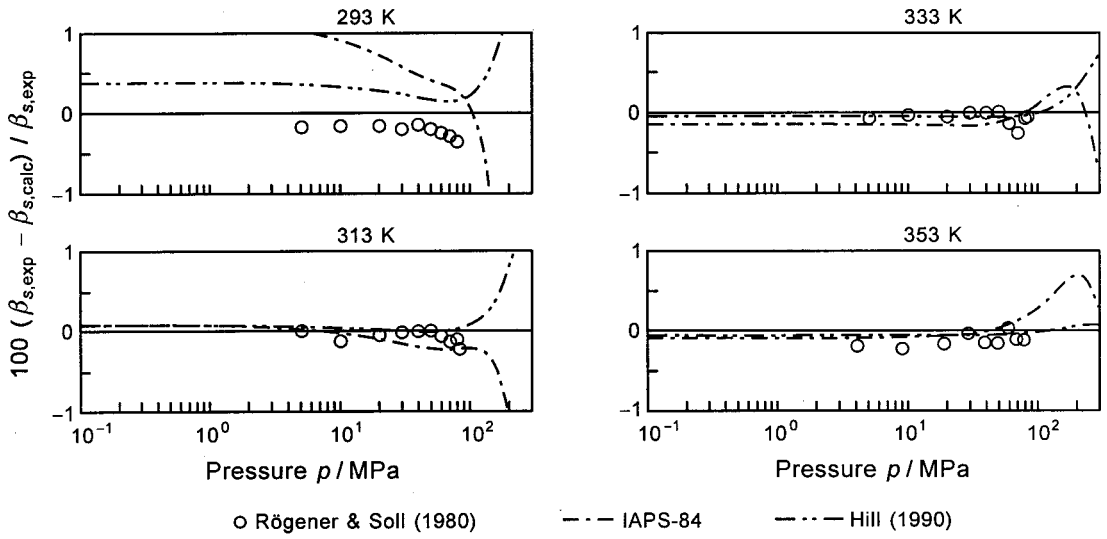

FIG. 7.44. Percentage deviations between experimental data of the isentropic temperature–pressure coefficient β_s and values calculated from IAPWS-95, Eq. (6.4). Values calculated from IAPS-84 and the equation of Hill (1990) are plotted for comparison.

zero pressure and for the second virial coefficient are not entirely mutually consistent. The reason for the opposite sign of the deviations in Figs. 7.42 and 7.43 is that in Fig. 7.42 the deviations are related to $\delta_{T,\mathrm{exp}}$ and these data have a negative sign.

7.2.8. Isentropic Temperature–Pressure Coefficient

The experimental data for the isentropic temperature–pressure coefficient $[\beta_s=(\partial T/\partial p)_s]$ reported by Rögener and Soll (1980) were not used to develop the IAPWS-95 formulation, because we know from the experience of Saul and Wagner (1989) that the accuracy of an equation of state for β_s data is comparable to that for the speed of sound in the corresponding region of state. This experience has also been confirmed in this work.

For four representative isotherms, Fig. 7.44 presents a comparison between the experimental β_s data and the values calculated from IAPWS-95, Eq. (6.4); the values from the other two equations of state are also plotted. It can be seen that IAPWS-95 represents these data to within their experimental uncertainty of $\Delta\beta_s=\pm 0.4\%$. The equation of Hill (1990) achieves a similarly good representation of the data, while IAPS-84 has some difficulties at low temperatures.

7.3. Selected Attributes of the IAPWS-95 Formulation

This section describes the behavior of the IAPWS-95 formulation with regard to the derivatives of the thermal properties, the behavior in the metastable regions, the results when extrapolating to very high pressures and temperatures, and the behavior with regard to the so-called ideal curves.

7.3.1. Derivatives of the Thermal Properties in the Liquid Phase

One important requirement for the development of the IAPWS-95 formulation was a reasonable course of the first and second derivatives of the thermal properties in the liquid region at low temperatures, see Sec. 1.3. The reason for this requirement was that IAPS-84 manifested some weaknesses in this respect and it was desired that IAPWS-95 yield a clear improvement in representing these derivatives. One example for the importance of this requirement is described in the following.

Solution chemists who study aqueous electrolytes make use of the Debye–Hückel limiting law for dilute solutions, which produces a characteristic ''Debye–Hückel slope'' for each property. For the activity and osmotic coefficients, the key parameter in the Debye–Hückel slope is the static dielectric constant ϵ of the solvent. However, derivative solution properties such as the partial molar volume or partial molar enthalpy are often studied. The Debye–Hückel slopes for these properties involve the derivatives of ϵ with respect to pressure and temperature $(\partial\epsilon/\partial\rho)_T$ and $(\partial\epsilon/\partial T)_p$. Since the wide-range equations for ϵ are given as a function of density and temperature, $\epsilon=\epsilon(\rho,T)$, one needs from an equation of state the derivatives $(\partial\rho/\partial p)_T$ and $(\partial p/\partial T)_\rho$. (Examples for such wide-range equations for the dielectric constant are the equation of Archer and Wang (1990) and the equation of Fernández *et al.* (1997) that was adopted as the IAPWS standard for ϵ [IAPWS (1997)].) For this purpose, but also for a number of similar applications, the first derivatives of the thermal properties of IAPWS-95 should be as accurate as possible. In order to ensure this, the IAPWS-95 formulation should also yield a reasonable course of the second derivatives of the thermal properties.

With this background, Archer and Wang (1990) pointed out that even small inaccuracies in the first density and pres-

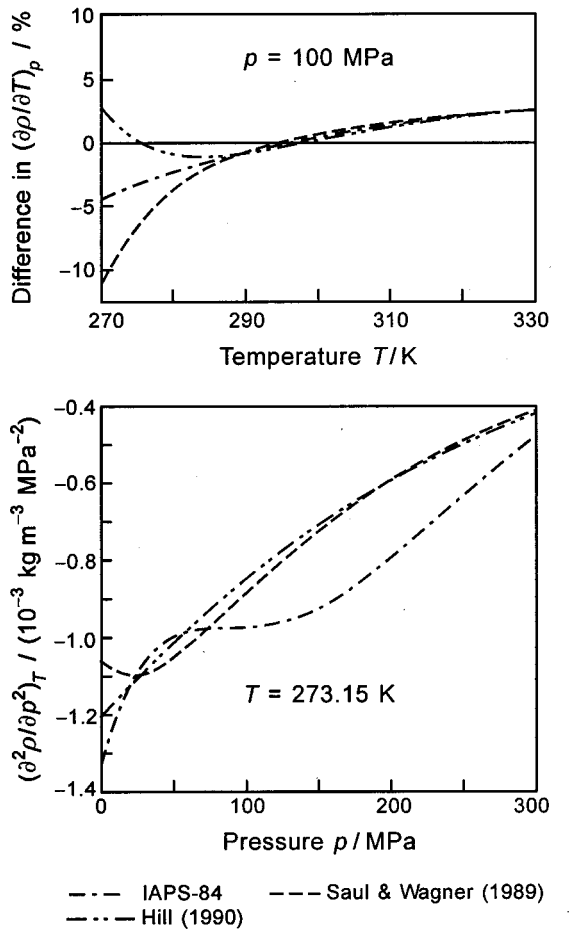

FIG. 7.45. (Upper diagram) Percentage differences of values of the derivative $(\partial\rho/\partial T)_p$ for $p=100$ MPa calculated from IAPS-84, the equation of Saul and Wagner (1989), and the equation of Hill (1990) from values calculated from an equation of Ter Minassian and Pruzan (1981) for the expansivity of water. (Lower diagram) Values of the derivative $(\partial^2\rho/\partial p^2)_T$ for $T=273.15$ K as a function of pressure as calculated from the same equations of state as mentioned for the upper diagram.

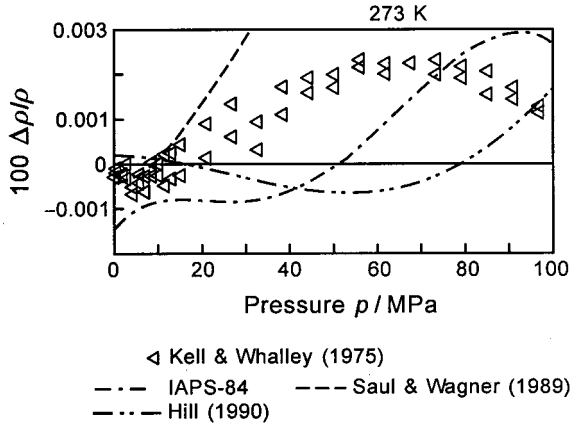

FIG. 7.46. Percentage density deviations $100\Delta\rho/\rho=100(\rho_{exp}-\rho_{calc})/\rho_{exp}$ between accurate experimental $p\rho T$ data for the isotherm $T=273.15$ K and values calculated from IAPWS-95, Eq. (6.4). Values calculated from IAPS-84 and the equation of Hill (1990) are plotted for comparison.

sure derivatives calculated from the various equations of state strongly affect the Debye–Hückel limiting slopes. Thus, with regard to these derivatives, they investigated the best equations of state for H_2O at that time, namely IAPS-84, the equation of Saul and Wagner (1989), and the equation of Hill (1990). They found out that the values of the derivatives calculated from these equations of state for liquid water at low temperatures are rather different. Figure 7.45 repeats the results of the investigations of Archer and Wang (1990) with regard to the first derivative $(\partial\rho/\partial T)_p$ and the second derivative $(\partial^2\rho/\partial p^2)_T$. The upper diagram of this figure shows that, for the isobar $p=100$ MPa and temperatures below 290 K, the values of the derivative $(\partial\rho/\partial T)_p$ calculated from the three equations of state clearly diverge, which leads at $T=270$ K to a difference of nearly 15% between IAPS-84 and the equation of Saul and Wagner (1989) and of about 7% between each of these two equations and the equation of Hill (1990). The lower diagram of Fig. 7.45 shows for the isotherm $T=273.15$ K the second derivative $(\partial^2\rho/\partial p^2)_T$ as a function of pressure calculated from IAPS-84, the equation of Saul and Wagner (1989), and the equation of Hill (1990). IAPS-84 shows a clearly oscillating course of this second derivative, while the equation of Saul and Wagner (1989) displays a minimum at a pressure of about 30 MPa. The equation of Hill represents this second derivative very steadily without oscillations and extrema, but does not correspond to the temperature scale ITS-90.

When starting the development of IAPWS-95, we investigated the possible reasons for the different course of the second derivative $(\partial^2\rho/\partial p^2)_T$ obtained from these three equations of state. The examination of the representation of the different types of experimental data in this region, namely:

(i) $p\rho T$ data and speeds of sound in the single-phase liquid region including the highly accurate $p\rho T$ and w data at $p=0.101\,325$ MPa; and

(ii) the saturation data ρ', p_σ, and h' along the saturated liquid line near the triple point led to the conclusion that the inadequate representation of the $p\rho T$ data of Kell and Whalley (1975) along the isotherm $T=273.15$ K is most likely the reason for the misguided behavior of the equation of Saul and Wagner (1989) and IAPS-84. Based on this knowledge, we paid attention to the isotherm $T=273.15$ K and the adjacent temperature range when developing the IAPWS-95 formulation. For this isotherm, the upper left diagram of Fig. 7.12 illustrates a comparison between the $p\rho T$ data and the values calculated from the various equations of state for pressures up to 100 MPa using a logarithmic pressure scale. For the same isotherm, but using a linear pressure scale and a higher resolution of the deviations, Fig. 7.46 shows the percentage density deviations between the very accurate $p\rho T$ data of Kell and Whalley (1975) and densities calculated from IAPWS-95, Eq. (6.4); values from IAPS-84, the equation of state of Saul and Wagner (1989), and the equation of Hill (1990) are plotted for

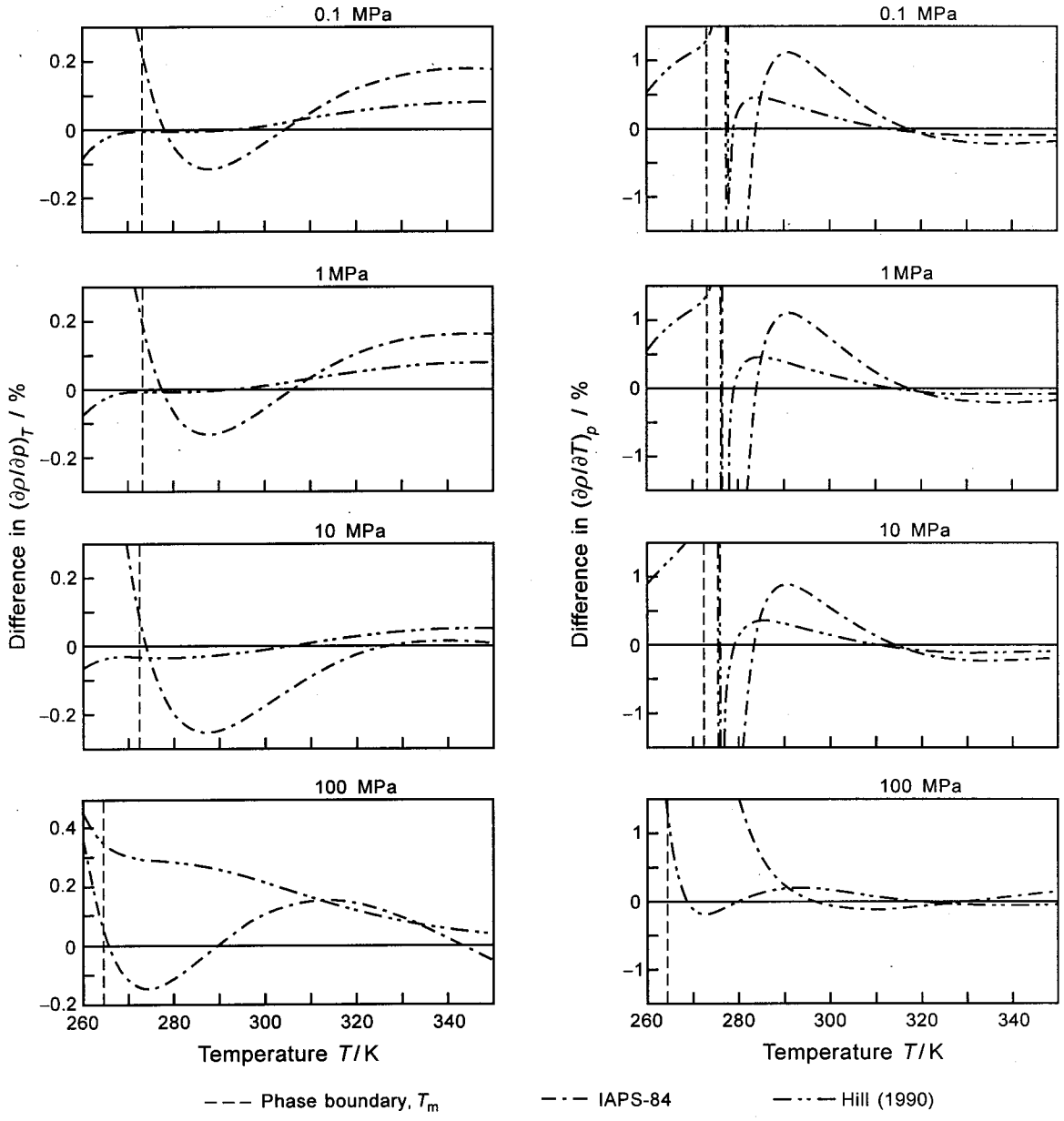

FIG. 7.47. Percentage differences of values of the derivatives $(\partial\rho/\partial p)_T$ and $(\partial\rho/\partial T)_p$ for the four pressures 0.1, 1, 10, and 100 MPa calculated with IAPS-84 and the equation of Hill (1990) from values calculated with IAPWS-95, Eq. (6.4).

comparison. It can be seen that, in comparison with the three other equations of state, IAPWS-95 represents these data best, and Hill's equation behaves similarly well. In contrast to these two equations, IAPS-84 but particularly the equation of Saul and Wagner (1989) show a different course in the percentage deviations, and therefore also a different course of the derivatives $(\partial p/\partial\rho)_T$ and $(\partial^2 p/\partial\rho^2)_T$. Given the quality of IAPWS-95 in this low-temperature part of the liquid region, if the very good representation of the $p\rho T$ data in this region was indeed the decisive precondition for a reasonable representation of the first and second derivatives of the thermal properties, then IAPWS-95 should not have any difficulties in this respect.

For the four pressures 0.1, 1, 10, and 100 MPa and temperatures from the melting temperature T_m to 350 K, Fig. 7.47 shows percentage differences between values of the two derivatives $(\partial\rho/\partial p)_T$ and $(\partial\rho/\partial T)_p$ calculated from IAPS-84 and the equation of Hill (1990) and the corresponding values calculated from IAPWS-95. In the diagrams on the left, the differences in the derivative $(\partial\rho/\partial p)_T$ between the equation of Hill (1990) and IAPWS-95 are less than 0.1% except for

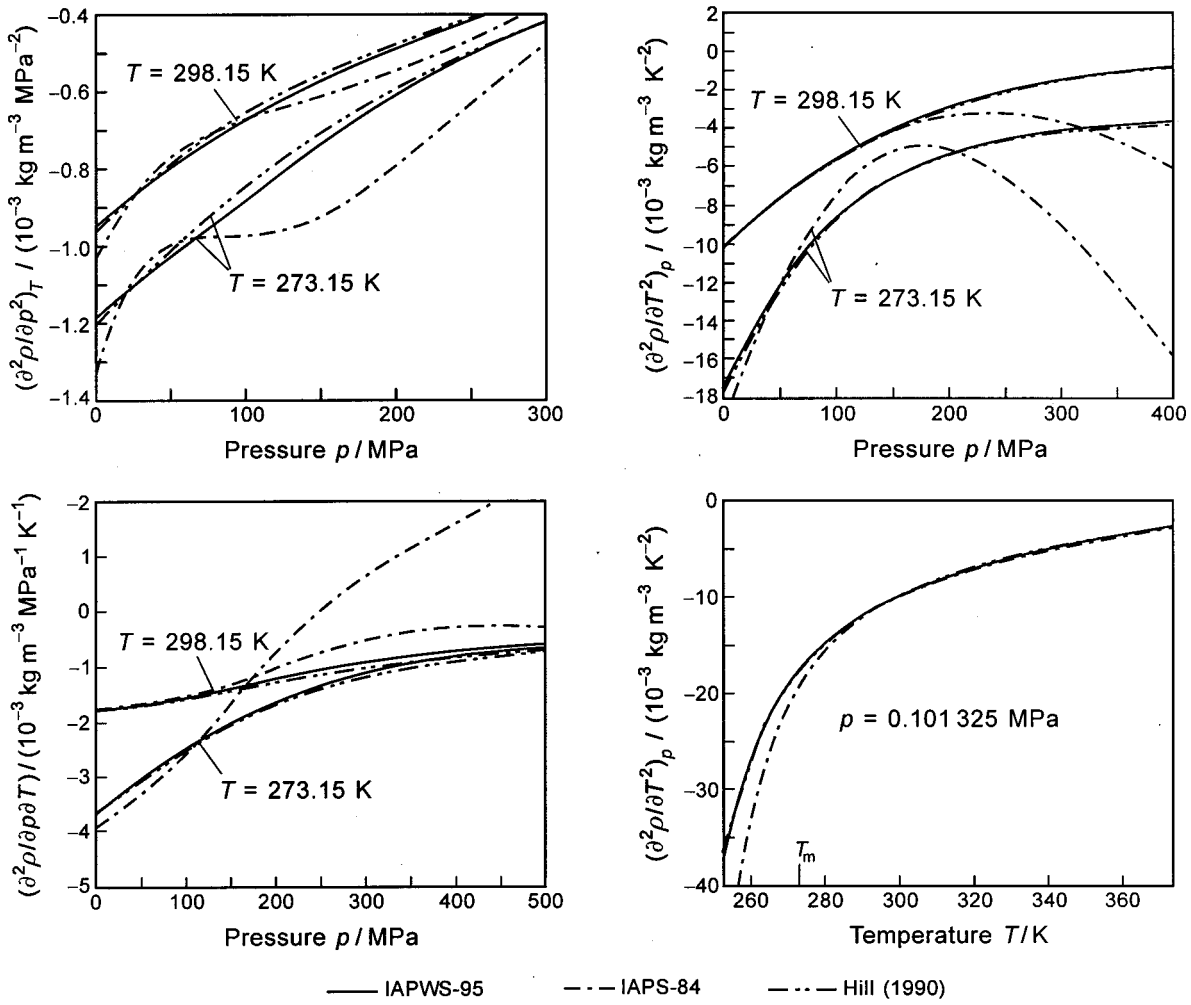

FIG. 7.48. Values of the derivatives $(\partial^2\rho/\partial p^2)_T$, $(\partial^2\rho/\partial T^2)_p$, and $(\partial^2\rho/\partial p\partial T)$ as a function of pressure for the temperatures 273.15 and 298.15 K and $(\partial^2\rho/\partial T^2)_p$ as a function of temperature for $p=0.101\,325$ MPa as calculated from IAPWS-95, IAPS-84, and the equation of Hill (1990).

the isobar $p=100$ MPa. From the diagrams on the right one can see that, except for $T\approx 277$ K and $p\leqslant 10$ MPa, IAPWS-95 and the equation of Hill agree with each other regarding the derivative $(\partial\rho/\partial T)_p$ within 0.5%. The reason for the large differences at about 277 K is the density maximum near this temperature; because $(\partial\rho/\partial T)_p=0$ at this point, very small absolute differences in this derivative cause large percentage differences. Except for the derivative $(\partial\rho/\partial T)_p$ at rather high pressures (for instance, $p=100$ MPa), the differences between IAPS-84 and the other two equations are not very large either. Thus, only the second derivatives are sensitive enough to detect significant differences between the equations of state in this respect.

Figure 7.48 summarizes the plots of the three second derivatives $(\partial^2\rho/\partial p^2)_T$, $(\partial^2\rho/\partial T^2)_p$, and $(\partial^2\rho/\partial p\partial T)$ as a function of pressure for the two temperatures 273.15 and 298.15 K, and the derivative $(\partial^2\rho/\partial T^2)_p$ as a function of temperature for $p=0.101\,325$ MPa, where each derivative was calculated from IAPWS-95, IAPS-84, and the equation of Hill (1990). The four diagrams show that the IAPWS-95 formulation yields in all cases a very steady course of the second derivatives, which is also true for the equation of Hill (1990); the differences between these two equations are marginal. In contrast, IAPS-84 shows significantly different courses of these derivatives, particularly for $T=273.15$ K but also for $T=298.15$ K and along the isobar $p=0.101\,325$ MPa; the maximum differences in the derivatives $(\partial^2\rho/\partial p\partial T)$ and $(\partial^2\rho/\partial T^2)_p$ in comparison with the two other equations reach several hundred percent with slopes that are even different in the sign.

Taking into account the requirements for a reasonable representation of the first and second derivatives of the thermal properties in connection with the need for representing the very accurate $p\rho T$ data and speeds of sound and the existence of a density maximum, the liquid range of H_2O places very high demands on an equation of state that are unique in comparison with those placed on the liquid region for other substances. The IAPWS-95 formulation meets these multiple requirements.

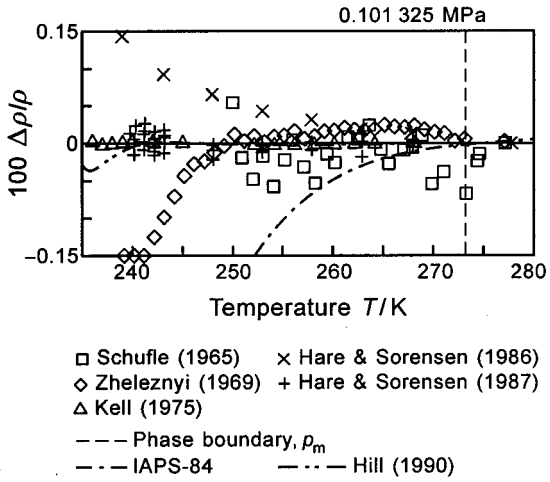

FIG. 7.49. Percentage density deviations $100\Delta\rho/\rho = 100(\rho_{exp} - \rho_{calc})/\rho_{exp}$ between experimental $p\rho T$ data in the subcooled liquid along the isobar $p = 0.101\,325$ MPa and values calculated from IAPWS-95, Eq. (6.4). Values calculated from IAPS-84 and the equation of Hill (1990) are plotted for comparison.

7.3.2. Representation of Thermodynamic Properties in Metastable Regions

The experimental data of the various properties cover two metastable regions, namely states in the subcooled liquid (metastable with respect to the solid) and in the superheated liquid (metastable with respect to the vapor). However, there are no data in the subcooled vapor (metastable with respect to the liquid). These three metastable regions are dealt with in separate subsections.

7.3.2.1. Subcooled Liquid. In the subcooled liquid, there are reliable experimental data for several properties only along the isobar $p = 0.101\,325$ MPa. The majority are $p\rho T$ data, whose density deviations from the values calculated with IAPWS-95, Eq. (6.4), are shown in Fig. 7.49. This figure is practically a continuation of Fig. 7.13 to temperatures below $T = 273.15$ K, the temperature on the melting curve at $p = 0.101\,325$ MPa. While for temperatures $T \geqslant 273.15$ K the data of Kell (1975) were not used [in favor of the $p\rho T$ data of Takenaka and Masui (1990)], for temperatures $T < 273.15$ K the data of Kell (1975) were the only $p\rho T$ data to which IAPWS-95 was fitted in this region. As can be seen from Fig. 7.49, these data are represented by IAPWS-95 well within their uncertainty of $\pm 0.05\%$ in density for temperatures down to 236 K. The very good representation of the data of Hare and Sorensen (1987) within $\pm 0.03\%$ confirm this data selection. The other data exhibit some scatter around the densities from IAPWS-95 and show systematic deviations in both directions that increase with decreasing temperature. IAPS-84 fails in representing the $p\rho T$ data in the subcooled liquid region for $T \leqslant 260$ K, and the equation of Hill behaves similarly to IAPWS-95 except for temperatures $T < 240$ K.

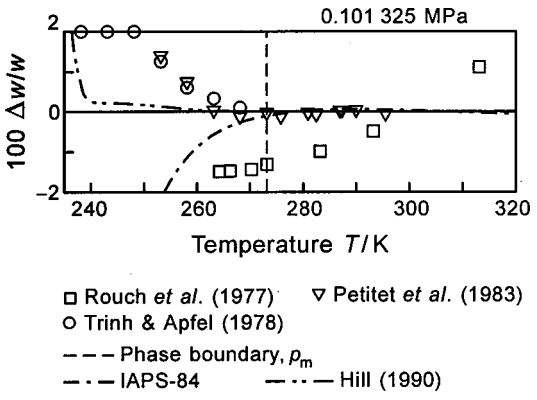

FIG. 7.50. Percentage deviations $100\Delta w/w = 100(w_{exp} - w_{calc})/w_{exp}$ between experimental data of the speed of sound w in the subcooled liquid along the isobar $p = 0.101\,325$ MPa and values calculated from IAPWS-95, Eq. (6.4). Values calculated from IAPS-84 and the equation of Hill (1990) are plotted for comparison.

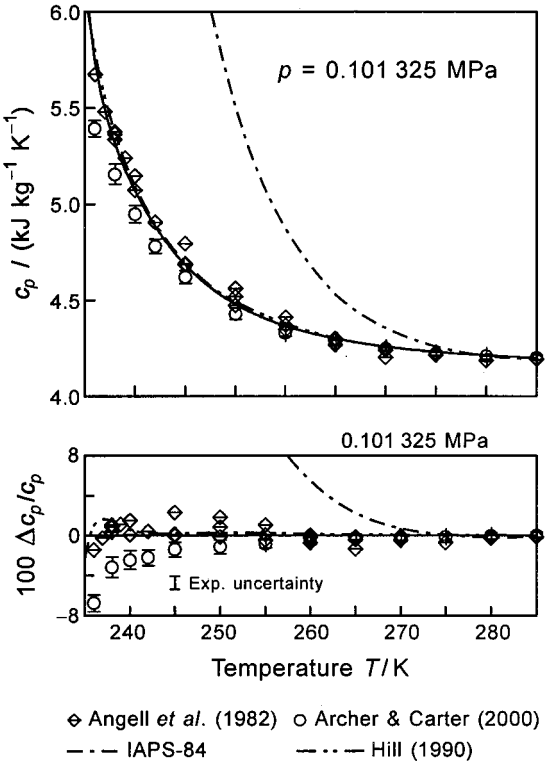

FIG. 7.51. Comparison between experimental data of the isobaric heat capacity c_p in the subcooled liquid for the isobar $p = 0.101\,325$ MPa and values calculated from IAPWS-95, Eq. (6.4), IAPS-84, and the equation of Hill (1990). The upper diagram shows the absolute plot of c_p as a function of temperature and the lower diagram percentage deviations. The data of Archer and Carter (2000) are combined with the experimental uncertainties estimated by these authors: $100\Delta c_p/c_p = 100(c_{p,exp} - c_{p,calc})/c_{p,exp}$.

Figure 7.50 shows a corresponding comparison between the experimental data for the speed of sound w and values calculated from IAPWS-95 for the same region of the subcooled liquid as plotted in Fig. 7.49 for the $p\rho T$ data. It can be seen that within the metastable region (on the left of the phase boundary), the agreement between the experimental data and the values from the equations of state is not so good, while the equation of Hill (1990) agrees well with

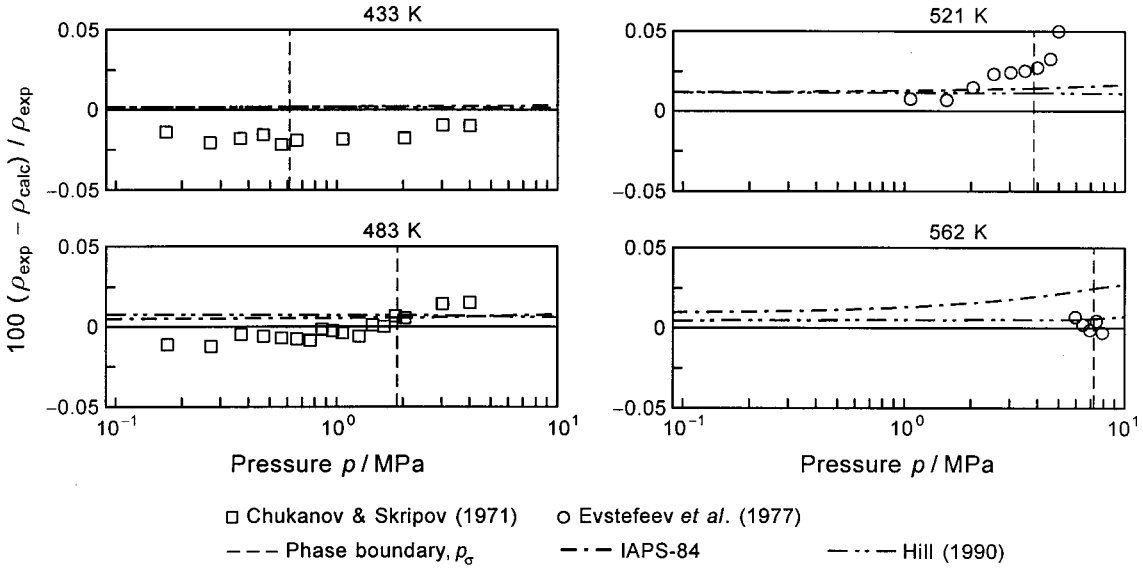

FIG. 7.52. Percentage density deviations between experimental $p\rho T$ data in the superheated liquid (left of the phase-boundary line) and values calculated from IAPWS-95, Eq. (6.4). Values calculated from IAPS-84 and the equation of Hill (1990) are plotted for comparison.

IAPWS-95 for temperatures down to 240 K. Attempts to bring IAPWS-95 for temperatures $T<265\,\mathrm{K}$ into better agreement with the *w* data of Trinh and Apfel (1978) and of Petitet *et al.* (1983) failed if one was not willing to accept systematic density deviations far outside the experimental uncertainty of the very accurate $p\rho T$ data of Kell (1975) for temperatures $T<250\,\mathrm{K}$ along this isobar. Without forcing IAPWS-95 to follow the *w* data of Trinh and Apfel (1978) and of Petitet *et al.* (1983) for $T<263\,\mathrm{K}$, the $p\rho T$ data of Kell (1975) and of Hare and Sorensen (1987) in this region can be very well represented, see Fig. 7.49. Obviously, for $p=0.101\,325\,\mathrm{MPa}$ and $T<263\,\mathrm{K}$ the speed-of-sound data of Trinh and Apfel (1978) and Petitet *et al.* (1983) are not consistent with the $p\rho T$ data of Kell (1975) and of Hare and Sorensen (1987). Therefore, we decided not to fit IAPWS-95 to any speed-of-sound data in the metastable region.

In the subcooled liquid at a pressure $p=0.101\,325\,\mathrm{MPa}$, there are data for the isobaric heat capacity c_p measured by Angell *et al.* (1982) and more recently by Archer and Carter (2000); both data sets cover temperatures down to 236 K, see Table 4.8. Figure 7.51 presents comparisons between these c_p data and values calculated from IAPWS-95. The upper diagram shows the absolute plot of the isobaric heat capacity as a function of temperature, and in the lower diagram the corresponding percentage deviations are given; values calculated from IAPS-84 and the equation of Hill (1990) are also plotted. It can be seen that IAPWS-95 represents the c_p data of Angell *et al.* (1982), to which IAPWS-95 was fitted, to within their experimental uncertainty, see below. Due to the discrepancy between Angell *et al.*'s data and the data of Archer and Carter (2000), see Sec. 4.5.2, there are also systematic differences between the values from IAPWS-95 and the data of Archer and Carter (2000). However, when taking into account the uncertainties of both data sets [±3% for the data of Angell *et al.* (1982) and between ±0.3% at 285 K and ±1% at 238 K for the data of Archer and Carter (2000), see Sec. 4.5.2], the values of IAPWS-95 are still within the coupled uncertainties (except for the lowest temperature $T=236\,\mathrm{K}$). The figure also shows that the equation of Hill (1990) follows the data of Angell *et al.* (1982) as well. IAPS-84 fails in representing the isobaric heat capacity in the subcooled liquid.

7.3.2.2. Superheated Liquid. In the superheated liquid, there are the $p\rho T$ data of Chukanov and Skripov (1971) and Evstefeev *et al.* (1977) and the speed-of-sound data measured by Evstefeev *et al.* (1979). The temperature and pressure ranges of these data are given in Secs. 4.2.1 and 4.3, respectively.

Comparisons between these data and values calculated from IAPWS-95, Eq. (6.4), are shown in Figs. 7.52 and 7.53 by using a few isotherms as examples; the corresponding values from IAPS-84 and the equation of Hill (1990) are plotted as well. Neither IAPWS-95 nor the two other equations of state were fitted to these $p\rho T$ and *w* data. Since, however, the course of the isotherms in the superheated liquid is very strongly determined by the accurate data in the stable homogeneous liquid, none of the equations of state discussed here has any difficulty in representing the $p\rho T$ and *w* data to within their experimental uncertainties; for the $p\rho T$ data we estimate the uncertainties to be less than ±0.05% in density. However, the data do not extend very far into the metastable region.

In the following the course of the spinodals on the saturated liquid side of the vapor–liquid two-phase region calculated from IAPWS-95, IAPS-84, and the equation of Hill (1990) is discussed. (The vapor and liquid spinodals are lines which connect, within the vapor–liquid two-phase region, all minima of the isotherms (liquid spinodal) and all maxima of the isotherms (vapor spinodal). The liquid spinodal, which is of interest here, describes the location on the isotherms at

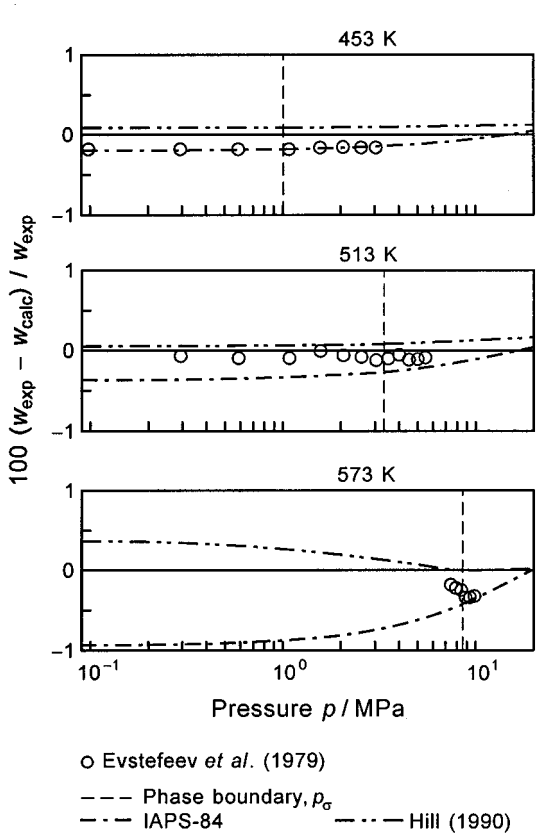

FIG. 7.53. Percentage deviations between experimental data of the speed of sound w in the superheated liquid (left of the phase-boundary line) and values calculated from IAPWS-95, Eq. (6.4). Values calculated from IAPS-84 and the equation of Hill (1990) are plotted for comparison.

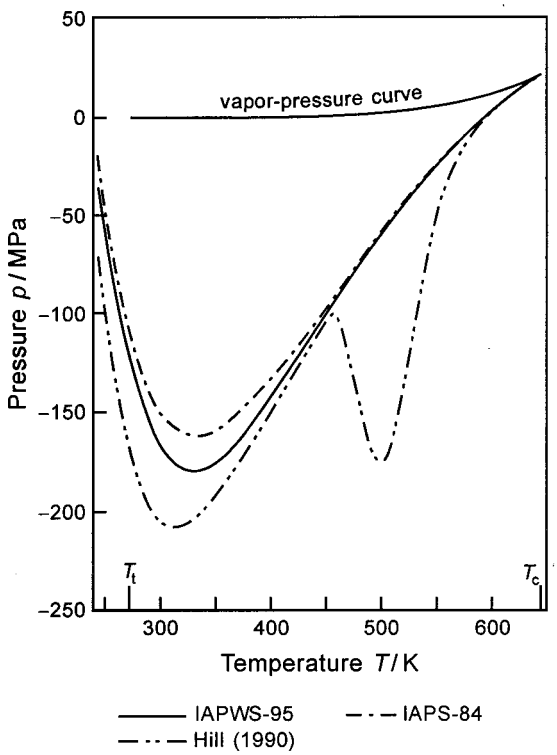

FIG. 7.54. The liquid spinodal of the vapor–liquid two-phase region as calculated from IAPWS-95, Eq. (6.4), IAPS-84 and the equation of Hill (1990). The vapor–pressure curve (IAPWS-95) is also plotted.

which, coming from the side of the saturated liquid, the mechanical stability condition $(\partial p/\partial v)_T \leqslant 0$ reaches the limiting value zero; here the isotherm has a horizontal tangent. The spinodals start at the critical point and extend, depending on the stability of the equation of state, to temperatures below the triple point.)

In contrast to an equation of state of the so-called van der Waals type whose isotherms form only *one* minimum and *one* maximum in the two-phase region, state-of-the-art multiparameter equations of state have, sufficiently far from the critical point, several minima and maxima along an isotherm. This is also true for the IAPWS-95 formulation. Taking this into account, the ''real'' spinodals are only those lines that connect the outermost minima and the maxima of the isotherms. The inner minima and maxima are only of mathematical and not of physical importance.

With this background, the course of many isotherms coming from the saturated-liquid line to the first minima in the pressure–density diagram was considered, and the $p-\rho$ values of these minima were determined so that one has the $p\rho T$ values at the minima of the isotherms. From these $p\rho T$ values, the corresponding $p-T$ combinations were used to plot the liquid spinodal in a $p-T$ diagram. As a result, Fig. 7.54 shows the liquid spinodal of H_2O as calculated from IAPWS-95, IAPS-84, and the equation of Hill (1990); for comparison the vapor–pressure curve is also plotted. From this figure, one can see that the three equations of state yield basically a similar course of the liquid spinodal. Only the equation of Hill (1990) shows an artifact in the course of the spinodal for temperatures from 450 to 580 K. In this range, Hill's equation forms a secondary minimum of the spinodal, which is based on corresponding indentations in the isotherms in this part of the two-phase region.

7.3.2.3. Subcooled Vapor. There are no experimental data for thermodynamic properties in the subcooled vapor that can be used to assess the behavior of IAPWS-95 in this metastable region, which is of importance for several technical applications (for example, in a steam turbine, the steam often expands into this metastable region).

However, when developing the industrial formulation IAPWS-IF97 (see Sec. 1.4), for which the IAPWS-95 formulation provided the input values, it became apparent that IAPWS-95 does not behave correctly within the subcooled vapor for pressures below 10 MPa. In this part of the vapor–liquid metastable region, IAPWS-95 yields a vapor spinodal that is significantly too close to the saturated-liquid line. After corresponding tests, the input values for IAPWS-IF97 (values of v, h, and c_p) for the subcooled vapor at pressures below 10 MPa were not calculated from IAPWS-95 but from the gas equation, Eq. (3.2), described in Sec. 3; for details see the international article on the industrial formulation IAPWS-IF97 of Wagner *et al.* (2000).

Therefore, values of thermodynamic properties in the sub-

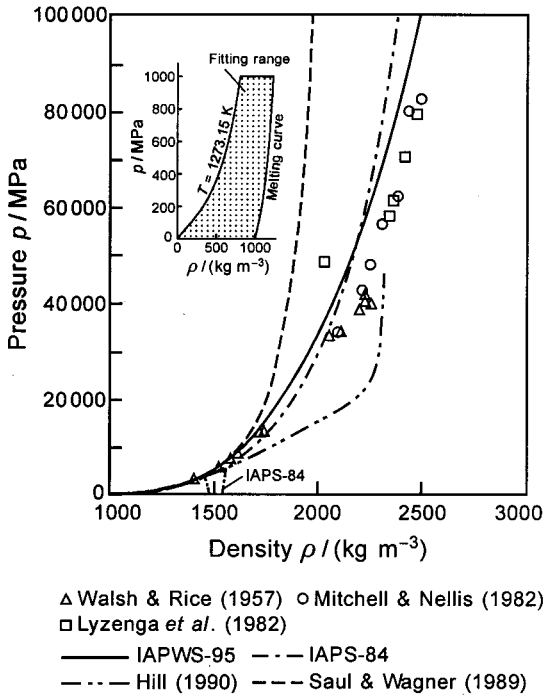

FIG. 7.55. Comparison of the Hugoniot curve as calculated from IAPWS-95, Eq. (6.4), IAPS-84, the equation of Saul and Wagner (1989), and the equation of Hill (1990) with the corresponding experimental data. The hatched range of the enlarged section corresponds to the range of data used for fitting IAPWS-95.

cooled vapor for pressures below 10 MPa should not be calculated from IAPWS-95, Eq. (6.4), but from the gas equation, Eq. (3.2); see also item (3) in Sec. 6.3.1. This statement does not include the saturated-vapor line on which IAPWS-95 is very accurate.

7.3.3. Extrapolation Behavior

Based on our experience with the development of the reference equations of state for methane [Setzmann and Wagner (1991)] and carbon dioxide [Span and Wagner (1996)], during the entire development of the IAPWS-95 formulation we attached importance to its reasonable extrapolation behavior. The extrapolation capability relates to the following three features:

(1) representation of experimental data outside the fitting (and validity) range of IAPWS-95;
(2) extrapolation beyond the range of primary data to very high pressures combined with high densities; and
(3) extrapolation beyond the range of primary data to very high temperatures combined with high and particularly with low densities.

The performance of IAPWS-95 with regard to item (1) was shown by a comparison of IAPWS-95 with reliable experimental data outside its range of validity (1000 MPa, 1273 K). Such comparisons have been carried out for $p\rho T$ data (Sec. 7.2.1), speeds of sound (Sec. 7.2.3), and isobaric heat

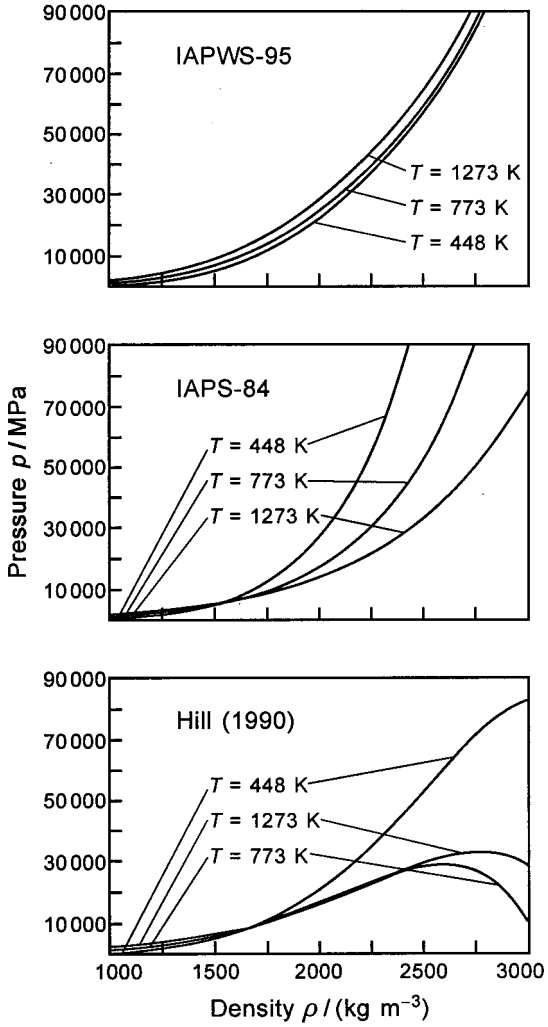

FIG. 7.56. Plot of three $p\rho T$ isotherms in the pressure–density diagram at extremely high pressures as calculated from IAPWS-95, Eq. (6.4), IAPS-84 and the equation of Hill (1990).

capacities (Sec. 7.2.5). The extrapolation behavior of IAPWS-95 with respect to the above-mentioned item (2) is mainly dealt with in the context of the Hugoniot curve in the following subsection, while the extrapolation capability with regard to the above-mentioned item (3) is discussed with the help of the so-called ideal curves in the subsection after that.

7.3.3.1. Hugoniot Curve and pρT Behavior at Extreme Pressures and Temperatures. The extrapolation capability of the IAPWS-95 formulation into the region of extremely high pressures and temperatures is tested with the help of shock-wave measurements meeting the so-called Hugoniot relation. For details of such Hugoniot-curve data, which are a combination of values of the three properties pressure, density, and specific enthalpy, see Sec. 4.9.

For water, such $p\rho h$ data were measured by three groups of authors: Walsh and Rice (1957), Lyzenga *et al.* (1982), and Mitchell and Nellis (1982). As already mentioned in Sec. 4.9, these data were not used for the development of the IAPWS-95 formulation because their use would have resulted in nonlinear relations that require iterative solutions

for temperature. Moreover, for an equation of state that had already been optimized with regard to its functional structure, nonlinear fits involving Hugoniot data hardly exercise an influence on the representation of these data—the extrapolation behavior of such equations of state is closely related to their functional form, see Span and Wagner (1997). Any attempt to use Hugoniot data in linear optimization algorithms, as applied for developing IAPWS-95 (see Sec. 5.3), requires a precorrelation of the temperature belonging to these data points. [Recently, during the development of the new reference equation of state for nitrogen [Span *et al.* (2000)], for the first time Hugoniot data were used directly in combination with the nonlinear optimization algorithm of Tegeler *et al.* (1997), (1999).] However, due to the absence of ''real'' $p\rho T$ data at these extreme conditions, such precorrelated temperatures cannot be checked. Therefore, such an approach risks distorting the experimental information given by Hugoniot data. For H_2O, one bad example in this respect is the $p\rho T$ values of Rice and Walsh (1957), which they derived from their Hugoniot measurements [Walsh and Rice (1957)], for details see Sec. 4.9. However, an equation of state fitted to these $p\rho T$ values yields totally unreasonable plots for the Hugoniot curve, with parts even having an unphysical negative slope.

Based on this knowledge, the reasonable extrapolation capability of IAPWS-95 was mainly achieved by choosing a suitable functional form for the bank of terms (limitations on the density and temperature exponents of the pure polynomial terms and the polynomial part combined with the exponential functions, see Secs. 5.4.1 and 5.4.2). These functional measures were slightly supported by adding to the data set used to fit IAPWS-95 (with very low weight) so-called ''artificial'' $p\rho T$ data determined in the optimization process from interim equations that reasonably represented the Hugoniot curve, see Sec. 4.11. The data of the Hugoniot curve themselves (see Sec. 4.9) were only used for comparison.

Figure 7.55 presents a plot of the Hugoniot curve for H_2O as calculated from IAPWS-95, Eq. (6.4), and three further equations of state; the experimental data of the corresponding shock-wave measurements, which extend to pressures beyond 80 000 MPa, are plotted as well. The four equations of state yield rather different Hugoniot curves. The equation of Saul and Wagner (1989) shows, in comparison to the experimental data, a Hugoniot curve that is too steep, although it was fitted to the $p\rho T$ data of Rice and Walsh (1957) that had been derived by these authors from their Hugoniot data. This confirms our statement on determining the temperature from the $p\rho h$ data obtained from Hugoniot measurements, see above. The equation of Hill (1990) is clearly too flat in the lower part up to densities of about 2200 $\mathrm{kg\,m^{-3}}$ and afterward much too steep; above the end point of this curve, no further equilibrium states according to Eq. (4.3) can be calculated from Hill's equation. At first glance it looks as if IAPS-84 represents the Hugoniot data quite well, but this equation yields a solution of Eq. (4.3) that extends into the solid phase of H_2O for densities near $\rho=1500$ $\mathrm{kg\,m^{-3}}$ and yields a maximum temperature of only 420 K for the $p\rho h$ data. Thus, the IAPWS-95 formulation is the only equation of state for H_2O that reasonably represents the Hugoniot data based on the shock wave measurements of the three groups of authors.

When testing an equation of state's extrapolation capability to extreme pressures and temperatures, a reasonable representation of the Hugoniot curve is a necessary but not a sufficient condition. It can happen that an equation meets the condition ''Hugoniot curve'' but displays an unphysical $p\rho T$ behavior in this region. With this background, Fig. 7.56 illustrates the $p\rho T$ behavior along the three isotherms $T=448\,\mathrm{K}$, $T=773\,\mathrm{K}$, and $T=1273\,\mathrm{K}$ in a $p-\rho$ diagram as calculated from three equations of state. It can be seen that IAPWS-95 (upper diagram) yields a very ''harmonic'' plot of the isotherms, while IAPS-84 and the equation of Hill (1990) produce physically unreasonable plots of these isotherms. IAPS-84 (middle diagram) yields a crossing point of the isotherms at the same value of the density at which the Hugoniot curve of this equation yields a solution in the solid region, see Fig. 7.55. Hill's equation shows a similar behavior, namely a crossing point of the isotherms at about $\rho=1675$ $\mathrm{kg\,m^{-3}}$ and, in addition, at higher densities the isotherms turn downward.

7.3.3.2. Ideal Curves. Plots of so-called ideal curves are useful in assessing the behavior of an equation of state in regions beyond the range of available data [Deiters and de Reuck (1997), Span and Wagner (1997), Span (2000)], as well as in revealing inconsistencies in the available data sets. (Ideal curves are curves along which one property of a real fluid is equal to the corresponding property of the hypothetical ideal gas at the same density and temperature. Based on this very general definition, ideal curves can be defined for almost every property, but usually the discussion is focused on the ideal curves of the compression factor and its first derivatives.) The most common ideal curves are those of the compression factor Z and its first derivatives. These curves are also considered here and their definitions are given in Table 7.1. Besides testing an equation of state at high pressures and high temperatures, these ideal curves are also very well suited to test the equations at high temperatures and low pressures and low densities, respectively.

Figure 7.57 illustrates in a double-logarithmic pressure–temperature diagram the plots of the four characteristic ideal curves for H_2O as calculated from the IAPWS-95 formulation, Eq. (6.4). The range in which reliable experimental data exist, to which IAPWS-95 was fitted, is marked by the dotted region. Although the curves in this figure do not provide any numerical information, reasonable shapes without visible oscillations as shown in the figure indicate a qualitatively correct extrapolation behavior of IAPWS-95. In contrast, IAPS-84 and the equation of Hill (1990) [and also the equation of Saul and Wagner (1989), which is not shown here] exhibit some serious shortcomings when describing both the Joule–Thomson inversion curve and the Joule inversion curve. As can be seen from Fig. 7.58, both equations show a physically unreasonable oscillating behavior of the Joule–

TABLE 7.1. The zeroth and first order ideal curves for the compression factor Z and their definitions in terms of the compression factor $Z(\rho,T)$ and of the residual part of the reduced Helmholtz free energy $\phi^{\mathrm{r}}(\rho,T)$ and the condition for the second virial coefficient B at the temperature T_{end}[a]

Designation	Definition in terms of: Compression factor	Definition in terms of: Residual Helmholtz free energy[b]	$B(T_{\mathrm{end}})$
(Classical) ideal curve	$Z=1$	$\phi^{\mathrm{r}}_{\delta}=0$	$B=0$
Boyle curve	$\left(\frac{\partial Z}{\partial \rho}\right)_T=0$	$\phi^{\mathrm{r}}_{\delta}+\delta\phi^{\mathrm{r}}_{\delta\delta}=0$	$B=0$
Joule–Thomson inversion curve	$\left(\frac{\partial Z}{\partial T}\right)_p=0$	$\phi^{\mathrm{r}}_{\delta}+\delta\phi^{\mathrm{r}}_{\delta\delta}+\tau\phi^{\mathrm{r}}_{\delta\tau}=0$	$B-T(\mathrm{d}B/\mathrm{d}T)=0$
Joule inversion curve	$\left(\frac{\partial Z}{\partial T}\right)_\rho=0$	$\phi^{\mathrm{r}}_{\delta\tau}=0$	$\mathrm{d}B/\mathrm{d}T=0$

[a]Temperatures where the ideal curves cross the axes $p=0$ and $\rho=0$, respectively, are called end temperatures, T_{end}. At these temperatures, the second virial coefficient must meet the condition given in the column on the right.
[b]For an explanation of the quantities $\phi^{\mathrm{r}}_{\delta}$, $\phi^{\mathrm{r}}_{\delta\delta}$, and $\phi^{\mathrm{r}}_{\delta\tau}$, see the footnote of Table 6.5.

Thomson inversion curve to the right of its maximum. In contrast, IAPWS-95, which is also plotted in Fig. 7.58 for comparison, is able to describe the course of this curve very smoothly and according to physical expectations, see Span and Wagner (1997).

Concerning the ideal curves, Fig. 7.58 also shows that the most significant discrepancy between IAPWS-95, IAPS-84, and the equation of Hill (1990) exists in their description of the Joule inversion curve. Only IAPWS-95 is able to represent the theoretically expected course of this curve. (The only substance for which the region of the Joule inversion curve is completely covered by experimental data is helium. Thus, for this substance the theoretically expected course of this curve is experimentally verified.) In particular, based on the fact that the other equations of state are not able to yield any zero crossing of this ideal curve, it can be concluded that they also behave incorrectly regarding the second virial coefficient B at these high temperatures. According to Table 7.1, for this ideal curve the condition for B at this zero crossing (corresponding to T_{end}) reads $\mathrm{d}B/\mathrm{d}T=0$, which requires a maximum in B at the temperature T_{end}. In this context, Fig. 7.59 presents the second virial coefficient for these extremely high temperatures as calculated from IAPWS-95, IAPS-84, and the equation of Hill (1990). For comparison purposes, the virial equation of Hill and MacMillan (1988) is also plotted. As can be seen, of all the wide-range equations of state [including the equation of Saul and Wagner (1989), which is not shown in the figure], only the IAPWS-95 formulation is able to produce a maximum in B at a reasonable temperature. The virial equation of Hill and MacMillan (1988) has the maximum at a very similar temperature, which confirms the course of the Joule inversion curve predicted by IAPWS-95.

During the development of IAPWS-95, the Joule inversion curve was the only ideal curve to which we had to pay attention and on whose representation we had to exert an influence. In order to produce the desired reasonable representation of the Joule inversion curve, ten data points of the second virial coefficient in this temperature range calculated from the gas equation, Eq. (3.2), were incorporated into the final data set used to develop IAPWS-95, see Sec. 4.10.

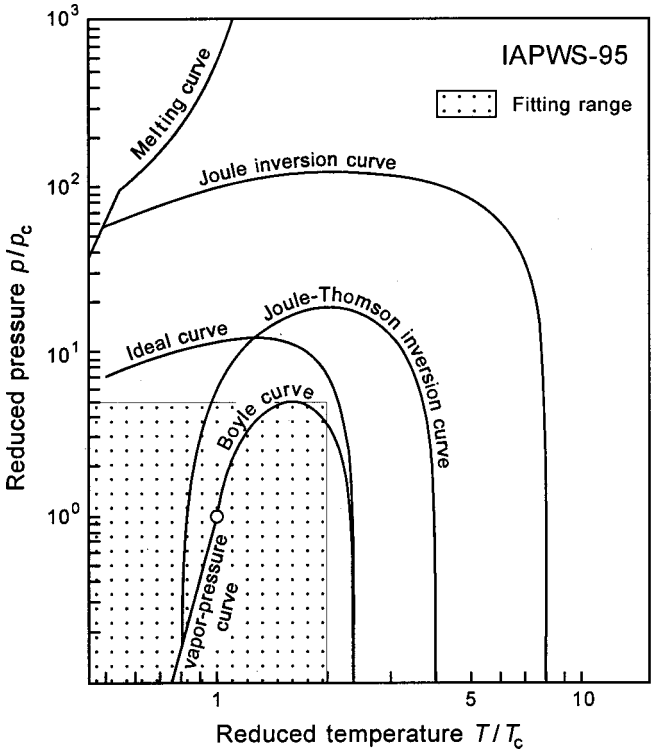

FIG. 7.57. The so-called ideal curves in a double logarithmic p/p_c vs T/T_c diagram as calculated from IAPWS-95, Eq. (6.4); for the definition of these curves see Table 7.1.

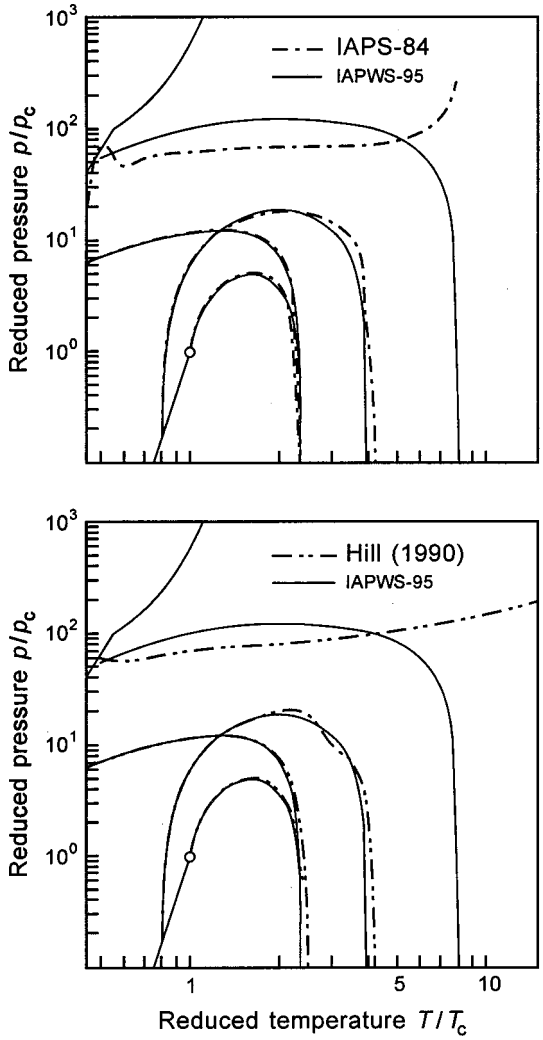

FIG. 7.58. The ideal curves in a double logarithmic p/p_c vs T/T_c diagram as calculated from IAPS-84 and the equation of Hill (1990); the curves calculated from IAPWS-95 are plotted for comparison. For the designation of the curves see Fig. 7.57.

Finally, Fig. 7.60 summarizes the plots of the four ideal curves as calculated from IAPWS-95, IAPS-84, and the equation of Hill (1990) in a density–temperature diagram. This diagram illustrates the location of the ideal curves in comparison to the saturated liquid and vapor line and again makes clear the smooth and ''natural'' representation of these curves by IAPWS-95. The oscillating representation of the Joule–Thomson inversion curve and the failure of IAPS-84 and Hill's equation for the Joule inversion curve are also obvious in this diagram.

In addition to its reasonable high-pressure, high-density behavior, IAPWS-95 is able to represent properties at high temperatures and low densities in a physically reasonable manner.

8. Uncertainty of the IAPWS-95 Formulation

Estimates for the uncertainty of an empirical equation of state must be guided by comparisons with experimental data

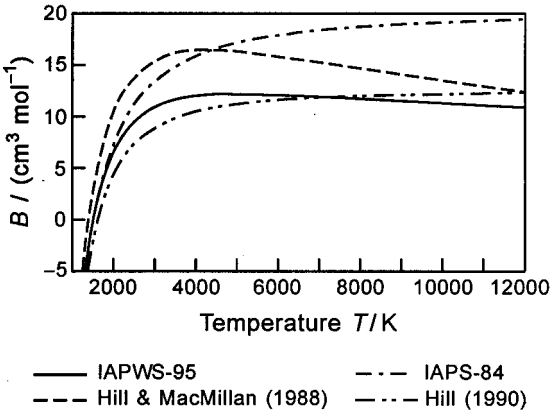

FIG. 7.59. Second virial coefficient at very high temperatures as calculated from IAPWS-95, Eq. (6.4), IAPS-84, the equation of Hill (1990), and the virial equation of Hill and MacMillan (1988).

and the assessment of their uncertainty. In regions where no data are available or where there are only data of lower accuracy, comparisons with existing equations of state can assist in the assessment. The estimates of the uncertainty of the $p\rho T$, w, and c_p values calculated from IAPWS-95, Eq. (6.4), were carried out by IAPWS, and the results are summarized in Sec. 6.3.2. Usually, the uncertainties of c_v in the gas and liquid region correspond to the uncertainties given for c_p (except for the critical region). However, due to the unclear data situation, a more conservative estimate has been made at the end of Sec. 7.2.4. The relative uncertainty of differences in enthalpy Δh is always smaller than the uncertainty in c_p. IAPWS plans to make a more specific statement on

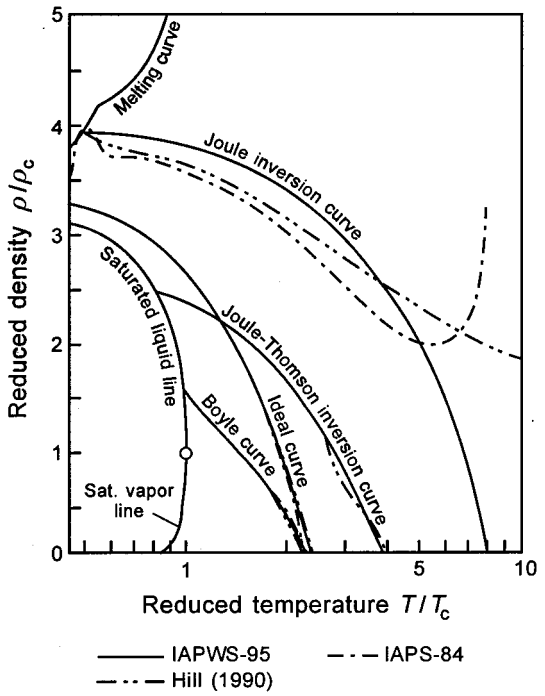

FIG. 7.60. The ideal curves in a ρ/ρ_c vs log (T/T_c) diagram as calculated from IAPWS-95, Eq. (6.4), IAPS-84, and the equation of Hill (1990).

the uncertainty in enthalpy, which will be given as an Informatory Note (see the IAPWS website from 2004 on).

Outside the range of its validity, IAPWS-95, Eq. (6.4), should yield reasonable results for the basic thermodynamic properties like pressure (density) and enthalpy within the whole chemically stable region of H_2O. Of course, the extrapolation results have an increased uncertainty that cannot be estimated. The calculation of derived properties such as speed of sound or specific isobaric and isochoric heat capacity is not recommended beyond the limits of validity of IAPWS-95. If such properties are calculated, the results should be checked carefully. For extrapolation into the three metastable regions; subcooled liquid, superheated liquid, and subcooled vapor, see Sec. 7.3.2.

9. Recommendations for Improving the Basis of the Experimental Data

The beginning of Sec. 4 stated that water is one of the best experimentally investigated fluids. This statement is particularly based on the very high accuracy of the $p\rho T$ data in the liquid region, on the accurate $p\rho T$ data in the gas region for not too high temperatures (see Fig. 6.1), and on the quantity of speed-of-sound and isobaric-heat-capacity data. However, if an improved equation of state is to be developed it would be helpful to have data with higher accuracies and, more importantly, to have data in those regions for which, at present, reliable experimental data are not available at all.

While it might be somewhat surprising, we consider the thermal properties ($p_\sigma \rho' \rho'' T$ data) along the entire vapor–liquid phase boundary a candidate for a remeasuring project. As discussed in several places in Sec. 7, there are inconsistencies between the properties on the phase boundary and those in the single-phase region near the saturation state. The data for the vapor pressure p_σ and the saturated-vapor density ρ'' are based mainly on data of Osborne *et al.* measured in the 1930's, see Table 2.1. Moreover, the ρ' and ρ'' data of Osborne *et al.* (1937), (1939) were not directly measured, but were determined from measurements of special caloric data in combination with further information, see Sec. 2.3.1. We also believe that the ρ' data of Kell *et al.* (1985) exhibit certain inconsistencies with the $p\rho T$ data in the single-phase liquid region. Thus, it would be interesting to see $\rho_\sigma \rho' \rho'' T$ data measured directly with a state-of-the-art two-sinker densimeter [see Wagner *et al.* (2002)] with which, for most of the liquid–vapor phase boundary of other substances, uncertainties in p_σ, ρ', and ρ'' of less than about $\pm 0.015\%$, $\pm 0.012\%$, and $\pm 0.025\%$, respectively, have been achieved.

In the single-phase region, the $p\rho T$ data of Vukalovich *et al.* (1961) should be replaced by more accurate data in the temperature range above 800 K at pressures of, if possible, up to 500 MPa. It would very desirable if such data had uncertainties in density of less than $\pm 0.1\%$, preferably on the order of $\pm 0.05\%$. Then, the discrepancies in the $p\rho T$ surface of H_2O in this high-temperature region (see Secs. 7.2.1.4 and 7.2.1.5) could be removed. For the pressure range from 100 to 500 MPa and temperatures below 800 K down to the melting-curve temperature, it would be helpful to have $p\rho T$ data with uncertainties in density on the order of $\pm 0.02\%$. With such data, the inconsistency between the $p\rho T$ data of Grindley and Lind (1971) and of Kell and Whalley (1975), see Fig. 4.2, could be clarified. At present, the gas region is covered by the $p\rho T$ data of Kell *et al.* (1989), which show, however, scatter on the order of $\pm 0.05\%$ and uncertainties of up to $+0.2\%$ at 423 and 448 K when approaching the phase boundary (see Fig. 4.3); moreover, the selected data of Kell *et al.* ''only'' extend down to 473 K. Therefore, in order to fix the derivatives of the $p\rho T$ surface in this region better, it would be desirable to have new $p\rho T$ data in the gas region, preferably covering a temperature range from 373 to 873 K at pressures up to the vapor pressure and for supercritical temperatures up to about 40 MPa. However, such remeasurements in the gas region only make sense if uncertainties in density of less than $\pm 0.02\%$ can be achieved; this is in principle possible with modern two-sinker densimeters in which the influence of adsorption is compensated, see Wagner *et al.* (2002). For the critical region, it would be desirable to have critical-region $p\rho T$ data with uncertainties in pressure of less than $\pm 0.01\%$–$\pm 0.02\%$. In this way, the increase of c_p in the critical region would be better fixed and water could catch up with other very well measured substances in the critical region (for example, CH_4, CO_2, N_2, Ar, C_2H_4, SF_6, and C_2H_6). Having a $p\rho T$ data set of the quality described above would to a large extent compensate for the absence of very accurate data for the isobaric and isochoric heat capacity, see below.

As usual, compared with the $p\rho T$ data, the data situation regarding the caloric properties is clearly worse. For the speed of sound w, the very well measured region [283–373 K, 10–100 MPa, Fujii (1994) to 200 MPa] with uncertainties between $\pm 0.005\%$ and $\pm 0.05\%$ should be extended to a greater range of temperatures and pressures. It would be desirable to have such measurements for pressures up to 500 MPa and up to supercritical temperatures, preferably up to about 900 K. It would be necessary that the experimental uncertainties of such data be less than $\pm 0.03\%$, at least for temperatures up to 650 K. In this case, the reason for the systematic deviation of the present w data in this region in comparison with the values from IAPWS-95 (see Fig. 7.21) could be clarified and the wpT surface in this region would be much better defined. Based on the present experimental possibilities for speed-of-sound measurements in the liquid region, uncertainties of this order are in principle achievable. It would also be very desirable to have new speed-of-sound measurements in the gas region for temperatures starting near the phase boundary and extending to 650 K (if possible to higher temperatures) at pressures from 0.1 MPa to near the vapor pressure, and for supercritical temperatures up to 25 MPa or even higher if possible. The experimental uncertainty of such w measurements should be less than $\pm 0.01\%$, which is achievable with spherical resonators [see Goodwin (2002)]. Then, such measurements would define a new quality of the wpT surface of H_2O at gas densities.

At present, the best data for the isobaric heat capacity c_p

are mostly confined to the middle density range from about 100 to 700 kg m^{-3} ($\rho_c = 322$ kg m^{-3}), supplemented by a few data in the gas region and in the liquid region at very high densities and low temperatures, see Fig. 4.8. Except for these very few c_p data in the liquid region, the uncertainties of all the other c_p data were given by the experimenters as $\pm 0.5\%$–$\pm 2\%$. However, in order to have a real test of an equation of state regarding its c_p behavior outside the critical region, the c_p data should have uncertainties on the order of $\pm 0.1\%$–$\pm 0.2\%$ in the gas and liquid region. At present, however, such a requirement cannot be experimentally realized. A possible alternative is given below.

Concerning the isochoric heat capacity c_v, the present data situation is worse than that for c_p. Except for the experimental verification of the steep increase of the c_v values when approaching the critical point and of the order of magnitude of this increase, and except for the high-density c_v data of Magee *et al.* (1998), the existing c_v data are unfortunately not accurate enough to serve as a real test of an equation of state regarding its c_v behavior. For this purpose one would need c_v measurements with uncertainties of $\pm 0.1\%$–$\pm 0.2\%$ (except for the critical region), but over the entire relevant part of the surface of state (i.e., temperatures to about 900 K and pressures to 100 MPa). As for c_p, this requirement is probably unrealistic.

A potentially achievable experimental compromise regarding the desirable c_p and c_v measurements might be as follows. The entire surface could be split into the gas region, for which c_p measurements are better suited, and into the liquid region, for which c_v measurements are better suited. At present, it should be possible to carry out c_p measurements in the gas region with experimental uncertainties between $\pm 0.1\%$ and $\pm 0.3\%$ and c_v measurements in the liquid region on the order of $\pm 0.2\%$–$\pm 0.4\%$, see the c_v data of Magee *et al.* (1998). Based on our assessment, it is not absolutely necessary to measure c_p data in the critical region, because the increase of c_p in this region is mainly based on the derivative $(\partial\rho/\partial p)_T$, see Eq. (6.11). This means that very good $p\rho T$ measurements would be sufficient to model the increase of c_p in the critical region. However, the behavior of an equation of state regarding the isochoric heat capacity in the critical region can only be reasonably modeled if one has good c_v data in this region. Besides a reasonable experimental accuracy, such data should particularly have very good internal consistency to guide the equation of state appropriately.

Finally, the inconsistency in the isobaric heat capacity in the ideal-gas state c_p°, which exists at high temperatures between the different c_p° data sets (see Sec. 4.5.1), should be clarified.

10. Conclusions

Based on a comprehensive study of the experimental data for the thermodynamic properties of ordinary water substance (H_2O), a new equation of state in the form of a fundamental equation explicit in the Helmholtz free energy has been developed. The functional form of this formulation has been determined by using a state-of-the-art linear structure-optimization method combined with nonlinear fitting processes in an iterative procedure. The new formulation has been adopted by the IAPWS as the new scientific standard equation of state for H_2O under the name ''The IAPWS Formulation 1995 for the Thermodynamic Properties of Ordinary Water Substance for General and Scientific Use,'' which we abbreviate to IAPWS-95 formulation or IAPWS-95 for short. This IAPWS-95 formulation is valid in the fluid region of H_2O up to temperatures of 1273 K at pressures up to 1000 MPa. IAPWS-95 is able to represent the most accurate experimental data in the single-phase region and on the vapor–liquid phase boundary to within their experimental uncertainty. In particular, in the liquid region IAPWS-95 is of an accuracy that has never been achieved before by a wide-range equation of state; for example, the standard densities along the isobar $p = 0.101\,325$ MPa are represented to within the 1 ppm level. Moreover, IAPWS-95 represents the experimental data of the thermal properties in the critical region without any difficulty.

Special interest has been focused on a reasonable representation of the caloric properties in the critical region and on a good extrapolation behavior of IAPWS-95. For the basic improvement of the caloric behavior in the critical region, the nonanalytical terms from the reference equation of state for carbon dioxide [Span and Wagner (1996)] were adopted. Although these terms are not perfect, they enable IAPWS-95 to represent the isochoric heat capacity and the speed of sound even in the immediate vicinity of the critical point; until the equation of state for CO_2 of Span and Wagner (1996), this attribute had only been a domain of scaled equations of state, which use iterative dependencies between different sets of variables and have a limited range of validity. Mostly because of its functional structure, the IAPWS-95 formulation can be extrapolated to extremely high pressures and very high temperatures and densities; at least for the basic properties of H_2O such as pressure (density) and specific enthalpy, IAPWS-95 should yield reasonable results within the whole region of chemical stability. The good representation of the so-called ideal curves has shown that IAPWS-95 can also be reasonably extrapolated to high temperatures at low densities and low pressures.

11. Acknowledgments

The authors are indebted to the members of the following IAPWS groups (so far as W. W. is not a member himself): Working Group ''Thermophysical Properties of Water and Steam,'' and its predecessor working groups with the same scope, Task Group ''New Scientific Formulation,'' and Task Group ''New Scientific Formulation–Evaluation.'' In particular, one of us (W.W.) is very grateful to his two colleagues in the Task Group ''New Scientific Formulation,'' P. G. Hill and J. V. Sengers (who became the chairman of this group in 1994) for their very fair and friendly collaboration, and also to D. G. Friend who joined this task group in 1995.

Similarly important has been the continuous support of this comprehensive project over all the years by the chairpersons of the Working Group ''Thermophysical Properties of Water and Steam'' and its predecessor groups, J. M. H. Levelt Sengers (1990), K. Watanabe (1991–1994), and J. R. Cooper (1995 and 1996). We are also grateful to the chairman of the Task Group ''New Scientific Formulation-Evaluation,'' J. Gallagher, and his colleagues A. Alexandrov, J. R. Cooper, H.-J. Kretzschmar, J. Patek, and H. Sato for their efforts in testing IAPWS-95 regarding the most relevant thermodynamic properties in the various regions of state. In addition, we are indebted to A. Kostrowicka Wyczalkowska and J. V. Sengers for investigating IAPWS-95 regarding its behavior in the near-critical and extended critical region. Moreover, we are grateful to all IAPWS colleagues who contributed to the entire project of the development of the IAPWS-95 formulation. On behalf of all of them we would like to thank the presidents of IAPWS who held office during the development period of IAPWS-95, namely M. Pichal, J. M. H. Levelt Sengers, J. R. Cooper, and K. Watanabe. We also wish to express our warmest thanks to D. Bücker for his help in handling the computer programs for plotting all the figures and to R. Gölzenleuchter for her postediting of these figures. Moreover, we would like to thank C. Bonsen, D. Bücker, R. Kleinrahm, O. Kunz, N. Kurzeja, and particularly R. Span for many fruitful discussions. In addition we thank A. Kostrowicka Wyczalkowska for providing us with the computer code of the crossover equation of Kostrowicka Wyczalkowska *et al.* (2000), I. M. Abdulagatov for providing us in electronic form with many c_v data measured at the Dagestan Scientific Center of the Russian Academy of Sciences, and K. Fujii for making very accurate speed-of-sound data available prior to their publication. Our special thanks go to A. H. Harvey for carefully reading the entire manuscript, for suggestions in improving certain details, for improving the grammar, and for some information on more recent articles on the properties of water. We also thank E. W. Lemmon for carefully reading the manuscript and for giving us helpful suggestions. Finally, we are particularly grateful to the Deutsche Forschungsgemeinschaft (German Research Association) for their financial support of the development of the IAPWS-95 formulation.

12. References

Abdulagatov, I. M. and V. I. Dvoryanchikov, J. Chem. Thermodyn. **25**, 823 (1993).

Abdulagatov, I. M., A. R. Bazaev, and A. E. Romazanova, J. Chem. Thermodyn. **25**, 249 (1993).

Abdulagatov, I. M., V. I. Dvoryanchikov, and A. N. Kamalov, J. Chem. Thermodyn. **29**, 1387 (1997).

Abdulagatov, I. M., V. I. Dvoryanchikov, and A. N. Kamalov, J. Chem. Eng. Data **43**, 830 (1998).

Abdulagatov, I. M., B. A. Mursalov, and N. M. Gamzatov, in *Proceedings of the 12th International Conference on the Properties of Water and Steam* (Begell House, New York, 1995), p. 94.

Abdulagatov, I. M., V. I. Dvoryanchikov, M. M. Aliev, and A. N. Kamalov, in *Proceedings of the 13th International Conference on the Properties of Water and Steam* (NRC, Ottawa, 2000), p. 157.

Alexandrov, A. A. and A. I. Kochetov, Teploenergetika **26**, 65 (1979); Thermal Eng. **26**, 558 (1979).

Alexandrov, A. A. and D. K. Larkin, Teploenergetika **23**, 75 (1976); Thermal Eng. **23**, 72 (1976).

Alexandrov, A. A. and A. I. Kochetov, *The Investigation of Velocity of Sound in Water and Steam—Their Properties and Current Industrial Applications*, Proceeding of the 9th International Conference on the Properties of Steam, Munich 1979, edited by J. Straub and K. Scheffler (Pergamon, Oxford, 1980), p. 221.

Amirkhanov, Kh. I., G. V. Stepanov, and B. G. Alibekov, in *Isochoric Heat Capacity of Water and Steam*, edited by M. P. Vukalovich (Akad. Nauk SSSR, Dagestanskii Filial, 1969), p. 217; English translation (Amerind Publ. Co., New Dehli, 1974), p. 203.

Angell, C. A., M. Oguni, and W. J. Sichina, J. Phys. Chem. **86**, 998 (1982).

Archer, D. G. and R. W. Carter, J. Phys. Chem. B **104**, 8563 (2000).

Archer, D. G. and P. Wang, J. Phys. Chem. Ref. Data **19**, 371 (1990).

Audi, G. and A. H. Wapstra, Nucl. Phys. A **565**, 1 (1993).

Baehr, H. D. and H. Schomäcker, Forsch. Ing.-Wes. **41**, 43 (1975).

Bedford, R. E. and C. G. M. Kirby, Metrologia **5**, 83 (1969).

Benedict, M., G. B. Webb, and L. C. Rubin, J. Chem. Phys. **8**, 334 (1940).

BIPM, *Supplementary Information for the International Temperature Scale of 1990* (Bureau International des Poids et Mesures, Pavillon de Breteuil, F-92310 Sèvres, France, 1990).

Bridgman, P. W., J. Chem. Phys. **3**, 597 (1935).

Bridgman, P. W., Proc. Am. Acad. Arts Sci. **74**, 419 (1942).

Castro-Gomez, R. C., K. R. Hall, J. C. Holste, B. E. Gammon, and K. N. Marsh, J. Chem. Thermodyn. **22**, 269 (1990).

Chase, M. W., *NIST-JANAF Thermochemical Tables*, 4th ed., Part II, J. Phys. Chem. Ref. Data, Monograph No. 9 (1998).

Chavez, M., V. Sosa, and R. Tsumura, J. Acoust. Soc. Am. **77**, 420 (1985).

Chen, Z. Y., A. Abacci, S. Tang, and J. V. Sengers, Phys. Rev. A **42**, 4470 (1990).

Chukanov, V. N. and V. P. Skripov, Teplofiz. Vys. Temp. **9**, 739 (1971); High Temp. **9**, 672 (1971).

Colina, C. M. and C. Olivera-Fuentes, Ind. Eng. Chem. Res. **41**, 1064 (2002).

Cooper, J. R., Int. J. Thermophys. **3**, 35 (1982).

Czarnota, I., High Temp.—High Press. **16**, 295 (1984).

Deiters, U. K. and K. M. de Reuck, Pure Appl. Chem. **69**, 1237 (1997).

Del Grosso, V. A. and C. W. Mader, J. Acoust. Soc. Am. **52**, 1442 (1972).

Ernst, G. and R. Philippi, J. Chem. Thermodyn. **22**, 211 (1990).

Erokhin, N. F. and B. I. Kal'yanov, Teplofiz. Vys. Temp. **17**, 290 (1979); High Temp. **17**, 245 (1979).

Erokhin, N. F. and B. I. Kal'yanov, Teploenergetika **27**, 50 (1980); Thermal Eng. **27**, 634 (1980).

Ertle, S., Dissertation, Technische Universität München, Germany, 1979.

Eubank, P. T., L. L. Joffrion, M. R. Patel, and W. Warowny, J. Chem. Thermodyn. **20**, 1009 (1988).

Evstefeev, V. N., V. N. Chukanov, and V. P. Skripov, Teplofiz. Vys. Temp. **15**, 659 (1977); High Temp. **15**, 550 (1977).

Evstefeev, V. N., V. P. Skripov, and V. N. Chukanov, Teplofiz. Vys. Temp. **17**, 299 (1979); High Temp. **17**, 252 (1979).

Ewers, J. and W. Wagner, *Proceedings of the 8th Symposium on Thermophysical Properties* (American Society of Mechanical Engineers, New York, 1982), Vol. 1, p. 78.

Fernández, D. P., A. H. R. Goodwin, E. W. Lemmon, J. M. H. Levelt Sengers, and R. C. Williams, J. Phys. Chem. Ref. Data **26**, 1125 (1997).

Fujii, K. and R. Masui, J. Acoust. Soc. Am. **93**, 276 (1993).

Fujii, K., ''Accurate measurements of the sound velocity in pure water under high pressure,'' 12th Symposium on Thermophysical Properties, Boulder, Colorado, USA, 1994.

Goodwin, A. R. H., ''Experimental Methods in Sound Speed'', in *IUPAC Experimental Thermodynamics, Vol VI: Measurements of the Thermodynamic Properties of Single Phases*, edited by A. R. H. Goodwin, K. N. Marsh, and W. A. Wakeham (Elsevier, Amsterdam, 2002).

Gonfiantini, R., Nature (London) **271**, 534 (1978).

Grindley, T. and J. E. Lind, Jr., J. Chem. Phys. **54**, 3983 (1971).

Guildner, L. A., D. P. Johnson, and E. F. Jones, J. Res. Natl. Bur. Stand. **80A**, 505 (1976).

Gurvich, L. V., I. V. Veyts, and C. B. Alcock, *Thermodynamic Properties of Individual Substances*, 4th ed. (Hemisphere, New York, 1989), Vol. 1, Part 2.

Haar, L., J. S. Gallagher, and G. S. Kell, *Proceedings of the 8th Symposium on Thermophysical Properties*, edited by J. V. Sengers (The American Society of Mechanical Engineers, New York, 1982), Vol. II, p. 298.

Haar, L., J. S. Gallagher, and G. S. Kell, *NBS/NRC Steam Tables* (Hemisphere, Washington, and McGraw-Hill, New York, 1984).

Hanafusa, H., T. Tsuchida, K. Kawai, H. Sato, M. Uematsu, and K. Watanabe, *Proceedings of the 10th International Conference on the Properties of Steam*, Moscow 1984, edited by V. V. Sytchev, and A. A. Aleksandrov (MIR, Moscow, 1984), p. 180.

Hare, D. E. and C. M. Sorensen, J. Chem. Phys. **84**, 5085 (1986).

Hare, D. E. and C. M. Sorensen, J. Chem. Phys. **87**, 4840 (1987).

Harvey, A. H., Minutes of the Meetings of the Executive Committee of IAPWS, London, 1998, p. 41.

Hendl, H., E. Bich, and E. Vogel, J. Chem. Thermodyn. **29**, 765 (1997).

Hilbert, R., K. Tödheide, and E. U. Franck, Ber. Bunsenges. Phys. Chem. **85**, 636 (1981).

Hill, P. G., J. Phys. Chem. Ref. Data **19**, 1233 (1990).

Hill, P. G. and R. D. C. MacMillan, Ind. Eng. Chem. Res. **27**, 874 (1988).

Holton, G., M. P. Hagelberg, S. Kao, and W. H. Johnson, Jr., J. Acoust. Soc. Am. **43**, 102 (1968).

IAPWS (International Association for the Properties of Water and Steam), *Release on the Values of Temperature, Pressure and Density of Ordinary and Heavy Water Substances at their Respective Critical Points* (IAPWS Secretariat, EPRI, Palo Alto, 1992). Also in White *et al.* (1995), p. A101 (All IAPWS releases and guidelines can also be found on the IAPWS website http://www.iapws.org.).

IAPWS (International Association for the Properties of Water and Steam), *Release on the Pressure along the Melting and the Sublimation Curves of Ordinary Water Substance* (IAPWS Secretariat, EPRI, Palo Alto, 1993). Also in Wagner *et al.* (1994), and in White *et al.* (1995), p. A9.

IAPWS (International Association for the Properties of Water and Steam), *Release on the Skeleton Tables 1985 for the Thermodynamic Properties of Ordinary Water Substance* (IAPWS Secretariat, EPRI, Palo Alto, 1994). Also in White *et al.* (1995), p. A13.

IAPWS (International Association for the Properties of Water and Steam), *Release on the IAPWS Formulation 1995 for the Thermodynamic Properties of Ordinary Water Substance for General and Scientific Use* (IAPWS Secretariat, EPRI, Palo Alto, 1996). Also in Tremaine *et al.* (2000), p. A106.

IAPWS (International Association for the Properties of Water and Steam), *Release on the Static Dielectric Constant of Ordinary Water Substance for Temperatures from 238 K to 873 K and Pressures up to 1000 MPa* (IAPWS Secretariat, EPRI, Palo Alto, 1997). Also in Tremaine *et al.* (2000), p. A97.

IAPWS (International Association for the Properties of Water and Steam), *Guideline on the Use of Fundamental Physical Constants and Basic Constants of Water* (IAPWS Secretariat; EPRI; Palo Alto, 2001).

IFC (International Formulation Committee of the Sixth International Conference on the Properties of Steam), *The 1967 Formulation for Industrial Use* (Verein Deutscher Ingenieure, Düsseldorf, 1967).

IFC (International Formulation Committee of the Sixth International Conference on the Properties of Steam), *The 1968 IFC Formulation for Scientific and General Use* (American Society of Mechanical Engineers, New York, 1968).

Keenan, J. H., F. G. Keyes, P. G. Hill, and J. G. Moore, *Steam Tables* (Wiley, New York, 1969).

Kell, G. S., J. Chem. Eng. Data **20**, 97 (1975).

Kell, G. S., J. Phys. Chem. Rev. Data **6**, 1109 (1977).

Kell, G. S. and E. Whalley, J. Chem. Phys. **62**, 3496 (1975).

Kell, G. S., G. E. McLaurin, and E. Whalley, in *Advances in Thermophysical Properties at Extreme Temperatures and Pressures, Proceedings of the Third Symposium on Thermophysical Properties*, edited by S. Gratch (American Society of Mechanical Engineers, New York, 1965), p. 104.

Kell, G. S., G. E. McLaurin, and E. Whalley, J. Chem. Phys. **48**, 3805 (1968).

Kell, G. S., G. E. McLaurin, and E. Whalley, Proc. Roy. Soc. London A **360**, 389 (1978).

Kell, G. S., G. E. McLaurin, and E. Whalley, Philos. Trans. R. Soc. London A **315**, 235 (1985).

Kell, G. S., G. E. McLaurin, and E. Whalley, Proc. R. Soc. London A **425**, 49 (1989).

Kerimov, A. M., Ph. D. thesis, Azneftechim, Azerbajdjan, Baku, 1964.

Kerimov, A. M. and M. K. Alieva, Teploenergetika **22**, 58 (1975); Therm. Eng. **22**, 76 (1976).

Kestin, J. and J. V. Sengers, J. Phys. Chem. Ref. Data **15**, 305 (1986).

Keyes, F. G., L. B. Smith, and H. T. Gerry, Proc. Am. Acad. Arts Sci. **70**, 319 (1936).

Kiselev, S. B. and D. G. Friend, Fluid Phase Equilibria **155**, 33 (1999).

Köster, H. and E. U. Franck, Ber. Bunsenges. Phys. Chem. **73**, 716 (1969).

Kostrowicka Wyczalkowska, A., Kh. S. Abdulkadirova, M. A. Anisimov, and J. V. Sengers, J. Chem. Phys. **113**, 4985 (2000).

Kubota, H., Y. Tanaka, and T. Makita, Int. J. Thermophys. **8**, 47 (1987).

Kurzeja, N. and W. Wagner, Int. J. Thermophys. **22** (to be submitted, 2002).

Kurzeja, N., Th. Tielkes, and W. Wagner, Int. J. Thermophys. **20**, 531 (1999).

Kurzeja, N., Th. Tielkes, and W. Wagner, Int. J. Thermophys. **22** (to be submitted 2002).

Le Fevre, E. J., M. R. Nightingale, and J. W. Rose, J. Mech. Eng. Sci. **17**, 243 (1975).

Levelt Sengers, J. M. H., B. Kamgar-Parsi, F. W. Balfour, and J. V. Sengers, J. Phys. Chem. Ref. Data **12**, 1 (1983).

Levelt Sengers, J. M. H., J. Straub, K. Watanabe, and P. G. Hill, J. Phys. Chem. Ref. Data **14**, 193 (1985).

Luettmer-Strathmann, J., ''A Parametric Model for the Global Thermodynamic Behavior of Fluids in the Critical Region'' (private communication, 1992).

Lyzenga, G. A., T. J. Ahrens, W. J. Nellis, and A. C. Mitchell, J. Chem. Phys. **76**, 6282 (1982).

Magee, J. W., R. J. Deal, and J. C. Blanco, J. Res. Natl. Inst. Stand. Technol. **103**, 63 (1998).

Maier, S. and E. U. Franck, Ber. Bunsenges. Phys. Chem. **70**, 639 (1966).

Masui, R., K. Fujii, and M. Takenaka, in *Physical Chemistry of Aqueous Systems: Meeting the Needs of Industry, Proceedings of the 12th International Conference on the Properties of Water and Steam*, edited by H. J. White, Jr. *et al.* (Begell House, New York, Wallingford, 1995), p. 78.

Masui, R., K. Fujii, and M. Takenaka, Metrologia **32**, 333 (1995/96).

Mamedov, A. M., Inzh. Fiz. Zh. **36**, 156 (1979).

McDade, J. C., D. R. Pardue, A. L. Hedrich, and F. Vrataric, J. Acoust. Soc. Am. **31**, 1380 (1959).

McGlashan, M. L. and C. J. Wormald, J. Chem. Thermodyn. **32**, 1489 (2000).

Menaché, M. and G. Girard, Metrologia **9**, 62 (1973).

Mitchell, A. C. and W. J. Nellis, J. Chem. Phys. **76**, 6273 (1982).

Mohr, P. J. and B. N. Taylor, J. Phys. Chem. Ref. Data **28**, 1713 (1999).

Morita, T., H. Sato, M. Uematsu, and K. Watanabe, Physica A **156**, 436 (1989).

Novikov, I. I. and V. I. Avdonin, ''Velocity of Sound in Saturated and Superheated Steam,'' Report at the 7th International Conference of the Properties of Steam, Tokyo, 1968.

Osborne, N. S., H. F. Stimson, E. F. Fiock, and D. C. Ginnings, J. Res. Natl. Bur. Stand. **10**, 155 (1933).

Osborne, N. S., H. F. Stimson, and D. C. Ginnings, J. Res. Natl. Bur. Stand. **18**, 389 (1937).

Osborne, N. S., H. F. Stimson, and D. C. Ginnings, J. Res. Natl. Bur. Stand. **23**, 197 (1939).

Patterson, J. B. and E. C. Morris, Metrologia **31**, 277 (1994).

Petitet, J. P., R. Tufeu, and B. Le Neindre, Int. J. Thermophys. **4**, 35 (1983).

Petitet, J. P., L. Denielou, R. Tufeu, and B. Le Neindre, Int. J. Thermophys. **7**, 1065 (1986).

Philippi, R., *Fortschritt-Berichte VDI*, Reihe 19, Nr. 13 (VDI, Düsseldorf, 1987).

Polikhronidi, N. G., I. M. Abdulagatov, J. W. Magee, and G. V. Stepanov, Int. J. Thermophys. **22**, 189 (2001).

Pollak, R., Dissertation, Ruhr-Universität Bochum, Germany, 1974; English Translation, Report PC/T (CEGB) 14 IUPAC Thermodynamic Tables Project Center, London (1976).

Pollak, R., Brennstoff-Wärme-Kraft **27**, 210 (1975).

Preston-Thomas, H., Metrologia **27**, 1 (1990).

Pruß, A. and W. Wagner, in *Physical Chemistry of Aqueous Systems: Meeting the Needs of Industry, Proceedings of the 12th International Conference on the Properties of Water and Steam*, edited by H. J. White, Jr. *et al.* (Begell House, New York, 1995a), p. 66.

Pruß, A. and W. Wagner, *Fortschritt-Berichte VDI*, Reihe 6, Nr. 320 (VDI, Düsseldorf, 1995b).

Rice, M. H. and J. M. Walsh, J. Chem. Phys. **26**, 824 (1957).

Rivkin, S. L. and T. S. Akhundov, Teploenergetika **9**, 57 (1962).

Rivkin, S. L. and T. S. Akhundov, Teploenergetika **10**, 66 (1963).

Rivkin, S. L. and G. V. Troyanovskaya, Teploenergetika **11**, 72 (1964); Thermal Eng. **11**, 91 (1964).

Rivkin, S. L., G. V. Troyanovskaya, and T. S. Akhundov, Teplofiz. Vys. Temp. **2**, 219 (1964); High Temp. **2**, 194 (1964).

Rivkin, S. L., T. S. Akhundov, E. A. Kremenevskaya, and N. N. Assadullaeva, Teploenergetika **13**, 59 (1966); Thermal Eng. **13**, 77 (1966).

Rögener, H. and P. Soll, Brennst.-Wärme-Kraft **32**, 472 (1980).

Rouch, J., C. Lai, and S.-H. Chen, J. Chem. Phys. **66**, 5031 (1977).

Rusby, R. L., J. Chem. Thermodyn. **23**, 1153 (1991).

Rusby, R. L., R. P., Hudson, and M. Durieux, Metrologia **31**, 149 (1994).

Sato, H., M. Uematsu, K. Watanabe, A. Saul, and W. Wagner, J. Phys. Chem. Ref. Data **17**, 1439 (1988).

Sato, H., K. Watanabe, J. M. H. Levelt Sengers, J. S. Gallagher, P. G. Hill, J. Straub, and W. Wagner, J. Phys. Chem. Ref. Data **20**, 1023 (1991).

Saul, A. and W. Wagner, J. Phys. Chem. Ref. Data **16**, 893 (1987).

Saul, A. and W. Wagner, J. Phys. Chem. Ref. Data **18**, 1537 (1989).

Schmidt, R. and W. Wagner, Fluid Phase Equilibria **19**, 175 (1985).

Schufle, J. A., Chem. Ind. (London), 690 (1965).

Setzmann, U. and W. Wagner, Int. J. Thermophys. **10**, 1103 (1989).

Setzmann, U. and W. Wagner, J. Phys. Chem. Ref. Data **20**, 1061 (1991).

Sirota, A. M., Teploenergetika **5**, 10 (1958).

Sirota, A. M., Inzh. Fiz. Zh. **6**, 52 (1963).

Sirota, A. M. and D. L. Timrot, Teploenergetika **3**, 16 (1956).

Sirota, A. M. and B. K. Mal'tsev, Teploenergetika **6**, 7 (1959).

Sirota, A. M. and B. K. Mal'tsev, Teploenergetika **7**, 67 (1960).

Sirota, A. M. and B. K. Mal'tsev, Teploenergetika **9**, 52 (1962a).

Sirota, A. M. and B. K. Mal'tsev, Teploenergetika **9**, 70 (1962b).

Sirota, A. M. and A. J. Grishkov, Teploenergetika **13**, 61 (1966).

Sirota, A. M. and A. J. Grishkov, ''Experimental Investigation Isobaric Heat Capacity of Water near the Solidification Curve,'' Preliminary report given at the 7th International Conference on the Properties of Steam, Tokyo (1968).

Sirota, A. M., B. K. Mal'tsev, and A. S. Grishkov, Teploenergetika **10**, 57 (1963).

Sirota, A. M., P. E. Belyakova, and Z. Kh. Shrago, Teploenergetika **13**, 84 (1966); Thermal Eng. **13**, 112 (1966).

Sirota, A. M., A. J. Grishkov, and A. G. Tomishko, Teploenergetika **17**, 60 (1970); Thermal Eng. **17**, 90 (1970).

Smith, L. B. and F. G. Keyes, Proc. Am. Acad. Arts Sci. **69**, 285 (1934).

Span, R., *Multiparameter Equations of State—An Accurate Source of Thermodynamic Property Data* (Springer, Berlin, 2000).

Span, R. and W. Wagner, J. Phys. Chem. Ref. Data **25**, 1509 (1996).

Span, R. and W. Wagner, Int. J. Thermophys. **18**, 1415 (1997).

Span, R., E. W. Lemmon, R. T Jacobsen, W. Wagner, and A. Yokozeki, J. Phys. Chem. Ref. Data **29**, 1361 (2000).

Stimson, H. F., J. Res. Natl. Bur. Stand. **73A**, 483 (1969).

Takenaka, M. and R. Masui, Metrologia **27**, 165 (1990).

Tammann, G. and W. Jellinghaus, Z. Anorg. Allgem. Chem. **174**, 225 (1928).

Tanaka, M., G. Girard, R. Davis, A. Peuto, and N. Bignell, Metrologia **38**, 301 (2001).

Taylor, B. N., W. H. Parker, and D. N. Langenberg, Rev. Mod. Phys. **41**, 375 (1969).

Tegeler, Ch., R. Span, and W. Wagner, *Fortschritt-Berichte VDI*, Reihe 3, Nr. 480 (VDI, Düsseldorf, 1997).

Tegeler, Ch., R. Span, and W. Wagner, J. Phys. Chem. Ref. Data **28**, 779 (1999).

Ter Minissian, L. and P. Pruzan, J. Chem. Phys. **75**, 3064 (1981).

TRC *Thermodynamic Tables*, Table tuv-25 (Thermodynamics Research Center, Texas A&M University, College Station, TX, 1988).

Tremaine, P., P. G. Hill, D. Irish, and P. V. Balakrishnan (eds.), *Steam, Water and Hydrothermal Systems: Physics and Chemistry Meeting the Needs of Industry*, Proceedings of the 13th International Conference on the Properties of Water and Steam (NRC, Ottawa, 2000).

Trinh, E. and R. E. Apfel, J. Chem. Phys. **69**, 4275 (1978).

Vidler, M. and J. Tennyson, J. Chem. Phys. **113**, 9766 (2000).

Vukalovich, M. P., W. N. Zubarev, and A. A. Alexandrov, Teploenergetika **8**, 79 (1961).

Vukalovich, M. P., W. N. Zubarev, and A. A. Alexandrov, Teploenergetika **9**, 49 (1962).

Vukalovich, M. P., M. S. Trakhtengerts, and G. A. Spiridonov, Teploenergetika **14**, 65 (1967); Thermal Eng. **14**, 86 (1967).

Wagner, W., *Fortschritt-Berichte VDI*, Reihe 3, Nr. 39 (VDI, Düsseldorf, 1974). Shortened English translation: Report PC/T15, IUPAC Thermodynamic Tables Project Center, London (1977).

Wagner, W. and K. M. de Reuck, *International Thermodynamic Tables of the Fluid State—13, Methane* (Blackwell Science, Oxford, 1996).

Wagner, W., N. Kurzeja, and B. Pieperbeck, Fluid Phase Equilibria **79**, 151 (1992).

Wagner, W. and A. Pruss, J. Phys. Chem. Ref. Data **22**, 783 (1993).

Wagner, W. and A. Saul, ''Correlation Equations for the Vapor Pressure and for the Orthobaric Densities of Water Substance,'' *Proceedings of the 10th International Conference on the Properties of Steam*, edited by V. V. Sytchev, and A. A. Aleksandrov (MIR, Moscow, 1986), Vol. 1, p. 199.

Wagner, W., A. Saul, and A. Pruß, J. Phys. Chem. Ref. Data **23**, 515 (1994).

Wagner, W., R. Kleinrahm, H. W. Lösch, and J. T. R. Watson, ''Hydrostatic Balance Densimeters with Magnetic Suspension Couplings'' in *IUPAC Experimental Thermodynamics, Vol VI: Measurements of the Thermodynamic Properties of Single Phases*, edited by A. R. H. Goodwin, K. N. Marsh, and W. A. Wakeham (Elsevier, Amsterdam, 2002).

Wagner, W., J. R. Cooper, A. Dittmann, J. Kijima, H.-J. Kretzschmar, A. Kruse, R. Mareš, K. Oguchi, H. Sato, I. Stöcker, O. Šifner, Y. Takaishi, I. Tanishita, J. Trübenbach, and Th. Willkommen, J. Eng. Gas Turbines Power **122**, 150 (2000).

Walsh, J. M. and M. H. Rice, J. Chem. Phys. **26**, 815 (1957).

Watanabe, H., Metrologia **28**, 33 (1991).

White, Jr., H. J., J. V. Sengers, D. B. Neumann, and J. C. Bellows, eds., *Physical Chemistry of Aqueous Systems: Meeting the Needs of Industry*, Proceedings of the 12th International Conference on the Properties of Water and Steam (Begell House, New York, 1995).

Wilson, W. D., J. Acoust. Soc. Am. **31**, 1067 (1959).

Wiryana, S., L. J. Slutsky, and J. M. Brown, Earth Planetary Sci. Lett. **163**, 123 (1998).

Woodburn, J., Trans. ASME **71**, 65 (1949).

Woolley, H. W., ''Thermodynamic Properties for H_2O in the Ideal Gas State,'' in *Water and Steam—Their Properties and Current Industrial Applications, Proceedings of the 9th International Conference on the Properties of Steam*, edited by J. Straub and K. Scheffler (Pergamon, Oxford, New York, 1980), p. 166.

Woolley, H. W., J. Res. Natl. Bur. Stand. **92**, 35 (1987).

Wormald, C. J., Ph. D. thesis, University of Reading, 1964.

Yokoyama, C. and S. Takahashi, Int. J. Thermophys. **10**, 35 (1989).

Zheleznyi, B. V., Russ. J. Phys. Chem. **43**, 1311 (1969).

Zubarev, V. N., P. G. Prusakov, and V. V. Barkovskii, Teploenergetika **24**, 77 (1977a); Thermal Eng. **24**, 62 (1977a).

Zubarev, V. N., P. G. Prusakov, and V. V. Barkovskii, Teploenergetika **24**, 80 (1977b); Thermal Eng. **24**, 68 (1977b).

13. Appendix: Tables of Thermodynamic Properties of Water

Tables are given here for the thermodynamic properties of ordinary water substance (H_2O) that cover the range of validity of the IAPWS-95 formulation. Table 13.1 lists the values along the vapor–liquid phase boundary. In order to preserve thermodynamic consistency with the values in the single-phase region, all values along the phase boundary were calculated from IAPWS-95 by applying the phase equilibrium condition, Eqs. (6.9a)–(6.9c), which means without using any auxiliary equations. Table 13.2 contains the corresponding values in the single-phase region and covers the entire range of validity of IAPWS-95, namely temperatures from the melting line to 1273 K and pressures up to 1000 MPa. For pressures below the critical pressure ($p_c = 22.064\,\mathrm{MPa}$), the isobaric values of the single-phase table also contain the values for the saturated liquid and saturated vapor at the phase boundary. The values of all properties, density, and derived properties, were calculated from the IAPWS-95 formulation, i.e., from Eq. (6.4) in combination with Eqs. (6.5) and (6.6). Tables 13.1 and 13.2 are given with five significant figures (six significant figures for the density up to $p = 100\,\mathrm{MPa}$), which is appropriate with respect to the uncertainties discussed in Secs. 6.3.2 and 8. However, interpolation between entries in the tables may result in uncertainties that are significantly larger than the uncertainties of Eq. (6.4). This must be particularly considered in the critical and extended critical region. For sophisticated applications, properties should be calculated directly from IAPWS-95, Eq. (6.4). For suitable software, see the IAPWS website http://www.iapws.org/newform.htm.

TABLE 13.1. Thermodynamic properties of water on the vapor–liquid phase boundary as a function on temperature[a]

T K	p MPa	ρ kg m^{-3}	h kJ kg^{-1}	s kJ kg^{-1} K^{-1}	c_v kJ kg^{-1} K^{-1}	c_p kJ kg^{-1} K^{-1}	w m s^{-1}
273.160[b]	0.000 612	999.793	0.001	0.0000	4.2174	4.2199	1402.3
		0.00485	2500.92	9.1555	1.4184	1.8844	409.00
274	0.000 650	999.843	3.544	0.0130	4.2156	4.2171	1406.5
		0.00514	2502.46	9.1331	1.4191	1.8852	409.61
276	0.000 750	999.914	11.972	0.0436	4.2108	4.2110	1416.1
		0.00589	2506.12	9.0804	1.4208	1.8872	411.05
278	0.000 863	999.919	20.389	0.0740	4.2057	4.2058	1425.3
		0.00673	2509.79	9.0287	1.4224	1.8893	412.49
280	0.000 992	999.862	28.796	0.1041	4.2003	4.2014	1434.1
		0.00768	2513.45	8.9779	1.4242	1.8913	413.92
282	0.001 137	999.746	37.195	0.1340	4.1945	4.1975	1442.5
		0.00874	2517.11	8.9280	1.4259	1.8935	415.35
284	0.001 300	999.575	45.587	0.1637	4.1884	4.1942	1450.4
		0.00993	2520.76	8.8791	1.4277	1.8956	416.77
286	0.001 483	999.352	53.973	0.1931	4.1820	4.1914	1458.0
		0.01125	2524.41	8.8310	1.4294	1.8978	418.18
288	0.001 689	999.079	62.353	0.2223	4.1753	4.1890	1465.2
		0.01272	2528.06	8.7838	1.4312	1.9000	419.59
290	0.001 920	998.758	70.729	0.2513	4.1684	4.1869	1472.1
		0.01436	2531.70	8.7374	1.4330	1.9023	420.99
292	0.002 178	998.392	79.101	0.2800	4.1612	4.1852	1478.6
		0.01618	2535.34	8.6918	1.4348	1.9046	422.38
294	0.002 465	997.983	87.471	0.3086	4.1539	4.1838	1484.8
		0.01820	2538.98	8.6471	1.4367	1.9069	423.77
296	0.002 786	997.532	95.837	0.3370	4.1463	4.1826	1490.6
		0.02042	2542.61	8.6031	1.4385	1.9092	425.15
298	0.003 142	997.042	104.202	0.3651	4.1385	4.1817	1496.1
		0.02288	2546.23	8.5599	1.4404	1.9116	426.52
300	0.003 537	996.513	112.565	0.3931	4.1305	4.1809	1501.4
		0.02559	2549.85	8.5174	1.4422	1.9141	427.89
302	0.003 975	995.948	120.926	0.4209	4.1223	4.1803	1506.3
		0.02857	2553.47	8.4756	1.4441	1.9166	429.25
304	0.004 459	995.346	129.287	0.4485	4.1140	4.1799	1510.9
		0.03184	2557.08	8.4346	1.4461	1.9191	430.61
306	0.004 993	994.711	137.647	0.4759	4.1054	4.1797	1515.3
		0.03543	2560.68	8.3943	1.4480	1.9217	431.95
308	0.005 582	994.042	146.007	0.5031	4.0967	4.1795	1519.4
		0.03936	2564.28	8.3546	1.4500	1.9243	433.29
310	0.006 231	993.342	154.366	0.5301	4.0879	4.1795	1523.2
		0.04366	2567.87	8.3156	1.4520	1.9270	434.63
312	0.006 944	992.610	162.726	0.5570	4.0789	4.1796	1526.8
		0.04835	2571.45	8.2773	1.4540	1.9298	435.95
314	0.007 726	991.848	171.086	0.5837	4.0698	4.1797	1530.1
		0.05347	2575.03	8.2396	1.4561	1.9326	437.27
316	0.008 583	991.056	179.447	0.6103	4.0605	4.1800	1533.2
		0.05904	2578.60	8.2025	1.4583	1.9356	438.58
318	0.009 521	990.235	187.808	0.6366	4.0511	4.1803	1536.1
		0.06509	2582.16	8.1660	1.4604	1.9386	439.89

TABLE 13.1. Thermodynamic properties of water on the vapor–liquid phase boundary as a function on temperature[a]—Continued

T K	p MPa	ρ kg m^{-3}	h kJ kg^{-1}	s kJ kg^{-1} K^{-1}	c_v kJ kg^{-1} K^{-1}	c_p kJ kg^{-1} K^{-1}	w m s^{-1}
320	0.010 546	989.387	196.170	0.6629	4.0416	4.1807	1538.7
		0.07166	2585.71	8.1302	1.4627	1.9417	441.18
322	0.011 664	988.512	204.533	0.6889	4.0320	4.1812	1541.1
		0.07879	2589.26	8.0949	1.4650	1.9449	442.47
324	0.012 882	987.610	212.897	0.7148	4.0223	4.1818	1543.3
		0.08650	2592.79	8.0601	1.4673	1.9482	443.75
326	0.014 208	986.682	221.262	0.7405	4.0124	4.1824	1545.3
		0.09484	2596.32	8.0260	1.4697	1.9516	445.02
328	0.015 649	985.728	229.629	0.7661	4.0025	4.1831	1547.1
		0.10385	2599.83	7.9923	1.4722	1.9551	446.29
330	0.017 213	984.750	237.997	0.7915	3.9925	4.1838	1548.7
		0.11357	2603.34	7.9592	1.4748	1.9587	447.54
332	0.018 909	983.747	246.367	0.8168	3.9825	4.1846	1550.1
		0.12404	2606.83	7.9267	1.4774	1.9625	448.79
334	0.020 744	982.721	254.739	0.8420	3.9723	4.1855	1551.3
		0.13532	2610.31	7.8946	1.4801	1.9664	450.03
336	0.022 730	981.671	263.112	0.8669	3.9621	4.1864	1552.3
		0.14743	2613.79	7.8630	1.4829	1.9705	451.26
338	0.024 874	980.599	271.488	0.8918	3.9519	4.1874	1553.2
		0.16045	2617.25	7.8319	1.4858	1.9747	452.47
340	0.027 188	979.503	279.866	0.9165	3.9416	4.1885	1553.9
		0.17440	2620.69	7.8013	1.4888	1.9790	453.68
342	0.029 681	978.386	288.246	0.9411	3.9312	4.1896	1554.4
		0.18936	2624.13	7.7711	1.4919	1.9835	454.88
344	0.032 366	977.247	296.628	0.9655	3.9208	4.1907	1554.7
		0.20537	2627.55	7.7414	1.4951	1.9882	456.07
346	0.035 253	976.086	305.013	0.9898	3.9104	4.1919	1554.9
		0.22249	2630.96	7.7122	1.4983	1.9931	457.25
348	0.038 354	974.904	313.401	1.0140	3.8999	4.1932	1555.0
		0.24077	2634.35	7.6833	1.5018	1.9981	458.42
350	0.041 682	973.702	321.791	1.0380	3.8895	4.1946	1554.8
		0.26029	2637.73	7.6549	1.5053	2.0033	459.58
352	0.045 249	972.479	330.185	1.0619	3.8790	4.1960	1554.5
		0.28110	2641.09	7.6270	1.5089	2.0088	460.73
354	0.049 070	971.235	338.581	1.0857	3.8685	4.1975	1554.1
		0.30326	2644.44	7.5994	1.5127	2.0144	461.87
356	0.053 158	969.972	346.981	1.1093	3.8580	4.1991	1553.6
		0.32685	2647.77	7.5722	1.5166	2.0202	463.00
358	0.057 527	968.689	355.384	1.1328	3.8475	4.2007	1552.8
		0.35193	2651.08	7.5454	1.5206	2.0263	464.12
360	0.062 194	967.386	363.791	1.1562	3.8369	4.2024	1552.0
		0.37858	2654.38	7.5190	1.5247	2.0326	465.22
362	0.067 172	966.064	372.202	1.1795	3.8264	4.2042	1551.0
		0.40686	2657.65	7.4929	1.5290	2.0391	466.32
364	0.072 478	964.723	380.616	1.2027	3.8159	4.2061	1549.9
		0.43686	2660.91	7.4672	1.5335	2.0458	467.40
366	0.078 129	963.363	389.034	1.2257	3.8055	4.2080	1548.6
		0.46865	2664.15	7.4419	1.5381	2.0528	468.47

TABLE 13.1. Thermodynamic properties of water on the vapor–liquid phase boundary as a function on temperature[a]—Continued

T K	p MPa	ρ kg m^{-3}	h kJ kg^{-1}	s kJ kg^{-1} K^{-1}	c_v kJ kg^{-1} K^{-1}	c_p kJ kg^{-1} K^{-1}	w m s^{-1}
368	0.084 142	961.984	397.457	1.2487	3.7950	4.2101	1547.3
		0.50231	2667.37	7.4169	1.5428	2.0601	469.53
370	0.090 535	960.587	405.884	1.2715	3.7846	4.2122	1545.8
		0.53792	2670.57	7.3923	1.5478	2.0676	470.57
372	0.097 326	959.171	414.316	1.2942	3.7741	4.2144	1544.1
		0.57557	2673.75	7.3680	1.5528	2.0754	471.61
374	0.104 53	957.737	422.752	1.3168	3.7637	4.2167	1542.4
		0.61534	2676.91	7.3440	1.5581	2.0835	472.63
376	0.112 18	956.285	431.194	1.3393	3.7534	4.2190	1540.5
		0.65732	2680.04	7.3203	1.5635	2.0919	473.64
378	0.120 28	954.815	439.640	1.3617	3.7431	4.2215	1538.6
		0.70161	2683.16	7.2969	1.5691	2.1006	474.63
380	0.128 85	953.327	448.092	1.3839	3.7328	4.2241	1536.5
		0.74830	2686.25	7.2738	1.5749	2.1096	475.61
382	0.137 93	951.822	456.550	1.4061	3.7225	4.2268	1534.2
		0.79748	2689.31	7.2510	1.5808	2.1189	476.58
384	0.147 52	950.298	465.013	1.4282	3.7123	4.2295	1531.9
		0.84926	2692.35	7.2286	1.5870	2.1285	477.54
386	0.157 66	948.758	473.482	1.4502	3.7022	4.2324	1529.5
		0.90372	2695.37	7.2063	1.5933	2.1385	478.48
388	0.168 36	947.199	481.957	1.4720	3.6920	4.2354	1526.9
		0.96099	2698.35	7.1844	1.5999	2.1488	479.41
390	0.179 64	945.624	490.439	1.4938	3.6820	4.2384	1524.3
		1.0212	2701.32	7.1627	1.6066	2.1594	480.32
392	0.191 54	944.030	498.928	1.5155	3.6719	4.2416	1521.5
		1.0843	2704.25	7.1413	1.6136	2.1705	481.22
394	0.204 08	942.420	507.423	1.5371	3.6620	4.2449	1518.7
		1.1506	2707.16	7.1202	1.6207	2.1818	482.11
396	0.217 28	940.793	515.926	1.5586	3.6520	4.2483	1515.7
		1.2202	2710.04	7.0992	1.6281	2.1936	482.98
398	0.231 17	939.148	524.435	1.5800	3.6422	4.2519	1512.6
		1.2931	2712.88	7.0786	1.6357	2.2058	483.83
400	0.245 77	937.486	532.953	1.6013	3.6324	4.2555	1509.5
		1.3694	2715.70	7.0581	1.6435	2.2183	484.67
402	0.261 11	935.807	541.478	1.6225	3.6226	4.2593	1506.2
		1.4494	2718.49	7.0379	1.6515	2.2312	485.50
404	0.277 22	934.111	550.011	1.6436	3.6129	4.2632	1502.8
		1.5330	2721.25	7.0180	1.6597	2.2446	486.31
406	0.294 13	932.398	558.553	1.6647	3.6033	4.2672	1499.4
		1.6205	2723.97	6.9982	1.6682	2.2583	487.10
408	0.311 87	930.668	567.103	1.6856	3.5937	4.2713	1495.8
		1.7120	2726.67	6.9787	1.6769	2.2725	487.88
410	0.330 45	928.921	575.662	1.7065	3.5842	4.2756	1492.2
		1.8076	2729.32	6.9593	1.6858	2.2871	488.65
412	0.349 93	927.157	584.231	1.7273	3.5748	4.2800	1488.4
		1.9074	2731.95	6.9402	1.6949	2.3021	489.39
414	0.370 32	925.375	592.808	1.7480	3.5654	4.2845	1484.6
		2.0116	2734.54	6.9213	1.7042	2.3176	490.13

TABLE 13.1. Thermodynamic properties of water on the vapor–liquid phase boundary as a function on temperature[a]—Continued

T K	p MPa	ρ kg m^{-3}	h kJ kg^{-1}	s kJ kg^{-1} K^{-1}	c_v kJ kg^{-1} K^{-1}	c_p kJ kg^{-1} K^{-1}	w m s^{-1}
416	0.391 66	923.577	601.396	1.7687	3.5560	4.2892	1480.6
		2.1203	2737.09	6.9025	1.7138	2.3334	490.84
418	0.413 97	921.761	609.993	1.7892	3.5468	4.2940	1476.6
		2.2336	2739.61	6.8840	1.7235	2.3498	491.54
420	0.437 30	919.929	618.601	1.8097	3.5376	4.2990	1472.5
		2.3518	2742.09	6.8656	1.7335	2.3666	492.22
422	0.461 67	918.079	627.219	1.8301	3.5285	4.3041	1468.3
		2.4750	2744.54	6.8474	1.7437	2.3838	492.89
424	0.487 11	916.212	635.848	1.8504	3.5194	4.3093	1464.0
		2.6032	2746.94	6.8294	1.7542	2.4015	493.54
426	0.513 67	914.328	644.488	1.8707	3.5104	4.3147	1459.6
		2.7367	2749.31	6.8116	1.7648	2.4196	494.17
428	0.541 38	912.426	653.140	1.8909	3.5015	4.3203	1455.2
		2.8757	2751.64	6.7939	1.7756	2.4382	494.79
430	0.570 26	910.507	661.804	1.9110	3.4926	4.3260	1450.6
		3.0202	2753.92	6.7764	1.7867	2.4573	495.39
432	0.600 36	908.571	670.479	1.9311	3.4838	4.3319	1446.0
		3.1705	2756.17	6.7590	1.7979	2.4768	495.97
434	0.631 72	906.617	679.167	1.9510	3.4751	4.3379	1441.2
		3.3268	2758.37	6.7418	1.8093	2.4968	496.53
436	0.664 36	904.645	687.868	1.9710	3.4664	4.3442	1436.4
		3.4891	2760.53	6.7248	1.8210	2.5173	497.08
438	0.698 33	902.656	696.582	1.9908	3.4578	4.3505	1431.5
		3.6578	2762.65	6.7079	1.8328	2.5383	497.61
440	0.733 67	900.649	705.310	2.0106	3.4493	4.3571	1426.5
		3.8329	2764.73	6.6911	1.8448	2.5597	498.12
442	0.770 41	898.624	714.051	2.0303	3.4408	4.3639	1421.5
		4.0146	2766.76	6.6745	1.8570	2.5816	498.61
444	0.808 59	896.580	722.807	2.0500	3.4324	4.3708	1416.3
		4.2032	2768.74	6.6580	1.8693	2.6040	499.09
446	0.848 26	894.519	731.576	2.0696	3.4241	4.3779	1411.1
		4.3988	2770.68	6.6416	1.8818	2.6269	499.55
448	0.889 45	892.439	740.361	2.0892	3.4159	4.3852	1405.8
		4.6017	2772.57	6.6253	1.8945	2.6503	499.99
450	0.932 20	890.341	749.162	2.1087	3.4077	4.3927	1400.4
		4.8120	2774.41	6.6092	1.9074	2.6742	500.41
452	0.976 56	888.225	757.977	2.1281	3.3996	4.4004	1394.9
		5.0300	2776.21	6.5932	1.9204	2.6986	500.82
454	1.0226	886.089	766.809	2.1475	3.3915	4.4084	1389.3
		5.2558	2777.95	6.5773	1.9335	2.7235	501.20
456	1.0703	883.935	775.658	2.1668	3.3835	4.4165	1383.7
		5.4897	2779.65	6.5615	1.9469	2.7490	501.57
458	1.1197	881.761	784.523	2.1861	3.3756	4.4248	1378.0
		5.7319	2781.29	6.5458	1.9603	2.7749	501.92
460	1.1709	879.569	793.406	2.2053	3.3678	4.4334	1372.2
		5.9826	2782.88	6.5303	1.9739	2.8014	502.24
462	1.2239	877.357	802.306	2.2245	3.3600	4.4422	1366.3
		6.2421	2784.42	6.5148	1.9876	2.8285	502.55

TABLE 13.1. Thermodynamic properties of water on the vapor–liquid phase boundary as a function on temperature[a]—Continued

T K	p MPa	ρ kg m^{-3}	h kJ kg^{-1}	s kJ kg^{-1} K^{-1}	c_v kJ kg^{-1} K^{-1}	c_p kJ kg^{-1} K^{-1}	w m s^{-1}
464	1.2788	875.125	811.225	2.2436	3.3523	4.4513	1360.3
		6.5107	2785.91	6.4994	2.0015	2.8561	502.85
466	1.3356	872.873	820.162	2.2627	3.3447	4.4606	1354.3
		6.7884	2787.34	6.4841	2.0155	2.8842	503.12
468	1.3943	870.601	829.118	2.2817	3.3371	4.4701	1348.2
		7.0757	2788.72	6.4689	2.0296	2.9129	503.37
470	1.4551	868.310	838.094	2.3007	3.3296	4.4799	1342.0
		7.3727	2790.04	6.4538	2.0439	2.9422	503.60
472	1.5179	865.997	847.089	2.3197	3.3222	4.4899	1335.7
		7.6798	2791.31	6.4388	2.0583	2.9721	503.81
474	1.5828	863.664	856.106	2.3386	3.3148	4.5003	1329.3
		7.9972	2792.51	6.4238	2.0727	3.0026	504.00
476	1.6498	861.310	865.143	2.3574	3.3075	4.5109	1322.9
		8.3251	2793.66	6.4089	2.0874	3.0337	504.17
478	1.7190	858.934	874.202	2.3762	3.3003	4.5218	1316.4
		8.6639	2794.75	6.3941	2.1021	3.0655	504.32
480	1.7905	856.537	883.283	2.3950	3.2932	4.5330	1309.8
		9.0139	2795.78	6.3794	2.1169	3.0979	504.45
482	1.8642	854.118	892.386	2.4138	3.2861	4.5445	1303.1
		9.3753	2796.74	6.3647	2.1319	3.1310	504.56
484	1.9403	851.678	901.513	2.4325	3.2791	4.5563	1296.4
		9.7485	2797.65	6.3501	2.1469	3.1648	504.65
486	2.0188	849.214	910.663	2.4512	3.2721	4.5684	1289.6
		10.134	2798.49	6.3356	2.1621	3.1993	504.71
488	2.0997	846.728	919.838	2.4698	3.2652	4.5809	1282.6
		10.532	2799.26	6.3211	2.1774	3.2345	504.76
490	2.1831	844.219	929.037	2.4884	3.2584	4.5937	1275.7
		10.942	2799.97	6.3066	2.1928	3.2705	504.78
492	2.2690	841.686	938.262	2.5070	3.2517	4.6069	1268.6
		11.366	2800.61	6.2923	2.2083	3.3073	504.78
494	2.3575	839.130	947.514	2.5256	3.2451	4.6204	1261.5
		11.803	2801.18	6.2779	2.2239	3.3450	504.76
496	2.4487	836.549	956.792	2.5441	3.2385	4.6344	1254.2
		12.254	2801.69	6.2636	2.2396	3.3834	504.71
498	2.5426	833.944	966.097	2.5626	3.2320	4.6487	1246.9
		12.719	2802.12	6.2494	2.2555	3.4228	504.64
500	2.6392	831.313	975.431	2.5810	3.2255	4.6635	1239.6
		13.199	2802.48	6.2351	2.2714	3.4631	504.55
502	2.7386	828.658	984.793	2.5995	3.2191	4.6786	1232.1
		13.694	2802.77	6.2210	2.2875	3.5043	504.43
504	2.8409	825.976	994.185	2.6179	3.2129	4.6943	1224.6
		14.204	2802.98	6.2068	2.3037	3.5465	504.29
506	2.9461	823.269	1003.61	2.6363	3.2066	4.7103	1216.9
		14.730	2803.11	6.1927	2.3200	3.5898	504.12
508	3.0543	820.534	1013.06	2.6547	3.2005	4.7269	1209.2
		15.273	2803.17	6.1786	2.3365	3.6342	503.93
510	3.1655	817.772	1022.55	2.6731	3.1944	4.7440	1201.5
		15.833	2803.15	6.1645	2.3530	3.6796	503.71

TABLE 13.1. Thermodynamic properties of water on the vapor–liquid phase boundary as a function on temperature[a]—Continued

T K	p MPa	ρ kg m^{-3}	h kJ kg^{-1}	s kJ kg^{-1} K^{-1}	c_v kJ kg^{-1} K^{-1}	c_p kJ kg^{-1} K^{-1}	w m s^{-1}
512	3.2798	814.982	1032.06	2.6914	3.1884	4.7616	1193.6
		16.409	2803.05	6.1504	2.3697	3.7263	503.47
514	3.3972	812.164	1041.62	2.7098	3.1825	4.7797	1185.6
		17.004	2802.87	6.1363	2.3866	3.7742	503.20
516	3.5179	809.318	1051.20	2.7281	3.1767	4.7984	1177.6
		17.617	2802.60	6.1223	2.4036	3.8233	502.90
518	3.6417	806.441	1060.82	2.7464	3.1709	4.8176	1169.5
		18.249	2802.25	6.1082	2.4207	3.8738	502.58
520	3.7690	803.535	1070.48	2.7647	3.1653	4.8375	1161.3
		18.900	2801.81	6.0942	2.4380	3.9257	502.23
522	3.8995	800.597	1080.18	2.7830	3.1597	4.8580	1153.0
		19.571	2801.28	6.0801	2.4554	3.9791	501.85
524	4.0336	797.629	1089.91	2.8013	3.1542	4.8792	1144.7
		20.264	2800.66	6.0661	2.4730	4.0341	501.45
526	4.1711	794.628	1099.68	2.8196	3.1488	4.9011	1136.2
		20.977	2799.95	6.0520	2.4907	4.0907	501.01
528	4.3122	791.594	1109.49	2.8379	3.1434	4.9237	1127.7
		21.712	2799.14	6.0379	2.5086	4.1490	500.54
530	4.4569	788.527	1119.35	2.8561	3.1382	4.9471	1119.1
		22.470	2798.23	6.0239	2.5267	4.2090	500.05
532	4.6052	785.425	1129.25	2.8744	3.1331	4.9713	1110.4
		23.252	2797.23	6.0097	2.5449	4.2710	499.52
534	4.7574	782.288	1139.19	2.8927	3.1280	4.9964	1101.6
		24.057	2796.12	5.9956	2.5634	4.3350	498.97
536	4.9133	779.115	1149.18	2.9110	3.1231	5.0223	1092.7
		24.887	2794.91	5.9814	2.5820	4.4011	498.38
538	5.0731	775.905	1159.21	2.9293	3.1182	5.0492	1083.7
		25.744	2793.59	5.9672	2.6008	4.4693	497.76
540	5.2369	772.657	1169.29	2.9476	3.1134	5.0770	1074.6
		26.627	2792.17	5.9530	2.6198	4.5400	497.10
542	5.4047	769.369	1179.42	2.9660	3.1088	5.1059	1065.5
		27.537	2790.63	5.9387	2.6390	4.6131	496.41
544	5.5765	766.042	1189.60	2.9843	3.1042	5.1359	1056.2
		28.476	2788.98	5.9243	2.6585	4.6888	495.69
546	5.7525	762.674	1199.84	3.0026	3.0998	5.1670	1046.9
		29.444	2787.21	5.9099	2.6781	4.7672	494.93
548	5.9327	759.263	1210.13	3.0210	3.0955	5.1994	1037.4
		30.443	2785.32	5.8955	2.6980	4.8487	494.14
550	6.1172	755.808	1220.47	3.0394	3.0913	5.2331	1027.9
		31.474	2783.30	5.8809	2.7181	4.9332	493.31
552	6.3060	752.308	1230.88	3.0579	3.0872	5.2681	1018.2
		32.538	2781.16	5.8663	2.7385	5.0210	492.44
554	6.4993	748.762	1241.34	3.0763	3.0833	5.3046	1008.4
		33.635	2778.88	5.8517	2.7591	5.1124	491.54
556	6.6970	745.169	1251.86	3.0948	3.0794	5.3427	998.58
		34.769	2776.48	5.8369	2.7800	5.2075	490.59
558	6.8993	741.525	1262.45	3.1133	3.0757	5.3824	988.62
		35.939	2773.93	5.8221	2.8011	5.3066	489.60

TABLE 13.1. Thermodynamic properties of water on the vapor–liquid phase boundary as a function on temperature[a]—Continued

T K	p MPa	ρ kg m^{-3}	h kJ kg^{-1}	s kJ kg^{-1} K^{-1}	c_v kJ kg^{-1} K^{-1}	c_p kJ kg^{-1} K^{-1}	w m s^{-1}
560	7.1062	737.831	1273.11	3.1319	3.0722	5.4239	978.54
		37.147	2771.24	5.8071	2.8225	5.4099	488.58
562	7.3179	734.084	1283.83	3.1505	3.0688	5.4673	968.35
		38.395	2768.40	5.7921	2.8442	5.5178	487.51
564	7.5344	730.283	1294.63	3.1691	3.0656	5.5126	958.05
		39.685	2765.41	5.7769	2.8662	5.6306	486.40
566	7.7557	726.425	1305.50	3.1878	3.0625	5.5602	947.63
		41.018	2762.26	5.7616	2.8885	5.7486	485.24
568	7.9819	722.508	1316.44	3.2066	3.0596	5.6100	937.09
		42.396	2758.95	5.7462	2.9110	5.8723	484.04
570	8.2132	718.530	1327.47	3.2254	3.0569	5.6624	926.44
		43.822	2755.47	5.7307	2.9340	6.0020	482.79
572	8.4496	714.489	1338.58	3.2443	3.0544	5.7175	915.66
		45.297	2751.82	5.7150	2.9572	6.1382	481.50
574	8.6912	710.382	1349.78	3.2632	3.0520	5.7754	904.75
		46.823	2747.99	5.6991	2.9808	6.2815	480.15
576	8.9381	706.206	1361.06	3.2823	3.0499	5.8365	893.71
		48.404	2743.97	5.6831	3.0048	6.4324	478.75
578	9.1903	701.959	1372.45	3.3014	3.0480	5.9010	882.54
		50.042	2739.75	5.6669	3.0291	6.5916	477.31
580	9.4480	697.638	1383.93	3.3205	3.0464	5.9691	871.23
		51.739	2735.33	5.6506	3.0539	6.7598	475.80
582	9.7112	693.238	1395.51	3.3398	3.0450	6.0413	859.78
		53.499	2730.71	5.6340	3.0790	6.9378	474.24
584	9.9800	688.757	1407.20	3.3592	3.0439	6.1179	848.19
		55.326	2725.86	5.6172	3.1046	7.1265	472.63
586	10.255	684.190	1419.00	3.3787	3.0430	6.1993	836.44
		57.222	2720.78	5.6002	3.1306	7.3269	470.95
588	10.535	679.533	1430.93	3.3983	3.0425	6.2859	824.55
		59.193	2715.46	5.5829	3.1571	7.5403	469.21
590	10.821	674.781	1442.98	3.4181	3.0423	6.3784	812.49
		61.242	2709.90	5.5654	3.1840	7.7679	467.41
592	11.113	669.930	1455.16	3.4379	3.0425	6.4773	800.26
		63.373	2704.06	5.5476	3.2115	8.0112	465.54
594	11.412	664.974	1467.48	3.4580	3.0431	6.5833	787.87
		65.593	2697.95	5.5295	3.2395	8.2720	463.60
596	11.716	659.907	1479.95	3.4781	3.0441	6.6973	775.29
		67.907	2691.55	5.5110	3.2681	8.5523	461.59
598	12.027	654.722	1492.57	3.4985	3.0455	6.8202	762.53
		70.321	2684.85	5.4923	3.2973	8.8543	459.50
600	12.345	649.411	1505.36	3.5190	3.0475	6.9532	749.57
		72.842	2677.81	5.4731	3.3271	9.1809	457.33
602	12.669	643.97	1518.33	3.5398	3.0500	7.0976	736.39
		75.479	2670.44	5.4536	3.3576	9.5350	455.07
604	12.999	638.38	1531.48	3.5607	3.0532	7.2549	722.99
		78.239	2662.69	5.4336	3.3889	9.9206	452.73
606	13.337	632.64	1544.84	3.5819	3.0571	7.4272	709.36
		81.134	2654.56	5.4132	3.4209	10.342	450.29

TABLE 13.1. Thermodynamic properties of water on the vapor–liquid phase boundary as a function on temperature[a]—Continued

T K	p MPa	ρ kg m^{-3}	h kJ kg^{-1}	s kJ kg^{-1} K^{-1}	c_v kJ kg^{-1} K^{-1}	c_p kJ kg^{-1} K^{-1}	w m s^{-1}
608	13.681	626.74	1558.42	3.6034	3.0617	7.6169	695.45
		84.173	2646.01	5.3922	3.4538	10.805	447.76
610	14.033	620.65	1572.24	3.6252	3.0673	7.8268	681.27
		87.369	2637.01	5.3707	3.4876	11.315	445.11
612	14.391	614.37	1586.31	3.6473	3.0738	8.0608	666.76
		90.738	2627.53	5.3486	3.5225	11.881	442.36
614	14.757	607.88	1600.67	3.6697	3.0815	8.3235	651.91
		94.295	2617.53	5.3258	3.5584	12.513	439.48
616	15.131	601.15	1615.33	3.6925	3.0906	8.6209	636.65
		98.060	2606.96	5.3023	3.5956	13.223	436.46
618	15.512	594.16	1630.34	3.7158	3.1014	8.9610	620.95
		102.05	2595.77	5.2780	3.6343	14.027	433.31
620	15.901	586.88	1645.74	3.7396	3.1140	9.3541	604.73
		106.31	2583.90	5.2528	3.6745	14.945	429.99
622	16.297	579.26	1661.57	3.7640	3.1290	9.8141	587.93
		110.85	2571.27	5.2266	3.7166	16.005	426.49
624	16.703	571.25	1677.90	3.7891	3.1470	10.360	570.46
		115.72	2557.80	5.1992	3.7608	17.243	422.80
626	17.116	562.81	1694.80	3.8150	3.1687	11.017	552.24
		120.96	2543.38	5.1705	3.8076	18.710	418.88
628	17.538	553.84	1712.37	3.8418	3.1952	11.822	533.18
		126.64	2527.86	5.1404	3.8576	20.479	414.70
630	17.969	544.25	1730.74	3.8698	3.2279	12.827	513.19
		132.84	2511.08	5.1084	3.9114	22.658	410.21
632	18.409	533.92	1750.06	3.8991	3.2689	14.105	492.23
		139.65	2492.80	5.0743	3.9701	25.412	405.36
634	18.858	522.71	1770.51	3.9301	3.3209	15.768	470.31
		147.22	2472.71	5.0376	4.0354	29.015	400.05
636	19.317	510.42	1792.35	3.9631	3.3873	17.995	447.58
		155.75	2450.34	4.9976	4.1098	33.945	394.16
638	19.786	496.82	1815.92	3.9986	3.4725	21.122	424.30
		165.55	2425.00	4.9533	4.1975	41.124	387.48
640	20.265	481.53	1841.77	4.0375	3.5815	25.942	400.66
		177.15	2395.51	4.9027	4.3061	52.586	379.64
641	20.509	473.01	1855.88	4.0587	3.6477	29.607	388.55
		183.90	2378.59	4.8742	4.3728	61.335	375.08
642	20.756	463.67	1871.12	4.0817	3.7256	34.929	375.90
		191.53	2359.67	4.8427	4.4520	73.787	369.90
643	21.006	453.14	1887.97	4.1071	3.8220	43.427	362.10
		200.38	2338.06	4.8070	4.5496	92.842	363.84
644	21.259	440.73	1907.35	4.1363	3.9543	58.910	346.01
		210.99	2312.57	4.7655	4.6763	125.31	356.41
645	21.515	425.05	1931.11	4.1722	4.1673	93.350	325.47
		224.45	2281.02	4.7147	4.8543	191.32	346.60
646	21.775	402.96	1963.49	4.2214	4.5943	204.58	297.13
		243.46	2238.06	4.6465	5.1457	385.23	331.61
647	22.038	357.34	2029.44	4.3224	6.2344	3905.2	251.19
		286.51	2148.56	4.5065	6.2740	5334.1	285.32

TABLE 13.1. Thermodynamic properties of water on the vapor–liquid phase boundary as a function on temperature[a]—Continued

T K	p MPa	ρ kg m^{-3}	h kJ kg^{-1}	s kJ kg^{-1} K^{-1}	c_v kJ kg^{-1} K^{-1}	c_p kJ kg^{-1} K^{-1}	w m s^{-1}
647.096[c]	22.064	322	2084.26	4.407			

[a]For each temperature, the values on the first line correspond to the saturated-liquid line and the values on the second line correspond to the saturated-vapor line.
[b]Triple point.
[c]Critical point.

TABLE 13.2. Thermodynamic properties of water in the single-phase region

T K	ρ kg m^{-3}	u kJ kg^{-1}	h kJ kg^{-1}	s kJ kg^{-1} K^{-1}	c_v kJ kg^{-1} K^{-1}	c_p kJ kg^{-1} K^{-1}	w m s^{-1}
			0.05 MPa				
273.156[a]	999.817	−0.016	0.034	−0.0001	4.2172	4.2197	1402.3
275	999.912	7.760	7.810	0.0283	4.2130	4.2137	1411.4
280	999.886	28.795	28.845	0.1041	4.2000	4.2011	1434.2
285	999.493	49.778	49.828	0.1784	4.1850	4.1926	1454.4
290	998.780	70.725	70.775	0.2513	4.1682	4.1868	1472.2
295	997.784	91.649	91.699	0.3228	4.1499	4.1830	1487.8
300	996.534	112.557	112.608	0.3931	4.1303	4.1808	1501.4
305	995.053	133.458	133.508	0.4622	4.1096	4.1797	1513.2
310	993.361	154.355	154.406	0.5301	4.0878	4.1794	1523.3
315	991.474	175.253	175.303	0.5970	4.0650	4.1797	1531.8
320	989.404	196.153	196.204	0.6628	4.0415	4.1807	1538.8
325	987.165	217.060	217.110	0.7277	4.0173	4.1820	1544.4
330	984.764	237.974	238.025	0.7915	3.9925	4.1838	1548.8
335	982.212	258.898	258.949	0.8545	3.9672	4.1859	1551.9
340	979.513	279.833	279.884	0.9165	3.9415	4.1884	1553.9
345	976.676	300.782	300.833	0.9777	3.9156	4.1913	1554.9
350	973.706	321.747	321.798	1.0380	3.8895	4.1946	1554.8
354.467[b]	970.942	340.490	340.542	1.0912	3.8660	4.1979	1554.0
354.467[c]	0.308 64	2483.21	2645.22	7.5930	1.5136	2.0157	462.14
355	0.308 15	2484.03	2646.29	7.5960	1.5121	2.0138	462.52
360	0.303 66	2491.66	2656.32	7.6241	1.5012	1.9987	466.05
365	0.299 31	2499.23	2666.28	7.6516	1.4935	1.9875	469.48
370	0.295 10	2506.76	2676.20	7.6786	1.4877	1.9788	472.84
375	0.291 01	2514.26	2686.07	7.7051	1.4833	1.9719	476.14
380	0.287 05	2521.73	2695.92	7.7311	1.4799	1.9662	479.40
385	0.283 20	2529.19	2705.74	7.7568	1.4772	1.9616	482.61
390	0.279 47	2536.62	2715.54	7.7821	1.4753	1.9579	485.79
395	0.275 83	2544.05	2725.32	7.8070	1.4738	1.9549	488.93
400	0.272 29	2551.46	2735.09	7.8316	1.4729	1.9525	492.04
410	0.265 50	2566.27	2754.59	7.8798	1.4722	1.9494	498.16
420	0.259 05	2581.07	2774.08	7.9267	1.4728	1.9479	504.17
430	0.252 92	2595.87	2793.56	7.9726	1.4743	1.9479	510.07
440	0.247 08	2610.68	2813.04	8.0173	1.4767	1.9488	515.88
450	0.241 51	2625.51	2832.54	8.0612	1.4797	1.9507	521.59
460	0.236 20	2640.37	2852.06	8.1041	1.4832	1.9532	527.22
470	0.231 12	2655.26	2871.60	8.1461	1.4872	1.9563	532.76
480	0.226 25	2670.19	2891.18	8.1873	1.4915	1.9599	538.23
490	0.221 59	2685.16	2910.80	8.2278	1.4961	1.9639	543.63
500	0.217 12	2700.18	2930.46	8.2675	1.5009	1.9681	548.96
510	0.212 83	2715.24	2950.17	8.3065	1.5060	1.9727	554.22
520	0.208 71	2730.35	2969.92	8.3449	1.5112	1.9775	559.41
530	0.204 74	2745.51	2989.72	8.3826	1.5166	1.9825	564.54
540	0.200 93	2760.72	3009.57	8.4197	1.5221	1.9877	569.62
550	0.197 26	2775.99	3029.47	8.4562	1.5278	1.9931	574.64
560	0.193 71	2791.32	3049.43	8.4922	1.5335	1.9985	579.60
570	0.190 30	2806.70	3069.44	8.5276	1.5394	2.0041	584.51
580	0.187 00	2822.14	3089.51	8.5625	1.5453	2.0098	589.37
590	0.183 82	2837.64	3109.64	8.5969	1.5513	2.0156	594.17
600	0.180 75	2853.19	3129.83	8.6308	1.5574	2.0215	598.93
610	0.177 77	2868.81	3150.07	8.6643	1.5635	2.0275	603.64
620	0.174 89	2884.49	3170.38	8.6973	1.5697	2.0335	608.31
630	0.172 11	2900.23	3190.74	8.7299	1.5760	2.0396	612.93
640	0.169 41	2916.03	3211.17	8.7621	1.5823	2.0458	617.50
650	0.166 80	2931.89	3231.66	8.7938	1.5886	2.0521	622.04
675	0.160 60	2971.83	3283.16	8.8716	1.6047	2.0679	633.19

TABLE 13.2. Thermodynamic properties of water in the single-phase region—Continued

T K	ρ kg m^{-3}	u kJ kg^{-1}	h kJ kg^{-1}	s kJ kg^{-1} K^{-1}	c_v kJ kg^{-1} K^{-1}	c_p kJ kg^{-1} K^{-1}	w m s^{-1}
			0.05 MPa—Continued				
700	0.154 85	3012.17	3335.05	8.9471	1.6210	2.0840	644.11
725	0.149 50	3052.92	3387.36	9.0205	1.6376	2.1004	654.79
750	0.144 51	3094.08	3440.08	9.0920	1.6544	2.1170	665.25
775	0.139 84	3135.67	3493.21	9.1617	1.6714	2.1339	675.51
800	0.135 47	3177.68	3546.77	9.2297	1.6885	2.1509	685.58
825	0.131 36	3220.12	3600.76	9.2961	1.7058	2.1682	695.46
850	0.127 49	3262.99	3655.18	9.3611	1.7233	2.1855	705.17
900	0.120 40	3350.05	3765.33	9.4870	1.7585	2.2206	724.09
950	0.114 06	3438.88	3877.25	9.6080	1.7939	2.2560	742.42
1000	0.108 35	3529.47	3990.93	9.7247	1.8294	2.2914	760.20
1050	0.103 19	3621.84	4106.39	9.8373	1.8648	2.3267	777.50
1100	0.098 50	3715.96	4223.59	9.9463	1.8998	2.3616	794.35
1150	0.094 21	3811.82	4342.54	10.052	1.9343	2.3961	810.79
1200	0.090 29	3909.39	4463.19	10.155	1.9681	2.4299	826.86
1250	0.086 67	4008.63	4585.51	10.255	2.0012	2.4629	842.59
1273	0.085 11	4054.84	4642.33	10.300	2.0161	2.4778	849.71
			0.1 MPa				
273.153[a]	999.843	−0.028	0.072	−0.0001	4.2170	4.2194	1402.4
275	999.937	7.760	7.860	0.0283	4.2128	4.2135	1411.5
280	999.910	28.794	28.894	0.1041	4.1998	4.2009	1434.3
285	999.517	49.776	49.876	0.1784	4.1848	4.1924	1454.4
290	998.803	70.722	70.822	0.2512	4.1680	4.1866	1472.3
295	997.807	91.645	91.745	0.3228	4.1498	4.1829	1487.9
300	996.556	112.553	112.654	0.3931	4.1302	4.1806	1501.5
305	995.075	133.453	133.554	0.4622	4.1094	4.1795	1513.3
310	993.383	154.350	154.450	0.5301	4.0876	4.1792	1523.4
315	991.496	175.246	175.347	0.5970	4.0649	4.1796	1531.9
320	989.426	196.146	196.247	0.6628	4.0414	4.1805	1538.9
325	987.187	217.052	217.153	0.7276	4.0172	4.1819	1544.5
330	984.786	237.966	238.067	0.7915	3.9923	4.1837	1548.9
335	982.233	258.889	258.991	0.8544	3.9671	4.1858	1552.0
340	979.535	279.823	279.926	0.9165	3.9414	4.1883	1554.0
345	976.699	300.772	300.874	0.9776	3.9155	4.1912	1555.0
350	973.728	321.735	321.838	1.0380	3.8894	4.1945	1554.9
355	970.628	342.716	342.820	1.0975	3.8631	4.1982	1554.0
360	967.403	363.717	363.821	1.1562	3.8369	4.2023	1552.1
365	964.057	384.740	384.844	1.2142	3.8107	4.2070	1549.3
370	960.591	405.787	405.891	1.2715	3.7845	4.2121	1545.8
372.756[b]	958.632	417.400	417.504	1.3028	3.7702	4.2152	1543.5
372.756[c]	0.590 34	2505.55	2674.95	7.3588	1.5548	2.0784	471.99
375	0.586 53	2509.11	2679.60	7.3713	1.5479	2.0686	473.59
380	0.578 24	2516.96	2689.90	7.3986	1.5356	2.0507	477.08
385	0.570 21	2524.74	2700.11	7.4253	1.5262	2.0366	480.47
390	0.562 45	2532.47	2710.27	7.4515	1.5189	2.0252	483.80
395	0.554 91	2540.16	2720.37	7.4772	1.5130	2.0157	487.08
400	0.547 61	2547.81	2730.43	7.5025	1.5082	2.0078	490.31
410	0.533 61	2563.04	2750.44	7.5519	1.5012	1.9954	496.63
420	0.520 38	2578.18	2770.35	7.5999	1.4968	1.9868	502.81
430	0.507 83	2593.27	2790.18	7.6466	1.4945	1.9809	508.86
440	0.495 92	2608.33	2809.97	7.6921	1.4938	1.9772	514.78
450	0.484 58	2623.37	2829.73	7.7365	1.4943	1.9752	520.60
460	0.473 78	2638.41	2849.48	7.7799	1.4957	1.9746	526.32
470	0.463 47	2653.46	2869.23	7.8224	1.4980	1.9751	531.94
480	0.453 61	2668.53	2888.99	7.8640	1.5009	1.9764	537.48

TABLE 13.2. Thermodynamic properties of water in the single-phase region—Continued

T K	ρ kg m^{-3}	u kJ kg^{-1}	h kJ kg^{-1}	s kJ kg^{-1} K^{-1}	c_v kJ kg^{-1} K^{-1}	c_p kJ kg^{-1} K^{-1}	w m s^{-1}
			0.1 MPa—Continued				
490	0.444 18	2683.62	2908.76	7.9047	1.5043	1.9785	542.93
500	0.435 14	2698.75	2928.56	7.9447	1.5082	1.9813	548.31
510	0.426 47	2713.91	2948.39	7.9840	1.5124	1.9845	553.62
520	0.418 15	2729.10	2968.25	8.0226	1.5169	1.9881	558.86
530	0.410 16	2744.34	2988.15	8.0605	1.5217	1.9921	564.03
540	0.402 47	2759.63	3008.09	8.0978	1.5267	1.9964	569.14
550	0.395 07	2774.96	3028.08	8.1344	1.5319	2.0010	574.19
560	0.387 94	2790.34	3048.11	8.1705	1.5373	2.0058	579.18
570	0.381 07	2805.78	3068.20	8.2061	1.5428	2.0108	584.12
580	0.374 44	2821.26	3088.33	8.2411	1.5484	2.0160	589.00
590	0.368 04	2836.80	3108.52	8.2756	1.5541	2.0213	593.83
600	0.361 85	2852.40	3128.76	8.3096	1.5600	2.0268	598.61
610	0.355 88	2868.06	3149.05	8.3432	1.5659	2.0324	603.34
620	0.350 10	2883.77	3169.40	8.3763	1.5719	2.0381	608.02
630	0.344 50	2899.54	3189.81	8.4089	1.5780	2.0439	612.65
640	0.339 09	2915.37	3210.28	8.4411	1.5841	2.0497	617.25
650	0.333 84	2931.27	3230.81	8.4730	1.5903	2.0557	621.79
675	0.321 41	2971.27	3282.39	8.5508	1.6061	2.0710	632.98
700	0.309 88	3011.66	3334.36	8.6264	1.6222	2.0867	643.92
725	0.299 15	3052.45	3386.73	8.6999	1.6386	2.1027	654.63
750	0.289 15	3093.66	3439.50	8.7715	1.6553	2.1191	665.11
775	0.279 79	3135.28	3492.68	8.8413	1.6721	2.1357	675.39
800	0.271 02	3177.32	3546.29	8.9093	1.6892	2.1525	685.47
825	0.262 79	3219.78	3600.31	8.9758	1.7064	2.1696	695.36
850	0.255 04	3262.68	3654.77	9.0408	1.7238	2.1868	705.08
900	0.240 85	3349.78	3764.98	9.1668	1.7589	2.2216	724.03
950	0.228 15	3438.64	3876.94	9.2879	1.7943	2.2568	742.37
1000	0.216 73	3529.26	3990.66	9.4045	1.8297	2.2921	760.17
1050	0.206 40	3621.65	4106.14	9.5172	1.8650	2.3273	777.47
1100	0.197 01	3715.79	4223.38	9.6263	1.9000	2.3621	794.33
1150	0.188 44	3811.67	4342.35	9.7321	1.9344	2.3965	810.78
1200	0.180 58	3909.25	4463.02	9.8348	1.9682	2.4302	826.85
1250	0.173 35	4008.50	4585.36	9.9346	2.0013	2.4632	842.59
1273	0.170 22	4054.71	4642.18	9.9797	2.0162	2.4781	849.72
			0.101 325 MPa				
273.153[a]	999.843	−0.028	0.074	−0.0001	4.2170	4.2194	1402.4
275	999.938	7.760	7.861	0.0283	4.2128	4.2135	1411.5
280	999.911	28.794	28.895	0.1041	4.1998	4.2009	1434.3
285	999.517	49.776	49.877	0.1784	4.1848	4.1924	1454.4
290	998.804	70.722	70.824	0.2512	4.1680	4.1866	1472.3
295	997.807	91.645	91.747	0.3228	4.1498	4.1829	1487.9
300	996.557	112.553	112.655	0.3931	4.1302	4.1806	1501.5
305	995.076	133.453	133.555	0.4622	4.1094	4.1795	1513.3
310	993.384	154.349	154.451	0.5301	4.0876	4.1792	1523.4
315	991.496	175.246	175.348	0.5970	4.0649	4.1796	1531.9
320	989.427	196.146	196.249	0.6628	4.0414	4.1805	1538.9
325	987.187	217.052	217.154	0.7276	4.0171	4.1819	1544.5
330	984.787	237.965	238.068	0.7915	3.9923	4.1837	1548.9
335	982.234	258.888	258.992	0.8544	3.9671	4.1858	1552.0
340	979.536	279.823	279.927	0.9165	3.9414	4.1883	1554.0
345	976.699	300.771	300.875	0.9776	3.9155	4.1912	1555.0
350	973.728	321.735	321.839	1.0380	3.8894	4.1945	1554.9
355	970.629	342.716	342.821	1.0975	3.8631	4.1982	1554.0
360	967.404	363.717	363.822	1.1562	3.8369	4.2023	1552.1

TABLE 13.2. Thermodynamic properties of water in the single-phase region—Continued

T K	ρ kg m^{-3}	u kJ kg^{-1}	h kJ kg^{-1}	s kJ kg^{-1} K^{-1}	c_v kJ kg^{-1} K^{-1}	c_p kJ kg^{-1} K^{-1}	w m s^{-1}
			0.101 325 MPa—Continued				
365	964.057	384.740	384.845	1.2142	3.8107	4.2070	1549.3
370	960.592	405.787	405.892	1.2715	3.7845	4.2121	1545.8
373.124[b]	958.367	418.952	419.058	1.3069	3.7683	4.2156	1543.2
373.124[c]	0.59766	2505.99	2675.53	7.3544	1.5558	2.0799	472.18
375	0.59442	2508.96	2679.42	7.3648	1.5499	2.0716	473.52
380	0.586 01	2516.83	2689.73	7.3921	1.5372	2.0532	477.01
385	0.577 87	2524.62	2699.96	7.4189	1.5277	2.0388	480.41
390	0.569 99	2532.36	2710.12	7.4451	1.5201	2.0271	483.75
395	0.562 36	2540.06	2720.24	7.4709	1.5141	2.0174	487.03
400	0.554 94	2547.72	2730.30	7.4962	1.5091	2.0093	490.26
410	0.540 75	2562.95	2750.33	7.5457	1.5020	1.9967	496.59
420	0.527 34	2578.10	2770.25	7.5937	1.4975	1.9878	502.78
430	0.514 62	2593.20	2790.09	7.6404	1.4951	1.9818	508.82
440	0.502 54	2608.26	2809.89	7.6859	1.4942	1.9780	514.75
450	0.491 05	2623.31	2829.66	7.7303	1.4947	1.9759	520.57
460	0.480 09	2638.36	2849.41	7.7737	1.4961	1.9752	526.29
470	0.469 64	2653.42	2869.17	7.8162	1.4983	1.9756	531.92
480	0.459 65	2668.49	2888.93	7.8578	1.5011	1.9769	537.46
490	0.450 09	2683.58	2908.71	7.8986	1.5045	1.9789	542.92
500	0.440 93	2698.71	2928.51	7.9386	1.5084	1.9816	548.30
510	0.432 15	2713.87	2948.34	7.9779	1.5126	1.9848	553.61
520	0.423 71	2729.07	2968.21	8.0164	1.5171	1.9884	558.84
530	0.415 61	2744.31	2988.11	8.0543	1.5219	1.9924	564.02
540	0.407 82	2759.60	3008.05	8.0916	1.5268	1.9967	569.13
550	0.400 32	2774.93	3028.04	8.1283	1.5320	2.0012	574.18
560	0.393 09	2790.32	3048.08	8.1644	1.5374	2.0060	579.17
570	0.386 13	2805.75	3068.16	8.2000	1.5429	2.0110	584.11
580	0.379 41	2821.24	3088.30	8.2350	1.5485	2.0161	588.99
590	0.372 92	2836.78	3108.49	8.2695	1.5542	2.0215	593.82
600	0.366 66	2852.38	3128.73	8.3035	1.5600	2.0269	598.60
610	0.360 60	2868.04	3149.03	8.3370	1.5659	2.0325	603.33
620	0.354 75	2883.75	3169.38	8.3701	1.5719	2.0382	608.01
630	0.349 08	2899.52	3189.79	8.4028	1.5780	2.0440	612.65
640	0.343 59	2915.36	3210.26	8.4350	1.5842	2.0498	617.24
650	0.338 27	2931.25	3230.79	8.4669	1.5904	2.0558	621.79
675	0.325 68	2971.25	3282.37	8.5447	1.6062	2.0711	632.98
700	0.313 99	3011.65	3334.34	8.6203	1.6223	2.0868	643.92
725	0.303 12	3052.44	3386.71	8.6938	1.6386	2.1028	654.62
750	0.292 98	3093.65	3439.49	8.7654	1.6553	2.1191	665.11
775	0.283 50	3135.26	3492.67	8.8352	1.6721	2.1357	675.39
800	0.274 62	3177.31	3546.27	8.9032	1.6892	2.1526	685.47
825	0.266 28	3219.77	3600.30	8.9697	1.7064	2.1696	695.36
850	0.258 43	3262.67	3654.76	9.0348	1.7238	2.1868	705.08
900	0.244 04	3349.77	3764.97	9.1607	1.7589	2.2217	724.03
950	0.231 18	3438.63	3876.93	9.2818	1.7943	2.2568	742.37
1000	0.219 60	3529.25	3990.65	9.3985	1.8297	2.2921	760.16
1050	0.209 14	3621.64	4106.14	9.5111	1.8650	2.3273	777.47
1100	0.199 62	3715.79	4223.37	9.6202	1.9000	2.3621	794.33
1150	0.190 93	3811.66	4342.34	9.7260	1.9344	2.3965	810.78
1200	0.182 97	3909.25	4463.01	9.8287	1.9682	2.4303	826.85
1250	0.175 65	4008.50	4585.35	9.9286	2.0013	2.4633	842.59
1273	0.172 48	4054.71	4642.18	9.9736	2.0162	2.4781	849.72
			0.25 MPa				
273.142[a]	999.918	−0.071	0.179	−0.0003	4.2163	4.2187	1402.6

TABLE 13.2. Thermodynamic properties of water in the single-phase region—Continued

T K	ρ kg m^{-3}	u kJ kg^{-1}	h kJ kg^{-1}	s kJ kg^{-1} K^{-1}	c_v kJ kg^{-1} K^{-1}	c_p kJ kg^{-1} K^{-1}	w m s^{-1}
			0.25 MPa—Continued				
275	1000.01	7.761	8.011	0.0283	4.2121	4.2128	1411.8
280	999.983	28.792	29.042	0.1041	4.1992	4.2003	1434.5
285	999.588	49.771	50.021	0.1784	4.1842	4.1918	1454.7
290	998.873	70.715	70.965	0.2512	4.1675	4.1861	1472.5
295	997.875	91.635	91.886	0.3227	4.1492	4.1824	1488.1
300	996.624	112.541	112.792	0.3930	4.1297	4.1802	1501.8
305	995.142	133.439	133.690	0.4621	4.1090	4.1791	1513.6
310	993.449	154.333	154.584	0.5301	4.0872	4.1789	1523.6
315	991.561	175.227	175.479	0.5969	4.0645	4.1793	1532.1
320	989.492	196.125	196.378	0.6627	4.0410	4.1802	1539.1
325	987.252	217.029	217.282	0.7276	4.0168	4.1816	1544.8
330	984.852	237.940	238.194	0.7914	3.9920	4.1833	1549.1
335	982.299	258.861	259.116	0.8543	3.9667	4.1855	1552.3
340	979.601	279.794	280.049	0.9164	3.9411	4.1880	1554.3
345	976.765	300.740	300.996	0.9775	3.9152	4.1909	1555.3
350	973.795	321.702	321.958	1.0379	3.8891	4.1941	1555.2
355	970.696	342.681	342.938	1.0974	3.8629	4.1979	1554.3
360	967.471	363.679	363.938	1.1561	3.8366	4.2020	1552.4
365	964.126	384.700	384.959	1.2141	3.8104	4.2066	1549.7
370	960.661	405.745	406.005	1.2714	3.7843	4.2118	1546.1
375	957.081	426.817	427.078	1.3279	3.7584	4.2175	1541.8
380	953.385	447.919	448.181	1.3838	3.7326	4.2238	1536.7
385	949.578	469.054	469.317	1.4391	3.7071	4.2307	1530.9
390	945.658	490.225	490.489	1.4937	3.6819	4.2383	1524.4
395	941.628	511.435	511.701	1.5478	3.6570	4.2465	1517.3
400	937.488	532.689	532.956	1.6013	3.6324	4.2555	1509.5
400.561[b]	937.016	535.078	535.345	1.6072	3.6296	4.2566	1508.6
400.561[c]	1.3915	2536.82	2716.49	7.0524	1.6457	2.2219	484.91
410	1.3551	2552.65	2737.14	7.1034	1.6045	2.1605	491.72
420	1.3191	2569.01	2758.53	7.1550	1.5790	2.1203	498.52
430	1.2854	2585.09	2779.59	7.2045	1.5620	2.0920	505.05
440	1.2536	2600.97	2800.40	7.2524	1.5501	2.0712	511.37
450	1.2236	2616.72	2821.03	7.2987	1.5417	2.0556	517.53
460	1.1952	2632.35	2841.52	7.3438	1.5361	2.0439	523.53
470	1.1682	2647.92	2861.92	7.3876	1.5327	2.0353	529.41
480	1.1426	2663.43	2882.24	7.4304	1.5308	2.0292	535.16
490	1.1181	2678.92	2902.51	7.4722	1.5304	2.0251	540.81
500	1.0947	2694.38	2922.75	7.5131	1.5310	2.0226	546.35
510	1.0724	2709.84	2942.97	7.5531	1.5325	2.0213	551.81
520	1.0510	2725.31	2963.18	7.5924	1.5347	2.0212	557.18
530	1.0305	2740.79	2983.39	7.6309	1.5375	2.0219	562.47
540	1.0108	2756.30	3003.62	7.6687	1.5409	2.0234	567.69
550	0.991 92	2771.82	3023.86	7.7058	1.5446	2.0255	572.84
560	0.973 73	2787.39	3044.13	7.7423	1.5487	2.0282	577.92
570	0.956 22	2802.98	3064.43	7.7783	1.5531	2.0313	582.93
580	0.939 35	2818.62	3084.76	7.8136	1.5578	2.0348	587.89
590	0.923 09	2834.29	3105.12	7.8484	1.5627	2.0386	592.78
600	0.907 40	2850.02	3125.53	7.8827	1.5678	2.0428	597.63
610	0.892 24	2865.79	3145.98	7.9165	1.5731	2.0472	602.41
620	0.877 60	2881.60	3166.47	7.9499	1.5785	2.0518	607.15
630	0.863 43	2897.47	3187.02	7.9827	1.5841	2.0566	611.83
640	0.849 73	2913.40	3207.61	8.0152	1.5897	2.0617	616.47
650	0.836 47	2929.37	3228.25	8.0472	1.5955	2.0668	621.06
675	0.805 08	2969.56	3280.09	8.1254	1.6105	2.0805	632.34
700	0.776 00	3010.12	3332.28	8.2013	1.6259	2.0948	643.36

TABLE 13.2. Thermodynamic properties of water in the single-phase region—Continued

T K	ρ kg m^{-3}	u kJ kg^{-1}	h kJ kg^{-1}	s kJ kg^{-1} K^{-1}	c_v kJ kg^{-1} K^{-1}	c_p kJ kg^{-1} K^{-1}	w m s^{-1}
			0.25 MPa—Continued				
725	0.748 98	3051.05	3384.83	8.2751	1.6417	2.1098	654.14
750	0.723 80	3092.37	3437.77	8.3469	1.6579	2.1252	664.68
775	0.700 27	3134.09	3491.10	8.4168	1.6744	2.1411	675.01
800	0.678 23	3176.22	3544.83	8.4851	1.6912	2.1573	685.14
825	0.657 55	3218.77	3598.97	8.5517	1.7082	2.1738	695.07
850	0.638 11	3261.74	3653.52	8.6168	1.7254	2.1906	704.83
900	0.602 49	3348.96	3763.90	8.7430	1.7601	2.2247	723.83
950	0.570 66	3437.91	3876.00	8.8642	1.7953	2.2593	742.22
1000	0.542 04	3528.61	3989.84	8.9810	1.8305	2.2942	760.05
1050	0.516 16	3621.07	4105.42	9.0938	1.8657	2.3290	777.39
1100	0.492 64	3715.27	4222.74	9.2029	1.9005	2.3636	794.27
1150	0.471 18	3811.19	4341.78	9.3088	1.9349	2.3978	810.75
1200	0.451 52	3908.82	4462.51	9.4115	1.9687	2.4314	826.84
1250	0.433 43	4008.11	4584.90	9.5114	2.0017	2.4642	842.59
1273	0.425 59	4054.33	4641.75	9.5565	2.0166	2.4791	849.73
			0.5 MPa				
273.123[a]	1000.04	−0.147	0.353	−0.0005	4.2152	4.2176	1402.9
275	1000.14	7.764	8.264	0.0283	4.2110	4.2116	1412.2
280	1000.10	28.789	29.289	0.1041	4.1981	4.1993	1434.9
285	999.706	49.763	50.263	0.1783	4.1832	4.1909	1455.1
290	998.989	70.702	71.203	0.2512	4.1665	4.1853	1472.9
295	997.989	91.619	92.120	0.3227	4.1484	4.1817	1488.6
300	996.736	112.520	113.022	0.3930	4.1289	4.1795	1502.2
305	995.253	133.414	133.916	0.4620	4.1082	4.1785	1514.0
310	993.559	154.305	154.808	0.5300	4.0864	4.1782	1524.1
315	991.671	175.196	175.700	0.5968	4.0638	4.1787	1532.6
320	989.601	196.090	196.595	0.6626	4.0403	4.1796	1539.6
325	987.361	216.990	217.497	0.7274	4.0161	4.1810	1545.2
330	984.961	237.898	238.406	0.7913	3.9914	4.1828	1549.6
335	982.409	258.816	259.325	0.8542	3.9662	4.1849	1552.7
340	979.711	279.745	280.255	0.9162	3.9406	4.1874	1554.8
345	976.876	300.688	301.200	0.9774	3.9147	4.1903	1555.8
350	973.906	321.646	322.159	1.0377	3.8886	4.1936	1555.7
355	970.808	342.621	343.136	1.0972	3.8624	4.1973	1554.8
360	967.585	363.616	364.133	1.1559	3.8362	4.2015	1552.9
365	964.241	384.633	385.152	1.2139	3.8100	4.2061	1550.2
370	960.778	405.674	406.195	1.2712	3.7839	4.2112	1546.6
375	957.199	426.743	427.265	1.3277	3.7580	4.2169	1542.3
380	953.505	447.841	448.365	1.3836	3.7322	4.2232	1537.3
385	949.699	468.971	469.498	1.4389	3.7068	4.2301	1531.5
390	945.782	490.138	490.667	1.4935	3.6815	4.2376	1525.0
395	941.754	511.345	511.875	1.5476	3.6566	4.2459	1517.9
400	937.617	532.594	533.127	1.6010	3.6321	4.2548	1510.1
410	929.012	575.236	575.774	1.7063	3.5840	4.2751	1492.6
420	919.964	618.097	618.640	1.8096	3.5375	4.2988	1472.7
424.981[b]	915.290	639.539	640.085	1.8604	3.5150	4.3120	1461.9
424.981[c]	2.6680	2560.71	2748.11	6.8207	1.7593	2.4103	493.85
430	2.6297	2569.90	2760.04	6.8486	1.7170	2.3469	497.85
440	2.5579	2587.60	2783.07	6.9015	1.6661	2.2671	505.18
450	2.4913	2604.77	2805.47	6.9519	1.6352	2.2159	512.04
460	2.4290	2621.59	2827.44	7.0001	1.6137	2.1787	518.62
470	2.3705	2638.15	2849.08	7.0467	1.5981	2.1504	524.96
480	2.3153	2654.51	2870.47	7.0917	1.5866	2.1285	531.12
490	2.2631	2670.72	2891.66	7.1354	1.5784	2.1116	537.12

TABLE 13.2. Thermodynamic properties of water in the single-phase region—Continued

T K	ρ kg m^{-3}	u kJ kg^{-1}	h kJ kg^{-1}	s kJ kg^{-1} K^{-1}	c_v kJ kg^{-1} K^{-1}	c_p kJ kg^{-1} K^{-1}	w m s^{-1}
			0.5 MPa—Continued				
500	2.2135	2686.83	2912.71	7.1779	1.5726	2.0984	542.97
510	2.1664	2702.85	2933.64	7.2194	1.5688	2.0883	548.70
520	2.1215	2718.80	2954.48	7.2599	1.5666	2.0807	554.31
530	2.0786	2734.72	2975.26	7.2994	1.5657	2.0752	559.81
540	2.0376	2750.61	2995.99	7.3382	1.5659	2.0713	565.22
550	1.9984	2766.49	3016.69	7.3762	1.5669	2.0687	570.54
560	1.9607	2782.36	3037.37	7.4134	1.5687	2.0674	575.77
570	1.9246	2798.24	3058.04	7.4500	1.5712	2.0670	580.93
580	1.8898	2814.14	3078.71	7.4860	1.5741	2.0674	586.01
590	1.8564	2830.05	3099.39	7.5213	1.5775	2.0686	591.02
600	1.8242	2845.99	3120.09	7.5561	1.5813	2.0703	595.97
610	1.7931	2861.96	3140.80	7.5903	1.5854	2.0726	600.86
620	1.7631	2877.96	3161.54	7.6241	1.5898	2.0754	605.68
630	1.7342	2894.00	3182.31	7.6573	1.5945	2.0785	610.45
640	1.7063	2910.08	3203.11	7.6901	1.5993	2.0820	615.17
650	1.6792	2926.20	3223.95	7.7224	1.6044	2.0858	619.83
675	1.6154	2966.71	3276.23	7.8013	1.6178	2.0965	631.28
700	1.5564	3007.53	3328.79	7.8777	1.6321	2.1085	642.43
725	1.5016	3048.69	3381.66	7.9520	1.6470	2.1216	653.32
750	1.4507	3090.21	3434.88	8.0241	1.6624	2.1355	663.97
775	1.4032	3132.11	3488.45	8.0944	1.6783	2.1501	674.38
800	1.3587	3174.39	3542.39	8.1629	1.6946	2.1653	684.59
825	1.3170	3217.07	3596.71	8.2298	1.7112	2.1809	694.59
850	1.2779	3260.16	3651.44	8.2951	1.7280	2.1969	704.40
900	1.2062	3347.58	3762.10	8.4216	1.7622	2.2299	723.50
950	1.1422	3436.70	3874.44	8.5431	1.7969	2.2636	741.97
1000	1.0848	3527.54	3988.47	8.6600	1.8319	2.2977	759.87
1050	1.0328	3620.11	4104.21	8.7730	1.8668	2.3320	777.26
1100	0.985 68	3714.40	4221.67	8.8822	1.9015	2.3662	794.19
1150	0.942 66	3810.41	4340.82	8.9882	1.9357	2.4000	810.69
1200	0.903 25	3908.10	4461.66	9.0910	1.9694	2.4333	826.82
1250	0.867 02	4007.45	4584.14	9.1910	2.0023	2.4659	842.59
1273	0.851 32	4053.70	4641.02	9.2361	2.0171	2.4806	849.74
			0.75 MPa				
273.105[a]	1000.17	−0.218	0.532	−0.0008	4.2140	4.2164	1403.2
275	1000.26	7.766	8.516	0.0283	4.2098	4.2104	1412.6
280	1000.23	28.786	29.536	0.1041	4.1971	4.1983	1435.3
285	999.824	49.755	50.505	0.1783	4.1822	4.1900	1455.5
290	999.104	70.690	71.441	0.2511	4.1656	4.1845	1473.3
295	998.103	91.602	92.353	0.3226	4.1475	4.1809	1489.0
300	996.848	112.500	113.252	0.3929	4.1280	4.1788	1502.6
305	995.364	133.390	134.143	0.4619	4.1074	4.1778	1514.4
310	993.669	154.277	155.031	0.5299	4.0857	4.1776	1524.5
315	991.780	175.164	175.920	0.5967	4.0631	4.1781	1533.0
320	989.710	196.055	196.813	0.6625	4.0397	4.1790	1540.0
325	987.470	216.952	217.711	0.7273	4.0155	4.1804	1545.7
330	985.070	237.856	238.617	0.7912	3.9908	4.1822	1550.0
335	982.518	258.770	259.534	0.8541	3.9656	4.1844	1553.2
340	979.821	279.696	280.462	0.9161	3.9400	4.1869	1555.3
345	976.986	300.635	301.403	0.9772	3.9142	4.1898	1556.2
350	974.018	321.590	322.360	1.0375	3.8881	4.1931	1556.2
355	970.920	342.562	343.334	1.0970	3.8619	4.1968	1555.3
360	967.699	363.553	364.328	1.1558	3.8357	4.2009	1553.4
365	964.355	384.566	385.344	1.2137	3.8096	4.2055	1550.7

TABLE 13.2. Thermodynamic properties of water in the single-phase region—Continued

T K	ρ kg m^{-3}	u kJ kg^{-1}	h kJ kg^{-1}	s kJ kg^{-1} K^{-1}	c_v kJ kg^{-1} K^{-1}	c_p kJ kg^{-1} K^{-1}	w m s^{-1}
			0.75 MPa—Continued				
370	960.894	405.604	406.384	1.2710	3.7835	4.2107	1547.2
375	957.316	426.668	427.452	1.3276	3.7576	4.2163	1542.9
380	953.625	447.762	448.549	1.3834	3.7319	4.2226	1537.8
385	949.821	468.889	469.679	1.4387	3.7064	4.2295	1532.1
390	945.906	490.052	490.845	1.4933	3.6812	4.2370	1525.6
395	941.880	511.254	512.050	1.5473	3.6563	4.2452	1518.5
400	937.745	532.498	533.298	1.6008	3.6318	4.2542	1510.7
410	929.145	575.131	575.938	1.7061	3.5838	4.2744	1493.2
420	920.104	617.982	618.797	1.8094	3.5373	4.2980	1473.3
430	910.613	661.087	661.910	1.9108	3.4924	4.3254	1451.1
440	900.659	704.486	705.319	2.0106	3.4493	4.3570	1426.6
440.899[b]	899.741	708.402	709.235	2.0195	3.4455	4.3601	1424.3
440.899[c]	3.9137	2574.01	2765.64	6.6836	1.8502	2.5695	498.34
450	3.8109	2591.53	2788.34	6.7346	1.7612	2.4320	505.86
460	3.7073	2609.88	2812.19	6.7870	1.7085	2.3456	513.27
470	3.6113	2627.65	2835.34	6.8368	1.6746	2.2872	520.21
480	3.5217	2645.02	2857.98	6.8845	1.6504	2.2438	526.85
490	3.4377	2662.08	2880.25	6.9304	1.6323	2.2101	533.24
500	3.3586	2678.90	2902.21	6.9747	1.6188	2.1837	539.44
510	3.2838	2695.54	2923.94	7.0178	1.6086	2.1627	545.46
520	3.2129	2712.05	2945.48	7.0596	1.6013	2.1462	551.33
530	3.1456	2728.44	2966.87	7.1003	1.5961	2.1331	557.06
540	3.0814	2744.76	2988.15	7.1401	1.5926	2.1229	562.68
550	3.0202	2761.01	3009.34	7.1790	1.5907	2.1151	568.18
560	2.9616	2777.22	3030.46	7.2171	1.5899	2.1091	573.57
570	2.9056	2793.40	3051.53	7.2543	1.5901	2.1048	578.88
580	2.8518	2809.57	3072.56	7.2909	1.5912	2.1018	584.10
590	2.8002	2825.73	3093.57	7.3268	1.5929	2.1000	589.23
600	2.7506	2841.90	3114.56	7.3621	1.5953	2.0991	594.29
610	2.7029	2858.07	3135.55	7.3968	1.5982	2.0991	599.28
620	2.6569	2874.26	3156.55	7.4310	1.6015	2.0998	604.20
630	2.6125	2890.48	3177.55	7.4646	1.6052	2.1011	609.06
640	2.5698	2906.72	3198.57	7.4977	1.6092	2.1030	613.85
650	2.5284	2922.99	3219.61	7.5303	1.6135	2.1053	618.59
675	2.4310	2963.83	3272.34	7.6099	1.6253	2.1129	630.20
700	2.3412	3004.93	3325.28	7.6869	1.6383	2.1225	641.49
725	2.2580	3046.33	3378.47	7.7616	1.6523	2.1337	652.50
750	2.1807	3088.05	3431.97	7.8341	1.6670	2.1460	663.25
775	2.1087	3130.12	3485.78	7.9047	1.6822	2.1593	673.75
800	2.0415	3172.56	3539.94	7.9735	1.6980	2.1734	684.03
825	1.9785	3215.37	3594.46	8.0406	1.7141	2.1881	694.10
850	1.9193	3258.58	3649.35	8.1061	1.7306	2.2033	703.97
900	1.8112	3346.21	3760.30	8.2329	1.7643	2.2350	723.18
950	1.7147	3435.49	3872.87	8.3547	1.7986	2.2678	741.72
1000	1.6282	3526.46	3987.10	8.4718	1.8332	2.3013	759.69
1050	1.5500	3619.14	4103.00	8.5849	1.8679	2.3350	777.13
1100	1.4791	3713.53	4220.60	8.6943	1.9024	2.3687	794.10
1150	1.4144	3809.62	4339.87	8.8004	1.9365	2.4022	810.64
1200	1.3552	3907.38	4460.80	8.9033	1.9701	2.4352	826.80
1250	1.3008	4006.79	4583.38	9.0034	2.0029	2.4676	842.60
1273	1.2772	4053.07	4640.30	9.0485	2.0177	2.4822	849.75
			1.0 MPa				
273.086[a]	1000.30	−0.294	0.706	−0.0011	4.2129	4.2152	1403.5
275	1000.39	7.769	8.768	0.0283	4.2087	4.2093	1413.0

TABLE 13.2. Thermodynamic properties of water in the single-phase region—Continued

T K	ρ kg m^{-3}	u kJ kg^{-1}	h kJ kg^{-1}	s kJ kg^{-1} K^{-1}	c_v kJ kg^{-1} K^{-1}	c_p kJ kg^{-1} K^{-1}	w m s^{-1}
			1.0 MPa—Continued				
280	1000.35	28.783	29.783	0.1041	4.1960	4.1973	1435.7
285	999.942	49.747	50.747	0.1783	4.1812	4.1891	1455.9
290	999.220	70.677	71.678	0.2511	4.1647	4.1836	1473.7
295	998.216	91.585	92.587	0.3226	4.1466	4.1802	1489.4
300	996.960	112.479	113.482	0.3928	4.1272	4.1781	1503.0
305	995.475	133.365	134.370	0.4619	4.1066	4.1771	1514.8
310	993.779	154.248	155.255	0.5298	4.0850	4.1770	1524.9
315	991.890	175.132	176.141	0.5966	4.0624	4.1774	1533.4
320	989.819	196.020	197.030	0.6624	4.0390	4.1784	1540.5
325	987.579	216.913	217.926	0.7272	4.0149	4.1798	1546.1
330	985.179	237.814	238.829	0.7910	3.9902	4.1816	1550.5
335	982.627	258.725	259.743	0.8539	3.9650	4.1838	1553.7
340	979.931	279.647	280.668	0.9159	3.9395	4.1863	1555.7
345	977.096	300.583	301.606	0.9771	3.9136	4.1892	1556.7
350	974.129	321.534	322.561	1.0374	3.8876	4.1925	1556.7
355	971.033	342.502	343.532	1.0969	3.8615	4.1962	1555.8
360	967.812	363.490	364.523	1.1556	3.8353	4.2004	1553.9
365	964.470	384.500	385.537	1.2136	3.8092	4.2050	1551.2
370	961.010	405.533	406.574	1.2708	3.7831	4.2101	1547.7
375	957.434	426.594	427.638	1.3274	3.7572	4.2158	1543.4
380	953.744	447.684	448.733	1.3832	3.7315	4.2220	1538.4
385	949.942	468.807	469.860	1.4385	3.7061	4.2289	1532.6
390	946.029	489.965	491.022	1.4931	3.6809	4.2364	1526.2
395	942.006	511.163	512.225	1.5471	3.6560	4.2446	1519.1
400	937.873	532.403	533.469	1.6005	3.6315	4.2535	1511.3
410	929.279	575.026	576.102	1.7058	3.5835	4.2737	1493.9
420	920.244	617.867	618.954	1.8091	3.5370	4.2972	1474.0
430	910.760	660.961	662.059	1.9105	3.4922	4.3245	1451.8
440	900.814	704.348	705.458	2.0103	3.4491	4.3561	1427.3
450	890.386	748.074	749.197	2.1086	3.4076	4.3924	1400.6
453.028[b]	887.129	761.388	762.515	2.1381	3.3954	4.4045	1392.0
453.028[c]	5.1450	2582.75	2777.11	6.5850	1.9271	2.7114	501.02
460	5.0376	2596.98	2795.49	6.6253	1.8387	2.5726	507.19
470	4.8960	2616.33	2820.57	6.6792	1.7677	2.4551	515.05
480	4.7658	2634.89	2844.72	6.7301	1.7239	2.3787	522.29
490	4.6451	2652.93	2868.22	6.7785	1.6930	2.3227	529.16
500	4.5323	2670.58	2891.22	6.8250	1.6699	2.2795	535.74
510	4.4265	2687.92	2913.84	6.8698	1.6523	2.2453	542.09
520	4.3268	2705.03	2936.15	6.9131	1.6389	2.2180	548.25
530	4.2325	2721.95	2958.21	6.9551	1.6288	2.1962	554.23
540	4.1431	2738.72	2980.09	6.9960	1.6213	2.1787	560.06
550	4.0581	2755.38	3001.80	7.0359	1.6159	2.1647	565.75
560	3.9771	2771.95	3023.39	7.0748	1.6123	2.1536	571.33
570	3.8998	2788.46	3044.88	7.1128	1.6101	2.1448	576.79
580	3.8258	2804.91	3066.29	7.1501	1.6090	2.1380	582.15
590	3.7550	2821.34	3087.65	7.1866	1.6090	2.1329	587.41
600	3.6871	2837.74	3108.96	7.2224	1.6098	2.1292	592.58
610	3.6218	2854.13	3130.23	7.2575	1.6114	2.1266	597.68
620	3.5591	2870.52	3151.49	7.2921	1.6135	2.1251	602.70
630	3.4986	2886.91	3172.74	7.3261	1.6161	2.1245	607.64
640	3.4404	2903.32	3193.98	7.3596	1.6193	2.1246	612.52
650	3.3843	2919.75	3215.23	7.3925	1.6227	2.1254	617.34
675	3.2521	2960.92	3268.41	7.4728	1.6329	2.1297	629.11
700	3.1305	3002.31	3321.74	7.5504	1.6447	2.1368	640.55

TABLE 13.2. Thermodynamic properties of water in the single-phase region—Continued

T K	ρ kg m^{-3}	u kJ kg^{-1}	h kJ kg^{-1}	s kJ kg^{-1} K^{-1}	c_v kJ kg^{-1} K^{-1}	c_p kJ kg^{-1} K^{-1}	w m s^{-1}
			1.0 MPa—Continued				
725	3.0182	3043.95	3375.27	7.6255	1.6576	2.1459	651.68
750	2.9140	3085.88	3429.05	7.6984	1.6715	2.1566	662.53
775	2.8170	3128.13	3483.11	7.7693	1.6862	2.1686	673.12
800	2.7265	3170.72	3537.49	7.8384	1.7014	2.1816	683.48
825	2.6418	3213.67	3592.20	7.9057	1.7171	2.1953	693.61
850	2.5624	3257.00	3647.26	7.9715	1.7332	2.2098	703.55
900	2.4174	3344.83	3758.50	8.0986	1.7663	2.2402	722.85
950	2.2882	3434.27	3871.30	8.2206	1.8003	2.2721	741.47
1000	2.1723	3525.38	3985.72	8.3380	1.8346	2.3048	759.50
1050	2.0678	3618.18	4101.79	8.4512	1.8691	2.3380	777.00
1100	1.9729	3712.66	4219.52	8.5608	1.9034	2.3713	794.01
1150	1.8865	3808.83	4338.91	8.6669	1.9373	2.4044	810.59
1200	1.8074	3906.66	4459.95	8.7699	1.9708	2.4371	826.77
1250	1.7347	4006.13	4582.61	8.8701	2.0035	2.4692	842.60
1273	1.7032	4052.43	4639.57	8.9152	2.0183	2.4838	849.77
			2.0 MPa				
273.012[a]	1000.80	−0.587	1.411	−0.0022	4.2084	4.2105	1404.7
275	1000.89	7.778	9.776	0.0284	4.2042	4.2046	1414.6
280	1000.83	28.770	30.769	0.1040	4.1918	4.1932	1437.3
285	1000.41	49.715	51.714	0.1782	4.1773	4.1855	1457.5
290	999.682	70.627	72.628	0.2509	4.1610	4.1804	1475.4
295	998.670	91.518	93.521	0.3223	4.1432	4.1771	1491.0
300	997.408	112.397	114.402	0.3925	4.1239	4.1753	1504.7
305	995.917	133.268	135.276	0.4615	4.1035	4.1745	1516.5
310	994.218	154.136	156.148	0.5294	4.0820	4.1745	1526.7
315	992.326	175.006	177.022	0.5962	4.0596	4.1750	1535.2
320	990.254	195.880	197.899	0.6620	4.0364	4.1761	1542.3
325	988.014	216.759	218.783	0.7267	4.0124	4.1776	1547.9
330	985.614	237.646	239.676	0.7905	3.9878	4.1794	1552.3
335	983.064	258.544	260.578	0.8534	3.9628	4.1816	1555.5
340	980.370	279.452	281.492	0.9154	3.9373	4.1842	1557.6
345	977.538	300.374	302.420	0.9765	3.9116	4.1871	1558.6
350	974.573	321.311	323.363	1.0367	3.8857	4.1903	1558.7
355	971.481	342.266	344.324	1.0962	3.8596	4.1940	1557.8
360	968.265	363.239	365.305	1.1549	3.8335	4.1982	1555.9
365	964.928	384.234	386.307	1.2128	3.8075	4.2027	1553.3
370	961.474	405.253	407.333	1.2700	3.7815	4.2078	1549.8
375	957.905	426.298	428.386	1.3266	3.7557	4.2135	1545.6
380	954.222	447.372	449.468	1.3824	3.7301	4.2197	1540.6
385	950.427	468.479	470.583	1.4376	3.7047	4.2265	1534.9
390	946.523	489.621	491.734	1.4922	3.6796	4.2339	1528.5
395	942.508	510.801	512.923	1.5462	3.6548	4.2420	1521.4
400	938.385	532.024	534.155	1.5996	3.6303	4.2508	1513.7
410	929.812	574.610	576.761	1.7048	3.5824	4.2708	1496.4
420	920.802	617.410	619.582	1.8080	3.5361	4.2941	1476.7
430	911.346	660.460	662.654	1.9093	3.4913	4.3211	1454.6
440	901.432	703.798	706.017	2.0090	3.4483	4.3522	1430.3
450	891.041	747.470	749.715	2.1072	3.4069	4.3881	1403.7
460	880.147	791.525	793.797	2.2041	3.3672	4.4294	1375.0
470	868.716	836.021	838.323	2.2999	3.3292	4.4768	1343.9
480	856.705	881.024	883.358	2.3947	3.2930	4.5316	1310.6
485.527[b]	849.798	906.145	908.498	2.4468	3.2737	4.5655	1291.2
485.527[c]	10.042	2599.12	2798.29	6.3390	2.1585	3.1910	504.70
490	9.8890	2609.96	2812.20	6.3675	2.0682	3.0364	509.47

TABLE 13.2. Thermodynamic properties of water in the single-phase region—Continued

T K	ρ kg m^{-3}	u kJ kg^{-1}	h kJ kg^{-1}	s kJ kg^{-1} K^{-1}	c_v kJ kg^{-1} K^{-1}	c_p kJ kg^{-1} K^{-1}	w m s^{-1}
			2.0 MPa—Continued				
500	9.5781	2632.56	2841.37	6.4265	1.9462	2.8185	518.77
510	9.2990	2653.76	2868.83	6.4808	1.8738	2.6822	527.02
520	9.0447	2674.02	2895.14	6.5319	1.8233	2.5841	534.66
530	8.8105	2693.59	2920.59	6.5804	1.7853	2.5087	541.89
540	8.5934	2712.63	2945.37	6.6267	1.7558	2.4489	548.78
550	8.3908	2731.25	2969.61	6.6712	1.7326	2.4007	555.40
560	8.2008	2749.53	2993.41	6.7141	1.7143	2.3614	561.78
570	8.0219	2767.54	3016.86	6.7556	1.6999	2.3292	567.96
580	7.8530	2785.33	3040.02	6.7959	1.6886	2.3028	573.96
590	7.6928	2802.95	3062.93	6.8350	1.6799	2.2809	579.79
600	7.5406	2820.42	3085.65	6.8732	1.6733	2.2629	585.49
610	7.3957	2837.77	3108.20	6.9105	1.6685	2.2480	591.05
620	7.2573	2855.03	3130.62	6.9470	1.6652	2.2358	596.49
630	7.1250	2872.22	3152.92	6.9826	1.6631	2.2258	601.82
640	6.9983	2889.35	3175.14	7.0176	1.6621	2.2177	607.06
650	6.8767	2906.44	3197.28	7.0520	1.6619	2.2112	612.20
675	6.5930	2949.07	3252.42	7.1352	1.6647	2.2008	624.68
700	6.3346	2991.65	3307.37	7.2151	1.6710	2.1965	636.71
725	6.0978	3034.29	3362.28	7.2922	1.6797	2.1968	648.34
750	5.8796	3077.08	3417.24	7.3667	1.6902	2.2004	659.61
775	5.6776	3120.06	3472.32	7.4390	1.7022	2.2067	670.57
800	5.4901	3163.30	3527.59	7.5092	1.7153	2.2150	681.24
825	5.3152	3206.81	3583.08	7.5775	1.7292	2.2248	691.65
850	5.1518	3250.63	3638.84	7.6441	1.7438	2.2360	701.83
900	4.8547	3339.29	3751.26	7.7726	1.7747	2.2613	721.53
950	4.5912	3429.40	3865.02	7.8956	1.8070	2.2893	740.48
1000	4.3558	3521.06	3980.22	8.0137	1.8401	2.3191	758.77
1050	4.1439	3614.31	4096.94	8.1276	1.8736	2.3500	776.47
1100	3.9521	3709.17	4215.23	8.2377	1.9072	2.3815	793.66
1150	3.7777	3805.67	4335.10	8.3443	1.9406	2.4132	810.38
1200	3.6182	3903.78	4456.54	8.4476	1.9735	2.4447	826.69
1250	3.4719	4003.50	4579.56	8.5481	2.0059	2.4759	842.62
1273	3.4085	4049.90	4636.67	8.5933	2.0205	2.4901	849.82
			3.0 MPa				
272.938[a]	1001.30	−0.880	2.116	−0.0032	4.2039	4.2059	1406.0
275	1001.39	7.786	10.782	0.0284	4.1997	4.2000	1416.2
280	1001.32	28.757	31.753	0.1040	4.1877	4.1892	1439.0
285	1000.89	49.683	52.680	0.1781	4.1734	4.1819	1459.2
290	1000.14	70.577	73.577	0.2507	4.1574	4.1771	1477.0
295	999.123	91.452	94.455	0.3221	4.1397	4.1742	1492.7
300	997.854	112.314	115.321	0.3923	4.1207	4.1725	1506.4
305	996.359	133.170	136.181	0.4612	4.1005	4.1719	1518.3
310	994.657	154.025	157.041	0.5291	4.0791	4.1720	1528.4
315	992.762	174.880	177.902	0.5958	4.0569	4.1726	1536.9
320	990.689	195.740	198.768	0.6615	4.0337	4.1738	1544.0
325	988.448	216.606	219.641	0.7263	4.0099	4.1753	1549.7
330	986.049	237.479	240.522	0.7900	3.9855	4.1772	1554.2
335	983.499	258.363	261.413	0.8529	3.9605	4.1794	1557.4
340	980.807	279.258	282.317	0.9148	3.9352	4.1820	1559.5
345	977.978	300.166	303.234	0.9759	3.9096	4.1849	1560.6
350	975.017	321.089	324.166	1.0361	3.8837	4.1882	1560.6
355	971.928	342.030	345.116	1.0955	3.8578	4.1919	1559.7
360	968.717	362.989	366.086	1.1542	3.8318	4.1960	1558.0
365	965.385	383.969	387.077	1.2121	3.8058	4.2005	1555.4

TABLE 13.2. Thermodynamic properties of water in the single-phase region—Continued

T K	ρ kg m^{-3}	u kJ kg^{-1}	h kJ kg^{-1}	s kJ kg^{-1} K^{-1}	c_v kJ kg^{-1} K^{-1}	c_p kJ kg^{-1} K^{-1}	w m s^{-1}
			3.0 MPa—Continued				
370	961.937	404.973	408.092	1.2693	3.7799	4.2056	1551.9
375	958.373	426.003	429.134	1.3258	3.7542	4.2112	1547.7
380	954.698	447.062	450.204	1.3816	3.7287	4.2173	1542.8
385	950.911	468.153	471.308	1.4368	3.7033	4.2240	1537.1
390	947.014	489.278	492.446	1.4913	3.6783	4.2314	1530.8
395	943.009	510.442	513.623	1.5453	3.6535	4.2395	1523.8
400	938.895	531.646	534.842	1.5986	3.6291	4.2482	1516.1
410	930.344	574.195	577.420	1.7038	3.5813	4.2679	1498.9
420	921.358	616.955	620.211	1.8069	3.5351	4.2910	1479.3
430	911.930	659.961	663.251	1.9082	3.4904	4.3177	1457.4
440	902.048	703.252	706.578	2.0078	3.4474	4.3484	1433.3
450	891.693	746.871	750.235	2.1059	3.4061	4.3839	1406.9
460	880.841	790.867	794.273	2.2027	3.3665	4.4245	1378.3
470	869.458	835.296	838.746	2.2983	3.3286	4.4713	1347.5
480	857.504	880.224	883.722	2.3930	3.2924	4.5252	1314.4
490	844.924	925.728	929.278	2.4869	3.2579	4.5876	1279.0
500	831.652	971.901	975.508	2.5803	3.2253	4.6603	1241.2
507.003[b]	821.900	1004.69	1008.34	2.6455	3.2035	4.7186	1213.1
507.003[c]	15.001	2603.16	2803.15	6.1856	2.3282	3.6119	504.03
510	14.828	2611.44	2813.76	6.2064	2.2525	3.4692	507.69
520	14.309	2637.05	2846.71	6.2704	2.0903	3.1531	518.33
530	13.852	2660.63	2877.21	6.3285	1.9946	2.9578	527.55
540	13.442	2682.88	2906.05	6.3825	1.9279	2.8186	535.96
550	13.070	2704.16	2933.69	6.4332	1.8776	2.7122	543.81
560	12.729	2724.69	2960.37	6.4812	1.8383	2.6280	551.23
570	12.413	2744.62	2986.30	6.5271	1.8070	2.5601	558.31
580	12.119	2764.08	3011.61	6.5712	1.7820	2.5047	565.09
590	11.845	2783.15	3036.43	6.6136	1.7620	2.4590	571.61
600	11.587	2801.90	3060.82	6.6546	1.7459	2.4212	577.91
610	11.343	2820.39	3084.87	6.6943	1.7331	2.3896	584.01
620	11.113	2838.67	3108.63	6.7330	1.7230	2.3633	589.94
630	10.894	2856.78	3132.15	6.7706	1.7150	2.3411	595.71
640	10.687	2874.74	3155.47	6.8073	1.7090	2.3226	601.34
650	10.488	2892.58	3178.61	6.8432	1.7045	2.3070	606.85
675	10.030	2936.81	3235.90	6.9297	1.6987	2.2785	620.11
700	9.6174	2980.69	3292.62	7.0122	1.6987	2.2608	632.77
725	9.2424	3024.42	3349.01	7.0914	1.7026	2.2509	644.92
750	8.8993	3068.11	3405.22	7.1676	1.7096	2.2466	656.64
775	8.5837	3111.87	3461.37	7.2412	1.7187	2.2465	667.98
800	8.2920	3155.77	3517.57	7.3126	1.7294	2.2496	678.98
825	8.0212	3199.87	3573.87	7.3819	1.7415	2.2553	689.67
850	7.7690	3244.20	3630.35	7.4493	1.7546	2.2630	700.10
900	7.3124	3333.71	3743.97	7.5792	1.7831	2.2827	720.21
950	6.9095	3424.51	3858.69	7.7033	1.8137	2.3068	739.49
1000	6.5506	3516.72	3974.69	7.8223	1.8456	2.3336	758.03
1050	6.2285	3610.43	4092.08	7.9368	1.8781	2.3621	775.95
1100	5.9377	3705.68	4210.93	8.0474	1.9110	2.3918	793.31
1150	5.6736	3802.50	4331.27	8.1544	1.9438	2.4220	810.18
1200	5.4325	3900.90	4453.13	8.2581	1.9763	2.4524	826.61
1250	5.2116	4000.86	4576.51	8.3588	2.0083	2.4826	842.64
1273	5.1160	4047.37	4633.76	8.4042	2.0228	2.4964	849.89
			4.0 MPa				
272.863[a]	1001.80	−1.178	2.815	−0.0043	4.1995	4.2013	1407.2
275	1001.89	7.794	11.787	0.0284	4.1953	4.1955	1417.8
280	1001.80	28.744	32.737	0.1039	4.1835	4.1853	1440.6

TABLE 13.2. Thermodynamic properties of water in the single-phase region—Continued

T K	ρ kg m^{-3}	u kJ kg^{-1}	h kJ kg^{-1}	s kJ kg^{-1} K^{-1}	c_v kJ kg^{-1} K^{-1}	c_p kJ kg^{-1} K^{-1}	w m s^{-1}
			4.0 MPa—Continued				
285	1001.36	49.650	53.645	0.1779	4.1696	4.1784	1460.8
290	1000.60	70.527	74.525	0.2506	4.1537	4.1739	1478.7
295	999.575	91.385	95.387	0.3219	4.1363	4.1712	1494.4
300	998.300	112.232	116.239	0.3920	4.1175	4.1698	1508.1
305	996.800	133.074	137.086	0.4609	4.0974	4.1693	1520.0
310	995.094	153.913	157.933	0.5287	4.0762	4.1695	1530.1
315	993.197	174.755	178.782	0.5954	4.0541	4.1703	1538.7
320	991.123	195.601	199.636	0.6611	4.0311	4.1715	1545.8
325	988.881	216.453	220.498	0.7258	4.0074	4.1731	1551.5
330	986.482	237.313	241.368	0.7895	3.9831	4.1750	1556.0
335	983.934	258.183	262.248	0.8523	3.9583	4.1773	1559.3
340	981.244	279.064	283.141	0.9142	3.9331	4.1798	1561.4
345	978.417	299.959	304.047	0.9753	3.9076	4.1828	1562.5
350	975.459	320.869	324.969	1.0355	3.8818	4.1860	1562.6
355	972.374	341.795	345.908	1.0949	3.8560	4.1897	1561.7
360	969.167	362.740	366.867	1.1535	3.8301	4.1938	1560.0
365	965.841	383.706	387.847	1.2114	3.8042	4.1983	1557.4
370	962.398	404.695	408.851	1.2685	3.7784	4.2034	1554.0
375	958.841	425.710	429.882	1.3250	3.7527	4.2089	1549.9
380	955.172	446.753	450.941	1.3808	3.7272	4.2150	1545.0
385	951.393	467.828	472.032	1.4359	3.7020	4.2217	1539.4
390	947.505	488.937	493.159	1.4904	3.6770	4.2290	1533.1
395	943.508	510.084	514.323	1.5444	3.6523	4.2369	1526.1
400	939.404	531.271	535.529	1.5977	3.6279	4.2456	1518.5
410	930.873	573.783	578.080	1.7028	3.5803	4.2651	1501.4
420	921.911	616.503	620.842	1.8058	3.5341	4.2879	1482.0
430	912.511	659.466	663.849	1.9070	3.4896	4.3143	1460.2
440	902.660	702.709	707.140	2.0065	3.4466	4.3447	1436.2
450	892.342	746.275	750.758	2.1046	3.4054	4.3796	1410.0
460	881.531	790.213	794.750	2.2012	3.3658	4.4198	1381.6
470	870.196	834.577	839.173	2.2968	3.3279	4.4658	1351.0
480	858.296	879.430	884.091	2.3913	3.2918	4.5189	1318.2
490	845.782	924.849	929.578	2.4851	3.2573	4.5802	1283.1
500	832.586	970.923	975.728	2.5784	3.2247	4.6515	1245.6
510	818.627	1017.76	1022.65	2.6713	3.1939	4.7352	1205.5
520	803.796	1065.51	1070.48	2.7642	3.1651	4.8345	1162.5
523.504[b]	798.368	1082.48	1087.49	2.7968	3.1555	4.8739	1146.8
523.504[c]	20.090	2601.72	2800.82	6.0696	2.4686	4.0203	501.55
530	19.553	2621.17	2825.75	6.1169	2.3067	3.6795	509.97
540	18.831	2648.36	2860.77	6.1824	2.1565	3.3517	520.97
550	18.202	2673.38	2893.14	6.2418	2.0595	3.1346	530.63
560	17.642	2696.92	2923.65	6.2968	1.9887	2.9751	539.46
570	17.136	2719.34	2952.76	6.3483	1.9342	2.8518	547.68
580	16.675	2740.89	2980.77	6.3970	1.8909	2.7536	555.42
590	16.251	2761.75	3007.90	6.4434	1.8562	2.6742	562.77
600	15.857	2782.05	3034.30	6.4878	1.8282	2.6090	569.79
610	15.491	2801.90	3060.11	6.5304	1.8055	2.5551	576.53
620	15.147	2821.36	3085.43	6.5716	1.7871	2.5102	583.02
630	14.825	2840.52	3110.34	6.6114	1.7722	2.4725	589.29
640	14.520	2859.43	3134.90	6.6501	1.7602	2.4408	595.37
650	14.232	2878.11	3159.17	6.6878	1.7506	2.4139	601.27
675	13.572	2924.12	3218.85	6.7778	1.7349	2.3634	615.39
700	12.985	2969.43	3277.49	6.8632	1.7278	2.3300	628.73
725	12.456	3014.32	3335.45	6.9445	1.7266	2.3084	641.44

TABLE 13.2. Thermodynamic properties of water in the single-phase region—Continued

T K	ρ kg m^{-3}	u kJ kg^{-1}	h kJ kg^{-1}	s kJ kg^{-1} K^{-1}	c_v kJ kg^{-1} K^{-1}	c_p kJ kg^{-1} K^{-1}	w m s^{-1}
			4.0 MPa—Continued				
750	11.976	3058.98	3392.98	7.0225	1.7295	2.2952	653.63
775	11.537	3103.55	3450.26	7.0977	1.7356	2.2881	665.36
800	11.134	3148.15	3507.42	7.1702	1.7439	2.2856	676.69
825	10.761	3192.85	3564.57	7.2406	1.7540	2.2867	687.68
850	10.415	3237.71	3621.78	7.3089	1.7655	2.2906	698.36
900	9.7910	3328.09	3736.63	7.4402	1.7916	2.3047	718.89
950	9.2430	3419.58	3852.34	7.5653	1.8205	2.3245	738.49
1000	8.7568	3512.36	3969.15	7.6851	1.8511	2.3482	757.30
1050	8.3217	3606.53	4087.20	7.8003	1.8827	2.3744	775.43
1100	7.9296	3702.18	4206.61	7.9114	1.9148	2.4022	792.97
1150	7.5742	3799.33	4327.44	8.0188	1.9471	2.4309	809.98
1200	7.2504	3898.02	4449.71	8.1229	1.9791	2.4601	826.53
1250	6.9538	3998.22	4573.45	8.2239	2.0107	2.4893	842.66
1273	6.8256	4044.83	4630.86	8.2694	2.0251	2.5027	849.95
			5.0 MPa				
272.788[a]	1002.30	−1.475	3.513	−0.0054	4.1950	4.1967	1408.4
275	1002.38	7.802	12.790	0.0284	4.1908	4.1910	1419.4
280	1002.28	28.731	33.719	0.1039	4.1794	4.1813	1442.2
285	1001.82	49.618	54.609	0.1778	4.1657	4.1749	1462.4
290	1001.06	70.477	75.472	0.2504	4.1501	4.1707	1480.3
295	1000.03	91.319	96.319	0.3217	4.1329	4.1683	1496.0
300	998.745	112.150	117.157	0.3917	4.1142	4.1670	1509.8
305	997.240	132.977	137.991	0.4606	4.0943	4.1667	1521.7
310	995.530	153.802	158.825	0.5283	4.0733	4.1670	1531.8
315	993.631	174.630	179.662	0.5950	4.0514	4.1679	1540.4
320	991.555	195.462	200.505	0.6607	4.0285	4.1692	1547.6
325	989.313	216.300	221.354	0.7253	4.0050	4.1708	1553.3
330	986.915	237.147	242.214	0.7890	3.9808	4.1728	1557.8
335	984.368	258.004	263.083	0.8518	3.9561	4.1751	1561.1
340	981.679	278.872	283.965	0.9136	3.9310	4.1777	1563.3
345	978.855	299.753	304.861	0.9747	3.9055	4.1806	1564.4
350	975.900	320.649	325.772	1.0348	3.8799	4.1839	1564.5
355	972.819	341.561	346.701	1.0942	3.8541	4.1876	1563.7
360	969.617	362.492	367.648	1.1528	3.8283	4.1916	1562.0
365	966.295	383.443	388.618	1.2106	3.8025	4.1961	1559.5
370	962.858	404.418	409.611	1.2678	3.7768	4.2011	1556.1
375	959.307	425.418	430.630	1.3242	3.7512	4.2066	1552.0
380	955.645	446.446	451.678	1.3800	3.7258	4.2127	1547.2
385	951.873	467.505	472.757	1.4351	3.7006	4.2193	1541.6
390	947.993	488.597	493.872	1.4896	3.6757	4.2265	1535.4
395	944.005	509.727	515.024	1.5434	3.6511	4.2344	1528.4
400	939.910	530.897	536.217	1.5968	3.6268	4.2430	1520.9
410	931.401	573.372	578.741	1.7018	3.5792	4.2623	1503.9
420	922.463	616.053	621.473	1.8047	3.5331	4.2848	1484.6
430	913.090	658.973	664.449	1.9059	3.4887	4.3109	1463.0
440	903.270	702.169	707.705	2.0053	3.4458	4.3410	1439.1
450	892.987	745.684	751.283	2.1032	3.4046	4.3755	1413.1
460	882.217	789.564	795.231	2.1998	3.3651	4.4151	1384.9
470	870.929	833.863	839.604	2.2953	3.3273	4.4605	1354.6
480	859.084	878.643	884.463	2.3897	3.2911	4.5127	1322.0
490	846.632	923.978	929.884	2.4833	3.2567	4.5729	1287.2
500	833.512	969.955	975.954	2.5764	3.2240	4.6429	1250.0
510	819.642	1016.68	1022.78	2.6691	3.1932	4.7248	1210.2
520	804.920	1064.29	1070.50	2.7618	3.1644	4.8219	1167.8

TABLE 13.2. Thermodynamic properties of water in the single-phase region—Continued

T K	ρ kg m^{-3}	u kJ kg^{-1}	h kJ kg^{-1}	s kJ kg^{-1} K^{-1}	c_v kJ kg^{-1} K^{-1}	c_p kJ kg^{-1} K^{-1}	w m s^{-1}
			5.0 MPa—Continued				
530	789.208	1112.95	1119.28	2.8547	3.1377	4.9386	1122.2
537.091[b]	777.369	1148.21	1154.64	2.9210	3.1204	5.0368	1087.8
537.091[c]	25.351	2596.98	2794.21	5.9737	2.5922	4.4380	498.04
540	25.004	2606.83	2806.80	5.9971	2.5029	4.2299	502.38
550	23.951	2637.70	2846.46	6.0698	2.2995	3.7464	515.19
560	23.058	2665.47	2882.31	6.1345	2.1745	3.4437	526.08
570	22.279	2691.20	2915.62	6.1934	2.0857	3.2283	535.84
580	21.586	2715.42	2947.05	6.2481	2.0178	3.0649	544.81
590	20.962	2738.51	2977.03	6.2993	1.9642	2.9365	553.18
600	20.393	2760.69	3005.87	6.3478	1.9212	2.8334	561.07
610	19.871	2782.14	3033.77	6.3939	1.8863	2.7494	568.55
620	19.387	2803.00	3060.90	6.4380	1.8580	2.6801	575.68
630	18.938	2823.38	3087.41	6.4805	1.8348	2.6225	582.52
640	18.517	2843.36	3113.38	6.5214	1.8158	2.5741	589.10
650	18.122	2863.00	3138.91	6.5609	1.8004	2.5333	595.46
675	17.228	2910.99	3201.22	6.6550	1.7734	2.4563	610.51
700	16.442	2957.85	3261.94	6.7433	1.7584	2.4045	624.59
725	15.743	3003.98	3321.59	6.8271	1.7515	2.3695	637.89
750	15.113	3049.66	3380.51	6.9070	1.7501	2.3463	650.57
775	14.540	3095.10	3438.97	6.9837	1.7529	2.3315	662.71
800	14.017	3140.42	3497.14	7.0575	1.7587	2.3229	674.39
825	13.535	3185.75	3555.16	7.1289	1.7667	2.3192	685.68
850	13.090	3231.15	3613.13	7.1982	1.7766	2.3191	696.61
900	12.291	3322.43	3729.24	7.3309	1.8002	2.3271	717.57
950	11.592	3414.63	3845.96	7.4571	1.8273	2.3426	737.50
1000	10.975	3507.98	3963.58	7.5778	1.8566	2.3630	756.57
1050	10.423	3602.63	4082.31	7.6936	1.8872	2.3868	774.92
1100	9.9280	3698.67	4202.29	7.8052	1.9186	2.4127	792.63
1150	9.4796	3796.16	4323.60	7.9131	1.9503	2.4399	809.78
1200	9.0717	3895.13	4446.29	8.0175	1.9819	2.4678	826.45
1250	8.6986	3995.58	4570.39	8.1188	2.0131	2.4960	842.69
1273	8.5374	4042.29	4627.95	8.1645	2.0274	2.5090	850.02
			6.0 MPa				
272.713[a]	1002.80	−1.772	4.211	−0.0065	4.1906	4.1921	1409.6
275	1002.88	7.809	13.792	0.0285	4.1864	4.1866	1421.0
280	1002.76	28.717	34.700	0.1038	4.1753	4.1774	1443.8
285	1002.29	49.585	55.571	0.1777	4.1619	4.1714	1464.1
290	1001.52	70.427	76.418	0.2502	4.1465	4.1676	1482.0
295	1000.48	91.253	97.250	0.3214	4.1295	4.1654	1497.7
300	999.189	112.069	118.074	0.3914	4.1110	4.1643	1511.4
305	997.679	132.880	138.894	0.4603	4.0913	4.1641	1523.4
310	995.966	153.692	159.716	0.5280	4.0705	4.1646	1533.6
315	994.064	174.505	180.541	0.5946	4.0486	4.1656	1542.2
320	991.987	195.324	201.372	0.6602	4.0260	4.1669	1549.3
325	989.744	216.149	222.211	0.7248	4.0025	4.1686	1555.1
330	987.346	236.982	243.059	0.7885	3.9784	4.1706	1559.6
335	984.800	257.825	263.918	0.8512	3.9539	4.1730	1563.0
340	982.113	278.680	284.789	0.9131	3.9289	4.1756	1565.2
345	979.291	299.547	305.674	0.9741	3.9035	4.1785	1566.3
350	976.340	320.429	326.575	1.0342	3.8780	4.1818	1566.5
355	973.263	341.328	347.493	1.0935	3.8523	4.1854	1565.7
360	970.065	362.245	368.430	1.1521	3.8266	4.1895	1564.0
365	966.748	383.182	389.388	1.2099	3.8009	4.1940	1561.5
370	963.317	404.142	410.370	1.2670	3.7752	4.1989	1558.2

TABLE 13.2. Thermodynamic properties of water in the single-phase region—Continued

T K	ρ kg m^{-3}	u kJ kg^{-1}	h kJ kg^{-1}	s kJ kg^{-1} K^{-1}	c_v kJ kg^{-1} K^{-1}	c_p kJ kg^{-1} K^{-1}	w m s^{-1}
			6.0 MPa—Continued				
375	959.772	425.127	431.379	1.3234	3.7497	4.2044	1554.1
380	956.117	446.140	452.415	1.3791	3.7244	4.2104	1549.3
385	952.352	467.183	473.483	1.4342	3.6993	4.2169	1543.8
390	948.480	488.259	494.585	1.4887	3.6744	4.2241	1537.6
395	944.501	509.373	515.725	1.5425	3.6499	4.2319	1530.8
400	940.415	530.525	536.905	1.5958	3.6256	4.2404	1523.3
410	931.926	572.964	579.402	1.7008	3.5782	4.2595	1506.4
420	923.012	615.606	622.106	1.8037	3.5322	4.2818	1487.2
430	913.666	658.483	665.050	1.9047	3.4878	4.3076	1465.7
440	903.877	701.633	708.271	2.0041	3.4450	4.3373	1442.1
450	893.629	745.096	751.810	2.1019	3.4039	4.3714	1416.2
460	882.899	788.919	795.714	2.1984	3.3644	4.4104	1388.2
470	871.657	833.154	840.037	2.2937	3.3266	4.4552	1358.1
480	859.865	877.862	884.840	2.3881	3.2905	4.5065	1325.7
490	847.477	923.114	930.194	2.4816	3.2561	4.5658	1291.2
500	834.430	968.996	976.187	2.5745	3.2234	4.6345	1254.3
510	820.648	1015.61	1022.92	2.6670	3.1926	4.7147	1215.0
520	806.031	1063.09	1070.53	2.7595	3.1637	4.8095	1172.9
530	790.450	1111.58	1119.17	2.8521	3.1369	4.9231	1127.9
540	773.728	1161.32	1169.08	2.9454	3.1126	5.0620	1079.5
548.735[b]	757.998	1206.01	1213.92	3.0278	3.0939	5.2116	1033.9
548.735[c]	30.818	2589.90	2784.59	5.8901	2.7054	4.8794	493.84
550	30.611	2594.68	2790.69	5.9012	2.6609	4.7634	495.95
560	29.166	2629.07	2834.79	5.9807	2.4167	4.1214	510.42
570	27.971	2659.42	2873.93	6.0500	2.2699	3.7334	522.43
580	26.947	2687.18	2909.84	6.1125	2.1666	3.4632	533.04
590	26.048	2713.08	2943.42	6.1699	2.0881	3.2613	542.70
600	25.247	2737.57	2975.22	6.2233	2.0262	3.1043	551.64
610	24.524	2760.95	3005.61	6.2736	1.9765	2.9791	560.00
620	23.865	2783.46	3034.88	6.3211	1.9362	2.8777	567.89
630	23.258	2805.25	3063.23	6.3665	1.9032	2.7943	575.38
640	22.697	2826.46	3090.81	6.4099	1.8762	2.7250	582.53
650	22.175	2847.19	3117.76	6.4517	1.8540	2.6670	589.39
675	21.008	2897.38	3182.99	6.5502	1.8143	2.5581	605.46
700	19.998	2945.93	3245.96	6.6418	1.7905	2.4848	620.34
725	19.107	2993.40	3307.42	6.7281	1.7773	2.4345	634.27
750	18.312	3040.17	3367.82	6.8100	1.7714	2.4001	647.46
775	17.595	3086.51	3427.51	6.8883	1.7706	2.3768	660.03
800	16.943	3132.59	3486.73	6.9635	1.7737	2.3616	672.07
825	16.345	3178.57	3545.65	7.0360	1.7797	2.3526	683.66
850	15.795	3224.53	3604.40	7.1062	1.7878	2.3483	694.86
900	14.812	3316.73	3721.80	7.2404	1.8088	2.3499	716.25
950	13.957	3409.66	3839.54	7.3677	1.8341	2.3609	736.51
1000	13.204	3503.59	3957.99	7.4892	1.8621	2.3780	755.85
1050	12.534	3598.71	4077.41	7.6057	1.8918	2.3993	774.41
1100	11.933	3695.15	4197.96	7.7179	1.9224	2.4232	792.29
1150	11.390	3792.97	4319.76	7.8262	1.9535	2.4489	809.60
1200	10.896	3892.23	4442.87	7.9310	1.9847	2.4756	826.38
1250	10.446	3992.94	4567.33	8.0326	2.0156	2.5028	842.72
1273	10.251	4039.75	4625.04	8.0783	2.0296	2.5154	850.09
			7.0 MPa				
272.638[a]	1003.30	−2.069	4.908	−0.0076	4.1862	4.1876	1410.9
275	1003.37	7.816	14.792	0.0285	4.1821	4.1822	1422.6
280	1003.24	28.703	35.680	0.1037	4.1713	4.1736	1445.4

TABLE 13.2. Thermodynamic properties of water in the single-phase region—Continued

T K	ρ kg m^{-3}	u kJ kg^{-1}	h kJ kg^{-1}	s kJ kg^{-1} K^{-1}	c_v kJ kg^{-1} K^{-1}	c_p kJ kg^{-1} K^{-1}	w m s^{-1}
			7.0 MPa—Continued				
285	1002.76	49.552	56.533	0.1776	4.1581	4.1680	1465.7
290	1001.98	70.377	77.363	0.2500	4.1429	4.1644	1483.6
295	1000.93	91.187	98.180	0.3212	4.1261	4.1625	1499.4
300	999.632	111.987	118.990	0.3911	4.1078	4.1616	1513.1
305	998.117	132.784	139.798	0.4599	4.0883	4.1616	1525.1
310	996.401	153.581	160.607	0.5276	4.0676	4.1622	1535.3
315	994.496	174.381	181.420	0.5942	4.0459	4.1632	1543.9
320	992.417	195.186	202.239	0.6598	4.0234	4.1647	1551.1
325	990.174	215.998	223.067	0.7244	4.0001	4.1664	1556.9
330	987.777	236.818	243.904	0.7880	3.9761	4.1685	1561.5
335	985.232	257.648	264.752	0.8507	3.9517	4.1708	1564.8
340	982.547	278.489	285.613	0.9125	3.9268	4.1735	1567.0
345	979.727	299.343	306.488	0.9734	3.9016	4.1764	1568.2
350	976.779	320.211	327.378	1.0336	3.8761	4.1797	1568.4
355	973.706	341.096	348.285	1.0929	3.8505	4.1833	1567.7
360	970.512	361.999	369.212	1.1514	3.8249	4.1874	1566.0
365	967.200	382.922	390.159	1.2092	3.7992	4.1918	1563.6
370	963.774	403.867	411.130	1.2663	3.7737	4.1967	1560.3
375	960.236	424.838	432.127	1.3226	3.7482	4.2021	1556.3
380	956.587	445.835	453.153	1.3783	3.7230	4.2081	1551.5
385	952.830	466.863	474.209	1.4334	3.6979	4.2146	1546.0
390	948.966	487.923	495.300	1.4878	3.6731	4.2217	1539.9
395	944.995	509.020	516.427	1.5416	3.6486	4.2294	1533.1
400	940.919	530.155	537.595	1.5949	3.6244	4.2378	1525.6
410	932.450	572.558	580.065	1.6998	3.5771	4.2567	1508.9
420	923.559	615.161	622.740	1.8026	3.5312	4.2788	1489.8
430	914.239	657.996	665.652	1.9036	3.4869	4.3043	1468.5
440	904.481	701.099	708.839	2.0029	3.4442	4.3336	1445.0
450	894.268	744.512	752.339	2.1006	3.4032	4.3673	1419.3
460	883.577	788.278	796.200	2.1970	3.3638	4.4058	1391.5
470	872.381	832.450	840.474	2.2922	3.3260	4.4499	1361.5
480	860.642	877.087	885.220	2.3864	3.2899	4.5005	1329.5
490	848.315	922.258	930.510	2.4798	3.2555	4.5588	1295.2
500	835.340	968.046	976.426	2.5726	3.2228	4.6262	1258.6
510	821.643	1014.55	1023.07	2.6649	3.1919	4.7048	1219.6
520	807.130	1061.90	1070.57	2.7572	3.1630	4.7975	1178.0
530	791.676	1110.24	1119.08	2.8496	3.1361	4.9082	1133.5
540	775.113	1159.78	1168.81	2.9425	3.1116	5.0429	1085.8
550	757.211	1210.80	1220.05	3.0365	3.0901	5.2108	1034.1
558.979[b]	739.724	1258.20	1267.66	3.1224	3.0740	5.4025	983.70
558.979[c]	36.525	2580.98	2772.63	5.8148	2.8115	5.3566	489.11
560	36.304	2585.22	2778.04	5.8244	2.7726	5.2421	490.98
570	34.419	2622.76	2826.14	5.9096	2.5055	4.4587	506.80
580	32.894	2655.43	2868.24	5.9828	2.3448	3.9933	519.78
590	31.606	2685.00	2906.48	6.0482	2.2313	3.6733	531.13
600	30.490	2712.39	2941.98	6.1078	2.1450	3.4365	541.38
610	29.503	2738.13	2975.39	6.1631	2.0770	3.2539	550.81
620	28.620	2762.59	3007.18	6.2148	2.0223	3.1092	559.59
630	27.819	2786.04	3037.67	6.2636	1.9779	2.9923	567.83
640	27.086	2808.66	3067.10	6.3099	1.9415	2.8965	575.63
650	26.411	2830.61	3095.65	6.3542	1.9115	2.8171	583.04
675	24.925	2883.26	3164.11	6.4575	1.8575	2.6697	600.25
700	23.658	2933.65	3229.54	6.5527	1.8240	2.5712	615.97
725	22.554	2982.56	3292.93	6.6417	1.8041	2.5037	630.58

TABLE 13.2. Thermodynamic properties of water in the single-phase region—Continued

T K	ρ kg m^{-3}	u kJ kg^{-1}	h kJ kg^{-1}	s kJ kg^{-1} K^{-1}	c_v kJ kg^{-1} K^{-1}	c_p kJ kg^{-1} K^{-1}	w m s^{-1}
			7.0 MPa—Continued				
750	21.578	3030.49	3354.90	6.7258	1.7932	2.4567	644.30
775	20.704	3077.78	3415.88	6.8057	1.7888	2.4241	657.31
800	19.913	3124.66	3476.19	6.8823	1.7891	2.4018	669.73
825	19.192	3171.30	3536.03	6.9560	1.7928	2.3871	681.63
850	18.531	3217.85	3595.59	7.0271	1.7991	2.3783	693.10
900	17.356	3310.99	3714.32	7.1628	1.8175	2.3732	714.93
950	16.338	3404.65	3833.10	7.2913	1.8409	2.3795	735.53
1000	15.445	3499.17	3952.39	7.4137	1.8676	2.3932	755.14
1050	14.653	3594.78	4072.50	7.5309	1.8964	2.4119	773.91
1100	13.944	3691.62	4193.63	7.6436	1.9263	2.4338	791.97
1150	13.305	3789.79	4315.92	7.7523	1.9568	2.4579	809.41
1200	12.725	3889.33	4439.44	7.8574	1.9874	2.4834	826.32
1250	12.196	3990.29	4564.27	7.9593	2.0180	2.5096	842.76
1273	11.967	4037.20	4622.13	8.0052	2.0319	2.5218	850.17
			8.0 MPa				
272.562[a]	1003.80	−2.370	5.600	−0.0087	4.1818	4.1831	1412.1
275	1003.87	7.822	15.791	0.0285	4.1778	4.1778	1424.2
280	1003.72	28.689	36.659	0.1037	4.1672	4.1698	1447.1
285	1003.23	49.519	57.494	0.1774	4.1543	4.1645	1467.3
290	1002.43	70.327	78.308	0.2498	4.1394	4.1613	1485.2
295	1001.37	91.120	99.109	0.3210	4.1228	4.1596	1501.0
300	1000.07	111.906	119.905	0.3909	4.1047	4.1589	1514.8
305	998.555	132.688	140.700	0.4596	4.0853	4.1590	1526.8
310	996.834	153.471	161.497	0.5272	4.0648	4.1597	1537.0
315	994.928	174.257	182.298	0.5938	4.0432	4.1609	1545.7
320	992.847	195.049	203.106	0.6593	4.0208	4.1624	1552.9
325	990.604	215.847	223.923	0.7239	3.9976	4.1642	1558.7
330	988.206	236.654	244.749	0.7875	3.9738	4.1663	1563.3
335	985.662	257.470	265.587	0.8502	3.9495	4.1687	1566.6
340	982.979	278.298	286.437	0.9119	3.9247	4.1714	1568.9
345	980.162	299.139	307.301	0.9728	3.8996	4.1743	1570.1
350	977.217	319.994	328.181	1.0329	3.8742	4.1776	1570.3
355	974.147	340.865	349.077	1.0922	3.8487	4.1812	1569.6
360	970.958	361.754	369.993	1.1507	3.8232	4.1852	1568.0
365	967.651	382.663	390.930	1.2085	3.7976	4.1897	1565.6
370	964.230	403.594	411.891	1.2655	3.7721	4.1945	1562.4
375	960.698	424.549	432.877	1.3219	3.7468	4.1999	1558.4
380	957.056	445.532	453.891	1.3775	3.7216	4.2058	1553.7
385	953.306	466.544	474.936	1.4325	3.6966	4.2123	1548.2
390	949.450	487.588	496.014	1.4869	3.6719	4.2193	1542.1
395	945.487	508.668	517.130	1.5407	3.6474	4.2269	1535.4
400	941.420	529.787	538.285	1.5940	3.6233	4.2353	1528.0
410	932.972	572.154	580.729	1.6988	3.5760	4.2540	1511.4
420	924.104	614.718	623.375	1.8015	3.5303	4.2758	1492.4
430	914.811	657.511	666.256	1.9024	3.4860	4.3010	1471.2
440	905.082	700.569	709.408	2.0016	3.4434	4.3300	1447.8
450	894.903	743.931	752.871	2.0993	3.4024	4.3632	1422.3
460	884.252	787.642	796.689	2.1956	3.3631	4.4013	1394.7
470	873.100	831.751	840.914	2.2907	3.3254	4.4447	1365.0
480	861.413	876.318	885.605	2.3848	3.2893	4.4946	1333.1
490	849.146	921.409	930.830	2.4781	3.2549	4.5519	1299.1
500	836.242	967.105	976.672	2.5707	3.2222	4.6180	1262.9
510	822.630	1013.50	1023.23	2.6629	3.1913	4.6951	1224.2
520	808.217	1060.72	1070.62	2.7549	3.1623	4.7857	1183.1

TABLE 13.2. Thermodynamic properties of water in the single-phase region—Continued

T K	ρ kg m^{-3}	u kJ kg^{-1}	h kJ kg^{-1}	s kJ kg^{-1} K^{-1}	c_v kJ kg^{-1} K^{-1}	c_p kJ kg^{-1} K^{-1}	w m s^{-1}
			8.0 MPa—Continued				
530	792.886	1108.91	1119.00	2.8470	3.1353	4.8936	1139.1
540	776.478	1158.26	1168.57	2.9397	3.1107	5.0243	1091.9
550	758.774	1209.05	1219.59	3.0333	3.0889	5.1866	1041.0
560	739.463	1261.63	1272.45	3.1285	3.0707	5.3942	985.65
568.158[b]	722.196	1306.23	1317.31	3.2081	3.0594	5.6141	936.26
568.158[c]	42.507	2570.48	2758.68	5.7450	2.9128	5.8823	483.94
570	41.997	2578.80	2769.29	5.7636	2.8397	5.6384	487.60
580	39.647	2618.96	2820.74	5.8531	2.5673	4.7449	504.42
590	37.777	2653.59	2865.36	5.9294	2.3999	4.2155	518.16
600	36.218	2684.72	2905.60	5.9971	2.2806	3.8537	530.11
610	34.878	2713.38	2942.75	6.0585	2.1894	3.5876	540.86
620	33.704	2740.20	2977.56	6.1151	2.1173	3.3835	550.69
630	32.657	2765.59	3010.56	6.1679	2.0593	3.2223	559.81
640	31.713	2789.85	3042.11	6.2176	2.0120	3.0925	568.35
650	30.854	2813.20	3072.49	6.2647	1.9732	2.9863	576.40
675	28.991	2868.60	3144.54	6.3735	1.9031	2.7923	594.85
700	27.431	2921.01	3212.65	6.4726	1.8591	2.6645	611.50
725	26.089	2971.47	3278.10	6.5644	1.8318	2.5772	626.82
750	24.914	3020.62	3341.73	6.6507	1.8157	2.5163	641.11
775	23.869	3068.90	3404.07	6.7325	1.8074	2.4735	654.58
800	22.929	3116.61	3465.51	6.8105	1.8047	2.4434	667.37
825	22.077	3163.96	3526.32	6.8854	1.8061	2.4227	679.60
850	21.299	3211.10	3586.70	6.9575	1.8106	2.4091	691.34
900	19.922	3305.21	3706.79	7.0948	1.8262	2.3969	713.61
950	18.735	3399.62	3826.62	7.2243	1.8478	2.3983	734.55
1000	17.698	3494.74	3946.76	7.3476	1.8732	2.4085	754.43
1050	16.781	3590.84	4067.57	7.4655	1.9009	2.4246	773.41
1100	15.962	3688.08	4189.28	7.5787	1.9301	2.4445	791.64
1150	15.224	3786.59	4312.06	7.6879	1.9600	2.4670	809.23
1200	14.556	3886.43	4436.02	7.7934	1.9902	2.4912	826.26
1250	13.948	3987.64	4561.20	7.8956	2.0204	2.5164	842.80
1273	13.686	4034.66	4619.22	7.9416	2.0341	2.5282	850.25
			10.0 MPa				
272.410[a]	1004.79	−2.972	6.981	−0.0110	4.1732	4.1742	1414.6
275	1004.85	7.834	17.785	0.0285	4.1692	4.1692	1427.5
280	1004.67	28.659	38.613	0.1035	4.1593	4.1622	1450.3
285	1004.16	49.453	59.412	0.1772	4.1468	4.1578	1470.6
290	1003.34	70.227	80.193	0.2495	4.1323	4.1552	1488.5
295	1002.27	90.988	100.966	0.3205	4.1161	4.1539	1504.3
300	1000.96	111.744	121.734	0.3903	4.0984	4.1536	1518.2
305	999.426	132.497	142.503	0.4589	4.0794	4.1540	1530.1
310	997.699	153.252	163.276	0.5265	4.0591	4.1550	1540.4
315	995.787	174.011	184.054	0.5930	4.0379	4.1563	1549.2
320	993.704	194.776	204.839	0.6585	4.0157	4.1580	1556.4
325	991.459	215.548	225.634	0.7229	3.9928	4.1599	1562.3
330	989.062	236.328	246.438	0.7865	3.9692	4.1621	1566.9
335	986.520	257.118	267.255	0.8491	3.9451	4.1645	1570.3
340	983.840	277.920	288.084	0.9108	3.9205	4.1672	1572.6
345	981.028	298.734	308.927	0.9717	3.8956	4.1702	1573.9
350	978.089	319.562	329.786	1.0317	3.8705	4.1734	1574.2
355	975.027	340.406	350.662	1.0909	3.8451	4.1770	1573.6
360	971.846	361.267	371.557	1.1493	3.8198	4.1810	1572.0
365	968.549	382.148	392.473	1.2070	3.7944	4.1854	1569.7
370	965.139	403.051	413.412	1.2640	3.7690	4.1902	1566.5

TABLE 13.2. Thermodynamic properties of water in the single-phase region—Continued

T K	ρ kg m^{-3}	u kJ kg^{-1}	h kJ kg^{-1}	s kJ kg^{-1} K^{-1}	c_v kJ kg^{-1} K^{-1}	c_p kJ kg^{-1} K^{-1}	w m s^{-1}
			10.0 MPa—Continued				
375	961.618	423.977	434.376	1.3203	3.7438	4.1955	1562.6
380	957.990	444.929	455.368	1.3759	3.7188	4.2013	1558.0
385	954.254	465.911	476.390	1.4309	3.6939	4.2076	1552.6
390	950.413	486.923	497.445	1.4852	3.6693	4.2145	1546.6
395	946.467	507.971	518.536	1.5389	3.6450	4.2221	1540.0
400	942.418	529.056	539.667	1.5921	3.6210	4.2302	1532.7
410	934.009	571.352	582.059	1.6968	3.5739	4.2486	1516.3
420	925.187	613.840	624.649	1.7994	3.5283	4.2699	1497.6
430	915.946	656.551	667.468	1.9002	3.4843	4.2946	1476.7
440	906.277	699.518	710.552	1.9992	3.4418	4.3229	1453.6
450	896.165	742.781	753.940	2.0967	3.4010	4.3553	1428.4
460	885.590	786.382	797.674	2.1928	3.3617	4.3923	1401.1
470	874.527	830.369	841.804	2.2877	3.3241	4.4346	1371.8
480	862.941	874.798	886.386	2.3816	3.2881	4.4829	1340.4
490	850.791	919.732	931.486	2.4746	3.2538	4.5384	1306.9
500	838.025	965.249	977.182	2.5669	3.2211	4.6022	1271.3
510	824.575	1011.44	1023.56	2.6588	3.1901	4.6763	1233.3
520	810.357	1058.41	1070.75	2.7504	3.1609	4.7630	1193.0
530	795.263	1106.30	1118.88	2.8421	3.1338	4.8656	1150.0
540	779.149	1155.30	1168.13	2.9341	3.1088	4.9891	1104.0
550	761.820	1205.63	1218.75	3.0270	3.0865	5.1407	1054.6
560	743.005	1257.62	1271.08	3.1213	3.0675	5.3323	1001.1
570	722.296	1311.75	1325.60	3.2178	3.0528	5.5838	942.46
580	699.049	1368.77	1383.07	3.3177	3.0445	5.9333	877.07
584.147[b]	688.424	1393.54	1408.06	3.3606	3.0438	6.1237	847.33
584.147[c]	55.463	2545.19	2725.49	5.6160	3.1065	7.1408	472.51
590	53.019	2575.48	2764.10	5.6817	2.8728	6.1343	485.55
600	49.773	2619.05	2819.96	5.7756	2.6239	5.1365	503.34
610	47.237	2656.39	2868.09	5.8552	2.4599	4.5319	517.99
620	45.151	2689.75	2911.22	5.9253	2.3391	4.1171	530.72
630	43.380	2720.28	2950.80	5.9887	2.2454	3.8129	542.12
640	41.840	2748.71	2987.72	6.0468	2.1707	3.5801	552.51
650	40.479	2775.53	3022.57	6.1009	2.1103	3.3968	562.10
675	37.639	2837.47	3103.16	6.2225	2.0020	3.0765	583.48
700	35.355	2894.51	3177.36	6.3305	1.9338	2.8741	602.20
725	33.447	2948.43	3247.42	6.4289	1.8901	2.7389	619.08
750	31.810	3000.28	3314.65	6.5200	1.8625	2.6452	634.58
775	30.378	3050.72	3379.90	6.6056	1.8458	2.5788	649.02
800	29.107	3100.19	3443.75	6.6867	1.8367	2.5313	662.61
825	27.966	3149.01	3506.58	6.7641	1.8332	2.4973	675.51
850	26.933	3197.40	3568.69	6.8382	1.8339	2.4732	687.81
900	25.123	3293.53	3691.57	6.9787	1.8439	2.4458	710.98
950	23.580	3389.49	3813.58	7.1107	1.8617	2.4369	732.61
1000	22.241	3485.83	3935.46	7.2357	1.8843	2.4397	753.03
1050	21.063	3582.92	4057.68	7.3549	1.9101	2.4503	772.44
1100	20.017	3680.99	4180.58	7.4693	1.9377	2.4661	791.02
1150	19.078	3780.19	4304.35	7.5793	1.9665	2.4854	808.90
1200	18.230	3880.62	4429.15	7.6855	1.9957	2.5070	826.16
1250	17.460	3982.33	4555.08	7.7884	2.0251	2.5301	842.90
1273	17.128	4029.56	4613.39	7.8346	2.0386	2.5410	850.43
			12.5 MPa				
272.218[a]	1006.03	−3.731	8.694	−0.0138	4.1625	4.1632	1417.7
275	1006.07	7.845	20.270	0.0285	4.1587	4.1587	1431.6
280	1005.86	28.621	41.048	0.1034	4.1494	4.1530	1454.4

TABLE 13.2. Thermodynamic properties of water in the single-phase region—Continued

T K	ρ kg m^{-3}	u kJ kg^{-1}	h kJ kg^{-1}	s kJ kg^{-1} K^{-1}	c_v kJ kg^{-1} K^{-1}	c_p kJ kg^{-1} K^{-1}	w m s^{-1}
			12.5 MPa—Continued				
285	1005.31	49.369	61.803	0.1768	4.1376	4.1495	1474.7
290	1004.47	70.101	82.546	0.2490	4.1237	4.1476	1492.7
295	1003.38	90.824	103.282	0.3199	4.1079	4.1470	1508.5
300	1002.05	111.542	124.017	0.3896	4.0906	4.1471	1522.4
305	1000.51	132.260	144.754	0.4581	4.0720	4.1479	1534.4
310	998.774	152.981	165.496	0.5256	4.0522	4.1491	1544.7
315	996.857	173.706	186.245	0.5920	4.0313	4.1506	1553.5
320	994.770	194.437	207.003	0.6574	4.0094	4.1525	1560.8
325	992.523	215.176	227.770	0.7218	3.9868	4.1545	1566.7
330	990.127	235.924	248.549	0.7852	3.9635	4.1568	1571.4
335	987.588	256.682	269.339	0.8477	3.9397	4.1593	1574.9
340	984.912	277.451	290.142	0.9094	3.9154	4.1620	1577.3
345	982.105	298.232	310.960	0.9702	3.8907	4.1650	1578.6
350	979.174	319.027	331.793	1.0301	3.8658	4.1683	1579.0
355	976.120	339.838	352.643	1.0893	3.8407	4.1719	1578.4
360	972.949	360.665	373.513	1.1476	3.8155	4.1758	1577.0
365	969.664	381.511	394.402	1.2053	3.7903	4.1801	1574.7
370	966.268	402.378	415.315	1.2622	3.7652	4.1849	1571.7
375	962.762	423.268	436.252	1.3184	3.7402	4.1901	1567.9
380	959.149	444.184	457.216	1.3739	3.7153	4.1958	1563.3
385	955.431	465.127	478.210	1.4288	3.6906	4.2020	1558.1
390	951.609	486.101	499.237	1.4831	3.6661	4.2087	1552.2
395	947.683	507.108	520.298	1.5367	3.6420	4.2161	1545.7
400	943.656	528.152	541.398	1.5898	3.6181	4.2240	1538.5
410	935.296	570.361	583.726	1.6943	3.5713	4.2419	1522.4
420	926.529	612.755	626.246	1.7968	3.5260	4.2627	1504.0
430	917.352	655.364	668.990	1.8974	3.4821	4.2867	1483.4
440	907.754	698.221	711.992	1.9962	3.4398	4.3142	1460.6
450	897.724	741.363	755.287	2.0935	3.3991	4.3456	1435.9
460	887.243	784.830	798.919	2.1894	3.3600	4.3815	1409.1
470	876.286	828.668	842.933	2.2841	3.3225	4.4223	1380.2
480	864.823	872.930	887.384	2.3777	3.2866	4.4689	1349.4
490	852.815	917.675	932.332	2.4703	3.2523	4.5221	1316.5
500	840.213	962.975	977.852	2.5623	3.2196	4.5832	1281.6
510	826.957	1008.91	1024.03	2.6537	3.1886	4.6538	1244.5
520	812.970	1055.59	1070.97	2.7449	3.1594	4.7360	1205.1
530	798.155	1103.13	1118.80	2.8360	3.1320	4.8326	1163.2
540	782.385	1151.70	1167.68	2.9273	3.1067	4.9479	1118.5
550	765.490	1201.51	1217.84	3.0194	3.0838	5.0879	1070.8
560	747.237	1252.82	1269.55	3.1126	3.0639	5.2622	1019.4
570	727.289	1306.06	1323.24	3.2076	3.0477	5.4862	963.63
580	705.135	1361.81	1379.53	3.3055	3.0368	5.7879	902.18
590	679.923	1421.05	1439.44	3.4079	3.0341	6.2229	833.01
600	650.039	1485.63	1504.86	3.5178	3.0462	6.9279	751.97
600.963[b]	646.807	1492.26	1511.58	3.5290	3.0486	7.0212	743.25
600.963[c]	74.097	2505.61	2674.31	5.4638	3.3417	9.3478	456.25
610	67.912	2562.29	2746.35	5.5828	2.9481	6.9550	480.22
620	63.188	2611.20	2809.03	5.6847	2.7016	5.7061	499.85
630	59.612	2652.42	2862.11	5.7697	2.5339	4.9656	515.87
640	56.733	2688.80	2909.13	5.8437	2.4085	4.4663	529.67
650	54.326	2721.80	2951.89	5.9101	2.3106	4.1046	541.93
675	49.625	2794.66	3046.55	6.0530	2.1409	3.5257	568.04
700	46.085	2858.90	3130.14	6.1747	2.0359	3.1881	589.89
725	43.252	2917.95	3206.96	6.2825	1.9684	2.9723	609.00

TABLE 13.2. Thermodynamic properties of water in the single-phase region—Continued

T K	ρ kg m^{-3}	u kJ kg^{-1}	h kJ kg^{-1}	s kJ kg^{-1} K^{-1}	c_v kJ kg^{-1} K^{-1}	c_p kJ kg^{-1} K^{-1}	w m s^{-1}
			12.5 MPa—Continued				
750	40.894	2973.66	3279.33	6.3807	1.9244	2.8263	626.19
775	38.878	3027.11	3348.63	6.4716	1.8960	2.7240	641.95
800	37.120	3079.02	3415.76	6.5568	1.8782	2.6505	656.60
825	35.563	3129.84	3481.32	6.6375	1.8681	2.5971	670.37
850	34.169	3179.91	3545.74	6.7144	1.8637	2.5581	683.41
900	31.758	3278.70	3672.30	6.8591	1.8663	2.5096	707.74
950	29.730	3376.67	3797.12	6.9941	1.8792	2.4867	730.24
1000	27.987	3474.60	3921.23	7.1214	1.8983	2.4797	751.33
1050	26.466	3572.96	4045.26	7.2425	1.9215	2.4831	771.28
1100	25.122	3672.08	4169.66	7.3582	1.9472	2.4935	790.29
1150	23.922	3772.16	4294.69	7.4694	1.9745	2.5086	808.52
1200	22.842	3873.33	4420.56	7.5765	2.0026	2.5269	826.08
1250	21.864	3975.68	4547.41	7.6801	2.0311	2.5473	843.06
1273	21.443	4023.18	4606.11	7.7266	2.0442	2.5572	850.69
			15.0 MPa				
272.025[a]	1007.27	−4.493	10.398	−0.0167	4.1519	4.1524	1420.8
275	1007.29	7.854	22.746	0.0285	4.1484	4.1485	1435.6
280	1007.04	28.581	43.476	0.1032	4.1398	4.1440	1458.5
285	1006.46	49.285	64.189	0.1765	4.1285	4.1414	1478.8
290	1005.60	69.976	84.892	0.2485	4.1151	4.1403	1496.8
295	1004.49	90.660	105.593	0.3193	4.0998	4.1401	1512.7
300	1003.14	111.342	126.295	0.3889	4.0830	4.1407	1526.5
305	1001.59	132.024	147.001	0.4573	4.0647	4.1418	1538.6
310	999.844	152.711	167.713	0.5247	4.0453	4.1433	1549.0
315	997.920	173.403	188.434	0.5910	4.0247	4.1451	1557.8
320	995.830	194.101	209.164	0.6563	4.0032	4.1471	1565.2
325	993.582	214.808	229.905	0.7206	3.9809	4.1493	1571.2
330	991.186	235.524	250.657	0.7840	3.9579	4.1516	1575.9
335	988.649	256.249	271.422	0.8464	3.9343	4.1542	1579.5
340	985.977	276.986	292.200	0.9080	3.9103	4.1570	1581.9
345	983.176	297.735	312.992	0.9687	3.8859	4.1600	1583.3
350	980.251	318.498	333.800	1.0286	3.8612	4.1632	1583.8
355	977.207	339.275	354.625	1.0876	3.8363	4.1668	1583.3
360	974.046	360.069	375.468	1.1459	3.8113	4.1707	1581.9
365	970.772	380.881	396.332	1.2035	3.7863	4.1750	1579.8
370	967.389	401.713	417.219	1.2603	3.7614	4.1796	1576.8
375	963.897	422.567	438.129	1.3165	3.7365	4.1847	1573.1
380	960.300	443.447	459.067	1.3719	3.7118	4.1903	1568.6
385	956.599	464.352	480.033	1.4267	3.6873	4.1964	1563.5
390	952.795	485.288	501.031	1.4809	3.6630	4.2030	1557.7
395	948.890	506.256	522.064	1.5345	3.6390	4.2101	1551.3
400	944.884	527.258	543.133	1.5875	3.6152	4.2179	1544.3
410	936.572	569.382	585.398	1.6919	3.5687	4.2354	1528.4
420	927.859	611.684	627.850	1.7942	3.5236	4.2556	1510.3
430	918.743	654.194	670.521	1.8946	3.4800	4.2790	1490.0
440	909.216	696.943	713.441	1.9933	3.4379	4.3057	1467.6
450	899.265	739.967	756.647	2.0904	3.3973	4.3362	1443.2
460	888.874	783.303	800.179	2.1860	3.3584	4.3709	1416.9
470	878.020	826.997	844.081	2.2804	3.3210	4.4104	1388.5
480	866.675	871.096	888.404	2.3738	3.2852	4.4553	1358.2
490	854.803	915.659	933.207	2.4661	3.2509	4.5065	1326.0
500	842.359	960.750	978.557	2.5578	3.2182	4.5650	1291.7
510	829.288	1006.45	1024.54	2.6488	3.1872	4.6324	1255.3
520	815.520	1052.85	1071.24	2.7395	3.1578	4.7104	1216.8

TABLE 13.2. Thermodynamic properties of water in the single-phase region—Continued

T K	ρ kg m^{-3}	u kJ kg^{-1}	h kJ kg^{-1}	s kJ kg^{-1} K^{-1}	c_v kJ kg^{-1} K^{-1}	c_p kJ kg^{-1} K^{-1}	w m s^{-1}
			15.0 MPa—Continued				
530	800.967	1100.06	1118.79	2.8301	3.1303	4.8016	1176.0
540	785.517	1148.23	1167.33	2.9208	3.1047	4.9096	1132.6
550	769.020	1197.55	1217.05	3.0120	3.0813	5.0395	1086.4
560	751.276	1248.25	1268.22	3.1042	3.0606	5.1990	1036.9
570	732.003	1300.68	1321.17	3.1979	3.0433	5.4004	983.55
580	710.785	1355.33	1376.43	3.2940	3.0304	5.6647	925.40
590	686.967	1412.96	1434.80	3.3938	3.0240	6.0308	861.00
600	659.407	1474.91	1497.65	3.4994	3.0282	6.5830	787.74
610	625.747	1543.83	1567.81	3.6154	3.0539	7.5565	699.84
615.305[b]	603.518	1585.35	1610.20	3.6846	3.0873	8.5132	642.00
615.305[c]	96.727	2455.62	2610.70	5.3106	3.5826	12.967	437.53
620	90.362	2497.64	2663.64	5.3963	3.2813	9.9684	455.29
630	81.553	2563.70	2747.63	5.5308	2.9240	7.2506	482.00
640	75.640	2614.79	2813.10	5.6339	2.7066	5.9668	501.93
650	71.186	2657.89	2868.61	5.7200	2.5511	5.1902	518.37
675	63.337	2746.51	2983.34	5.8933	2.2981	4.1243	551.01
700	57.942	2820.07	3078.95	6.0324	2.1479	3.5762	576.75
725	53.850	2885.38	3163.93	6.1517	2.0524	3.2474	598.48
750	50.564	2945.61	3242.26	6.2580	1.9899	3.0329	617.57
775	47.826	3002.49	3316.13	6.3549	1.9484	2.8855	634.77
800	45.484	3057.10	3386.89	6.4448	1.9212	2.7808	650.56
825	43.441	3110.11	3455.41	6.5291	1.9040	2.7047	665.24
850	41.632	3161.99	3522.29	6.6090	1.8941	2.6486	679.04
900	38.548	3263.61	3652.73	6.7581	1.8890	2.5765	704.55
950	35.988	3363.69	3780.49	6.8963	1.8968	2.5382	727.93
1000	33.811	3463.26	3906.90	7.0259	1.9124	2.5207	749.69
1050	31.925	3562.94	4032.79	7.1488	1.9329	2.5165	770.17
1100	30.268	3663.13	4158.70	7.2659	1.9567	2.5213	789.62
1150	28.796	3764.10	4285.01	7.3782	1.9825	2.5320	808.20
1200	27.475	3866.02	4411.97	7.4863	2.0095	2.5469	826.04
1250	26.282	3969.02	4539.75	7.5906	2.0371	2.5646	843.26
1273	25.771	4016.79	4598.84	7.6375	2.0498	2.5734	850.99
			17.5 MPa				
271.830[a]	1008.50	−5.263	12.089	−0.0196	4.1415	4.1418	1423.9
275	1008.50	7.861	25.213	0.0284	4.1382	4.1385	1439.7
280	1008.21	28.539	45.896	0.1029	4.1303	4.1352	1462.6
285	1007.61	49.200	66.567	0.1761	4.1196	4.1335	1482.9
290	1006.72	69.850	87.233	0.2480	4.1067	4.1330	1500.9
295	1005.59	90.496	107.899	0.3187	4.0919	4.1334	1516.8
300	1004.23	111.142	128.568	0.3881	4.0754	4.1344	1530.7
305	1002.66	131.790	149.244	0.4565	4.0576	4.1358	1542.8
310	1000.91	152.443	169.927	0.5237	4.0385	4.1376	1553.3
315	998.979	173.102	190.620	0.5900	4.0183	4.1396	1562.1
320	996.884	193.769	211.323	0.6552	3.9971	4.1417	1569.5
325	994.635	214.443	232.038	0.7194	3.9751	4.1441	1575.6
330	992.239	235.127	252.764	0.7827	3.9523	4.1465	1580.4
335	989.704	255.821	273.503	0.8451	3.9290	4.1492	1584.0
340	987.036	276.526	294.256	0.9066	3.9052	4.1520	1586.5
345	984.241	297.243	315.023	0.9672	3.8810	4.1550	1588.0
350	981.323	317.973	335.806	1.0270	3.8566	4.1583	1588.5
355	978.287	338.718	356.606	1.0860	3.8319	4.1618	1588.1
360	975.136	359.479	377.425	1.1442	3.8072	4.1656	1586.8
365	971.873	380.257	398.263	1.2017	3.7824	4.1698	1584.7
370	968.502	401.055	419.124	1.2585	3.7576	4.1744	1581.9

TABLE 13.2. Thermodynamic properties of water in the single-phase region—Continued

T K	ρ kg m^{-3}	u kJ kg^{-1}	h kJ kg^{-1}	s kJ kg^{-1} K^{-1}	c_v kJ kg^{-1} K^{-1}	c_p kJ kg^{-1} K^{-1}	w m s^{-1}
			17.5 MPa—Continued				
375	965.025	421.874	440.008	1.3146	3.7329	4.1794	1578.3
380	961.443	442.717	460.919	1.3700	3.7084	4.1849	1573.9
385	957.759	463.586	481.858	1.4247	3.6840	4.1908	1568.9
390	953.973	484.484	502.828	1.4788	3.6599	4.1973	1563.2
395	950.087	505.413	523.832	1.5323	3.6360	4.2043	1556.9
400	946.102	526.376	544.873	1.5853	3.6124	4.2119	1550.0
410	937.836	568.415	587.075	1.6895	3.5662	4.2290	1534.4
420	929.177	610.627	629.461	1.7916	3.5213	4.2487	1516.6
430	920.121	653.039	672.059	1.8918	3.4778	4.2714	1496.6
440	910.662	695.683	714.900	1.9903	3.4359	4.2974	1474.6
450	900.788	738.591	758.018	2.0872	3.3956	4.3270	1450.5
460	890.485	781.800	801.453	2.1827	3.3567	4.3606	1424.6
470	879.730	825.353	845.246	2.2769	3.3194	4.3988	1396.7
480	868.499	869.296	889.445	2.3699	3.2837	4.4421	1366.9
490	856.757	913.682	934.107	2.4620	3.2495	4.4914	1335.2
500	844.465	958.573	979.296	2.5533	3.2169	4.5476	1301.6
510	831.569	1004.04	1025.09	2.6440	3.1858	4.6119	1266.0
520	818.009	1050.17	1071.57	2.7342	3.1564	4.6861	1228.3
530	803.703	1097.07	1118.85	2.8243	3.1287	4.7724	1188.4
540	788.552	1144.87	1167.07	2.9144	3.1028	4.8739	1146.2
550	772.423	1193.73	1216.39	3.0049	3.0791	4.9948	1101.4
560	755.143	1243.87	1267.05	3.0962	3.0577	5.1416	1053.6
570	736.472	1295.58	1319.34	3.1888	3.0394	5.3241	1002.4
580	716.070	1349.26	1373.70	3.2833	3.0249	5.5584	947.07
590	693.418	1405.54	1430.77	3.3808	3.0157	5.8728	886.56
600	667.671	1465.39	1491.60	3.4831	3.0146	6.3228	819.13
610	637.271	1530.63	1558.09	3.5930	3.0278	7.0397	741.49
620	598.616	1605.36	1634.60	3.7173	3.0734	8.4602	645.14
627.821[b]	554.662	1679.22	1710.77	3.8394	3.1926	11.743	534.92
627.821[c]	126.12	2390.54	2529.30	5.1431	3.8530	20.306	415.08
630	119.56	2421.73	2568.10	5.2048	3.6249	15.833	428.07
640	102.67	2514.88	2685.32	5.3896	3.1125	9.2496	465.31
650	93.225	2578.00	2765.72	5.5143	2.8484	7.0988	489.66
675	79.472	2691.43	2911.64	5.7348	2.4758	4.9568	532.05
700	71.230	2777.45	3023.13	5.8971	2.2699	4.0638	562.73
725	65.396	2850.47	3118.07	6.0304	2.1421	3.5737	587.53
750	60.907	2916.01	3203.33	6.1460	2.0586	3.2690	608.75
775	57.274	2976.80	3282.35	6.2497	2.0029	3.0654	627.51
800	54.231	3034.41	3357.11	6.3446	1.9655	2.9231	644.51
825	51.619	3089.81	3428.83	6.4329	1.9408	2.8204	660.15
850	49.337	3143.64	3498.35	6.5160	1.9251	2.7448	674.73
900	45.498	3248.26	3632.89	6.6698	1.9120	2.6463	701.45
950	42.358	3350.56	3763.70	6.8112	1.9144	2.5915	725.71
1000	39.714	3451.82	3892.47	6.9434	1.9264	2.5628	748.14
1050	37.440	3552.84	4020.25	7.0680	1.9444	2.5506	769.14
1100	35.455	3654.13	4147.72	7.1866	1.9662	2.5494	789.01
1150	33.698	3756.01	4275.32	7.3001	1.9905	2.5557	807.93
1200	32.129	3858.70	4403.37	7.4091	2.0163	2.5671	826.06
1250	30.716	3962.35	4532.09	7.5142	2.0430	2.5820	843.51
1273	30.111	4010.38	4591.56	7.5613	2.0554	2.5898	851.33
			20.0 MPa				
271.633[a]	1009.72	−6.041	13.767	−0.0225	4.1311	4.1313	1427.0
275	1009.70	7.864	27.672	0.0283	4.1282	4.1288	1443.9
280	1009.38	28.496	48.310	0.1027	4.1209	4.1265	1466.7

TABLE 13.2. Thermodynamic properties of water in the single-phase region—Continued

T K	ρ kg m^{-3}	u kJ kg^{-1}	h kJ kg^{-1}	s kJ kg^{-1} K^{-1}	c_v kJ kg^{-1} K^{-1}	c_p kJ kg^{-1} K^{-1}	w m s^{-1}
			20.0 MPa—Continued				
285	1008.74	49.113	68.940	0.1757	4.1108	4.1257	1487.0
290	1007.83	69.724	89.569	0.2475	4.0984	4.1259	1505.0
295	1006.68	90.333	110.200	0.3180	4.0840	4.1268	1521.0
300	1005.31	110.943	130.838	0.3874	4.0680	4.1282	1534.9
305	1003.73	131.558	151.483	0.4557	4.0505	4.1300	1547.1
310	1001.97	152.177	172.138	0.5228	4.0318	4.1320	1557.5
315	1000.03	172.804	192.803	0.5890	4.0119	4.1342	1566.4
320	997.933	193.439	213.480	0.6541	3.9910	4.1365	1573.9
325	995.682	214.082	234.169	0.7182	3.9693	4.1389	1580.0
330	993.286	234.734	254.870	0.7814	3.9468	4.1415	1584.8
335	990.753	255.397	275.584	0.8437	3.9238	4.1442	1588.5
340	988.089	276.071	296.312	0.9052	3.9002	4.1470	1591.1
345	985.299	296.756	317.054	0.9657	3.8763	4.1501	1592.7
350	982.388	317.454	337.813	1.0255	3.8520	4.1533	1593.2
355	979.360	338.167	358.588	1.0844	3.8276	4.1568	1592.9
360	976.219	358.894	379.382	1.1426	3.8031	4.1607	1591.7
365	972.967	379.640	400.195	1.2000	3.7784	4.1648	1589.7
370	969.608	400.403	421.030	1.2567	3.7539	4.1693	1586.9
375	966.145	421.188	441.889	1.3127	3.7294	4.1742	1583.4
380	962.578	441.996	462.773	1.3680	3.7050	4.1796	1579.2
385	958.910	462.829	483.686	1.4227	3.6808	4.1854	1574.2
390	955.142	483.689	504.628	1.4767	3.6568	4.1917	1568.7
395	951.275	504.580	525.604	1.5302	3.6331	4.1986	1562.5
400	947.311	525.503	546.615	1.5830	3.6096	4.2060	1555.7
410	939.090	567.459	588.757	1.6871	3.5636	4.2226	1540.3
420	930.482	609.583	631.077	1.7891	3.5189	4.2419	1522.8
430	921.485	651.900	673.604	1.8891	3.4757	4.2640	1503.1
440	912.092	694.440	716.368	1.9874	3.4340	4.2893	1481.4
450	902.294	737.235	759.401	2.0841	3.3938	4.3180	1457.7
460	892.075	780.321	802.741	2.1794	3.3551	4.3506	1432.2
470	881.417	823.737	846.427	2.2733	3.3179	4.3875	1404.7
480	870.296	867.527	890.508	2.3662	3.2823	4.4294	1375.4
490	858.680	911.742	935.034	2.4580	3.2482	4.4768	1344.3
500	846.532	956.440	980.066	2.5489	3.2155	4.5308	1311.3
510	833.805	1001.69	1025.67	2.6393	3.1845	4.5924	1276.3
520	820.441	1047.57	1071.94	2.7291	3.1550	4.6631	1239.5
530	806.369	1094.17	1118.97	2.8187	3.1271	4.7449	1200.5
540	791.497	1141.62	1166.89	2.9082	3.1011	4.8404	1159.4
550	775.710	1190.06	1215.84	2.9981	3.0770	4.9533	1115.8
560	758.855	1239.67	1266.03	3.0885	3.0551	5.0891	1069.6
570	740.728	1290.72	1317.72	3.1800	3.0359	5.2556	1020.3
580	721.044	1343.55	1371.28	3.2731	3.0201	5.4654	967.43
590	699.386	1398.65	1427.24	3.3688	3.0087	5.7396	910.18
600	675.109	1456.79	1486.41	3.4682	3.0038	6.1168	847.35
610	647.113	1519.27	1550.18	3.5736	3.0091	6.6775	776.90
620	613.229	1588.62	1621.24	3.6891	3.0337	7.6336	694.57
630	567.644	1671.50	1706.73	3.8259	3.1104	9.8619	587.65
638.899[b]	490.188	1786.41	1827.21	4.0156	3.5181	22.997	413.72
638.899[c]	170.50	2295.04	2412.35	4.9314	4.2431	45.550	384.13
640	160.50	2328.35	2452.96	4.9950	3.9874	30.849	397.61
650	126.49	2467.03	2625.15	5.2622	3.2490	11.643	451.23
675	99.221	2626.90	2828.47	5.5698	2.6761	6.1893	510.66
700	86.380	2730.24	2961.78	5.7639	2.4016	4.6890	547.76
725	78.088	2812.91	3069.03	5.9145	2.2368	3.9636	576.19

TABLE 13.2. Thermodynamic properties of water in the single-phase region—Continued

T K	ρ kg m^{-3}	u kJ kg^{-1}	h kJ kg^{-1}	s kJ kg^{-1} K^{-1}	c_v kJ kg^{-1} K^{-1}	c_p kJ kg^{-1} K^{-1}	w m s^{-1}
			20.0 MPa—Continued				
750	72.027	2884.73	3162.40	6.0411	2.1304	3.5394	599.77
775	67.280	2949.97	3247.24	6.1524	2.0593	3.2657	620.23
800	63.396	3010.92	3326.40	6.2530	2.0110	3.0783	638.50
825	60.121	3068.93	3401.60	6.3456	1.9783	2.9447	655.14
850	57.296	3124.86	3473.93	6.4319	1.9566	2.8470	670.52
900	52.615	3232.66	3612.79	6.5907	1.9351	2.7193	698.45
950	48.841	3337.27	3746.76	6.7356	1.9322	2.6465	723.58
1000	45.696	3440.28	3877.96	6.8702	1.9405	2.6058	746.67
1050	43.012	3542.69	4007.67	6.9968	1.9558	2.5853	768.20
1100	40.682	3645.09	4136.71	7.1168	1.9757	2.5780	788.47
1150	38.630	3747.89	4265.62	7.2314	1.9985	2.5796	807.72
1200	36.804	3851.36	4394.78	7.3414	2.0231	2.5875	826.13
1250	35.164	3955.67	4524.44	7.4472	2.0488	2.5996	843.81
1273	34.463	4003.98	4584.30	7.4947	2.0609	2.6062	851.73
			22.5 MPa				
271.435[a]	1010.95	−6.821	15.435	−0.0255	4.1209	4.1210	1430.1
275	1010.90	7.866	30.123	0.0283	4.1184	4.1193	1448.0
280	1010.54	28.451	50.716	0.1025	4.1118	4.1181	1470.8
285	1009.87	49.026	71.306	0.1754	4.1022	4.1181	1491.1
290	1008.94	69.598	91.899	0.2470	4.0902	4.1190	1509.2
295	1007.77	90.170	112.497	0.3174	4.0763	4.1204	1525.1
300	1006.38	110.746	133.103	0.3867	4.0606	4.1222	1539.1
305	1004.79	131.326	153.719	0.4548	4.0435	4.1242	1551.3
310	1003.02	151.913	174.346	0.5219	4.0251	4.1265	1561.8
315	1001.08	172.508	194.984	0.5879	4.0056	4.1289	1570.7
320	998.976	193.111	215.634	0.6530	3.9850	4.1313	1578.2
325	996.723	213.723	236.297	0.7171	3.9636	4.1339	1584.4
330	994.328	234.345	256.973	0.7802	3.9414	4.1365	1589.3
335	991.797	254.977	277.663	0.8424	3.9186	4.1393	1593.0
340	989.136	275.619	298.366	0.9038	3.8953	4.1422	1595.7
345	986.351	296.273	319.085	0.9643	3.8716	4.1452	1597.3
350	983.447	316.940	339.819	1.0239	3.8476	4.1485	1597.9
355	980.427	337.621	360.570	1.0828	3.8233	4.1520	1597.7
360	977.295	358.316	381.339	1.1409	3.7990	4.1557	1596.6
365	974.054	379.028	402.128	1.1982	3.7746	4.1598	1594.6
370	970.707	399.759	422.938	1.2549	3.7501	4.1643	1591.9
375	967.257	420.510	443.771	1.3108	3.7258	4.1691	1588.5
380	963.705	441.282	464.630	1.3661	3.7016	4.1744	1584.4
385	960.053	462.079	485.516	1.4207	3.6776	4.1801	1579.5
390	956.302	482.903	506.431	1.4746	3.6537	4.1863	1574.1
395	952.454	503.756	527.379	1.5280	3.6301	4.1930	1568.0
400	948.510	524.640	548.362	1.5808	3.6068	4.2002	1561.3
410	940.334	566.515	590.443	1.6847	3.5611	4.2165	1546.2
420	931.776	608.552	632.699	1.7865	3.5166	4.2352	1528.9
430	922.836	650.775	675.157	1.8864	3.4736	4.2568	1509.5
440	913.508	693.214	717.844	1.9846	3.4321	4.2813	1488.1
450	903.782	735.899	760.794	2.0811	3.3920	4.3092	1464.8
460	893.646	778.864	804.042	2.1761	3.3535	4.3409	1439.7
470	883.081	822.146	847.625	2.2699	3.3164	4.3766	1412.6
480	872.066	865.789	891.590	2.3624	3.2809	4.4171	1383.8
490	860.571	909.839	935.984	2.4540	3.2468	4.4628	1353.2
500	848.562	954.350	980.866	2.5446	3.2142	4.5146	1320.8
510	835.996	999.387	1026.30	2.6346	3.1832	4.5736	1286.5
520	822.820	1045.02	1072.37	2.7241	3.1536	4.6411	1250.4

TABLE 13.2. Thermodynamic properties of water in the single-phase region—Continued

T K	ρ kg m^{-3}	u kJ kg^{-1}	h kJ kg^{-1}	s kJ kg^{-1} K^{-1}	c_v kJ kg^{-1} K^{-1}	c_p kJ kg^{-1} K^{-1}	w m s^{-1}
			22.5 MPa—Continued				
530	808.969	1091.34	1119.16	2.8132	3.1257	4.7188	1212.3
540	794.360	1138.46	1166.78	2.9022	3.0994	4.8089	1172.1
550	778.891	1186.50	1215.39	2.9914	3.0750	4.9148	1129.8
560	762.428	1235.64	1265.15	3.0810	3.0527	5.0408	1085.0
570	744.794	1286.08	1316.29	3.1716	3.0328	5.1935	1037.4
580	725.750	1338.14	1369.14	3.2635	3.0159	5.3830	986.68
590	704.954	1392.21	1424.13	3.3575	3.0028	5.6253	932.21
600	681.900	1448.91	1481.91	3.4546	2.9950	5.9481	873.13
610	655.778	1509.22	1543.53	3.5564	2.9949	6.4043	808.11
620	625.149	1574.83	1610.82	3.6658	3.0078	7.1128	734.76
630	586.927	1649.38	1687.71	3.7888	3.0474	8.4284	647.47
640	531.385	1744.16	1786.50	3.9443	3.1724	12.142	529.59
650	218.278	2221.62	2324.70	4.7753	4.2412	65.272	368.68
675	124.87	2548.45	2728.64	5.3885	2.9018	8.1990	486.04
700	104.02	2677.42	2893.72	5.6289	2.5422	5.5112	531.81
725	92.178	2772.36	3016.45	5.8013	2.3359	4.4330	564.50
750	84.043	2851.62	3119.34	5.9409	2.2046	3.8495	590.71
775	77.909	2921.95	3210.75	6.0608	2.1171	3.4885	612.98
800	73.017	2986.61	3294.76	6.1675	2.0574	3.2473	632.57
825	68.967	3047.46	3373.71	6.2647	2.0164	3.0780	650.23
850	65.523	3105.65	3449.04	6.3547	1.9884	2.9552	666.43
900	59.903	3216.82	3592.43	6.5186	1.9584	2.7953	695.57
950	55.439	3323.83	3729.68	6.6671	1.9500	2.7031	721.57
1000	51.757	3428.66	3863.38	6.8042	1.9545	2.6498	745.31
1050	48.640	3532.48	3995.06	6.9327	1.9672	2.6205	767.34
1100	45.949	3636.02	4125.69	7.0543	1.9851	2.6069	788.01
1150	43.591	3739.75	4255.92	7.1701	2.0064	2.6038	807.59
1200	41.499	3844.00	4386.19	7.2809	2.0299	2.6079	826.26
1250	39.626	3948.98	4516.80	7.3876	2.0547	2.6171	844.16
1273	38.827	3997.56	4577.05	7.4353	2.0664	2.6226	852.17
			25.0 MPa				
271.235[a]	1012.16	−7.609	17.090	−0.0285	4.1109	4.1109	1433.3
275	1012.09	7.865	32.566	0.0282	4.1088	4.1100	1452.2
280	1011.69	28.404	53.115	0.1022	4.1027	4.1099	1474.9
285	1011.00	48.939	73.667	0.1750	4.0936	4.1107	1495.3
290	1010.04	69.472	94.224	0.2465	4.0821	4.1121	1513.3
295	1008.85	90.008	114.789	0.3168	4.0686	4.1140	1529.3
300	1007.45	110.549	135.364	0.3859	4.0534	4.1162	1543.3
305	1005.85	131.096	155.951	0.4540	4.0366	4.1186	1555.5
310	1004.07	151.651	176.550	0.5210	4.0186	4.1211	1566.0
315	1002.12	172.215	197.162	0.5869	3.9993	4.1236	1575.0
320	1000.01	192.787	217.786	0.6519	3.9791	4.1262	1582.6
325	997.759	213.368	238.424	0.7159	3.9579	4.1289	1588.8
330	995.364	233.959	259.076	0.7790	3.9360	4.1316	1593.7
335	992.834	254.560	279.741	0.8411	3.9134	4.1344	1597.5
340	990.177	275.172	300.420	0.9024	3.8904	4.1374	1600.2
345	987.397	295.795	321.114	0.9628	3.8669	4.1404	1601.9
350	984.499	316.431	341.825	1.0224	3.8431	4.1437	1602.6
355	981.487	337.080	362.552	1.0812	3.8191	4.1472	1602.4
360	978.365	357.744	383.297	1.1392	3.7949	4.1509	1601.4
365	975.134	378.424	404.061	1.1965	3.7707	4.1549	1599.5
370	971.799	399.121	424.847	1.2531	3.7465	4.1593	1596.9
375	968.362	419.838	445.655	1.3089	3.7223	4.1641	1593.6
380	964.824	440.576	466.488	1.3641	3.6982	4.1692	1589.5

TABLE 13.2. Thermodynamic properties of water in the single-phase region—Continued

T K	ρ kg m^{-3}	u kJ kg^{-1}	h kJ kg^{-1}	s kJ kg^{-1} K^{-1}	c_v kJ kg^{-1} K^{-1}	c_p kJ kg^{-1} K^{-1}	w m s^{-1}
			25.0 MPa—Continued				
385	961.188	461.338	487.348	1.4187	3.6744	4.1748	1584.8
390	957.454	482.126	508.237	1.4726	3.6507	4.1809	1579.5
395	953.624	502.941	529.157	1.5259	3.6272	4.1874	1573.5
400	949.699	523.788	550.112	1.5786	3.6040	4.1945	1566.9
410	941.567	565.583	592.134	1.6823	3.5585	4.2104	1552.0
420	933.059	607.534	634.327	1.7840	3.5143	4.2287	1535.0
430	924.174	649.665	676.716	1.8838	3.4715	4.2496	1515.9
440	914.909	692.005	719.330	1.9817	3.4302	4.2736	1494.8
450	905.254	734.582	762.198	2.0781	3.3903	4.3007	1471.9
460	895.198	777.429	805.355	2.1729	3.3519	4.3314	1447.1
470	884.724	820.582	848.839	2.2664	3.3149	4.3660	1420.5
480	873.811	864.080	892.691	2.3588	3.2795	4.4051	1392.1
490	862.433	907.970	936.958	2.4500	3.2455	4.4492	1362.0
500	850.558	952.302	981.694	2.5404	3.2130	4.4991	1330.1
510	838.146	997.135	1026.96	2.6300	3.1819	4.5557	1296.5
520	825.149	1042.54	1072.83	2.7191	3.1523	4.6201	1261.1
530	811.506	1088.59	1119.40	2.8078	3.1243	4.6940	1223.8
540	797.145	1135.39	1166.75	2.8963	3.0979	4.7793	1184.6
550	781.973	1183.06	1215.03	2.9849	3.0732	4.8788	1143.3
560	765.873	1231.75	1264.39	3.0738	3.0505	4.9962	1099.8
570	748.690	1281.64	1315.03	3.1635	3.0300	5.1370	1053.8
580	730.221	1333.00	1367.23	3.2543	3.0122	5.3093	1005.0
590	710.183	1386.16	1421.36	3.3468	2.9977	5.5256	952.89
600	688.169	1441.63	1477.96	3.4419	2.9876	5.8064	896.95
610	663.563	1500.15	1537.82	3.5408	2.9837	6.1881	836.23
620	635.349	1562.94	1602.29	3.6457	2.9891	6.7440	769.29
630	601.635	1632.29	1673.84	3.7601	3.0110	7.6523	693.27
640	557.980	1713.51	1758.31	3.8931	3.0696	9.5042	601.48
650	488.846	1825.21	1876.35	4.0760	3.2506	15.701	479.26
675	161.60	2447.09	2601.79	5.1743	3.1528	12.032	456.98
700	125.09	2617.54	2817.39	5.4885	2.6894	6.6244	514.91
725	107.99	2728.40	2959.91	5.6887	2.4382	5.0021	552.58
750	97.098	2816.56	3074.03	5.8436	2.2806	4.2055	581.65
775	89.232	2892.68	3172.84	5.9732	2.1759	3.7360	605.82
800	83.132	2961.46	3262.18	6.0867	2.1044	3.4310	626.78
825	78.181	3025.40	3345.17	6.1889	2.0548	3.2206	645.48
850	74.032	3086.01	3423.70	6.2826	2.0205	3.0696	662.49
900	67.367	3200.74	3571.84	6.4520	1.9817	2.8742	692.84
950	62.153	3310.24	3712.48	6.6041	1.9677	2.7613	719.69
1000	57.899	3416.94	3848.73	6.7439	1.9685	2.6947	744.06
1050	54.324	3522.21	3982.41	6.8744	1.9785	2.6563	766.58
1100	51.256	3626.91	4114.66	6.9974	1.9945	2.6361	787.64
1150	48.579	3731.59	4246.22	7.1144	2.0143	2.6281	807.53
1200	46.213	3836.64	4377.61	7.2262	2.0366	2.6285	826.46
1250	44.101	3942.29	4509.17	7.3336	2.0605	2.6348	844.57
1273	43.202	3991.14	4569.82	7.3817	2.0718	2.6391	852.66
			30.0 MPa				
270.829[a]	1014.59	−9.207	20.362	−0.0346	4.0910	4.0910	1439.6
275	1014.45	7.855	37.428	0.0279	4.0900	4.0922	1460.5
280	1013.98	28.307	57.893	0.1016	4.0851	4.0940	1483.2
285	1013.23	48.761	78.369	0.1741	4.0770	4.0963	1503.5
290	1012.23	69.220	98.857	0.2454	4.0664	4.0989	1521.6
295	1011.00	89.685	119.359	0.3155	4.0537	4.1017	1537.6
300	1009.57	110.159	139.874	0.3844	4.0392	4.1046	1551.6

TABLE 13.2. Thermodynamic properties of water in the single-phase region—Continued

T K	ρ kg m^{-3}	u kJ kg^{-1}	h kJ kg^{-1}	s kJ kg^{-1} K^{-1}	c_v kJ kg^{-1} K^{-1}	c_p kJ kg^{-1} K^{-1}	w m s^{-1}
			30.0 MPa—Continued				
305	1007.95	130.641	160.405	0.4523	4.0231	4.1075	1563.9
310	1006.15	151.133	180.950	0.5191	4.0057	4.1105	1574.5
315	1004.19	171.634	201.509	0.5849	3.9871	4.1134	1583.6
320	1002.07	192.146	222.083	0.6497	3.9674	4.1163	1591.2
325	999.815	212.667	242.672	0.7136	3.9468	4.1192	1597.5
330	997.419	233.197	263.275	0.7765	3.9254	4.1220	1602.5
335	994.893	253.739	283.893	0.8385	3.9033	4.1250	1606.4
340	992.242	274.290	304.525	0.8996	3.8807	4.1279	1609.2
345	989.472	294.853	325.172	0.9599	3.8577	4.1310	1611.0
350	986.586	315.428	345.835	1.0194	3.8343	4.1343	1611.9
355	983.589	336.015	366.515	1.0780	3.8107	4.1377	1611.8
360	980.484	356.616	387.213	1.1359	3.7869	4.1414	1610.9
365	977.274	377.232	407.930	1.1931	3.7631	4.1453	1609.3
370	973.962	397.865	428.667	1.2495	3.7392	4.1496	1606.8
375	970.550	418.516	449.426	1.3052	3.7154	4.1542	1603.6
380	967.040	439.187	470.209	1.3603	3.6916	4.1591	1599.8
385	963.434	459.879	491.018	1.4147	3.6680	4.1645	1595.2
390	959.733	480.596	511.855	1.4685	3.6446	4.1703	1590.1
395	955.939	501.339	532.722	1.5216	3.6215	4.1766	1584.3
400	952.052	522.111	553.621	1.5742	3.5985	4.1834	1577.9
410	944.003	563.749	595.529	1.6777	3.5535	4.1985	1563.5
420	935.590	605.534	637.599	1.7791	3.5098	4.2159	1547.0
430	926.813	647.487	679.856	1.8785	3.4674	4.2359	1528.4
440	917.669	689.634	722.325	1.9761	3.4264	4.2585	1508.0
450	908.150	732.002	765.036	2.0721	3.3868	4.2842	1485.7
460	898.248	774.621	808.020	2.1666	3.3487	4.3131	1461.6
470	887.947	817.524	851.310	2.2597	3.3120	4.3457	1435.8
480	877.229	860.748	894.946	2.3516	3.2768	4.3823	1408.3
490	866.073	904.332	938.971	2.4423	3.2429	4.4234	1379.1
500	854.451	948.321	983.432	2.5322	3.2105	4.4697	1348.3
510	842.328	992.769	1028.38	2.6212	3.1795	4.5219	1315.8
520	829.664	1037.73	1073.89	2.7095	3.1498	4.5809	1281.7
530	816.410	1083.28	1120.03	2.7974	3.1217	4.6481	1246.0
540	802.505	1129.50	1166.89	2.8850	3.0950	4.7248	1208.4
550	787.873	1176.49	1214.56	2.9725	3.0699	4.8133	1169.1
560	772.424	1224.36	1263.20	3.0601	3.0466	4.9162	1127.9
570	756.037	1273.27	1312.95	3.1482	3.0252	5.0375	1084.6
580	738.563	1323.41	1364.03	3.2370	3.0059	5.1825	1039.0
590	719.799	1375.03	1416.71	3.3270	2.9893	5.3592	990.96
600	699.473	1428.47	1471.36	3.4189	2.9760	5.5795	940.02
610	677.200	1484.20	1528.50	3.5133	2.9668	5.8628	885.78
620	652.409	1542.95	1588.93	3.6116	2.9634	6.2422	827.64
630	624.203	1605.81	1653.87	3.7155	2.9681	6.7805	764.68
640	591.011	1674.75	1725.52	3.8283	2.9860	7.6179	695.25
650	549.640	1753.80	1808.38	3.9567	3.0286	9.1195	616.53
675	332.51	2111.81	2202.03	4.5488	3.4341	27.030	416.55
700	184.24	2468.61	2631.44	5.1754	2.9775	10.351	480.01
725	146.51	2628.50	2833.26	5.4590	2.6431	6.5382	528.88
750	127.00	2740.01	2976.24	5.6531	2.4337	5.0795	564.09
775	114.27	2830.23	3092.77	5.8060	2.2946	4.3121	592.18
800	105.00	2908.58	3194.29	5.9349	2.1990	3.8442	615.89
825	97.796	2979.51	3286.27	6.0482	2.1321	3.5339	636.64
850	91.943	3045.46	3371.75	6.1503	2.0848	3.3166	655.24
900	82.840	3167.87	3530.02	6.3313	2.0283	3.0408	687.91

TABLE 13.2. Thermodynamic properties of water in the single-phase region—Continued

T K	ρ kg m^{-3}	u kJ kg^{-1}	h kJ kg^{-1}	s kJ kg^{-1} K^{-1}	c_v kJ kg^{-1} K^{-1}	c_p kJ kg^{-1} K^{-1}	w m s^{-1}
			30.0 MPa—Continued				
950	75.936	3282.68	3677.75	6.4911	2.0031	2.8822	716.38
1000	70.420	3393.26	3819.28	6.6363	1.9964	2.7869	741.96
1050	65.857	3501.52	3957.06	6.7707	2.0010	2.7292	765.39
1100	61.984	3608.60	4092.59	6.8968	2.0131	2.6953	787.18
1150	58.636	3715.22	4226.85	7.0162	2.0299	2.6772	807.66
1200	55.698	3821.87	4360.49	7.1300	2.0500	2.6700	827.07
1250	53.089	3928.88	4493.97	7.2389	2.0720	2.6702	845.58
1273	51.983	3978.29	4555.41	7.2876	2.0826	2.6722	853.83
			40.0 MPa				
269.997[a]	1019.38	−12.472	26.768	−0.0473	4.0526	4.0530	1452.4
270	1019.38	−12.460	26.780	−0.0473	4.0526	4.0530	1452.4
275	1019.09	7.809	47.060	0.0272	4.0543	4.0590	1477.4
280	1018.49	28.095	67.369	0.1003	4.0514	4.0644	1500.0
285	1017.63	48.397	87.703	0.1723	4.0452	4.0694	1520.2
290	1016.54	68.713	108.062	0.2431	4.0362	4.0740	1538.2
295	1015.24	89.044	128.443	0.3128	4.0250	4.0784	1554.2
300	1013.75	109.389	148.846	0.3814	4.0119	4.0826	1568.3
305	1012.08	129.747	169.269	0.4489	3.9971	4.0866	1580.7
310	1010.25	150.117	189.711	0.5154	3.9809	4.0903	1591.4
315	1008.26	170.500	210.172	0.5809	3.9634	4.0939	1600.5
320	1006.13	190.894	230.650	0.6454	3.9448	4.0973	1608.3
325	1003.86	211.298	251.144	0.7089	3.9252	4.1005	1614.8
330	1001.47	231.713	271.655	0.7715	3.9048	4.1037	1620.0
335	998.945	252.139	292.181	0.8333	3.8837	4.1068	1624.1
340	996.306	272.574	312.722	0.8941	3.8620	4.1099	1627.1
345	993.552	293.020	333.280	0.9542	3.8398	4.1130	1629.1
350	990.690	313.477	353.853	1.0134	3.8172	4.1162	1630.2
355	987.721	333.945	374.442	1.0718	3.7944	4.1196	1630.4
360	984.649	354.425	395.049	1.1294	3.7713	4.1231	1629.8
365	981.477	374.919	415.674	1.1863	3.7482	4.1269	1628.4
370	978.208	395.427	436.318	1.2425	3.7250	4.1309	1626.2
375	974.843	415.951	456.983	1.2980	3.7018	4.1352	1623.3
380	971.385	436.492	477.670	1.3528	3.6787	4.1398	1619.8
385	967.836	457.052	498.381	1.4069	3.6557	4.1448	1615.6
390	964.196	477.633	519.118	1.4604	3.6328	4.1501	1610.8
395	960.468	498.237	539.883	1.5133	3.6102	4.1559	1605.5
400	956.652	518.865	560.678	1.5657	3.5878	4.1621	1599.5
410	948.761	560.206	602.366	1.6686	3.5437	4.1759	1586.0
420	940.526	601.673	644.203	1.7694	3.5009	4.1918	1570.4
430	931.950	643.288	686.209	1.8683	3.4592	4.2098	1552.8
440	923.031	685.071	728.407	1.9653	3.4190	4.2302	1533.5
450	913.765	727.047	770.822	2.0606	3.3800	4.2533	1512.4
460	904.145	769.241	813.482	2.1543	3.3425	4.2791	1489.6
470	894.161	811.680	856.415	2.2467	3.3063	4.3080	1465.2
480	883.800	854.395	899.654	2.3377	3.2715	4.3403	1439.2
490	873.045	897.418	943.234	2.4276	3.2380	4.3764	1411.8
500	861.876	940.785	987.195	2.5164	3.2058	4.4166	1382.9
510	850.268	984.537	1031.58	2.6043	3.1749	4.4614	1352.5
520	838.192	1028.72	1076.44	2.6914	3.1453	4.5116	1320.7
530	825.613	1073.39	1121.83	2.7778	3.1170	4.5679	1287.5
540	812.489	1118.59	1167.82	2.8638	3.0900	4.6313	1252.8
550	798.768	1164.41	1214.49	2.9494	3.0644	4.7030	1216.8
560	784.392	1210.92	1261.92	3.0349	3.0403	4.7846	1179.2
570	769.287	1258.22	1310.22	3.1204	3.0176	4.8781	1140.2

TABLE 13.2. Thermodynamic properties of water in the single-phase region—Continued

T K	ρ kg m^{-3}	u kJ kg^{-1}	h kJ kg^{-1}	s kJ kg^{-1} K^{-1}	c_v kJ kg^{-1} K^{-1}	c_p kJ kg^{-1} K^{-1}	w m s^{-1}
			40.0 MPa—Continued				
580	753.362	1306.43	1359.53	3.2061	2.9966	4.9863	1099.6
590	736.505	1355.70	1410.01	3.2924	2.9774	5.1128	1057.3
600	718.577	1406.19	1461.86	3.3796	2.9603	5.2625	1013.3
610	699.396	1458.16	1515.36	3.4680	2.9456	5.4425	967.45
620	678.725	1511.91	1570.84	3.5582	2.9339	5.6629	919.63
630	656.249	1567.85	1628.80	3.6509	2.9256	5.9386	869.73
640	631.536	1626.54	1689.88	3.7471	2.9217	6.2932	817.65
650	603.968	1688.82	1755.05	3.8481	2.9234	6.7657	763.26
675	515.48	1870.15	1947.74	4.1388	2.9639	8.9652	619.27
700	383.02	2118.62	2223.05	4.5388	3.0488	13.079	503.64
725	264.65	2380.67	2531.81	4.9725	2.9186	10.653	503.90
750	206.98	2560.85	2754.10	5.2742	2.6956	7.4503	538.91
775	176.03	2690.03	2917.26	5.4883	2.5134	5.7787	571.46
800	156.30	2793.11	3049.03	5.6558	2.3790	4.8437	599.19
825	142.27	2881.18	3162.35	5.7953	2.2811	4.2635	623.16
850	131.58	2959.79	3263.79	5.9164	2.2096	3.8756	644.33
900	116.01	3099.72	3444.53	6.1232	2.1193	3.4031	680.82
950	104.90	3226.18	3607.48	6.2995	2.0723	3.1386	711.99
1000	96.389	3345.12	3760.11	6.4561	2.0508	2.9790	739.56
1050	89.550	3459.69	3906.37	6.5988	2.0450	2.8792	764.53
1100	83.873	3571.72	4048.63	6.7312	2.0494	2.8160	787.55
1150	79.046	3682.33	4188.37	6.8554	2.0605	2.7767	809.01
1200	74.867	3792.28	4326.56	6.9731	2.0760	2.7534	829.23
1250	71.196	3902.06	4463.89	7.0852	2.0946	2.7412	848.41
1273	69.650	3952.60	4526.90	7.1351	2.1038	2.7385	856.93
			50.0 MPa				
269.134[a]	1024.11	−15.846	32.977	−0.0606	4.0156	4.0169	1465.4
270	1024.07	−12.369	36.456	−0.0477	4.0169	4.0188	1469.9
275	1023.62	7.730	56.576	0.0262	4.0208	4.0289	1494.6
280	1022.90	27.862	76.742	0.0988	4.0198	4.0373	1516.9
285	1021.94	48.021	96.948	0.1703	4.0152	4.0446	1537.0
290	1020.77	68.204	117.187	0.2407	4.0077	4.0511	1555.0
295	1019.40	88.409	137.457	0.3101	3.9979	4.0569	1570.9
300	1017.85	108.632	157.755	0.3783	3.9860	4.0622	1585.0
305	1016.13	128.872	178.078	0.4455	3.9724	4.0670	1597.4
310	1014.26	149.128	198.425	0.5116	3.9573	4.0714	1608.1
315	1012.25	169.398	218.792	0.5768	3.9408	4.0755	1617.4
320	1010.11	189.680	239.180	0.6410	3.9232	4.0793	1625.3
325	1007.83	209.974	259.585	0.7043	3.9046	4.0829	1631.8
330	1005.43	230.278	280.008	0.7667	3.8851	4.0863	1637.2
335	1002.91	250.593	300.448	0.8281	3.8648	4.0896	1641.4
340	1000.28	270.918	320.904	0.8887	3.8439	4.0927	1644.6
345	997.546	291.252	341.375	0.9485	3.8225	4.0959	1646.9
350	994.703	311.597	361.863	1.0075	3.8007	4.0991	1648.2
355	991.760	331.951	382.366	1.0656	3.7786	4.1024	1648.6
360	988.718	352.316	402.887	1.1230	3.7563	4.1058	1648.2
365	985.581	372.693	423.424	1.1797	3.7338	4.1094	1647.1
370	982.351	393.082	443.981	1.2356	3.7112	4.1131	1645.2
375	979.030	413.485	464.556	1.2909	3.6887	4.1172	1642.6
380	975.621	433.903	485.153	1.3454	3.6661	4.1215	1639.4
385	972.124	454.338	505.771	1.3993	3.6437	4.1261	1635.5
390	968.541	474.790	526.414	1.4526	3.6214	4.1310	1631.1
395	964.874	495.262	547.083	1.5053	3.5993	4.1364	1626.0
400	961.124	515.756	567.778	1.5573	3.5773	4.1421	1620.4

TABLE 13.2. Thermodynamic properties of water in the single-phase region—Continued

T K	ρ kg m^{-3}	u kJ kg^{-1}	h kJ kg^{-1}	s kJ kg^{-1} K^{-1}	c_v kJ kg^{-1} K^{-1}	c_p kJ kg^{-1} K^{-1}	w m s^{-1}
			50.0 MPa—Continued				
410	953.376	556.816	609.261	1.6598	3.5342	4.1547	1607.7
420	945.305	597.986	650.879	1.7601	3.4922	4.1692	1592.9
430	936.912	639.284	692.651	1.8583	3.4513	4.1856	1576.3
440	928.199	680.730	734.598	1.9548	3.4117	4.2041	1558.0
450	919.161	722.343	776.741	2.0495	3.3735	4.2249	1537.9
460	909.796	764.146	819.104	2.1426	3.3365	4.2481	1516.3
470	900.097	806.162	861.712	2.2342	3.3008	4.2740	1493.2
480	890.053	848.416	904.592	2.3245	3.2664	4.3027	1468.7
490	879.652	890.935	947.775	2.4135	3.2332	4.3345	1442.7
500	868.880	933.748	991.293	2.5015	3.2013	4.3697	1415.4
510	857.719	976.888	1035.18	2.5884	3.1707	4.4088	1386.8
520	846.146	1020.39	1079.48	2.6744	3.1412	4.4520	1356.9
530	834.136	1064.30	1124.24	2.7596	3.1129	4.5000	1325.8
540	821.660	1108.65	1169.50	2.8442	3.0858	4.5534	1293.5
550	808.683	1153.50	1215.33	2.9283	3.0600	4.6130	1260.0
560	795.163	1198.90	1261.78	3.0120	3.0353	4.6796	1225.4
570	781.053	1244.93	1308.95	3.0955	3.0120	4.7545	1189.6
580	766.295	1291.66	1356.91	3.1789	2.9899	4.8392	1152.6
590	750.822	1339.18	1405.77	3.2624	2.9693	4.9356	1114.4
600	734.552	1387.60	1455.67	3.3463	2.9502	5.0460	1075.1
610	717.387	1437.05	1506.75	3.4307	2.9328	5.1736	1034.6
620	699.207	1487.70	1559.21	3.5160	2.9173	5.3225	993.00
630	679.867	1539.74	1613.29	3.6026	2.9039	5.4980	950.21
640	659.185	1593.43	1669.28	3.6907	2.8928	5.7072	906.36
650	636.940	1649.07	1727.57	3.7811	2.8843	5.9596	861.56
675	572.50	1799.66	1887.00	4.0217	2.8762	6.8759	746.93
700	491.03	1974.15	2075.98	4.2964	2.8846	8.3131	639.75
725	394.85	2175.77	2302.40	4.6141	2.8757	9.6057	568.02
750	309.93	2375.10	2536.43	4.9315	2.7930	8.8011	554.67
775	253.76	2538.96	2736.00	5.1934	2.6553	7.1758	571.69
800	218.07	2669.21	2898.49	5.3999	2.5197	5.9041	595.46
825	193.89	2776.85	3034.73	5.5677	2.4077	5.0529	618.89
850	176.31	2869.85	3153.43	5.7095	2.3205	4.4788	640.55
900	152.03	3029.35	3358.22	5.9437	2.2034	3.7869	678.60
950	135.62	3168.48	3537.17	6.1373	2.1375	3.4054	711.23
1000	123.48	3296.34	3701.26	6.3057	2.1025	3.1763	740.02
1050	113.98	3417.54	3856.19	6.4569	2.0871	3.0316	766.00
1100	106.26	3534.70	4005.26	6.5956	2.0843	2.9377	789.83
1150	99.786	3649.42	4150.49	6.7248	2.0899	2.8762	811.98
1200	94.250	3762.73	4293.24	6.8463	2.1012	2.8365	832.76
1250	89.434	3875.32	4434.39	6.9615	2.1164	2.8118	852.43
1273	87.417	3927.00	4498.97	7.0127	2.1243	2.8042	861.15
			75.0 MPa				
266.843[a]	1035.67	−24.734	47.683	−0.0963	3.9271	3.9325	1499.0
270	1035.31	−12.322	60.120	−0.0500	3.9366	3.9466	1515.0
275	1034.53	7.404	79.901	0.0226	3.9455	3.9649	1538.5
280	1033.53	27.196	99.763	0.0942	3.9486	3.9794	1560.0
285	1032.33	47.040	119.691	0.1648	3.9476	3.9913	1579.5
290	1030.96	66.925	139.673	0.2343	3.9432	4.0013	1597.0
295	1029.43	86.845	159.701	0.3027	3.9362	4.0098	1612.7
300	1027.75	106.794	179.769	0.3702	3.9270	4.0172	1626.6
305	1025.93	126.767	199.872	0.4366	3.9158	4.0237	1638.9
310	1023.98	146.761	220.004	0.5021	3.9031	4.0294	1649.6
315	1021.90	166.772	240.164	0.5666	3.8889	4.0344	1658.9

TABLE 13.2. Thermodynamic properties of water in the single-phase region—Continued

T K	ρ kg m^{-3}	u kJ kg^{-1}	h kJ kg^{-1}	s kJ kg^{-1} K^{-1}	c_v kJ kg^{-1} K^{-1}	c_p kJ kg^{-1} K^{-1}	w m s^{-1}
			75.0 MPa—Continued				
320	1019.71	186.798	260.348	0.6302	3.8734	4.0390	1666.9
325	1017.41	206.837	280.553	0.6929	3.8568	4.0431	1673.7
330	1015.00	226.887	300.778	0.7546	3.8393	4.0469	1679.3
335	1012.49	246.947	321.022	0.8155	3.8209	4.0504	1683.9
340	1009.88	267.016	341.282	0.8755	3.8019	4.0537	1687.4
345	1007.17	287.092	361.558	0.9347	3.7822	4.0568	1690.0
350	1004.37	307.177	381.850	0.9931	3.7621	4.0599	1691.7
355	1001.49	327.268	402.157	1.0507	3.7416	4.0630	1692.6
360	998.509	347.368	422.480	1.1076	3.7208	4.0661	1692.8
365	995.447	367.475	442.818	1.1637	3.6999	4.0693	1692.2
370	992.303	387.591	463.173	1.2191	3.6788	4.0726	1690.9
375	989.078	407.716	483.544	1.2738	3.6576	4.0760	1688.9
380	985.773	427.851	503.933	1.3278	3.6364	4.0797	1686.3
385	982.391	447.997	524.341	1.3811	3.6153	4.0835	1683.2
390	978.933	468.155	544.769	1.4338	3.5942	4.0876	1679.4
395	975.399	488.326	565.218	1.4859	3.5733	4.0920	1675.2
400	971.792	508.513	585.690	1.5374	3.5525	4.0967	1670.4
410	964.361	548.935	626.707	1.6387	3.5115	4.1070	1659.3
420	956.645	589.435	667.834	1.7378	3.4715	4.1186	1646.4
430	948.649	630.024	709.084	1.8349	3.4324	4.1317	1631.8
440	940.377	670.718	750.474	1.9301	3.3945	4.1464	1615.5
450	931.829	711.531	792.018	2.0234	3.3577	4.1628	1597.8
460	923.006	752.479	833.735	2.1151	3.3221	4.1809	1578.7
470	913.905	793.577	875.642	2.2052	3.2877	4.2009	1558.2
480	904.522	834.842	917.759	2.2939	3.2544	4.2228	1536.5
490	894.853	876.292	960.105	2.3812	3.2222	4.2468	1513.6
500	884.891	917.946	1002.70	2.4673	3.1912	4.2730	1489.5
510	874.626	959.822	1045.57	2.5522	3.1612	4.3016	1464.4
520	864.050	1001.94	1088.74	2.6360	3.1322	4.3328	1438.3
530	853.151	1044.33	1132.24	2.7188	3.1043	4.3668	1411.3
540	841.915	1087.01	1176.09	2.8008	3.0774	4.4037	1383.4
550	830.327	1130.00	1220.32	2.8820	3.0515	4.4439	1354.6
560	818.370	1173.33	1264.98	2.9624	3.0265	4.4877	1325.1
570	806.024	1217.04	1310.09	3.0423	3.0025	4.5354	1294.8
580	793.269	1261.16	1355.70	3.1216	2.9795	4.5875	1263.9
590	780.080	1305.71	1401.86	3.2005	2.9574	4.6445	1232.4
600	766.431	1350.75	1448.61	3.2791	2.9363	4.7069	1200.3
610	752.293	1396.32	1496.01	3.3574	2.9162	4.7753	1167.7
620	737.634	1442.46	1544.14	3.4357	2.8970	4.8505	1134.6
630	722.419	1489.23	1593.05	3.5139	2.8790	4.9332	1101.3
640	706.609	1536.69	1642.83	3.5923	2.8619	5.0245	1067.6
650	690.165	1584.90	1693.57	3.6710	2.8460	5.1251	1033.8
675	646.01	1709.19	1825.28	3.8698	2.8108	5.4237	949.62
700	597.04	1839.75	1965.37	4.0735	2.7815	5.7946	868.17
725	543.17	1977.33	2115.41	4.2841	2.7551	6.2090	794.10
750	485.93	2120.80	2275.14	4.5007	2.7252	6.5419	734.99
775	429.18	2265.86	2440.62	4.7177	2.6841	6.6487	695.45
800	377.56	2406.25	2604.90	4.9263	2.6281	6.4422	675.70
825	334.22	2536.37	2760.77	5.1182	2.5601	6.0028	671.84
850	299.47	2654.01	2904.45	5.2899	2.4883	5.4909	677.56
900	250.00	2855.72	3155.71	5.5773	2.3613	4.6087	701.13
950	217.46	3025.43	3370.32	5.8095	2.2714	4.0194	728.73
1000	194.44	3175.44	3561.16	6.0054	2.2140	3.6417	755.67
1050	177.14	3313.25	3736.65	6.1767	2.1803	3.3945	781.04

TABLE 13.2. Thermodynamic properties of water in the single-phase region—Continued

T K	ρ kg m^{-3}	u kJ kg^{-1}	h kJ kg^{-1}	s kJ kg^{-1} K^{-1}	c_v kJ kg^{-1} K^{-1}	c_p kJ kg^{-1} K^{-1}	w m s^{-1}
			75.0 MPa—Continued				
1100	163.51	3443.28	3901.96	6.3305	2.1630	3.2284	804.77
1150	152.41	3568.27	4060.35	6.4714	2.1572	3.1144	827.05
1200	143.13	3689.96	4213.98	6.6021	2.1593	3.0354	848.07
1250	135.19	3809.53	4364.29	6.7249	2.1671	2.9805	867.99
1273	131.91	3864.05	4432.61	6.7790	2.1721	2.9613	876.84
			100 MPa				
264.347[a]	1046.87	−34.278	61.245	−0.1356	3.8401	3.8512	1534.2
265	1046.78	−31.770	63.761	−0.1261	3.8439	3.8562	1537.4
270	1045.92	−12.481	83.128	−0.0537	3.8667	3.8889	1561.3
275	1044.86	6.931	102.637	0.0179	3.8802	3.9136	1583.4
280	1043.62	26.435	122.255	0.0886	3.8869	3.9328	1603.8
285	1042.22	46.010	141.959	0.1583	3.8888	3.9481	1622.4
290	1040.67	65.640	161.732	0.2271	3.8870	3.9606	1639.2
295	1038.99	85.315	181.562	0.2949	3.8823	3.9710	1654.4
300	1037.19	105.025	201.439	0.3617	3.8751	3.9798	1667.9
305	1035.27	124.764	221.357	0.4276	3.8660	3.9872	1679.9
310	1033.25	144.528	241.310	0.4924	3.8551	3.9937	1690.5
315	1031.12	164.311	261.293	0.5564	3.8426	3.9993	1699.7
320	1028.88	184.109	281.302	0.6194	3.8289	4.0043	1707.7
325	1026.55	203.921	301.335	0.6815	3.8140	4.0086	1714.5
330	1024.13	223.744	321.388	0.7428	3.7980	4.0125	1720.2
335	1021.62	243.576	341.459	0.8031	3.7812	4.0161	1724.9
340	1019.02	263.415	361.548	0.8627	3.7637	4.0194	1728.7
345	1016.34	283.260	381.653	0.9214	3.7455	4.0224	1731.6
350	1013.58	303.111	401.772	0.9793	3.7269	4.0253	1733.6
355	1010.73	322.967	421.906	1.0364	3.7078	4.0281	1734.9
360	1007.81	342.828	442.053	1.0927	3.6883	4.0309	1735.4
365	1004.81	362.694	462.215	1.1483	3.6687	4.0338	1735.2
370	1001.74	382.564	482.391	1.2032	3.6488	4.0366	1734.4
375	998.590	402.440	502.582	1.2575	3.6289	4.0396	1732.9
380	995.373	422.323	522.787	1.3110	3.6089	4.0427	1730.9
385	992.087	442.211	543.009	1.3638	3.5889	4.0460	1728.2
390	988.732	462.108	563.247	1.4161	3.5689	4.0494	1725.1
395	985.311	482.013	583.503	1.4677	3.5491	4.0530	1721.4
400	981.823	501.927	603.778	1.5187	3.5293	4.0569	1717.3
410	974.655	541.788	644.389	1.6190	3.4903	4.0654	1707.6
420	967.235	581.701	685.089	1.7170	3.4521	4.0749	1696.2
430	959.568	621.676	725.890	1.8130	3.4147	4.0855	1683.2
440	951.659	661.724	766.803	1.9071	3.3783	4.0974	1668.7
450	943.511	701.855	807.842	1.9993	3.3430	4.1105	1652.8
460	935.126	742.081	849.018	2.0898	3.3087	4.1249	1635.7
470	926.505	782.413	890.345	2.1787	3.2755	4.1407	1617.3
480	917.647	822.863	931.838	2.2661	3.2433	4.1579	1597.8
490	908.551	863.444	973.509	2.3520	3.2121	4.1766	1577.2
500	899.215	904.167	1015.38	2.4366	3.1820	4.1968	1555.7
510	889.635	945.045	1057.45	2.5199	3.1528	4.2186	1533.2
520	879.807	986.092	1099.75	2.6020	3.1246	4.2421	1509.9
530	869.727	1027.32	1142.30	2.6831	3.0972	4.2673	1485.8
540	859.387	1068.74	1185.11	2.7631	3.0708	4.2944	1461.0
550	848.783	1110.38	1228.19	2.8421	3.0452	4.3234	1435.5
560	837.905	1152.24	1271.58	2.9203	3.0205	4.3545	1409.4
570	826.746	1194.33	1315.29	2.9977	2.9965	4.3877	1382.8
580	815.297	1236.69	1359.34	3.0743	2.9734	4.4233	1355.7
590	803.550	1279.32	1403.76	3.1502	2.9511	4.4613	1328.3

TABLE 13.2. Thermodynamic properties of water in the single-phase region—Continued

T K	ρ kg m^{-3}	u kJ kg^{-1}	h kJ kg^{-1}	s kJ kg^{-1} K^{-1}	c_v kJ kg^{-1} K^{-1}	c_p kJ kg^{-1} K^{-1}	w m s^{-1}
			100 MPa—Continued				
600	791.493	1322.23	1448.58	3.2256	2.9295	4.5019	1300.4
610	779.117	1365.46	1493.81	3.3003	2.9087	4.5454	1272.3
620	766.412	1409.02	1539.49	3.3746	2.8886	4.5917	1244.0
630	753.366	1452.92	1585.66	3.4485	2.8693	4.6413	1215.6
640	739.969	1497.19	1632.33	3.5220	2.8507	4.6941	1187.1
650	726.212	1541.85	1679.55	3.5952	2.8329	4.7503	1158.6
675	690.18	1655.32	1800.21	3.7773	2.7913	4.9065	1088.1
700	651.77	1771.62	1925.05	3.9589	2.7538	5.0832	1020.0
725	611.07	1890.83	2054.48	4.1405	2.7194	5.2716	956.15
750	568.52	2012.65	2188.54	4.3223	2.6866	5.4492	898.84
775	525.06	2136.05	2326.51	4.5033	2.6532	5.5753	850.76
800	482.23	2259.17	2466.55	4.6811	2.6169	5.6108	813.97
825	441.66	2379.77	2606.18	4.8530	2.5762	5.5432	788.45
850	404.66	2495.78	2742.90	5.0163	2.5315	5.3803	773.05
900	343.61	2709.10	3000.13	5.3104	2.4386	4.8879	765.30
950	298.61	2896.69	3231.58	5.5608	2.3567	4.3823	775.22
1000	265.45	3063.40	3440.12	5.7749	2.2950	3.9788	792.50
1050	240.32	3215.15	3631.27	5.9615	2.2533	3.6833	812.32
1100	220.62	3356.58	3809.84	6.1276	2.2276	3.4715	832.67
1150	204.71	3490.92	3979.41	6.2784	2.2142	3.3195	852.75
1200	191.53	3620.37	4142.49	6.4172	2.2098	3.2098	872.28
1250	180.37	3746.46	4300.89	6.5466	2.2119	3.1303	891.15
1273	175.78	3803.64	4372.55	6.6034	2.2146	3.1014	899.61
			200 MPa				
252.462[a]	1087.98	−76.248	107.580	−0.3187	3.3346	3.3550	1684.9
255	1087.46	−67.707	116.208	−0.2847	3.4118	3.4417	1694.1
260	1086.21	−50.361	133.766	−0.2165	3.5251	3.5739	1712.2
265	1084.72	−32.497	151.882	−0.1475	3.6009	3.6673	1730.0
270	1083.06	−14.268	170.394	−0.0783	3.6511	3.7335	1747.0
275	1081.27	4.218	189.186	−0.0093	3.6838	3.7808	1763.1
280	1079.38	22.888	208.180	0.0591	3.7044	3.8148	1778.1
285	1077.41	41.688	227.319	0.1269	3.7166	3.8397	1792.2
290	1075.37	60.583	246.566	0.1938	3.7226	3.8582	1805.1
295	1073.26	79.545	265.893	0.2599	3.7242	3.8721	1817.0
300	1071.10	98.558	285.282	0.3251	3.7224	3.8828	1827.9
305	1068.89	117.607	304.717	0.3893	3.7179	3.8911	1837.7
310	1066.62	136.681	324.190	0.4527	3.7113	3.8977	1846.5
315	1064.30	155.774	343.692	0.5151	3.7030	3.9029	1854.4
320	1061.92	174.880	363.217	0.5766	3.6932	3.9072	1861.4
325	1059.50	193.994	382.762	0.6372	3.6821	3.9106	1867.6
330	1057.02	213.112	402.323	0.6969	3.6700	3.9135	1872.9
335	1054.49	232.232	421.896	0.7558	3.6571	3.9159	1877.5
340	1051.91	251.352	441.481	0.8138	3.6433	3.9180	1881.3
345	1049.28	270.469	461.076	0.8710	3.6289	3.9198	1884.5
350	1046.60	289.584	480.679	0.9274	3.6140	3.9214	1887.0
355	1043.87	308.695	500.290	0.9831	3.5986	3.9229	1888.9
360	1041.09	327.800	519.908	1.0379	3.5829	3.9243	1890.2
365	1038.25	346.901	539.532	1.0921	3.5669	3.9256	1890.9
370	1035.38	365.997	559.164	1.1455	3.5506	3.9270	1891.1
375	1032.45	385.088	578.802	1.1982	3.5342	3.9283	1890.8
380	1029.47	404.173	598.447	1.2503	3.5177	3.9298	1890.1
385	1026.45	423.254	618.100	1.3016	3.5011	3.9312	1888.9
390	1023.39	442.330	637.760	1.3524	3.4845	3.9328	1887.2
395	1020.28	461.403	657.428	1.4025	3.4679	3.9345	1885.1

TABLE 13.2. Thermodynamic properties of water in the single-phase region—Continued

T K	ρ kg m^{-3}	u kJ kg^{-1}	h kJ kg^{-1}	s kJ kg^{-1} K^{-1}	c_v kJ kg^{-1} K^{-1}	c_p kJ kg^{-1} K^{-1}	w m s^{-1}
			200 MPa—Continued				
400	1017.12	480.471	677.105	1.4520	3.4513	3.9363	1882.7
410	1010.68	518.601	716.487	1.5492	3.4184	3.9402	1876.6
420	1004.08	556.723	755.910	1.6442	3.3860	3.9446	1869.1
430	997.312	594.842	795.381	1.7371	3.3542	3.9496	1860.4
440	990.390	632.963	834.904	1.8280	3.3230	3.9551	1850.4
450	983.316	671.091	874.485	1.9169	3.2926	3.9612	1839.4
460	976.096	709.231	914.129	2.0041	3.2629	3.9677	1827.3
470	968.734	747.386	953.841	2.0895	3.2339	3.9748	1814.3
480	961.233	785.561	993.627	2.1732	3.2058	3.9824	1800.4
490	953.596	823.759	1033.49	2.2554	3.1784	3.9905	1785.7
500	945.828	861.984	1073.44	2.3361	3.1518	3.9990	1770.3
510	937.929	900.238	1113.47	2.4154	3.1258	4.0080	1754.2
520	929.903	938.524	1153.60	2.4933	3.1006	4.0174	1737.5
530	921.752	976.844	1193.82	2.5699	3.0761	4.0272	1720.3
540	913.478	1015.20	1234.15	2.6453	3.0523	4.0374	1702.5
550	905.083	1053.60	1274.57	2.7195	3.0291	4.0480	1684.3
560	896.569	1092.03	1315.11	2.7925	3.0065	4.0589	1665.7
570	887.937	1130.51	1355.75	2.8645	2.9845	4.0702	1646.8
580	879.189	1169.03	1396.51	2.9353	2.9631	4.0818	1627.6
590	870.328	1207.59	1437.39	3.0052	2.9422	4.0937	1608.2
600	861.354	1246.19	1478.39	3.0741	2.9219	4.1059	1588.6
610	852.271	1284.84	1519.51	3.1421	2.9021	4.1184	1568.8
620	843.079	1323.53	1560.75	3.2092	2.8829	4.1311	1549.0
630	833.782	1362.26	1602.13	3.2754	2.8641	4.1440	1529.1
640	824.383	1401.03	1643.64	3.3407	2.8458	4.1572	1509.2
650	814.883	1439.84	1685.27	3.4053	2.8280	4.1705	1489.4
675	790.72	1537.02	1789.96	3.5633	2.7855	4.2043	1440.2
700	766.01	1634.40	1895.49	3.7168	2.7458	4.2385	1392.3
725	740.84	1731.91	2001.88	3.8662	2.7086	4.2720	1346.1
750	715.30	1829.48	2109.08	4.0115	2.6738	4.3038	1302.3
775	689.52	1926.98	2217.04	4.1531	2.6414	4.3319	1261.3
800	663.65	2024.26	2325.62	4.2910	2.6110	4.3538	1223.5
825	637.89	2121.12	2434.65	4.4252	2.5826	4.3668	1189.4
850	612.45	2217.30	2543.86	4.5556	2.5559	4.3680	1159.0
900	563.38	2406.51	2761.51	4.8045	2.5072	4.3280	1109.8
950	518.03	2589.67	2975.74	5.0361	2.4644	4.2335	1075.0
1000	477.38	2765.29	3184.25	5.2501	2.4274	4.1026	1052.1
1050	441.66	2932.94	3385.78	5.4467	2.3967	3.9577	1038.6
1100	410.60	3092.98	3580.07	5.6275	2.3727	3.8153	1032.1
1150	383.70	3246.27	3767.52	5.7942	2.3553	3.6852	1031.0
1200	360.35	3393.84	3948.86	5.9486	2.3440	3.5714	1033.8
1250	340.01	3536.72	4124.94	6.0924	2.3380	3.4749	1039.5
1273	331.52	3601.12	4204.41	6.1554	2.3368	3.4360	1042.8
			400 MPa				
259.820[a]	1144.46	−51.611	297.897	−0.2741	3.0567	3.1768	2041.4
260	1144.39	−51.060	298.470	−0.2719	3.0641	3.1853	2041.9
265	1142.35	−35.232	314.925	−0.2092	3.2361	3.3852	2054.1
270	1140.15	−18.608	332.224	−0.1445	3.3547	3.5264	2064.4
275	1137.84	−1.423	350.119	−0.0789	3.4356	3.6254	2073.5
280	1135.47	16.152	368.428	−0.0129	3.4897	3.6941	2081.6
285	1133.06	33.996	387.023	0.0529	3.5248	3.7411	2089.0
290	1130.61	52.022	405.814	0.1183	3.5465	3.7729	2095.7
295	1128.14	70.170	424.735	0.1830	3.5586	3.7939	2102.0
300	1125.66	88.394	443.740	0.2469	3.5638	3.8073	2107.8

TABLE 13.2. Thermodynamic properties of water in the single-phase region—Continued

T K	ρ kg m^{-3}	u kJ kg^{-1}	h kJ kg^{-1}	s kJ kg^{-1} K^{-1}	c_v kJ kg^{-1} K^{-1}	c_p kJ kg^{-1} K^{-1}	w m s^{-1}
			400 MPa—Continued				
305	1123.17	106.664	462.799	0.3099	3.5641	3.8154	2113.2
310	1120.67	124.959	481.889	0.3719	3.5607	3.8199	2118.2
315	1118.16	143.263	500.994	0.4331	3.5547	3.8218	2122.7
320	1115.64	161.565	520.104	0.4933	3.5467	3.8220	2127.0
325	1113.11	179.858	539.212	0.5525	3.5373	3.8211	2130.8
330	1110.57	198.137	558.314	0.6109	3.5268	3.8195	2134.3
335	1108.01	216.399	577.407	0.6683	3.5155	3.8175	2137.4
340	1105.44	234.641	596.489	0.7248	3.5036	3.8152	2140.1
345	1102.85	252.862	615.559	0.7805	3.4912	3.8129	2142.5
350	1100.24	271.061	634.618	0.8353	3.4785	3.8106	2144.5
355	1097.62	289.239	653.665	0.8894	3.4655	3.8083	2146.1
360	1094.97	307.396	672.702	0.9426	3.4524	3.8062	2147.5
365	1092.31	325.531	691.728	0.9951	3.4391	3.8043	2148.5
370	1089.62	343.646	710.745	1.0469	3.4258	3.8025	2149.1
375	1086.92	361.740	729.754	1.0979	3.4124	3.8010	2149.5
380	1084.19	379.816	748.755	1.1482	3.3990	3.7996	2149.5
385	1081.44	397.873	767.750	1.1979	3.3857	3.7984	2149.3
390	1078.67	415.913	786.739	1.2469	3.3724	3.7974	2148.7
395	1075.88	433.936	805.724	1.2953	3.3592	3.7966	2147.9
400	1073.07	451.943	824.705	1.3430	3.3461	3.7959	2146.8
410	1067.38	487.911	862.660	1.4367	3.3201	3.7951	2143.7
420	1061.61	523.823	900.609	1.5282	3.2947	3.7949	2139.7
430	1055.76	559.685	938.559	1.6175	3.2697	3.7951	2134.7
440	1049.83	595.500	976.513	1.7047	3.2453	3.7958	2128.8
450	1043.83	631.271	1014.48	1.7901	3.2214	3.7968	2122.1
460	1037.76	667.003	1052.45	1.8735	3.1981	3.7981	2114.6
470	1031.62	702.696	1090.44	1.9552	3.1753	3.7995	2106.4
480	1025.41	738.353	1128.44	2.0352	3.1531	3.8012	2097.6
490	1019.14	773.975	1166.46	2.1136	3.1315	3.8030	2088.1
500	1012.82	809.563	1204.50	2.1905	3.1103	3.8048	2078.0
510	1006.44	845.117	1242.56	2.2658	3.0897	3.8067	2067.5
520	1000.01	880.637	1280.63	2.3398	3.0695	3.8086	2056.5
530	993.523	916.123	1318.73	2.4123	3.0499	3.8105	2045.0
540	986.994	951.575	1356.85	2.4836	3.0306	3.8124	2033.1
550	980.421	986.991	1394.98	2.5536	3.0119	3.8143	2020.9
560	973.807	1022.37	1433.13	2.6223	2.9935	3.8160	2008.4
570	967.153	1057.71	1471.30	2.6899	2.9756	3.8177	1995.6
580	960.463	1093.02	1509.49	2.7563	2.9581	3.8194	1982.6
590	953.738	1128.28	1547.69	2.8216	2.9410	3.8209	1969.3
600	946.982	1163.51	1585.90	2.8858	2.9243	3.8223	1955.9
610	940.195	1198.69	1624.13	2.9490	2.9080	3.8236	1942.3
620	933.381	1233.83	1662.37	3.0112	2.8921	3.8248	1928.6
630	926.543	1268.92	1700.63	3.0724	2.8765	3.8259	1914.7
640	919.681	1303.96	1738.89	3.1326	2.8613	3.8269	1900.9
650	912.798	1338.95	1777.17	3.1920	2.8465	3.8277	1886.9
675	895.52	1426.21	1872.88	3.3365	2.8110	3.8292	1852.0
700	878.15	1513.12	1968.62	3.4757	2.7776	3.8298	1817.3
725	860.74	1599.65	2064.36	3.6101	2.7463	3.8296	1783.1
750	843.32	1685.78	2160.09	3.7399	2.7170	3.8284	1749.6
775	825.93	1771.47	2255.78	3.8654	2.6898	3.8265	1717.0
800	808.59	1856.72	2351.41	3.9869	2.6645	3.8237	1685.5
825	791.35	1941.49	2446.96	4.1045	2.6411	3.8202	1655.2
850	774.24	2025.77	2542.41	4.2185	2.6195	3.8159	1626.4
900	740.52	2192.77	2732.94	4.4363	2.5815	3.8046	1573.4

TABLE 13.2. Thermodynamic properties of water in the single-phase region—Continued

T K	ρ kg m^{-3}	u kJ kg^{-1}	h kJ kg^{-1}	s kJ kg^{-1} K^{-1}	c_v kJ kg^{-1} K^{-1}	c_p kJ kg^{-1} K^{-1}	w m s^{-1}
			400 MPa—Continued				
950	707.72	2357.60	2922.79	4.6416	2.5501	3.7887	1527.1
1000	676.11	2520.08	3111.71	4.8354	2.5245	3.7668	1487.8
1050	645.93	2680.08	3299.35	5.0185	2.5041	3.7374	1455.6
1100	617.41	2837.46	3485.32	5.1915	2.4883	3.7005	1430.0
1150	590.69	2992.13	3669.30	5.3551	2.4767	3.6575	1410.3
1200	565.84	3144.10	3851.01	5.5098	2.4687	3.6106	1395.5
1250	542.84	3293.48	4030.34	5.6562	2.4638	3.5627	1384.8
1273	532.86	3361.37	4112.03	5.7210	2.4625	3.5409	1381.0
			600 MPa				
271.691[a]	1183.60	−15.760	491.170	−0.1929	3.1871	3.4202	2316.4
275	1181.96	−4.990	502.641	−0.1509	3.2654	3.5099	2320.4
280	1179.45	11.748	520.460	−0.0867	3.3527	3.6116	2325.5
285	1176.90	28.893	538.705	−0.0221	3.4117	3.6821	2329.8
290	1174.34	46.318	557.243	0.0423	3.4502	3.7298	2333.5
295	1171.77	63.929	575.976	0.1064	3.4738	3.7610	2336.8
300	1169.19	81.659	594.833	0.1698	3.4865	3.7803	2339.8
305	1166.62	99.459	613.764	0.2324	3.4914	3.7911	2342.6
310	1164.05	117.293	632.734	0.2941	3.4907	3.7959	2345.2
315	1161.49	135.137	651.716	0.3548	3.4860	3.7965	2347.7
320	1158.92	152.973	670.695	0.4146	3.4784	3.7944	2349.9
325	1156.37	170.790	689.657	0.4734	3.4688	3.7903	2352.1
330	1153.81	188.580	708.596	0.5312	3.4578	3.7851	2354.0
335	1151.26	206.338	727.507	0.5881	3.4458	3.7793	2355.8
340	1148.71	224.061	746.388	0.6440	3.4333	3.7732	2357.4
345	1146.15	241.747	765.239	0.6991	3.4204	3.7670	2358.9
350	1143.59	259.397	784.059	0.7532	3.4073	3.7610	2360.2
355	1141.03	277.010	802.849	0.8065	3.3942	3.7552	2361.2
360	1138.47	294.587	821.611	0.8590	3.3810	3.7498	2362.1
365	1135.90	312.130	840.347	0.9107	3.3680	3.7447	2362.8
370	1133.32	329.640	859.059	0.9616	3.3551	3.7400	2363.3
375	1130.73	347.118	877.748	1.0118	3.3424	3.7357	2363.6
380	1128.14	364.567	896.417	1.0612	3.3299	3.7318	2363.7
385	1125.54	381.987	915.067	1.1100	3.3176	3.7283	2363.6
390	1122.92	399.381	933.700	1.1581	3.3054	3.7251	2363.2
395	1120.30	416.749	952.319	1.2055	3.2935	3.7223	2362.7
400	1117.67	434.093	970.924	1.2523	3.2818	3.7198	2362.0
410	1112.38	468.716	1008.10	1.3441	3.2591	3.7156	2359.9
420	1107.05	503.258	1045.24	1.4336	3.2371	3.7124	2357.1
430	1101.68	537.728	1082.35	1.5210	3.2158	3.7101	2353.6
440	1096.27	572.132	1119.44	1.6062	3.1953	3.7083	2349.3
450	1090.82	606.476	1156.52	1.6895	3.1754	3.7071	2344.4
460	1085.34	640.764	1193.59	1.7710	3.1561	3.7063	2338.8
470	1079.82	675.000	1230.65	1.8507	3.1373	3.7058	2332.6
480	1074.27	709.186	1267.70	1.9287	3.1190	3.7054	2325.9
490	1068.70	743.323	1304.76	2.0051	3.1012	3.7052	2318.7
500	1063.09	777.413	1341.81	2.0800	3.0839	3.7051	2311.0
510	1057.46	811.457	1378.86	2.1534	3.0669	3.7049	2302.8
520	1051.80	845.454	1415.91	2.2253	3.0504	3.7048	2294.3
530	1046.12	879.405	1452.95	2.2959	3.0342	3.7046	2285.3
540	1040.42	913.308	1490.00	2.3651	3.0184	3.7043	2276.1
550	1034.71	947.164	1527.04	2.4331	3.0029	3.7040	2266.5
560	1028.97	980.971	1564.08	2.4998	2.9878	3.7035	2256.6
570	1023.23	1014.73	1601.11	2.5654	2.9730	3.7029	2246.5
580	1017.47	1048.44	1638.13	2.6298	2.9584	3.7022	2236.1

TABLE 13.2. Thermodynamic properties of water in the single-phase region—Continued

T K	ρ kg m^{-3}	u kJ kg^{-1}	h kJ kg^{-1}	s kJ kg^{-1} K^{-1}	c_v kJ kg^{-1} K^{-1}	c_p kJ kg^{-1} K^{-1}	w m s^{-1}
			600 MPa—Continued				
590	1011.70	1082.09	1675.15	2.6930	2.9442	3.7014	2225.6
600	1005.92	1115.69	1712.16	2.7552	2.9303	3.7005	2214.9
610	1000.14	1149.24	1749.16	2.8164	2.9167	3.6994	2204.0
620	994.345	1182.74	1786.15	2.8765	2.9034	3.6982	2193.0
630	988.549	1216.18	1823.13	2.9357	2.8903	3.6969	2181.9
640	982.750	1249.56	1860.09	2.9939	2.8776	3.6954	2170.7
650	976.950	1282.88	1897.03	3.0512	2.8651	3.6938	2159.4
675	962.45	1365.92	1989.32	3.1905	2.8351	3.6894	2131.0
700	947.98	1448.57	2081.50	3.3246	2.8069	3.6842	2102.5
725	933.54	1530.82	2173.53	3.4538	2.7803	3.6784	2074.2
750	919.17	1612.65	2265.41	3.5784	2.7555	3.6721	2046.0
775	904.88	1694.06	2357.13	3.6987	2.7323	3.6653	2018.4
800	890.69	1775.04	2448.68	3.8149	2.7107	3.6581	1991.2
825	876.62	1855.59	2540.04	3.9274	2.6908	3.6507	1964.8
850	862.67	1935.69	2631.21	4.0363	2.6724	3.6430	1939.0
900	835.22	2094.60	2812.97	4.2441	2.6400	3.6275	1890.0
950	808.44	2251.79	2993.96	4.4398	2.6132	3.6121	1844.7
1000	782.41	2407.33	3174.19	4.6247	2.5916	3.5972	1803.2
1050	757.19	2561.29	3353.69	4.7998	2.5744	3.5828	1765.9
1100	732.85	2713.76	3532.48	4.9662	2.5613	3.5685	1732.8
1150	709.44	2864.80	3710.54	5.1245	2.5517	3.5538	1704.1
1200	687.01	3014.48	3887.84	5.2754	2.5451	3.5379	1679.6
1250	665.59	3162.85	4064.31	5.4195	2.5410	3.5207	1659.3
1273	656.08	3230.67	4145.19	5.4836	2.5399	3.5123	1651.2
			800 MPa				
286.725[a]	1212.69	32.019	691.710	−0.0723	3.3575	3.6685	2537.5
290	1210.98	43.167	703.786	−0.0304	3.3891	3.7047	2538.6
295	1208.38	60.374	722.415	0.0333	3.4224	3.7442	2540.1
300	1205.79	77.738	741.204	0.0965	3.4420	3.7690	2541.4
305	1203.20	95.195	760.088	0.1589	3.4515	3.7832	2542.6
310	1200.62	112.701	779.022	0.2205	3.4536	3.7895	2543.6
315	1198.05	130.224	797.973	0.2811	3.4503	3.7902	2544.7
320	1195.50	147.740	816.918	0.3408	3.4432	3.7871	2545.7
325	1192.95	165.233	835.841	0.3994	3.4335	3.7814	2546.6
330	1190.41	182.692	854.730	0.4571	3.4220	3.7740	2547.5
335	1187.88	200.110	873.579	0.5138	3.4092	3.7656	2548.3
340	1185.36	217.483	892.385	0.5695	3.3958	3.7568	2549.0
345	1182.84	234.808	911.147	0.6243	3.3819	3.7478	2549.7
350	1180.33	252.085	929.863	0.6782	3.3680	3.7389	2550.3
355	1177.82	269.314	948.536	0.7312	3.3540	3.7303	2550.8
360	1175.31	286.497	967.167	0.7833	3.3402	3.7221	2551.2
365	1172.81	303.635	985.758	0.8346	3.3267	3.7145	2551.4
370	1170.31	320.731	1004.31	0.8850	3.3135	3.7073	2551.6
375	1167.80	337.785	1022.83	0.9348	3.3006	3.7007	2551.6
380	1165.30	354.802	1041.32	0.9837	3.2880	3.6947	2551.4
385	1162.79	371.782	1059.78	1.0320	3.2758	3.6891	2551.2
390	1160.29	388.729	1078.21	1.0796	3.2640	3.6841	2550.8
395	1157.78	405.643	1096.62	1.1265	3.2525	3.6796	2550.2
400	1155.27	422.528	1115.01	1.1727	3.2413	3.6755	2549.5
410	1150.23	456.217	1151.73	1.2634	3.2200	3.6685	2547.6
420	1145.18	489.807	1188.38	1.3517	3.1998	3.6630	2545.1
430	1140.12	523.311	1224.99	1.4379	3.1806	3.6586	2542.1
440	1135.04	556.739	1261.56	1.5219	3.1624	3.6551	2538.4
450	1129.95	590.098	1298.10	1.6040	3.1450	3.6524	2534.2

TABLE 13.2. Thermodynamic properties of water in the single-phase region—Continued

T K	ρ kg m^{-3}	u kJ kg^{-1}	h kJ kg^{-1}	s kJ kg^{-1} K^{-1}	c_v kJ kg^{-1} K^{-1}	c_p kJ kg^{-1} K^{-1}	w m s^{-1}
			800 MPa—Continued				
460	1124.84	623.395	1334.61	1.6843	3.1282	3.6503	2529.5
470	1119.71	656.634	1371.10	1.7628	3.1121	3.6486	2524.3
480	1114.58	689.819	1407.58	1.8396	3.0966	3.6472	2518.6
490	1109.43	722.953	1444.05	1.9148	3.0815	3.6460	2512.4
500	1104.27	756.038	1480.50	1.9884	3.0668	3.6449	2505.9
510	1099.10	789.074	1516.95	2.0606	3.0526	3.6439	2498.9
520	1093.92	822.063	1553.38	2.1313	3.0386	3.6430	2491.6
530	1088.73	855.004	1589.80	2.2007	3.0250	3.6420	2484.0
540	1083.54	887.898	1626.22	2.2688	3.0117	3.6409	2476.0
550	1078.34	920.744	1662.62	2.3356	2.9987	3.6397	2467.8
560	1073.14	953.541	1699.01	2.4012	2.9859	3.6385	2459.3
570	1067.94	986.289	1735.39	2.4655	2.9734	3.6372	2450.6
580	1062.74	1018.99	1771.76	2.5288	2.9611	3.6357	2441.7
590	1057.54	1051.63	1808.11	2.5909	2.9491	3.6341	2432.7
600	1052.34	1084.23	1844.44	2.6520	2.9373	3.6324	2423.4
610	1047.15	1116.77	1880.75	2.7120	2.9257	3.6306	2414.0
620	1041.96	1149.26	1917.05	2.7710	2.9143	3.6286	2404.5
630	1036.77	1181.70	1953.32	2.8291	2.9032	3.6265	2394.9
640	1031.59	1214.07	1989.58	2.8862	2.8923	3.6244	2385.2
650	1026.41	1246.40	2025.81	2.9423	2.8816	3.6221	2375.4
675	1013.5	1326.95	2116.29	3.0789	2.8558	3.6159	2350.7
700	1000.7	1407.14	2206.60	3.2103	2.8314	3.6092	2325.8
725	987.91	1486.96	2296.75	3.3368	2.8084	3.6021	2300.9
750	975.24	1566.40	2386.71	3.4588	2.7869	3.5946	2276.1
775	962.67	1645.45	2476.48	3.5766	2.7667	3.5869	2251.5
800	950.20	1724.12	2566.05	3.6903	2.7478	3.5789	2227.3
825	937.86	1802.41	2655.42	3.8003	2.7304	3.5708	2203.6
850	925.64	1880.32	2744.59	3.9068	2.7143	3.5627	2180.3
900	901.63	2035.04	2922.32	4.1100	2.6859	3.5466	2135.4
950	878.21	2188.32	3099.26	4.3013	2.6624	3.5311	2093.1
1000	855.43	2340.25	3275.45	4.4821	2.6433	3.5167	2053.5
1050	833.31	2490.93	3450.95	4.6533	2.6282	3.5036	2016.6
1100	811.87	2640.45	3625.83	4.8161	2.6167	3.4919	1982.5
1150	791.12	2788.94	3800.16	4.9710	2.6083	3.4816	1951.3
1200	771.06	2936.47	3974.01	5.1190	2.6026	3.4725	1923.0
1250	751.68	3083.15	4147.43	5.2606	2.5991	3.4643	1897.5
1273	743.01	3150.36	4227.07	5.3237	2.5982	3.4607	1886.8
			1000 MPa				
300.243[a]	1237.39	76.834	884.986	0.0301	3.4179	3.7697	2723.3
305	1234.94	93.201	902.957	0.0895	3.4296	3.7845	2723.2
310	1232.38	110.461	921.901	0.1511	3.4337	3.7917	2723.1
315	1229.83	127.743	940.864	0.2118	3.4317	3.7927	2723.0
320	1227.29	145.020	959.820	0.2715	3.4251	3.7891	2723.0
325	1224.77	162.272	978.749	0.3302	3.4154	3.7823	2723.0
330	1222.26	179.486	997.640	0.3879	3.4034	3.7735	2723.0
335	1219.77	196.654	1016.48	0.4446	3.3901	3.7634	2723.0
340	1217.28	213.770	1035.27	0.5002	3.3758	3.7526	2723.0
345	1214.81	230.831	1054.01	0.5550	3.3611	3.7416	2723.0
350	1212.34	247.836	1072.69	0.6087	3.3463	3.7306	2722.9
355	1209.88	264.786	1091.31	0.6615	3.3315	3.7198	2722.9
360	1207.43	281.680	1109.89	0.7135	3.3169	3.7096	2722.7
365	1204.98	298.523	1128.41	0.7646	3.3027	3.6999	2722.5
370	1202.54	315.314	1146.89	0.8149	3.2889	3.6908	2722.2
375	1200.10	332.059	1165.32	0.8644	3.2755	3.6823	2721.9

TABLE 13.2. Thermodynamic properties of water in the single-phase region—Continued

T K	ρ kg m^{-3}	u kJ kg^{-1}	h kJ kg^{-1}	s kJ kg^{-1} K^{-1}	c_v kJ kg^{-1} K^{-1}	c_p kJ kg^{-1} K^{-1}	w m s^{-1}
			1000 MPa—Continued				
380	1197.67	348.758	1183.71	0.9131	3.2627	3.6745	2721.4
385	1195.24	365.415	1202.07	0.9611	3.2503	3.6673	2720.9
390	1192.82	382.032	1220.39	1.0083	3.2383	3.6607	2720.2
395	1190.39	398.613	1238.67	1.0549	3.2269	3.6547	2719.5
400	1187.97	415.159	1256.93	1.1009	3.2158	3.6493	2718.6
410	1183.12	448.157	1293.38	1.1909	3.1951	3.6399	2716.5
420	1178.28	481.044	1329.74	1.2785	3.1758	3.6324	2713.9
430	1173.44	513.835	1366.03	1.3639	3.1578	3.6263	2710.9
440	1168.60	546.541	1402.27	1.4472	3.1410	3.6214	2707.4
450	1163.75	579.174	1438.46	1.5285	3.1252	3.6175	2703.4
460	1158.91	611.740	1474.62	1.6080	3.1102	3.6143	2699.0
470	1154.06	644.246	1510.75	1.6857	3.0960	3.6118	2694.1
480	1149.22	676.698	1546.86	1.7617	3.0823	3.6096	2688.8
490	1144.37	709.099	1582.94	1.8361	3.0692	3.6078	2683.2
500	1139.52	741.451	1619.01	1.9090	3.0565	3.6062	2677.2
510	1134.67	773.756	1655.07	1.9804	3.0442	3.6047	2670.8
520	1129.83	806.016	1691.11	2.0504	3.0322	3.6033	2664.2
530	1124.98	838.231	1727.13	2.1190	3.0205	3.6019	2657.2
540	1120.14	870.402	1763.14	2.1863	3.0091	3.6004	2650.0
550	1115.31	902.527	1799.14	2.2524	2.9979	3.5989	2642.5
560	1110.47	934.608	1835.12	2.3172	2.9869	3.5974	2634.9
570	1105.65	966.642	1871.09	2.3809	2.9762	3.5957	2627.0
580	1100.83	998.631	1907.04	2.4434	2.9656	3.5939	2618.9
590	1096.02	1030.57	1942.97	2.5048	2.9552	3.5920	2610.7
600	1091.21	1062.47	1978.88	2.5652	2.9450	3.5901	2602.3
610	1086.42	1094.31	2014.77	2.6245	2.9350	3.5879	2593.8
620	1081.63	1126.11	2050.64	2.6828	2.9252	3.5857	2585.2
630	1076.85	1157.85	2086.48	2.7402	2.9155	3.5834	2576.5
640	1072.09	1189.54	2122.30	2.7966	2.9060	3.5810	2567.7
650	1067.33	1221.19	2158.10	2.8521	2.8967	3.5785	2558.8
675	1055.5	1300.06	2247.48	2.9870	2.8741	3.5718	2536.4
700	1043.8	1378.61	2336.69	3.1168	2.8527	3.5647	2513.7
725	1032.1	1456.81	2425.71	3.2417	2.8325	3.5573	2491.0
750	1020.5	1534.68	2514.55	3.3622	2.8134	3.5496	2468.4
775	1009.1	1612.21	2603.19	3.4785	2.7954	3.5417	2445.9
800	997.76	1689.39	2691.64	3.5908	2.7787	3.5338	2423.7
825	986.55	1766.24	2779.88	3.6994	2.7631	3.5259	2401.8
850	975.46	1842.77	2867.93	3.8046	2.7487	3.5180	2380.3
900	953.67	1994.86	3043.45	4.0052	2.7233	3.5027	2338.7
950	932.43	2145.74	3218.21	4.1942	2.7022	3.4881	2299.0
1000	911.77	2295.50	3392.27	4.3727	2.6851	3.4745	2261.5
1050	891.69	2444.21	3565.68	4.5420	2.6716	3.4622	2226.3
1100	872.20	2591.99	3738.51	4.7028	2.6612	3.4513	2193.2
1150	853.30	2738.92	3910.83	4.8560	2.6536	3.4418	2162.3
1200	834.99	2885.10	4082.72	5.0023	2.6485	3.4338	2133.6
1250	817.25	3030.62	4254.24	5.1423	2.6454	3.4271	2107.0
1273	809.28	3097.36	4333.03	5.2048	2.6446	3.4245	2095.5

[a]Temperature on the melting curve.
[b]Saturated liquid.
[c]Saturated vapor.